DEPARTMENT R... WME-101-104-1

LEVEL II

2

DP

MOISTURE AND THERMAL EXPANSION OF COMPOSITE MATERIALS

Douglas S. Cairns

Donald F. Adams

November 1981

INTERIM REPORT

U.S. Army Research Office

Grant No. DAAG 29-79-C-0189

Approved for Public Release; Distribution Unlimited

COMPOSITE MATERIALS RESEARCH GROUP

DEPARTMENT of MECHANICAL ENGINEERING

University of Wyoming Laramie, Wyoming 82071

THE VIEWS, OPINIONS, AND/OR FINDINGS CONTAINED IN THIS REPORT ARE THOSE OF THE AUTHORS AND SHOULD NOT BE CONSTRUED AS AN OFFICIAL DEPARTMENT OF THE ARMY POSITION, POLICY, OR DECISION, UNLESS SO DESIGNATED BY OTHER DOCUMENTATION.

DEPARTMENT REPORT
UWME-DR-101-104-1

MOISTURE AND THERMAL EXPANSION OF COMPOSITE MATERIALS

(2)

INTERIM REPORT

DOUGLAS S. CAIRNS
DONALD F. ADAMS

NOVEMBER 1981

U.S. ARMY RESEARCH OFFICE
GRANT NO. DAAG 29-79-C-0189

COMPOSITE MATERIALS RESEARCH GROUP
MECHANICAL ENGINEERING DEPARTMENT
UNIVERSITY OF WYOMING
LARAMIE, WYOMING 82071

Unclassified

SECURITY CLASSIFICATION OF THIS PAGE (When Data Entered)

REPORT DOCUMENTATION PAGE		READ INSTRUCTIONS BEFORE COMPLETING FORM
1. REPORT NUMBER ARO	2. GOVT ACCESSION NO. AD-A109 131	3. RECIPIENT'S CATALOG NUMBER
4. TITLE (and Subtitle) Moisture and Thermal Expansion of Composite Materials		5. TYPE OF REPORT & PERIOD COVERED Interim Report
		6. PERFORMING ORG. REPORT NUMBER UWME-DR-101-104-1
7. AUTHOR(s) Douglas S. Cairns Donald F. Adams		8. CONTRACT OR GRANT NUMBER(s) DAAG 29-79-C-0189
9. PERFORMING ORGANIZATION NAME AND ADDRESS Composite Materials Research Group Mechanical Engineering Department University of Wyoming Laramie, WY 82071		10. PROGRAM ELEMENT, PROJECT, TASK AREA & WORK UNIT NUMBERS
11. CONTROLLING OFFICE NAME AND ADDRESS U.S. Army Research Office P.O. Box 12211 Research Triangle Park, NC 27709		12. REPORT DATE November 1981 13. NUMBER OF PAGES 204
14. MONITORING AGENCY NAME & ADDRESS (if different from Controlling Office)		15. SECURITY CLASS. (of this report) Unclassified 15a. DECLASSIFICATION/DOWNGRADING SCHEDULE NA

16. DISTRIBUTION STATEMENT (of this Report)

Approved for Public Release; Distribution Unlimited

17. DISTRIBUTION STATEMENT (of the abstract entered in Block 20, if different from Report)

18. SUPPLEMENTARY NOTES

The views, opinion, and/or findings contained in this report are those of the authors and should not be construed as an official Department of the Army position, policy, or decision, unless so designated by other documentation.

19. KEY WORDS (Continue on reverse side if necessary and identify by block number)

Composite Materials
Moisture Expansion
Thermal Expansion
Unidirectional Composites
Experimental Measurements
Micromechanical Analyses

20. ABSTRACT (Continue on reverse side if necessary and identify by block number)

An experimental technique is presented for determining the moisture and thermal expansion coefficients of polymers, and polymer-matrix composite materials. Materials tested included Hercules 3501-6 neat epoxy resin, Hercules AS/3501-6 graphite/epoxy composite and Owens-Corning S2 glass fibers in the same Hercules 3501-6 epoxy matrix. Correlations of the experimentally determined moisture and thermal expansion properties with a nonlinear finite element micromechanics analysis are presented. Thermal expansion results for all three -

(continued)

DD FORM 1 JAN 73 1473 EDITION OF 1 NOV 65 IS OBSOLETE

Unclassified

SECURITY CLASSIFICATION OF THIS PAGE (When Data Entered)

materials, both dry and moisture-conditioned, were obtained. Diffusivity constants were also experimentally determined. It is demonstrated that the moisture and thermal expansion of composite materials can be determined experimentally, and predicted numerically, with generally good results.

FORWARD

This Interim Report presents the preliminary results of one phase of a comprehensive study, "Laminate Analyses, Micromechanical Creep Response, and Fatigue Behavior of Polymer Matrix Composites," being performed under Grant DAAG 29-79-C-0189 for the U.S. Army Research Office, Durham, North Carolina. The study was initiated in September 1979. The ARO Project Monitor is Dr. John C. Hurt, Associate Director, Metallurgy and Materials Science Division.

Program Manager and Principal Investigator at the University of Wyoming is Dr. Donald F. Adams, Professor of Mechanical Engineering. Co-Principal Investigator is Mr. David E. Walrath, Staff Scientist in Mechanical Engineering.

The task being reported here was performed by Mr. Douglas S. Cairns, Graduate Student in Mechanical Engineering, as a Masters Thesis under the direction of Dr. D. F. Adams.

Special thanks are due to Mr. Mark Walker for his innovative work on the data acquisition system, and Mr. David E. Walrath for sharing his knowledge of mechanical and electrical hardware.

The assistance of Mr. John Miller and Mr. Dean Logan in the machining and welding is also gratefully acknowledged.

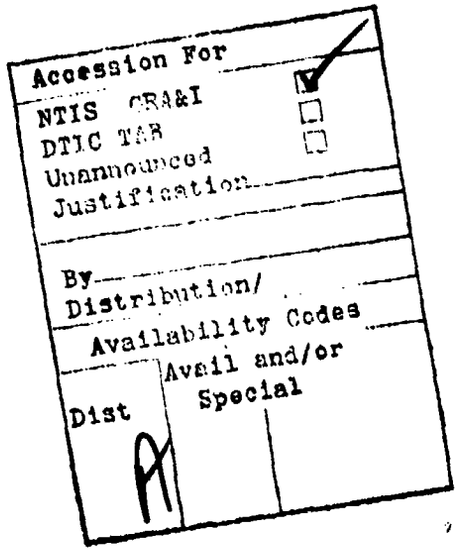

TABLE OF CONTENTS

LIST OF FIGURES

Figure Page

Figure | Page

Figure Page

Figure Page

Figure Page

Figure Page

Figure Page

LIST OF TABLES

LIST OF SYMBOLS

ϵ = linear strain

β = coefficient of moisture expansion

M = weight percent moisture

α = coefficient of thermal expansion

T = temperature

ν = Poisson's ratio

E = Young's modulus

V_f = fiber volume

ρ = mass density (mass/volume)

x_i = coordinates axes

K_{ij} = thermal conductivity tensor

q_i = heat flux vector

$a_{\alpha\beta}$ = direction cosines

K_r = thermal conductivity of epoxy resin

K_f = thermal conductivity of fiber

c = concentration of moisture (mass/volume)

t = time

D_{ij} = diffusivity tensor

D_r = diffusivity of epoxy resin

D_f = diffusivity of fiber

J_i = moisture flux vector

F_r = weight fraction of the epoxy resin

SECTION 1

INTRODUCTION

In recent years, materials known as composite materials have been developed extensively for use in structural components. A composite material typically consists of a load-carrying material phase, such as fibers, held together by a binder or matrix material, often an organic polymer. Composite materials have the advantage of high strength-to-weight and stiffness-to-weight ratios compared to metals [1,2].

However, matrix materials typically exhibit drastically different coefficients of thermal expansion than fibers. Composites used for primary structural applications requiring strength and stiffness are known as high performance composites. These high performance composites are cured at elevated temperatures. At the cure temperature, the matrix and fiber can usually be considered to be at a zero stress state. When the composite is cooled to room temperature, this mismatch of thermal expansion coefficients causes stresses at the interface. If the composite is cycled several times, the matrix material may actually be forced into the plastic region [3], causing permanent deformation of the composite.

As analysis methods continue to improve, designers are learning to utilize the anisotropy of composites consisting of laminae (plies) of oriented fibers to obtain unique properties. Typically, this is accomplished by orienting unidirectional laminae at various angles to obtain a laminate with the desired properties [4].

The coefficient of thermal expansion is usually higher in the transverse direction than the longitudinal direction of a unidirectional lamina. This is due to the fact that the fibers do not restrict matrix expansion in the transverse direction as much as in the longitudinal direction. Stresses are hence generated in the laminate. A composite can actually fail due to these thermally-induced stresses, even though no mechanical loads have been applied. Thus, these thermal stresses must be considered in design and analysis. Another design consideration is dimensional stability. For example, graphite fibers actually have a slightly negative coefficient of thermal expansion in their longitudinal direction, while polymer matrix materials have a positive coefficient of thermal expansion. By combining these materials in the proper ratio, a composite may be obtained which has virtually a zero coefficient of thermal expansion. As a typical design application, snow skis need to be dimensionally stable over a wide temperature range. If the curvature of a ski changes, it can cause the ski to perform differently. Knowing the properties of each individual lamina, a ski can be designed to be dimensionally stable while still retaining essential mechanical responses [5]. As another design example, spacecraft antennae need to maintain dimensional stability over a wide range of temperatures so that they may transmit high frequencies precisely. Graphite/epoxy antenna structures have been designed to exhibit little dimensional change throughout their lifetime [6].

A similar problem of dimensional stability is posed by the absorption of moisture into the matrix material. Polymers currently used as matrices in composites absorb moisture, while fibers such as glass and

graphite absorb little or none [7,8]. As moisture diffuses into the matrix, expansion occurs. This expansion again causes internal stresses along with dimensional changes. The moisture-induced dimensional change in the transverse direction of a unidirectional lamina is greater than the dimensional change in the longitudinal direction, since the stiff fibers restrict this motion. The same laminate design problems mentioned for thermal expansion exist due to moisture expansion also. For example, telescopes must be designed to insure moisture stability [9]. This is necessary since any dimensional changes affect precision optics.

In light of the above, it is necessary to determine the nature of moisture and thermal expansion of a unidirectional lamina prior to any design. The matrix material as well as the resulting laminae need to be characterized, so that not only may reliable data for individual laminae be obtained, but predictions based on material constituent properties be formulated, also. The purpose of the present study was to address both of these problems.

SECTION 2

LITERATURE SURVEY

2.1 Classic Works

Classic works have been conducted to determine the equations of diffusion in anisotropic media. Carslaw and Yaeger [10] formulated the equations of thermal diffusion for the most generally anisotropic solid, and reduced the equations to the isotropic case. Springer and Tsai [11] extrapolated these equations to provide the equations of thermal diffusion for a transversely isotropic (material properties independent of direction transverse to a fiber) lamina. Crank [12] and Jost [13] have solved the mass diffusion problem (Fick's Second Law). Later, Springer and Shen [14] extended this work to solve the moisture diffusion problem, which includes the effect of edges. These works present the governing differential equations for mass and moisture diffusion in anisotropic media. A more in-depth review of these works may be found in Appendix A.

2.2 Studies of Composite Laminates

Much work has been done to characterize diffusion in composite laminates. Springer has developed a numerical solution technique to determine moisture distributions through the thickness of a composite material [15,16,17]. The solution includes time-dependent boundary conditions and effects of surface coatings. McKague, et al., have developed a multiple input parameter numerical model which compares favorably with tests using a finite difference scheme [18]. Augl and

Berger [19] also provide a numerical solution to Fick's Second Law, Eq. (A.11) of Appendix A. In general, the solution provides the same information as Springer's program [15]. Augl [20] has characterized diffusion in Kevlar 49 fibers, which adds the further complication of moisture absorbing reinforcing fibers.

While the above solutions are important in determining the rate at which moisture is absorbed in a real environment, the amount of strain induced by this moisture absorption is not determined. Thus, other investigators have pursued this problem. Walrath and Adams [9] have characterized moisture expansion of graphite/epoxy laminates. Crossman, et al. [21] have also characterized the moisture expansion of unidirectional composites.

The similar thermal expansion problem has also been studied experimentally. Freeman and Campbell [22] have characterized several different laminates over a wide temperature range. Room temperature to glass transition temperature tests have also been performed at the University of Wyoming [23].

In addition to testing actual composite materials, numerical models have been developed. Knowing the properties of the constituents, predictions of the composite behavior can be made. Wolff and Eselun [24] used a volume fraction approach to predict moisture expansion. Mauri, et al., [25] predicted in-plane and out-of-plane moisture expansion, taking into account viscoelastic response of the matrix material. Adams and Monib [26] took a micromechanics approach, which included nonlinearities of the matrix material. Viscoelastic effects were included in the above analysis by Schaffer and Adams [27].

Models have also been developed to theoretically determine thermal expansion. Ashton, et al., [28] presented a fiber volume approach to predict thermal expansion. Ishikawa [29] used a micromechanics technique to numerically predict thermal expansion. Miller and Adams [3] used another micromechanics approach, which again included nonlinearities of the matrix and also predicted the onset of plastic deformation due to hygrothermal cycling. Viscoelastic effects have also been included [27].

The above survey is by no means complete. However, it represents a general overview of previous work. The general progression has been to apply the classical works of Carslaw and Yaeger [10], Crank [12] and Jost [13] to composite materials consisting of unidirectional lamina [11,14]. Then, data for dimensional changes due to temperature and moisture diffusion have been generated both experimentally and numerically. Many discrepancies are found in the literature and it is hoped that the present study will shed light on some of the unanswered questions.

SECTION 3

EXPERIMENTAL PROCEDURES

3.1 Introduction

Since little has been done to date to determine the moisture expansion coefficients of unidirectional composite materials, the main thrust of the present study was to characterize a typical matrix material, and two composites with very different fiber materials, but with this same matrix. Since the Hercules AS/3501-6 graphite/epoxy composite system is widely used and was readily available [8], as was the Hercules 3501-6 epoxy resin system [8], these materials were chosen for the study. Owens-Corning S2 glass fiber [7] in the same 3501-6 epoxy matrix was chosen as the third material system.

These three materials were also used for the thermal expansion tests since analysis of both the moisture dilatation and thermal dilatation is similar. One goal of the present study was knowing the mechanical and physical property characteristics of both the matrix material and fiber, to be able to predict the properties of a lamina. Using these unidirectional ply properties, a composite laminate may be analyzed, using existing laminate analyses [4,28]. This would be cost effective since these materials are expensive to manufacture, fabricate, and test.

3.2 Specimen Fabrication

Producing thin, neat resin plates (free of all voids, foreign objects, and surface imperfections) is difficult, especially for the high volatile

content, viscous, high thermal expansion resin systems such as the Hercules 3501-6 epoxy.

Special techniques have been developed at the University of Wyoming for casting the high temperature cure matrix systems used in advanced composites. These techniques include injection molding, open mold casting, and casting in elastomer molds having a coefficient of thermal expansion compatible with the resin system being cast.

The technique chosen for this study was open mold casting. This technique involved making flat casting molds from 0.127 mm (0.005 in) thick aluminum sheet. The molds were approximately 15 cm x 30 cm (6 in x 12 in). These molds were coated with a dry release agent, such as Miller-Stephenson Release Agent Dry Lubricant, to prevent bonding of the resin to the pan. The resin in solid (granular) form, was placed in one of these pans and heated to 49°C (120°F), to form a viscous liquid. The resin was then placed in a vacuum oven until all volatiles were removed from the resin. The pan was moved to a Blue M (Power-O-Matic 60) forced convection oven and made as level as possible. The resin was cured at 100°C (212°F) for one hour, followed by 177°C (350°F) for three hours. After cooling, the cured resin plate was surface ground (see Figure 1). This grinding was accomplished by holding the plate in position with double-faced tape. After one side was fully surfaced, the specimen was flipped over and ground to the proper thickness of 1.27 mm (0.050 in).

The above procedure offers several advantages over other techniques. First, for small volume production, the open casting technique is the most time and cost efficient method. Initial setup of other techniques

requires much more time. Also, while the process is being perfected for a particular resin system, initial specimen attrition is high. Therefore, more material is used for small production runs. Injection molding between two plates is, at this point, still more of an art than a science and requires much practice to perfect the technique. Second, it has been postulated [16] that release agents may affect the surface properties, thereby affecting the diffusivity constants. The surface grinding technique removes all as-cast surfaces, thereby eliminating this problem. Also, with injection molding, residual stresses may be induced in the molded plate during the curing cycle. This is because not only is the resin injected under pressure, mismatch of thermal expansion of the mold and resin may cause stresses. Elastomer molds are not particularly well suited for making thin plates since uniform thickness control of the epoxy resin plate is a problem. Examination in a polariscope [30] showed the residual stresses for the open cast plates to be lower than in injection molded plates. The technique involved examining the fringe order of the stresses under polarized light. The injection molded plates exhibited higher fringe orders and consequently higher stresses.

After curing, all plates were placed in a dessicator to prevent moisture absorption prior to use.

The graphite/epoxy specimens were fabricated from commercially available, 305 mm (12 in) wide Hercules AS/3501-6 prepreg tape. The tape was cut to size and five plies were layed up by hand to the proper dimensions of 305 mm x 610 mm x 0.64 mm (12 in x 24 in x 0.025 in) on a release agent coated, stainless steel plate. On the top were placed, in order, a layer of teflon release cloth, a layer of open cell foam/random

fiber bleeder cloth, and a layer of polyethylene film. This whole unit was placed in a blanket press and cured (see Figure 2) following the same cure cycle as for the neat resin specimens. The blanket press is a pressure chamber used for curing composite plates. Air pressure forces a rubber blanket against the composite to provide debulking during the curing process. These plates were also placed in a moisture absorbing dessicator until used.

Figure 1. Surface Grinding of Six Hercules 3501-6 Epoxy Specimens Held Down by Double-faced Tape

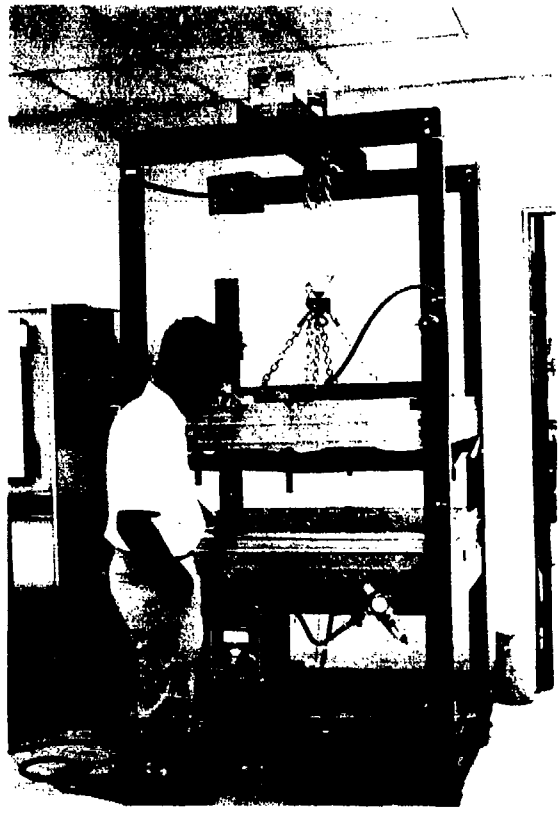

Figure 2. Blanket Press

No prepreg of the S2 glass fiber and 3501-6 epoxy resin was available; this had to be fabricated. S2 glass continuous strand roving (Owens-Corning 470AA-1250) was tightly wound around a rotating drum and then impregnated with the 3501-6 epoxy resin. The homemade prepreg was somewhat greater in thickness than the commercially available AS/3501-6 graphite/epoxy prepreg, so only two layers were needed to produce approximately the same cured composite plate thickness as for the graphite/epoxy system. The rest of the fabrication procedure was exactly the same as

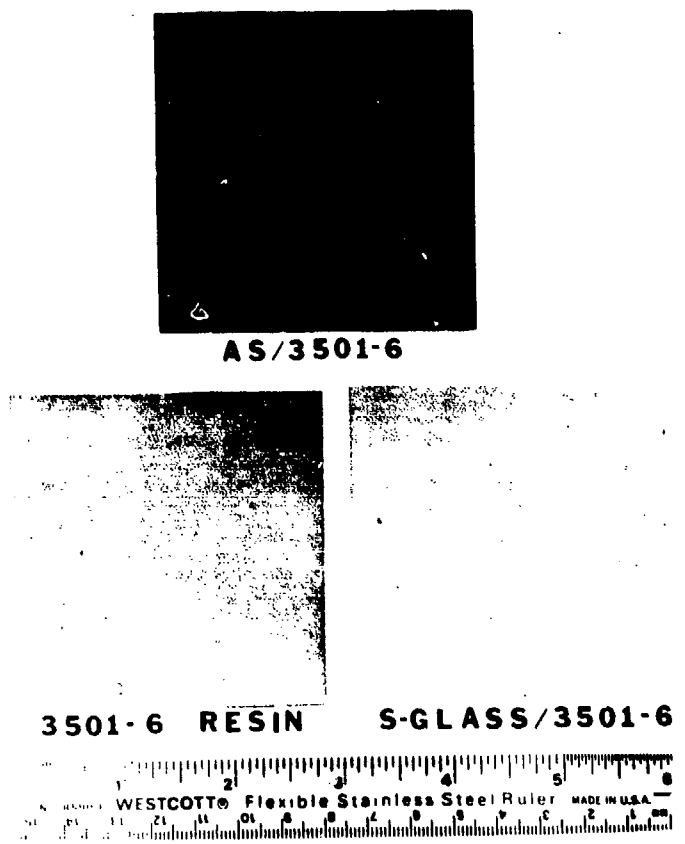

Figure 3. Moisture Dilatation and Diffusion Specimens

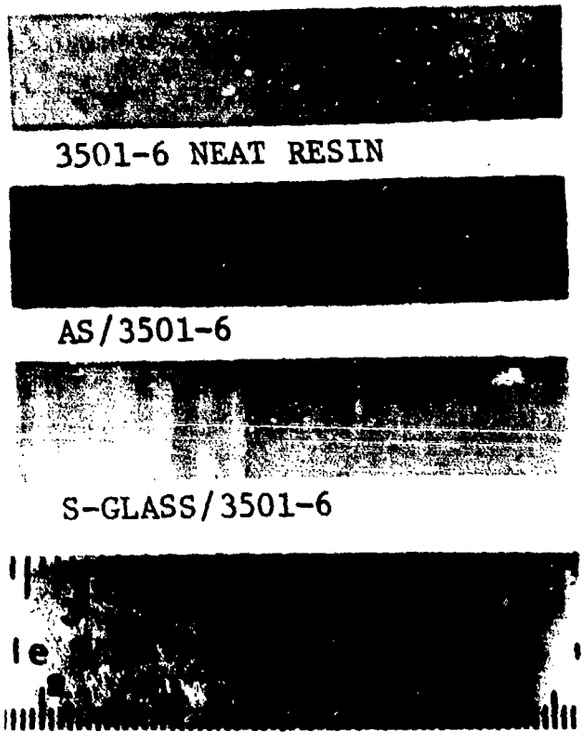

Figure 4. Thermal Dilatation Specimens (note lines indicating fiber orientation)

for the graphite/epoxy specimens. These, too, were placed into the dessicator until needed.

All of the plates were cut with a diamond saw (Diachrome continuous rim 80/100 grit) blade into specimens 73 mm x 73 mm (2.875 in x 2.875 in) for the moisture expansion experiments, and 6.35 mm x 57.2 mm (0.25 in x 2.25 in) for the thermal expansion experiments (see Figures 3 and 4). Actual dimensions of each specimen were taken with a dial caliber (Helios 52-010-006), and fiber volume measurements (Table 6) were made following the procedure described in Appendix B. The S-Glass specimens in Figures 3 and 4 are actually Owens-Corning S2 glass/3501-6 specimens. Tables 1 and 2 show the basic test plans established and the conditioning of each specimen.

3.3 Experimental Method for Moisture Dilatation Tests

Three Blue M Stabiltherm Model OV-U60A Gravity Ovens were used to provide heat for the accelerated moisture conditioning (see Figures 5 and 6). Each oven contains a semi-vapor proof insert made of Plexiglas to provide a chamber for the moisture conditioning. The chambers are not totally vapor proof since holes for instrumentation allow some water vapor to escape. Housed inside the chambers are the quartz glass dilatation measuring assemblies and the specimens used for determining weight gain and diffusivity constants (Figure 7). The ovens may be used with distilled water to obtain 98 percent relative humidity, or saturated salt baths to provide a controlled moisture environment at lower relative humidities. Information concerning this may be found in References [31 and 32].

TABLE 1

MOISTURE TESTS

Test Series	Specimen Number	Specimen Type	Material	Relative Humidity	Temperature	Length of Conditioning (days)
1	0,0	dilatation	AS/3501-6	98%	65.5°C (150°F)	8
	1,0	dilatation				
	1,1	diffusion				
	2,0	dilatation				
	2,1	diffusion				
2	0,0	dilatation	S2 glass/ 3501-6	98%	65.5°C (150°F)	8
	1,0	dilatation				
	1,1	diffusion				
	2,0	dilatation				
	2,1	diffusion				
3	0,0	dilatation	3501-6 resin	98%	65.5°C (150°F)	8
	1,0	dilatation				
	1,1	diffusion				
	2,0	dilatation				
	2,1	diffusion				
4	0,0	dilatation	AS/3501-6	98%	65.5°C (150°F)	30
	1,0	dilatation				
	1,1	diffusion				
	2,0	dilatation				
	2,1	diffusion				

TABLE 1 (continued)

MOISTURE TESTS

Test Series	Specimen Number	Specimen Type	Material	Relative Humidity	Temperature	Length of Conditioning (days)
5	0,0	dilatation	3501-6 resin	98%	65.5°C (150°F)	30
	1,0	dilatation				
	1,1	diffusion				
	2,0	dilatation				
	2,1	diffusion				
	2,2	diffusion				
6	0,0	dilatation	S2 glass/ 3501-6	98%	65.5°C (150°F)	30
	1,0	dilatation				
	1,1	diffusion				
	2,0	dilatation				
	2,1	diffusion				
	2,2	diffusion				
7	2,0	dilatation	S2 glass/ 3501-6	98%	70.0°C (167°F)	20
	2,1	diffusion				
	2,2	diffusion				

TABLE 2

THERMAL TESTS

Test Series	Specimen Number	Material	Conditioning
1	S1	S2 glass/3501-6	Dry
2	S2		
3	S3		
4	G1	AS/3501-6	Dry
5	G2		
6	G3		
7	R1	3501-6 resin	Dry
8	R2		
9	R3		
10	S4	S2 glass/3501-6	98% RH*, 65.5°C for 90 days
11	S5		
12	S6		
13	G4	AS/3501-6	98% RH*, 65.5°C for 90 days
14	G5		
15	G6		
16	R4	3501-6 resin	98% RH*, 65.5°C for 90 days
17	R5		
18	R6		

*RH = Relative Humidity

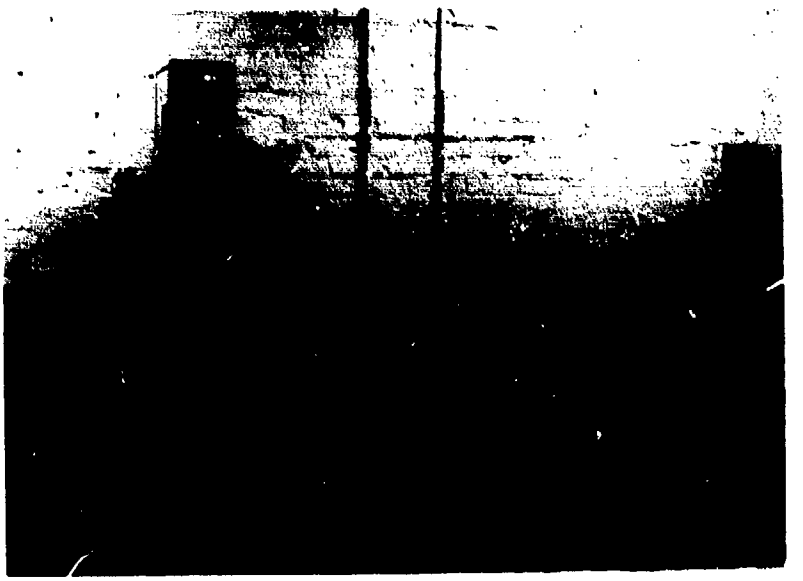

Figure 5. Three-Station Moisture Dilatation Test Facility (note microprocessor at left and analytical balance above left station)

On the outside of the ovens are Daytronic Model DS200 LVDTs (Linear Variable Differential Transformers), with calibration assemblies, used to monitor the dilatation of the specimens via a quartz glass push-rod. The external mounting is desirable since the LVDTs are not particularly well-suited for the high temperature, high humidity environment present inside the chambers. The LVDTs are repeatable to ±0.00015 mm (±0.000006 in) according to specifications. A Daytronic Model 9130 LVDT conditioner (Figure 8) provides a linear ±5V DC output to a microcomputer analog-to-digital (A/D) converter (Figure 7). The extensional measuring system is accurate to ±0.00254 mm (±0.0001 in) with 0.1 percent error. This accuracy is adequate for measuring the transverse dilatation of any unidirectional composite and may be suitable for longitudinal measurements

on some unidirectional composites also, such as the S2 glass/epoxy of the present work. The above statement assumes that the matrix material exhibits moisture dilatation while the fibers do not.

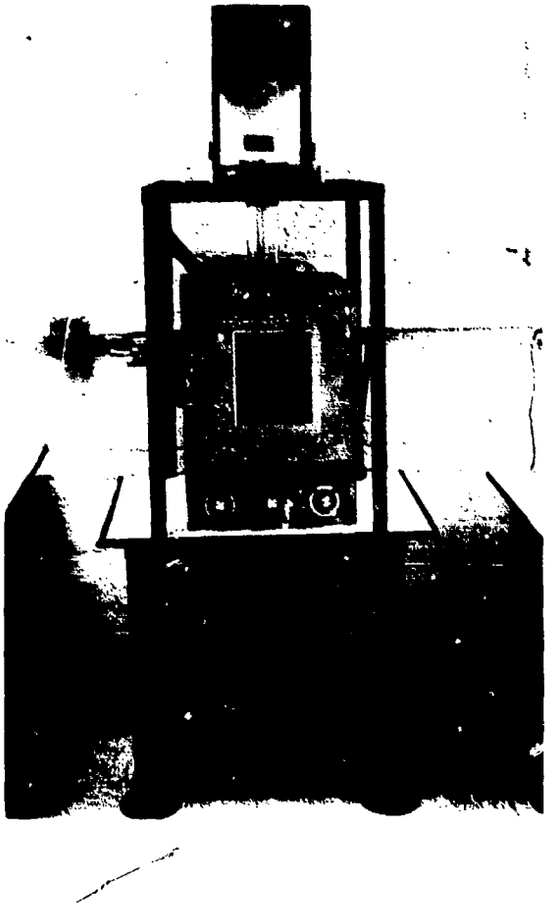

Figure 6. Moisture Dilatometer with Analytical Balance

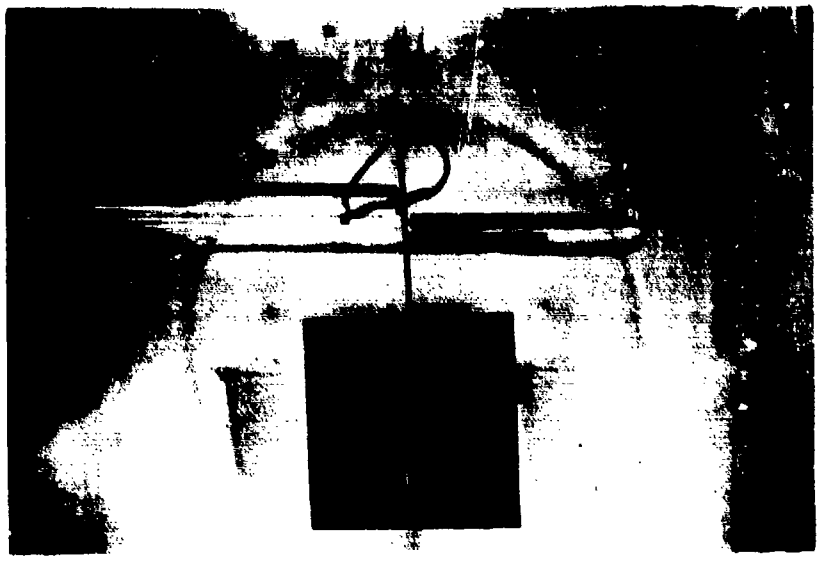

Figure 7. Semi-vapor Proof Plexiglas Insert Chamber Inside Oven, with Test Specimens and Quartz Tube in Place

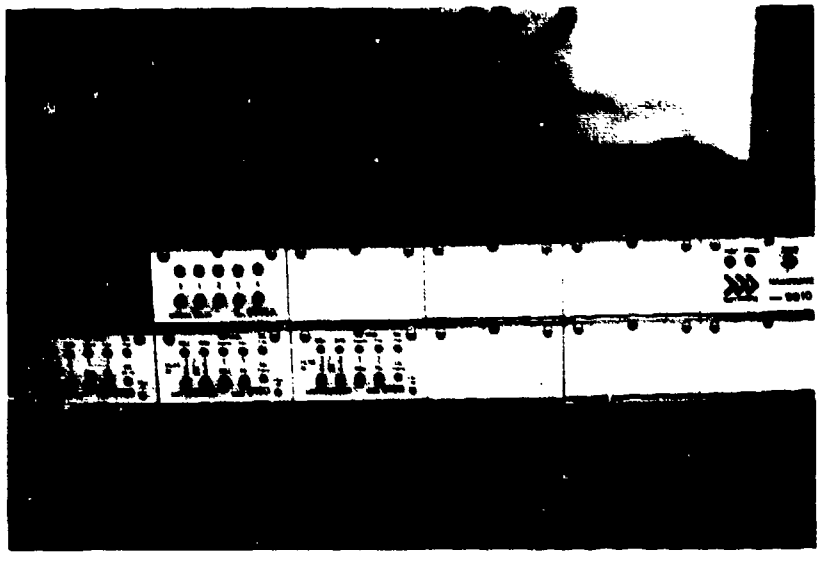

Figure 8. Daytronic LVDT Conditioner (located below the center test unit in Figure 5)

A Mettler Model HL 32 analytical balance was used for the constant monitoring of the specimen weights. It has the advantage that it can be tared externally by a voltage input, and has an "unstable output" signal allowing the computer to select stable periods to read the balance. The output is in Binary Coded Decimal (BCD) form. This has the advantage that the information can be read directly into the microprocessor without having to be converted to digital data. This reduces errors in weight data acquisition.

A 1.59 mm (0.0625 in) solid brass rod was used to hang the diffusion specimen below the balance. A rigid frame structure surrounds the oven and supports the balance (see Figure 6). The rod must be isolated from all wind currents, so Plexiglas shields are placed around all exposed balance parts. Convective currents are present inside the chambers also, so the specimens must be sufficiently large to provide air damping and inertia, in order that fluctuations due to these convective currents are minimized. The specimen configuration described meets this criterion. Nothing less than an air table (a table supported by air dampers which provide isolation from vibration) can provide isolation from the large hydraulic earth tamper being used in nearby construction, which plagued portions of the last two series of experiments. To minimize these vibration problems, massive analytical balance tables were used and rubber vibration isolation pads were placed under both the tables and the balance.

In addition to recording time, displacement, and weight, a Beckman Hygroline Model 5415 temperature and humidity transmitter was used to monitor temperature and humidity during some of the testing. The signal

was processed in much the same was as was the Daytronic signal. Unfortunately, the humidity sensors proved to be inadequate. No sensor lasted more than three weeks at the temperature and humidity levels used for testing. A search to obtain high temperature, high humidity, high reliability equipment to monitor temperature and humidity has been unsuccessful to date. Software has already been developed for this data acquisition, however.

The data acquisition system for the moisture experiments is unique, and totally developed by the Composite Materials Research Group at the University of Wyoming. It is based on a Zilog Z-80 microprocessor (see Figures 5 and 9) which, upon starting a test, requires no additional operator assistance. Specimen names are input to a mini-floppy disk. Weight, dilatation, and time are recorded. The system provides several advantages over other moisture dilatation systems. For example, it constantly monitors times, displacements, and weights. It records power failures and is capable of retaring the balance after a power failure. This is particularly useful since minimal specific history of a test needs to be known.

At any point during a test, a new floppy disk may be inserted while previously recorded data are reduced. This is a convenient feature because the operator can reduce and interpret data before completion of the tests. Also, the operator may monitor any data desired through a digital readout on the front panel display. The floppy disk storage system is inherently more stable than other types of data acquisition, especially strip chart recorders. With the data stored on the disk, it may be manipulated to get any information that is desired. The software

is programmed into ROM (Read Only Memory). This has the advantage that additional support units, such as a disk drive or a CRT, are not required. Program modifications can still be made, however, thereby further increasing the flexibility of the machine.

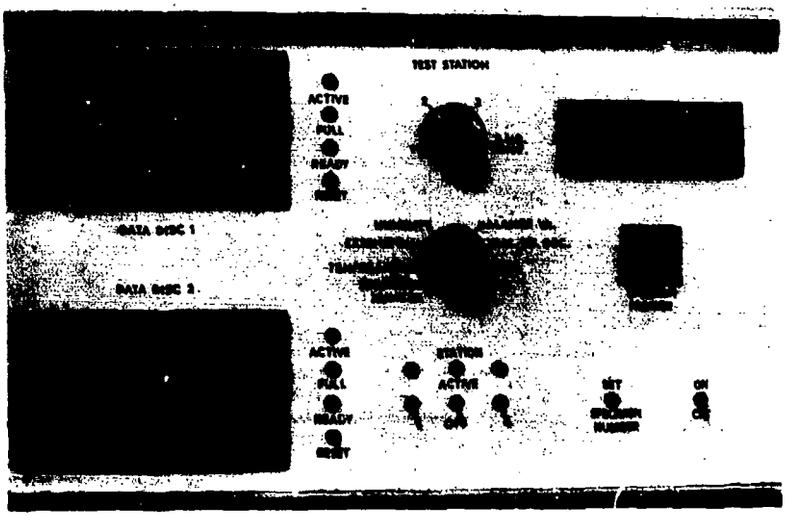

Figure 9. Microprocessor Data Acquisition Computer (located at the left in Figure 5)

Figure 10 is a simplified block diagram of the microprocessor setup. It will be noted that the microcomputer does not control much of the data acquisition system other than the balance. The data are monitored along with important historical parameters such as power outages, retaring of the balance, temperature, humidity, and the unstable indicator on the balance. Also, the CRT and printer are only needed for initial startup of the program or program modifications. This is especially advantageous since these expensive pieces of equipment do not need to be tied up during the course of the lengthy moisture absorption tests.

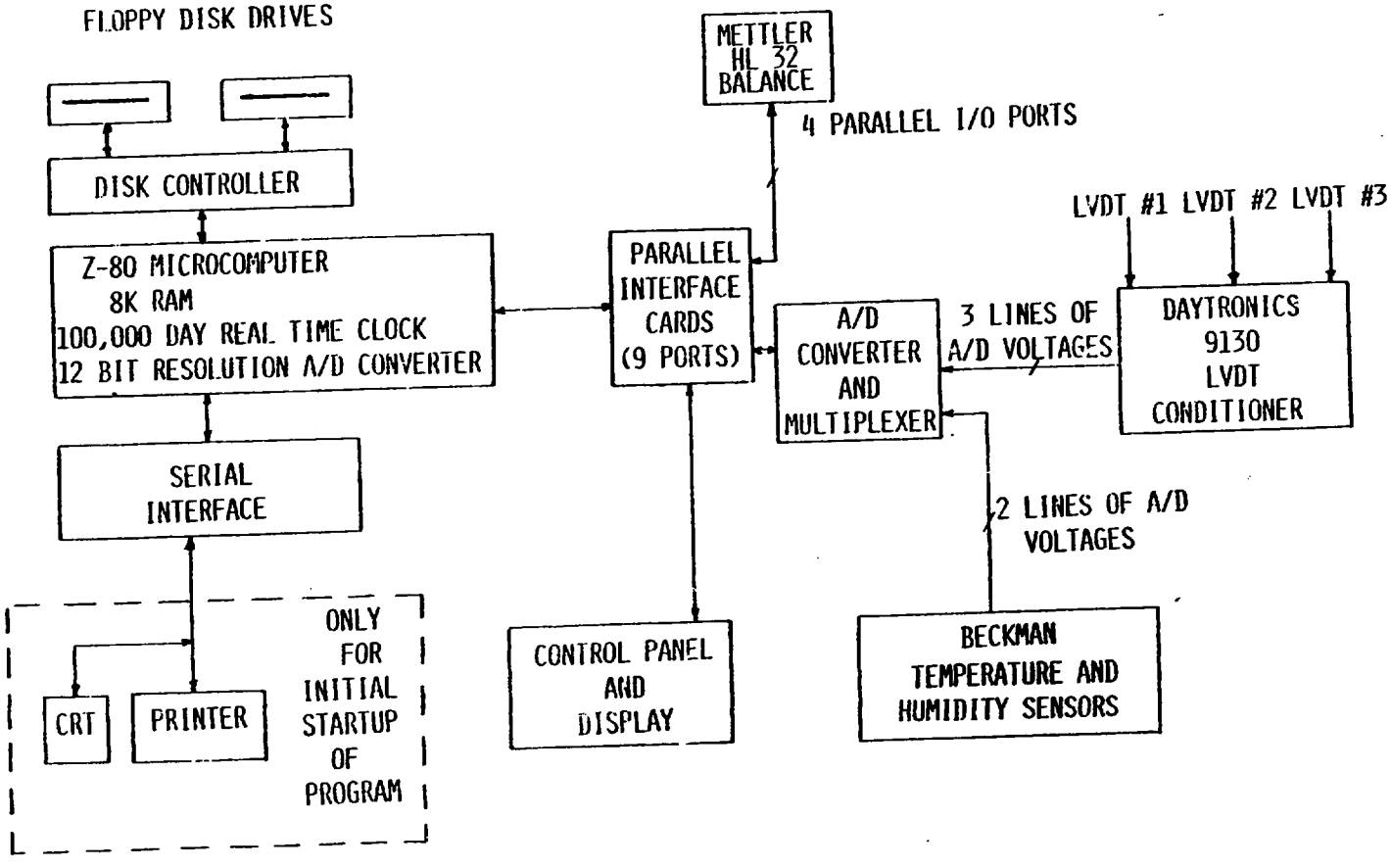

Figure 10. Simplified Block Diagram of Moisture Test Facility Hardware

Figure 11 is a simplified flow diagram of the software developed at the University of Wyoming directly in assembler language. The interval for taking data is a variable. The first data are taken at intervals of 60 seconds. This increment progresses to two minutes, four minutes, nine minutes, 16 minutes. . . ., until increments of 64 minutes are reached. At this point, data are taken at intervals of 64 minutes. These data are then stored on the mini-floppy disk.

Each mini-floppy disk has 350 blocks of storage with 256 bytes per block. Blocks 1 and 10 are broken down as shown in Table 3. These blocks store system information in the event of a power failure. Blocks 2-9 are reserved for future expansion. Blocks 11-350 contain eight records of the actual data for each station, which are stored in 32 byte blocks broken down as shown in Table 4. According to this breakdown, 2720 readings may be stored on a mini-floppy disk. This represents approximately 40 days before disks must be changed. Since the two disk drives change automatically, 80 days worth of data may be taken before the operator needs to insert new disks.

In the event of a power failure, the real time clock is operational, but no data are taken. The clock is powered by a 9V DC cell on standby at all times. A power fail circuit within the system reinitializes the program by using information stored according to Table 3, and continues to take data as before, when line voltage returns.

Once a test is terminated, the mini-floppy disks are read into a mini-floppy disk drive interface connected to a Hewlett-Packard 21MX-E minicomputer system (Figure 12). Here, the 32 byte data readings are converted to the 16 bit words required by the HP 21MX-E minicomputer.

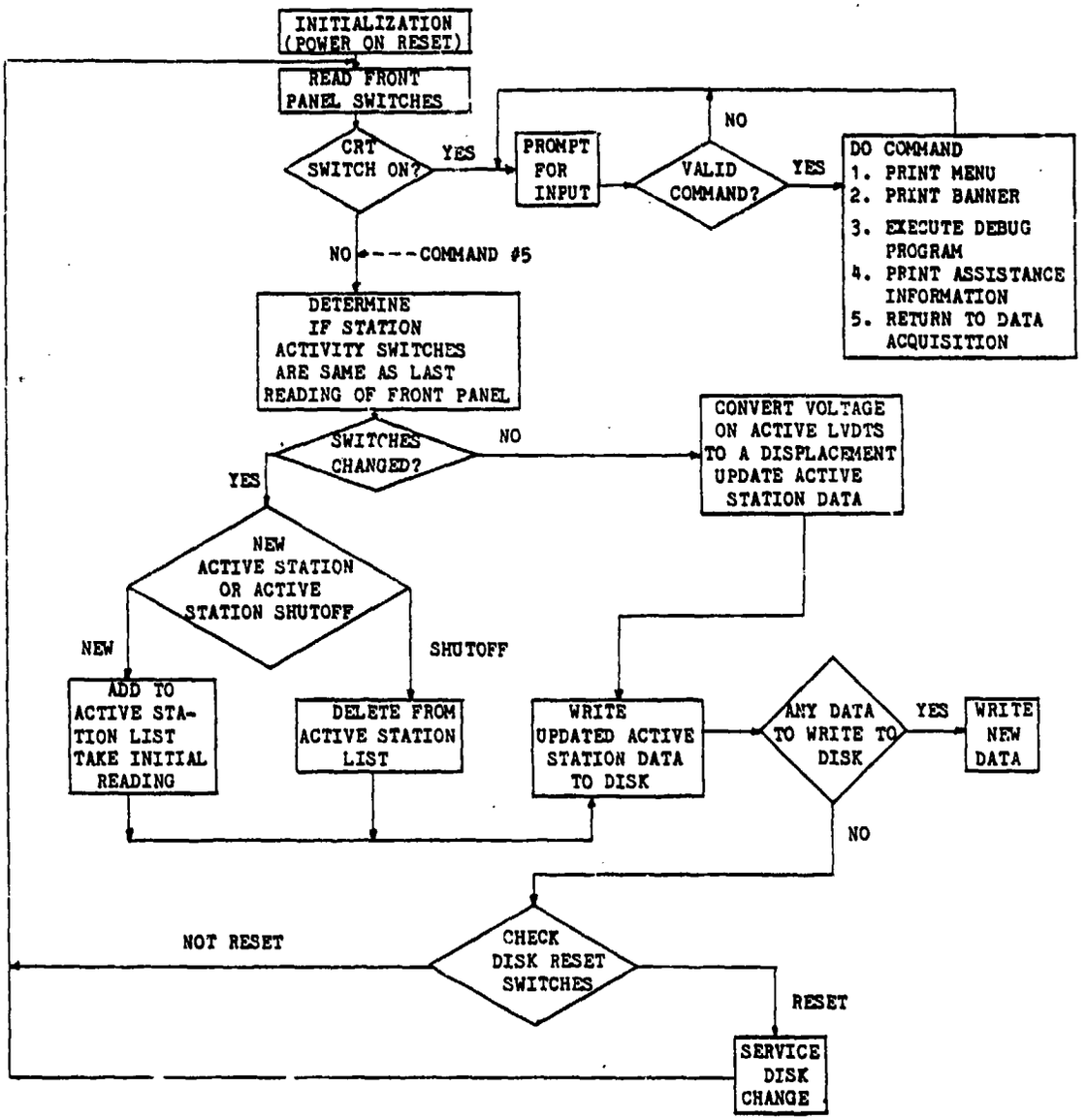

Figure 11. Simplified Block Diagram of Moisture Test Facility Software

TABLE 3

BREAKDOWN OF MINI-FLOPPY DISK
(BLOCKS 1 AND 10)

Byte	Contents
1-6	DISK NUMBER
7	DISK STATUS
8-15	TIME DISK INSTALLED
16-17	CURRENT DATA SECTOR
18	CURRENT DATA SECTOR NEXT FREE BYTE
19-26	DATE AND TIME OF LAST UPDATE TO DISK
113-160	STATION 1 SYSTEM ACTIVITY INFORMATION
161-208	STATION 2 SYSTEM ACTIVITY INFORMATION
209-256	STATION 3 SYSTEM ACTIVITY INFORMATION

TABLE 4

BREAKDOWN OF MINI-FLOPPY DISK
(BLOCKS 11-350)

Byte	Contents
1	STATION NUMBER
2	SPECIMEN # TYPE (NUMERIC OR ALPHANUMERIC)
3-8	SPECIMEN NUMBER
9-16	DAY AND TIME READING WAS TAKEN
17-18	TEMPERATURE
19-20	DISPLACEMENT
21-22	HUMIDITY
23-26	WEIGHT
27	BALANCE TARE INDICATOR
28-32	EXTRA

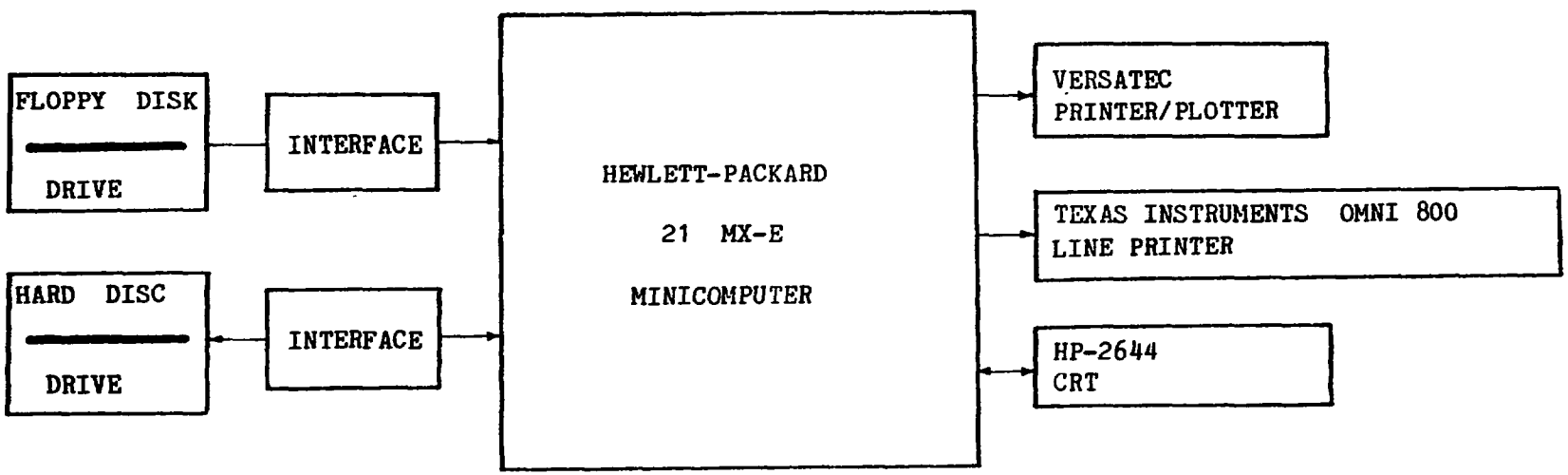

Figure 12. Data Reduction for Moisture Tests

At this point, a program known as DLTLG converts these words into real numbers and stores them in a data file in the HP 21MX-E minicomputer system. The DLTLG program was developed specifically for this purpose. Data were stored on a hard disk drive; a tape drive unit now is operational, so that in the future, all data will probably be stored on tapes. The data are then manipulated by a program called NPLOT, discussed in Section 3.5, to obtain information about diffusivity and moisture expansion.

3.4 Thermal Dilatation Tests

The thermal dilatation data acquisition was much less automated than the moisture system. Prior to the present work, the thermal dilatometer was not capable of temperature excursions below room temperature. Therefore, a new test station had to be designed to obtain data over a wide temperature range. The criteria for design were as follows:

1) The temperature chamber must be capable of large temperature ranges; -73°C to 177°C (-100°F to 350°F),
2) The fixture must interface to existing equipment,
3) The fixture must be of a sufficiently large thermal mass so as to obtain uniform and steady temperature changes.

Figures 13-16 show the final design, developed as part of the present study. Liquid nitrogen (LN_2) is pumped into the chamber to provide cooling, and a heater element is integral with the system. All of the above criteria were met with the additional feature that the chamber is actually capable of going above 316°C (600°F). This allows the fixture to be used for testing materials capable of withstanding much higher

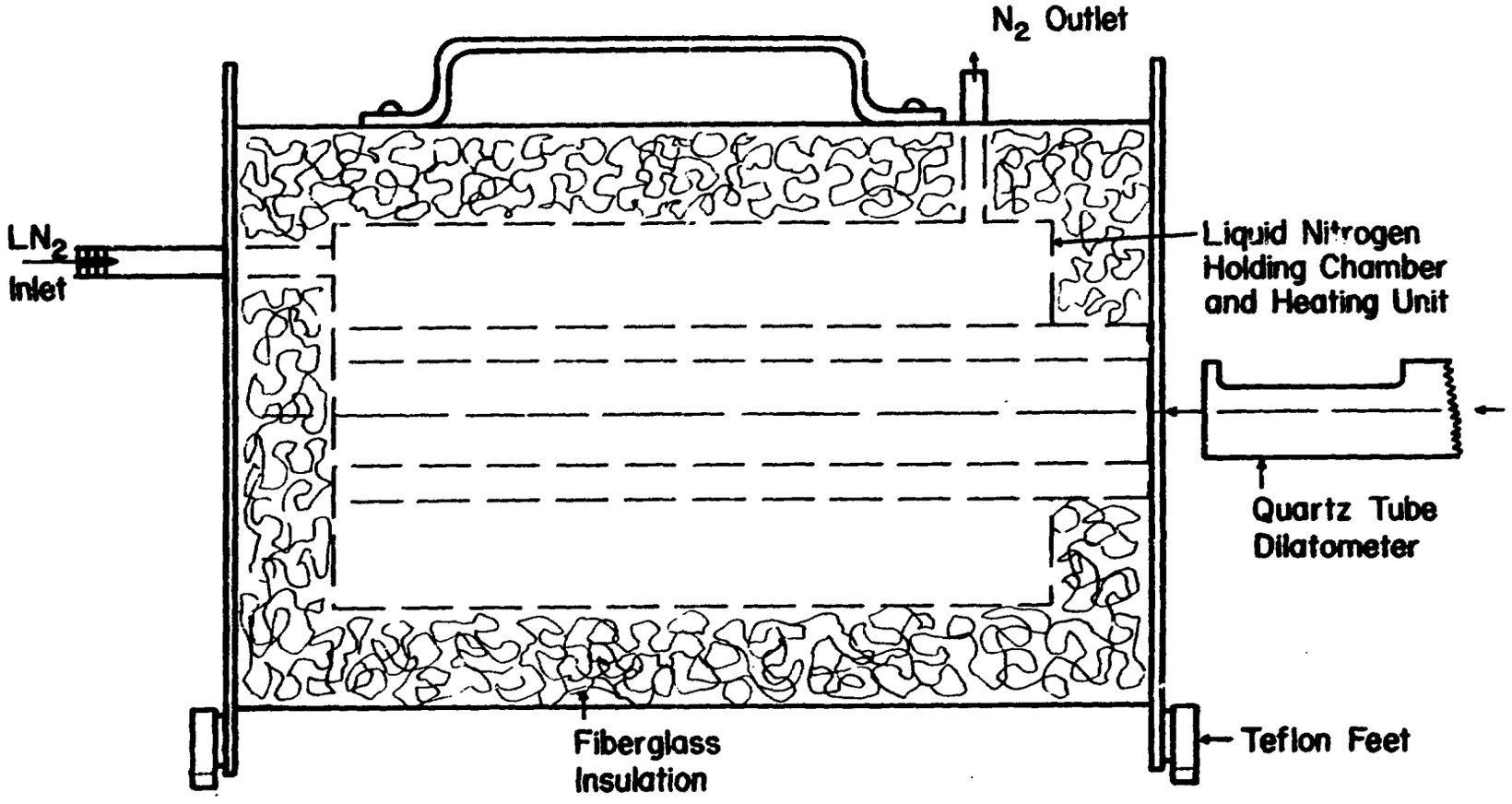

Figure 13. Thermal Dilatation Test Chamber Insulating Vessel (half scale)

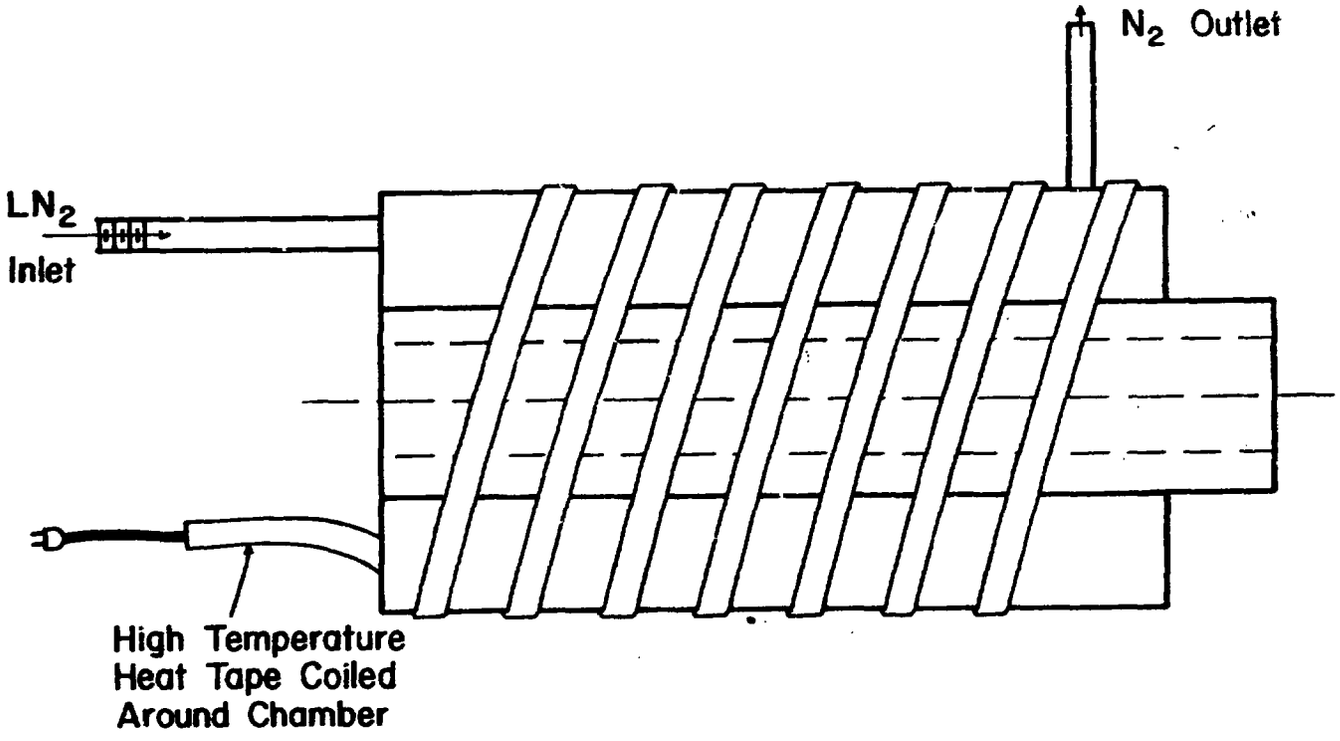

Figure 14. Thermal Dilatation Test Chamber Liquid Nitrogen Holding Tank and Heating Unit (half scale)

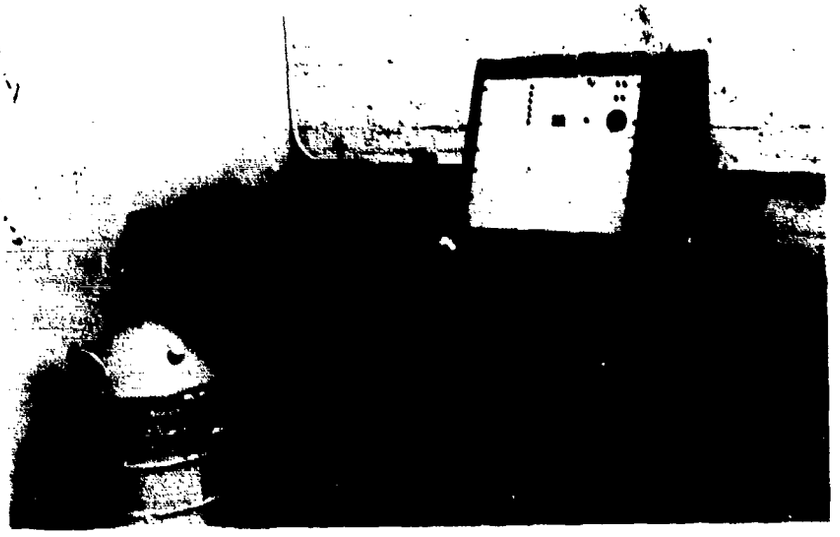

Figure 15. Thermal Dilatometer Apparatus

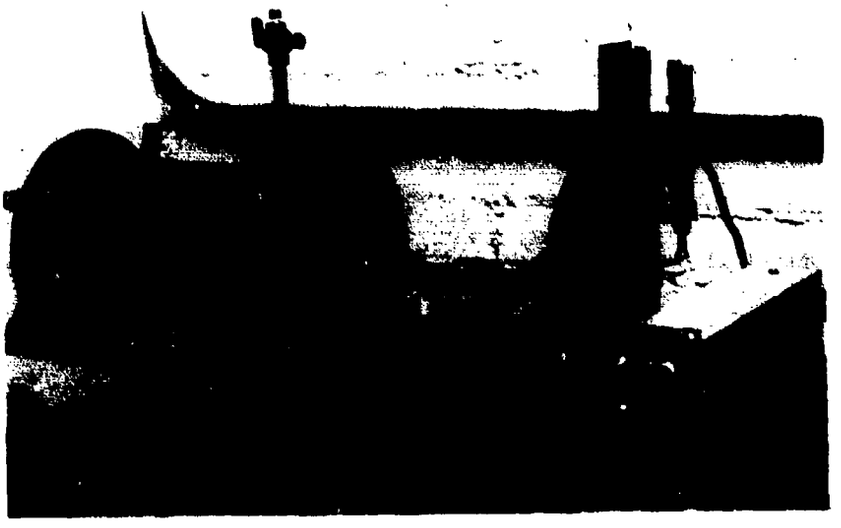

Figure 16. Closeup of Thermal Dilatometer and Temperature Chamber

temperatures. Power input is made through an AC rheostat controller. Currently, a microprocessor-controlled temperature programmer is under development for use with the above test facility.

Data acquisition was not particularly sophisticated. The specimen was placed in a quartz tube and a quartz pushrod was mounted up against it. The other end of this pushrod was in contact with an LVDT interfaced to a Daytronic Model 201C amplifier. Temperature was measured by an iron-constantan thermocouple. Nonlinearity of the thermocouple was 1 percent or less over the present tests. An electric cold compensation junction was used to provide a stable reference point for the thermocouple.

Displacement and temperature values were recorded on a Hewlett-Packard Model 7004B X-Y plotter. These data were reduced manually and best-fit curves were generated numerically.

Since such low temperatures can be generated, it is mandatory that the entire system be as moisture-free as possible, to prevent erroneous data due to freezing of the pushrod assembly. Therefore, the specimens were first cycled to a relatively high temperature in the chamber, but below the glass transition temperature of the matrix material. During this process it was assumed that a negligible amount of moisture was driven out of the moisture-conditioned thermal expansion specimens. The temperature was then lowered to the desired minimum value, the starting value for data acquisition. The specimen was heated to and slightly above the glass transition temperature, noted by a rapid rolloff of the curve due to bending of the specimen, while data were recorded. The bending is induced by the small force of the LVDT core pushing on the specimen (approximately nine grams). Tests were terminated at this point.

3.5 Data Reduction

All final data reduction, with the exception of the analytical correlations (Section 4), was accomplished using the HP 21MX-E mini-computer and a Versatec Model D1200A Matrix plotter. This system allows the operator to present the data in virtually any manner desired. The data reduction codes are included in Appendix C.

The computer program MPLOT, used for moisture data reduction (see Appendix C), requires that times, weights, and displacements be typed in at the terminal by hand. This was necessary since only one oven had the analytical balance. This problem has been remedied for future work with the recent addition of new Sartorius Model 1207 MP2A analytical balances specifically intended for this purpose. The important features, such as BCD and external tare are the same as for the Mettler Model HL32 balance used in the present study. In the present study, two other weight gain specimens were recorded by hand during a test, using an Ainsworth Type BCT balance (accurate to ±0.0001 g also).

MPLOT reads the data from a file generated by the operator. It calculates percent moisture gain, square root of time, and strain. These data points are then plotted on the Versatec mentioned above. At the operator's option, a complete listing of data points and calculated values may be had via a Texas Instruments OMNI 800 line printer. This is an easy check to make sure the operator has entered all data points correctly. Another option is a linear regression fit of the data points for linear analyses.

NPLOT will serve as the core for future work, now that all three balances are installed. It takes data from files generated by the mini-

floppy disk system and calculates square root of time from the real time clock in the microcomputer. All data are automatically adjusted in the event of a power failure resulting in the balance being retared. Statistically, this system is much better than the method of entering the data by hand since approximately 600 data points are taken as opposed to the 35 taken by hand for a 30-day test. The operator may see any calculations or data desired. A linear regression fit routine is also available, just as in MPLOT.

The program DILGLAS, on the University of Wyoming's CDC Cyber 730/760 dual processor computer system, is an example of the nonlinear regression routine used to calculate strain versus percent moisture relations. The equation used to accomplish this is (as will be discussed in Section 4.1)

$$\varepsilon = a_0 + a_1(\%\ \text{Moisture}) + a_2(\%\ \text{Moisture})^2 + a_3(\%\ \text{Moisture})^3 \qquad (1)$$

where ε is the moisture induced strain.

The codes were written in BASIC since simple matrix manipulations are much easier than in FORTRAN. The coefficients a_0, a_1, a_2, a_3 are calculated.

CARBON and MCAR are examples of the routines used for thermal dilatation curve fitting. These routines calculate the coefficients according to the equation

$$\varepsilon = a_0 + a_1(\text{Temperature}) + a_2(\text{Temperature})^2 \qquad (2)$$

as will be discussed in Section 4.2.

NLDIL is a plotting routine for the equations generated in programs such as DILGLAS. The operator need merely type in the coefficients and the total span of strain and the plots are generated.

Similar to NLDIL are GLASS and MGLAS, to provide plots of the thermal dilatation experiments.

SECTION 4

EXPERIMENTAL DATA

4.1 Moisture Dilatation Data

At a given percent moisture content below the equilibrium value, the moisture is not uniform through the thickness. That is, at an average 0.5 percent moisture content in the composite, it is not 0.5 percent everywhere. The moisture content varies from a high value at the exposed surface, to a low value in the center of the specimen, as represented by Eq. (A.17) of Appendix A. Therefore, a model was devised to check the difference between uniform moisture distribution and a moisture gradient through the thickness. The model was constructed using a laminated-plate computer program based on References [4 and 28]. This code was further modified to predict moisture and thermal dilatation at the University of Wyoming. Moisture distribution through the thickness was calculated based on previous works [15,16,17,33,34,35]. Moisture expansion based on limited experimental data [9,23,33] was then calculated based on this distribution. In thin specimens, such as the AS/3501-6 which was 0.64 mm (0.025 in) thick and the S2 glass/3501-6 which was 0.89 mm (0.035 in) thick, a negligible difference was found. The neat resin specimens were slightly thicker due to fabrication techniques (1.27 mm, 0.050 in); this thickness is approaching the limit for which the effects of non-uniform moisture distribution can be neglected.

The following data represent the results of the experimental effort of the present study. Figures 17, 18 and 19 represent strain vs. moisture

plots for the specimens. The remaining plots may be found in Appendix D. A few comments will be noted here and discussed in detail later. The starred data points are points recorded by a strip chart recorder and the smooth solid lines are best-fit curves generated by DILGLAS and plotted by NLDIL. It was necessary during initial tests to take data by hand since the microprocessor data acquisition system was not yet fully operational. Only the data of Figures 17 and D15 were totally obtained using the microprocessor system, although the system is now fully operational. The S2 glass/3501-6 composite tests show the most data scatter from one specimen to another. Also, the highly nonlinear moisture expansion curves for the S2 glass/3501-6 specimens will be noted. The 3501-6 epoxy resin curves appear to be the most linear. The AS/3501-6 and S2 glass/3501-6 composite specimen data were fit to cubic equations of the form of Eq. (1). This equation was used since it most closely modeled the behavior of the moisture expansion of the composites. The epoxy resin showed only slight nonlinearity so a linear moisture expansion behavior was assumed.

The solid jagged lines in Figures 17 and D15 are data taken by the microprocessor test station. The seemingly sporadic nature of Figure D15 is due to the second order moisture fluctuations discussed in Section 4.3, and to the fact that the balance fluctuated due to low amplitude background vibrations. The new balances, presently being installed, appear to be much more stable in this respect. The moisture expansion curve fitting coefficients which were used are presented in Table 5. These coefficients will be useful in design, to calculate the moisture expansion of a composite laminate.

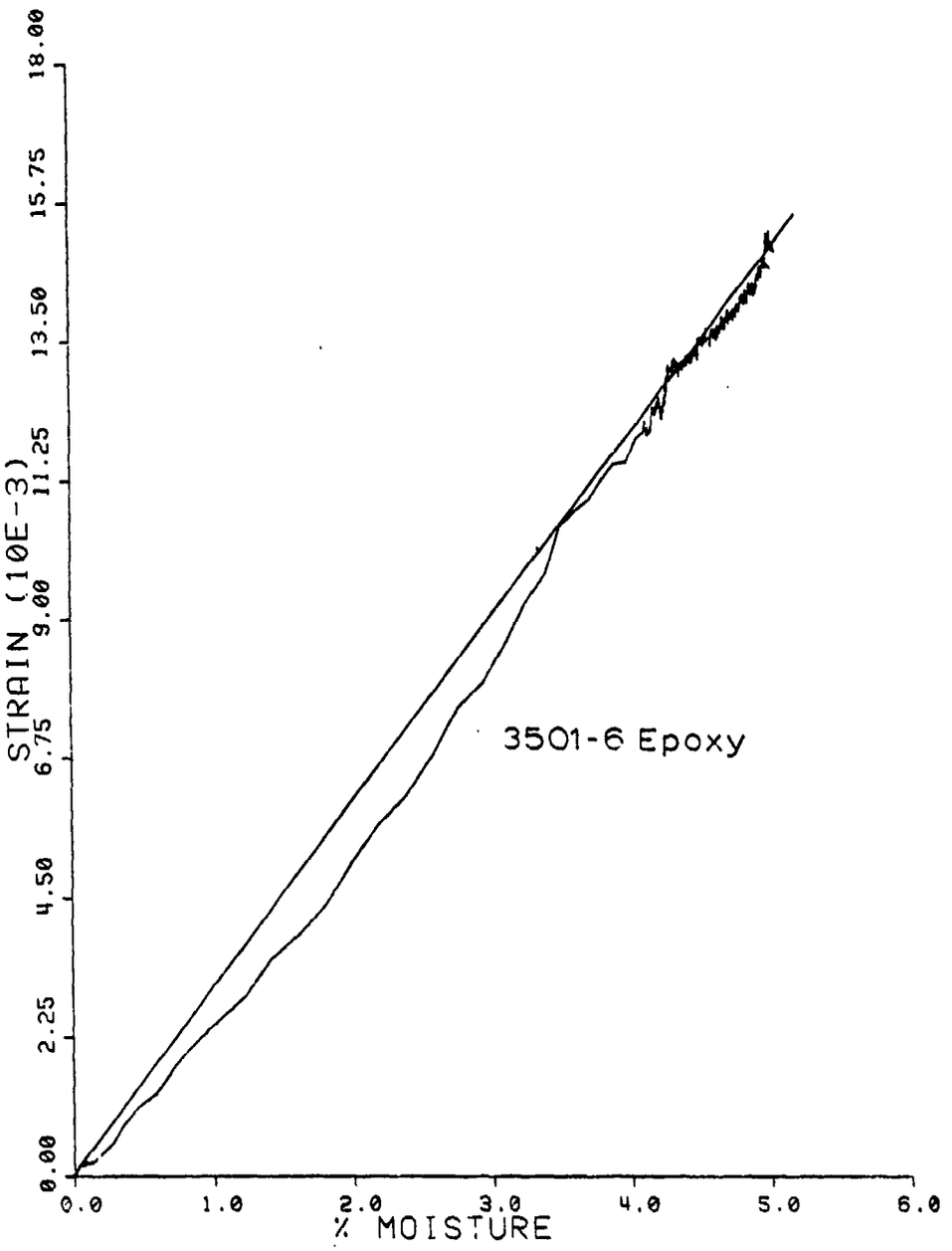

Figure 17. Results of Test 5, Station 2, 30 Days @ 98% RH, 65.5°C (150°F)

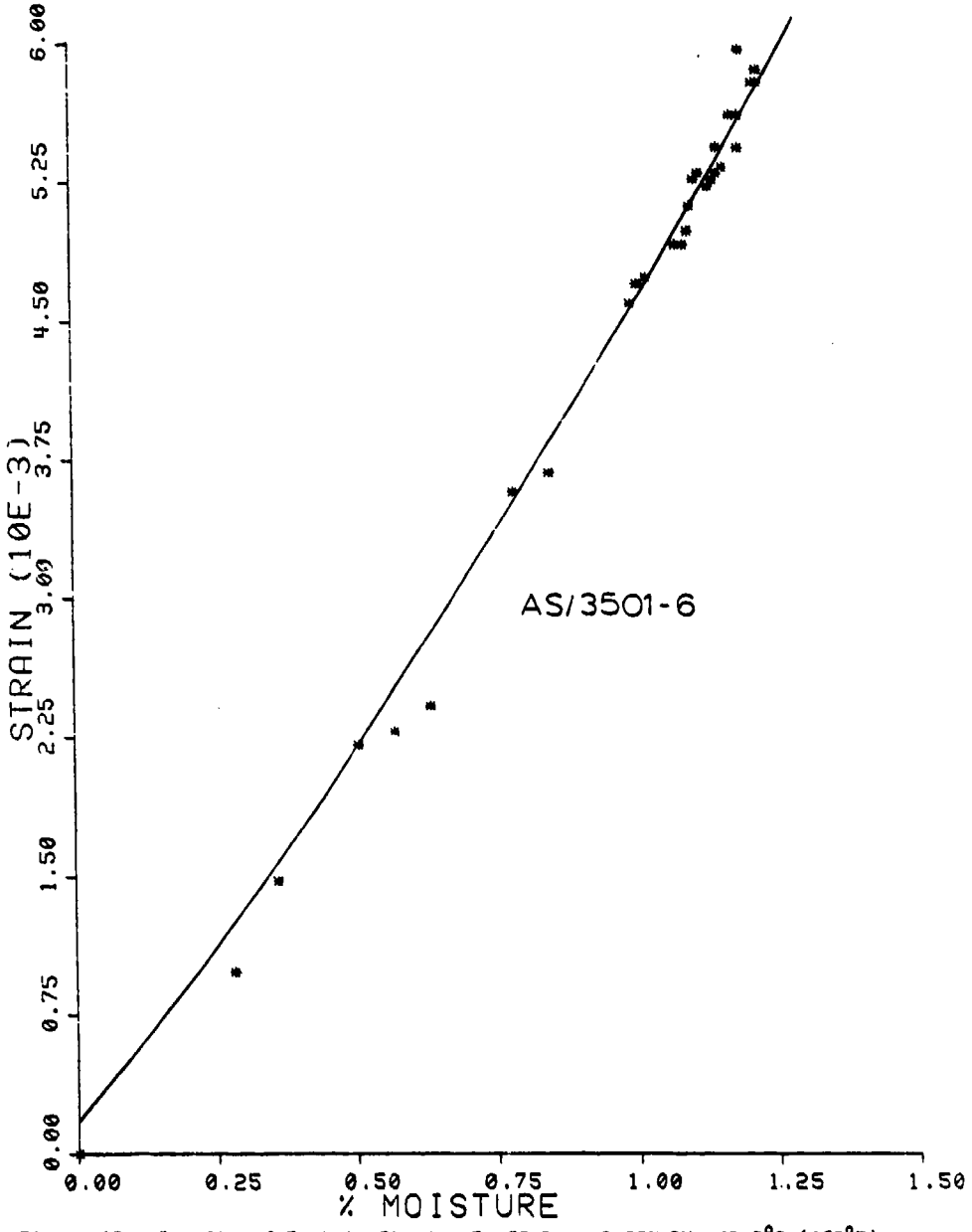

Figure 18. Results of Test 4, Station 3, 30 Days @ 98% RH, 65.5°C (150°F)

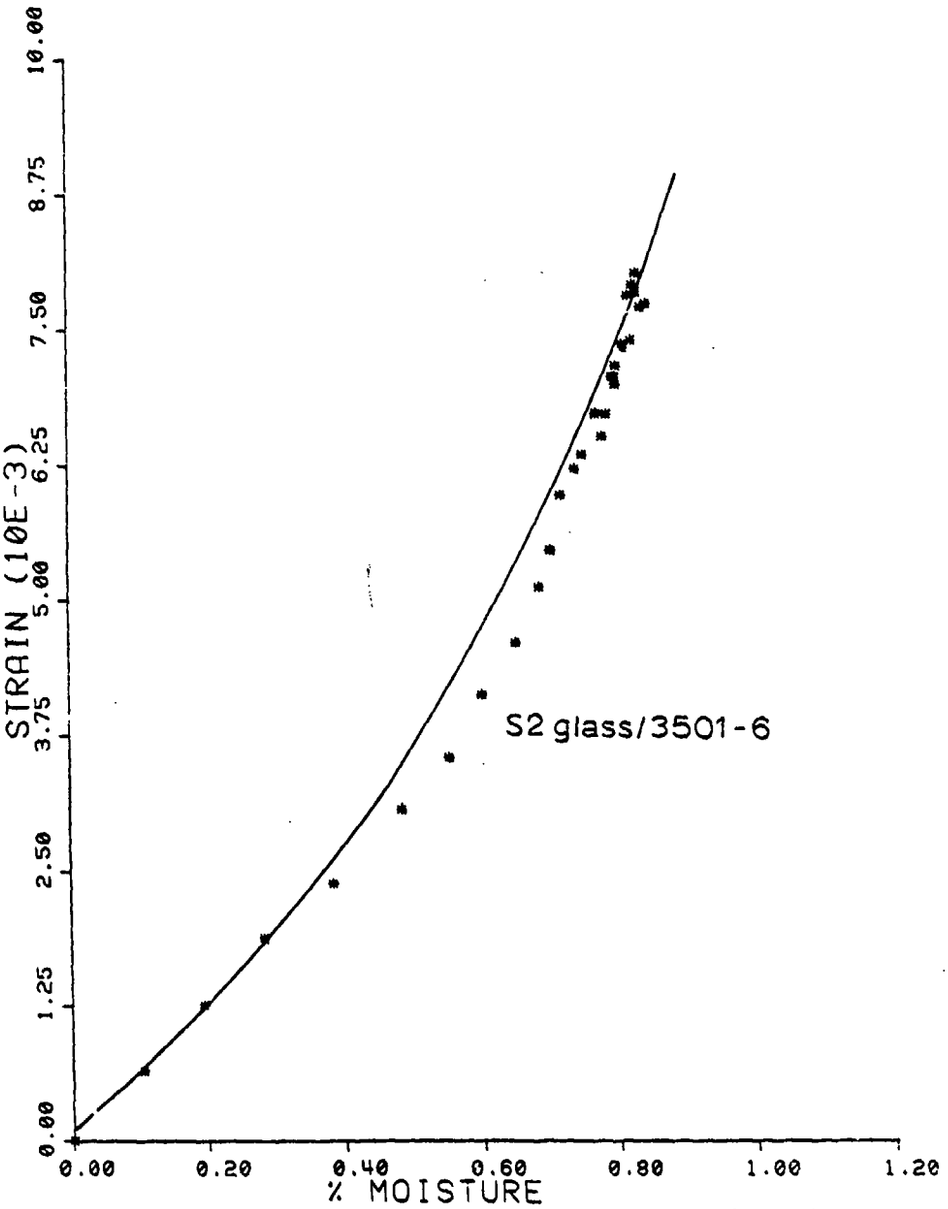

Figure 19. Results of Test 6, Station 3, 30 Days @ 98% RH, 65.5°C (150°F)

TABLE 5

MOISTURE EXPANSION CURVE FIT COEFFICIENTS

Best-fit coefficients to be used in the following equation (Eq. 1):

$$\varepsilon = a_0 + a_1(M) + a_2(M)^2 + a_3(M)^3$$

Material	Coefficients			
	a_0 (10^{-5})	a_1 (10^{-5})	a_2 (10^{-5})	a_3 (10^{-5})
3501-6 Neat Epoxy Resin	0.0	3.2	0.0	0.0
AS/3501-6	10.429	3.65039	1.30224	- .378363
S2 Glass/ 3501-6	8.05668	6.029	3.90029	5.42363

Often, the coefficient of moisture expansion is useful for analysis. This is defined as

$$\beta = \frac{\partial \epsilon}{\partial M} = a_1 + a_2 M + a_3 M^2 \qquad (3)$$

where β = coefficient of moisture expansion, and

M = weight percent moisture.

A linear interpolation may be suitable over small ranges of moisture content.

4.2 Thermal Dilatation Data

From experiment to experiment, the thermal dilatation experiments showed far less scatter than the moisture dilatation experiments. Representative examples are shown in Figures 20-22; the remainder of the data may be found in Appendix D. The circles, triangles and squares represent individual data points, while the solid lines represent numerically-generated curves by programs such as CARBON. Each type of symbol represents an individual test. These curves were of the form of Eq. (2), since it closely represents the physical behavior of polymer-matrix materials. This phenomenon has been noted previously [22,23,33]. That is, a parabolic thermal expansion curve is seen for the 3501-6 epoxy resin, and also for composites incorporating this epoxy.

It will be noted that the 3501-6 resin shows the highest thermal expansion, followed by the AS/3501-6 and S2 glass/3501-6, respectively. This is as expected since the transverse modulus of a graphite fiber is lower, and transverse thermal expansion is higher, than for an S2 glass fiber. The fiber volume of the S2 glass/3501-6 composite specimens was also higher than that of the AS/3501-6 composite, further reducing thermal

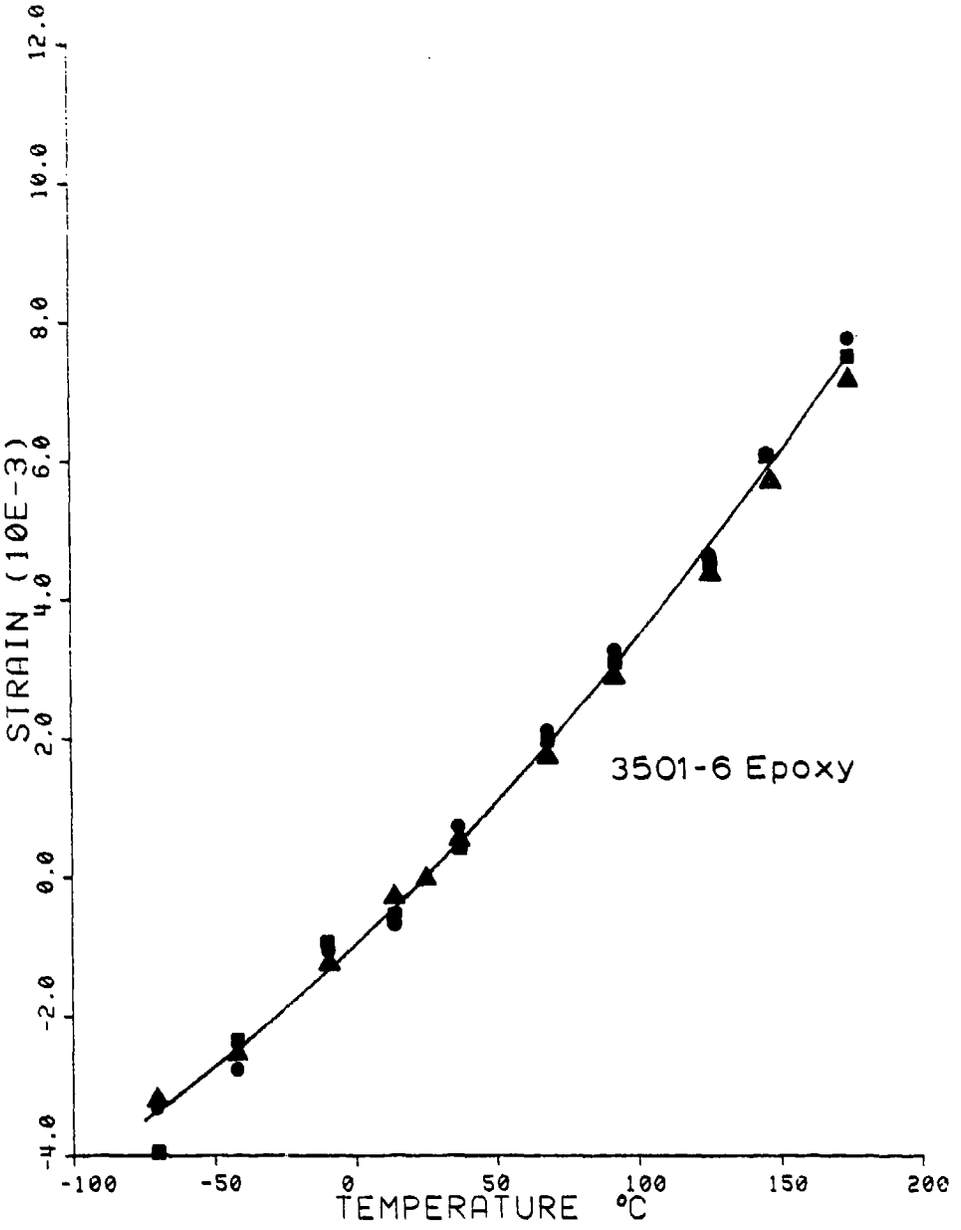

Figure 20. Thermal Expansion Data for Unconditioned 3501-6 Resin

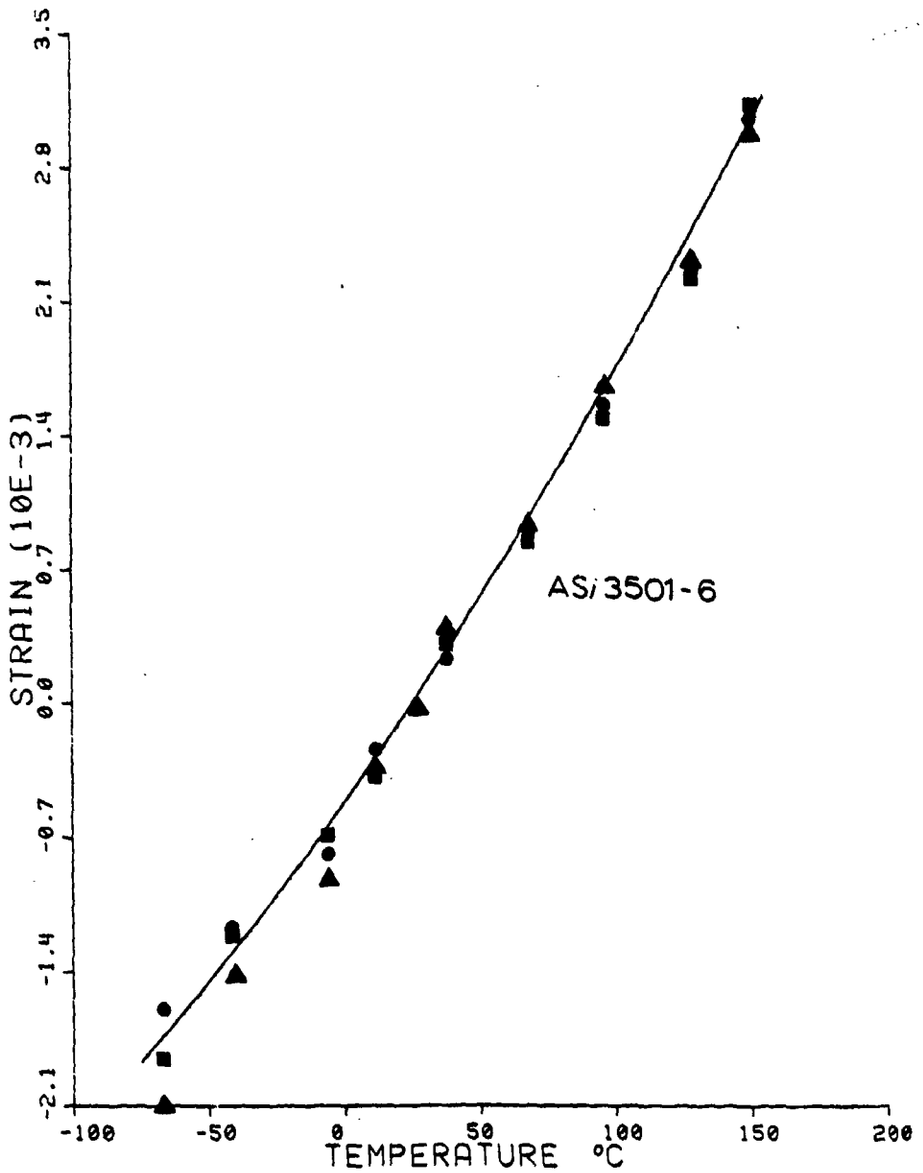

Figure 21. Thermal Expansion Data for Unconditioned AS/3501-6

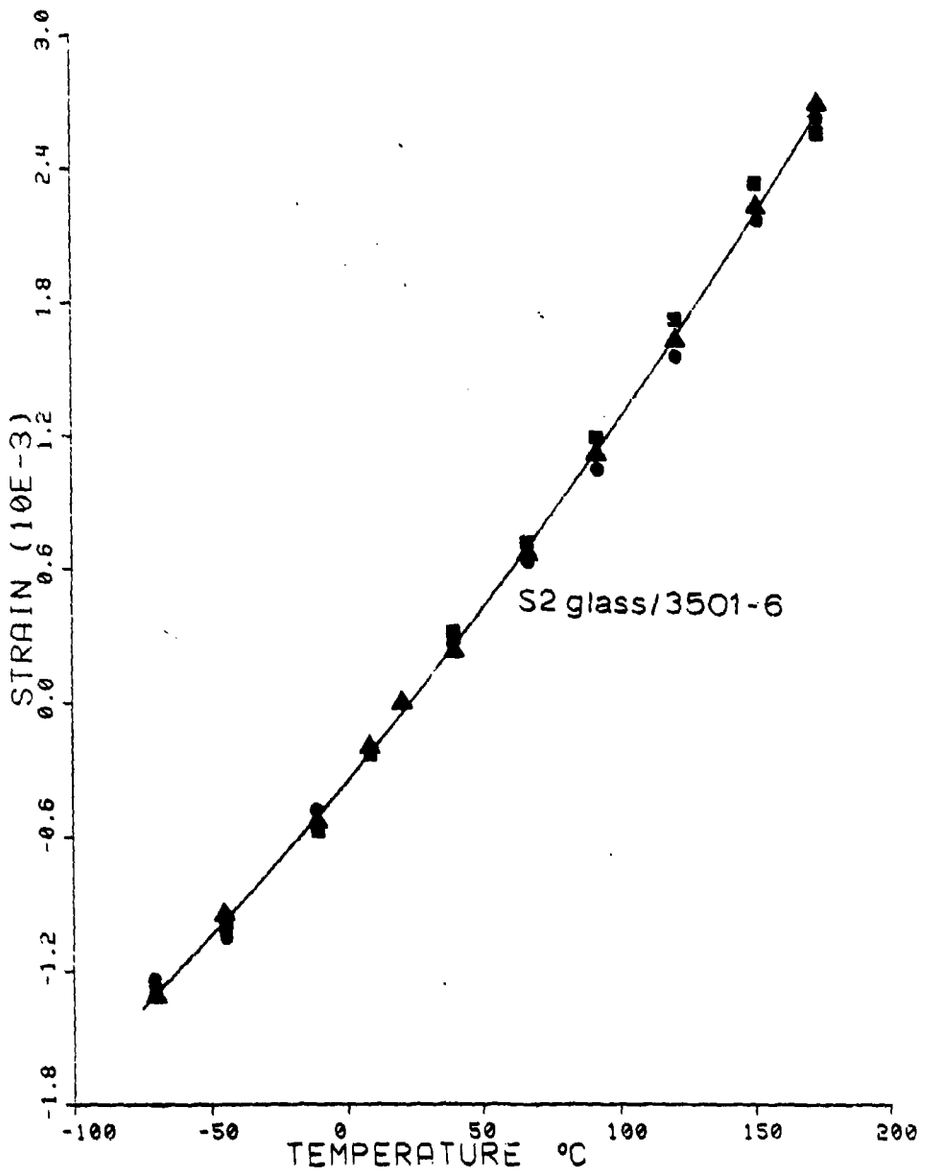

Figure 22. Thermal Expansion Data for Unconditioned S2 Glass/3501-6

expansion of the composites. Results of these measurements are found in Table 6.

Table 7 provides coefficients which may be used to calculate strain at any given temperature, based on zero reference strain at 23°C (73°F).

If the coefficient of thermal expansion is desired (the slope of the curve at any temperature), this may be determined by the equation

$$\alpha = \frac{\partial \varepsilon}{\partial T} = a_1 + 2a_2 T \qquad (4)$$

where T = temperature (°C)

α = coefficient of thermal expansion.

The above equation is independent of any reference temperature.

It should be noted that the thermal expansion is not linear over the present test temperature range. Also, since moisture serves as a plasticizer to the matrix material, higher nonlinearity is seen in moisture-conditioned composite specimens than dry composite specimens, due to a loss of modulus in the matrix. This loss of modulus affects the composite behavior on the micro level, which affects the resulting thermal expansion.

4.3 Moisture Diffusivity Data

As mentioned previously, the microprocessor test station may be used to calculate diffusivities of the various composite materials. The specimen geometry, i.e., 73 mm x 73 mm x 1.27 mm (2.88 in x 2.88 in x 0.050 in), was chosen so that essentially one-dimensional behavior (see Eq. (A.34) of Appendix A) is valid for calculating diffusivities. Less than 2 percent of the total surface area is represented by the edges. By contrast, a specimen that is 1.27 mm x 50.80 mm x 12.70 mm (0.050 in

TABLE 6

FIBER VOLUME CONTENTS (PERCENT BY WEIGHT)

Material	Specimen 1	Specimen 2	Specimen 3	Average
AS/3501-6	65	64	66	65
S2 glass/3501-6	60	74	70	68

TABLE 7

THERMAL EXPANSION CURVE FIT COEFFICIENTS

Coefficients to be used in the following equation (Eq. 2)
(based on 23°C (73°F) nominal zero value):

$$\epsilon = a_0 + a_1 T + a_2 T^2$$

Material	Ave. Moisture Content*	a_0 (10^{-4})	a_1 (10^{-5})	a_2 (10^{-6})
3501-6 Neat Resin	0	- 9.72023	3.83445	6.12029
S2 Glass/3501-6	0	- 3.52604	1.46491	1.50351
AS/3501-6	0	- 3.08472	2.00603	2.50517
3501-6 Neat Resin	6.23	-11.2567	4.48252	5.98654
S2 Glass/3501-6	1.16	3.334	1.38309	3.97577
AS/3501-6	1.87	- 6.74528	2.04744	4.54569

*Percent by weight

x 2.0 in x 0.5 in) has over 11 percent of its total surface area taken up by edges, so the one-dimensional edge correction equation is less valid.

The AS/3501-6 composite has been characterized previously [17,34, 35,36,37]. The resin system has also been characterized [34]. By knowing diffusivities, any moisture distribution through the thickness may be obtained by considering the time varying boundary problem of different humidities and temperatures [15,16,18,19,38]. Thus, accelerated environmental conditioning for testing other property changes (modulus, strength, glass transition temperature, etc.) may be obtained [5,21,36, 37,39,40].

A numerical model based on References [15 and 16] is operational at the University of Wyoming, but requires experimentally determined diffusivity constants to be input into the program.

The diffusivities are calculated by the method in Reference [13]. Figures 23-26 show typical percent moisture versus square root of time plots for the moisture dilatation tests. Diffusivities were calculated by the method of Reference [14]. Table 8 summarizes these data. The starred data for the neat resin are estimated from Eq. (A.27) of Appendix A and should be used only for purposes of comparison. As seen, there are still some discrepancies in reported data; however, all are well-ordered.

The composites were cured in a blanket press and the neat resin was cured in a forced convection oven. Even though the curing times were the same, the two-inch thick steel plate of the blanket press provided some extra postcuring, due to its high thermal inertia. Augl and Berger

[37] have noticed a 22 percent difference in diffusivities for the same resin batch due to different curing cycles. This could explain some of the discrepancy in reported experimental data.

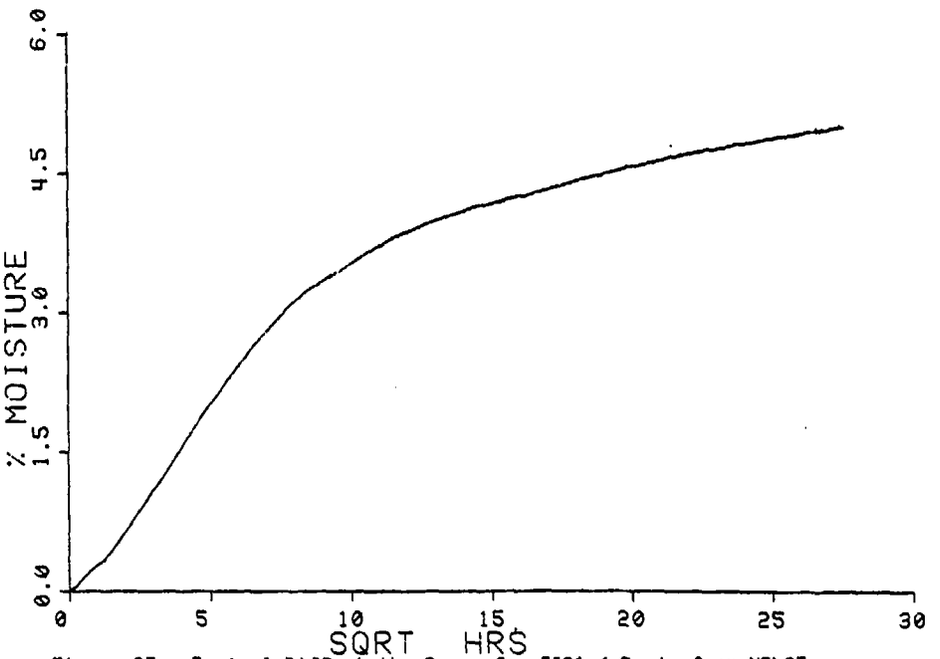

Figure 23. Typical Diffusivity Curve for 3501-6 Resin from NPLOT
RH = 98%, Temperature = 65.5°C (150°F), Thickness = 1.27 mm (0.050 in)

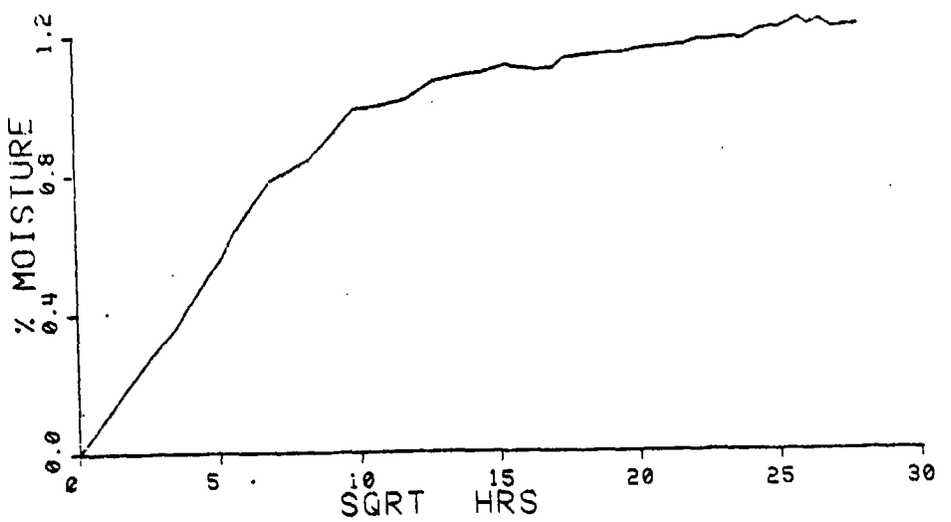

Figure 24. Typical Diffusivity Curve for AS/3501-6 from MPLOT
RH = 98%, Temperature = 65.5°C (150°F), Thickness = 0.64 mm (0.025 in)

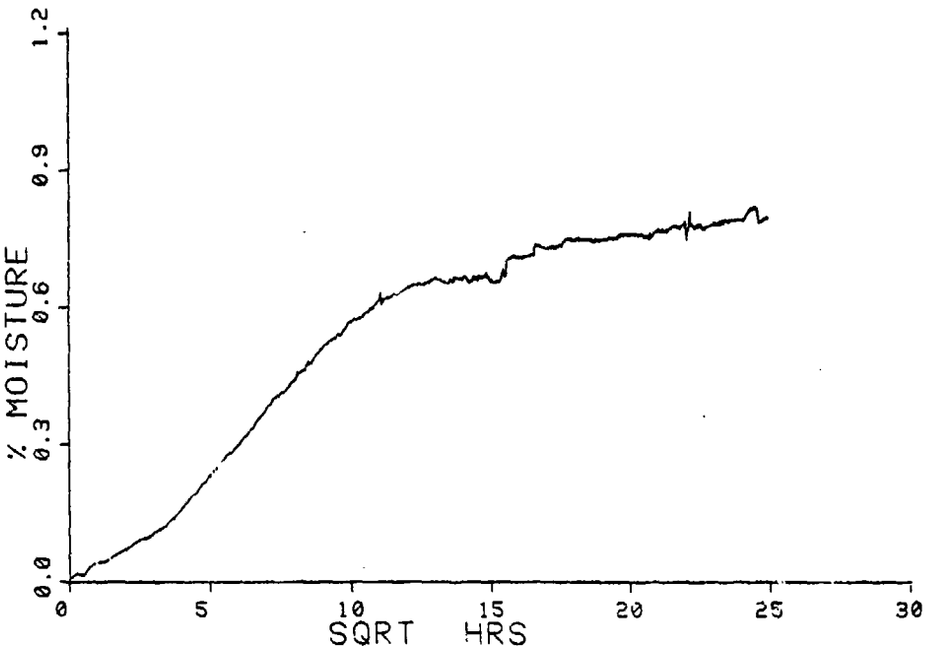

Figure 25. Typical Diffusivity Curve for S2 Glass/3501-6 from NPLOT
RH = 98%, Temperature = 65.5°C (150°F), Thickness = 0.86 mm (0.034 in)

Figure 26. Typical Diffusivity Curve for S2 Glass/3501-6 from MPLOT
RH = 98%, Temperature = 65.5°C (150°F), Thickness = 0.86 mm (0.034 in)

TABLE 8

VALUES OF MOISTURE DIFFUSIVITY
(mm²/sec) AT 65.5°C (150°F) AND 98 PERCENT RELATIVE HUMIDITY

Material	Present Data	DeIasi & Whiteside [34]	Loos & Springer [17]	Whitney & Browning [36]
3501-6 Epoxy	9.72×10^{-7}	8.06×10^{-7}	8.537×10^{-7}*	9.594×10^{-7}*
AS/3501-6	2.08×10^{-7}	1.55×10^{-7}	2.988×10^{-7}	3.358×10^{-7}
S2 Glass/3501-6	1.8902×10^{-7}	----	----	----

*Estimated from Eq. (A.27)

SECTION 5

EXPERIMENTAL/ANALYTICAL CORRELATIONS

5.1 Scanning Electron Microscope Investigation

The initial portions of the diffusivity curves appear to be very much Fickian in nature (see Eq. (A.11) of Appendix A). However, towards the latter stages of the diffusion curve (beyond the knee of the curve), the specimens showed fluctuations (see Figures 23-26). These fluctuations have been postulated to be due to microcracks on the surface [16,36,38]. Thus, it was desired to know if microcracks do, in fact, exist on the surface of a composite which has been preconditioned and exhibits the fluctuations noted.

The University of Wyoming's Jelco JSM-U3 Scanning Electron Microscope (SEM) was used to provide information about the composites after moisture preconditioning.

Specimens exhibiting non-Fickian moisture absorption were cut using a carborundum (carbide particles embedded in a polymer matrix) cutoff saw. These specimens were ultrasonically cleaned in lukewarm water and mounted on the special mounting studs required by the SEM. Since, through the nature of operation of the SEM, charge builds up on non-conductors such as composites, each specimen had to be vapor-coated with gold.

The neat epoxy resin specimens showed the least amount of fluctuation, while the S2 glass/3501-6 specimens showed the most, probably due to the less controlled prepregging technique compared to the commercial

AS/3501-6 system. The following series of figures show the results of the SEM study.

In Figure 27, a small void is seen on an S2 glass/3501-6 composite. While not a microcrack, these surface voids were seen on the side of the composite which faced the stainless steel caul plate during the curing process. It is noted that it is deeper than other surface aberrations. Most of the composites show cracks along edges which are sawcut prior

Figure 27. S2 Glass/3501-6, Test Series 6, Specimen 1,1, (600X); conditioned for 30 days at 65.5°C, 98% RH. Fibers cannot be seen, but run in the vertical direction in the photograph. This surface was adjacent to the release agent coated steel plate during curing.

to conditioning. These can be seen in an S2 glass/3501-6 composite in Figure 28. Note again the depth of the crack. The vertical lines are replicates of fibers in the bleeder cloth. These are quite shallow, and therefore probably do not alter the diffusion characteristics. Surface cracks are found on the neat 3501-6 epoxy specimens. A typical crack

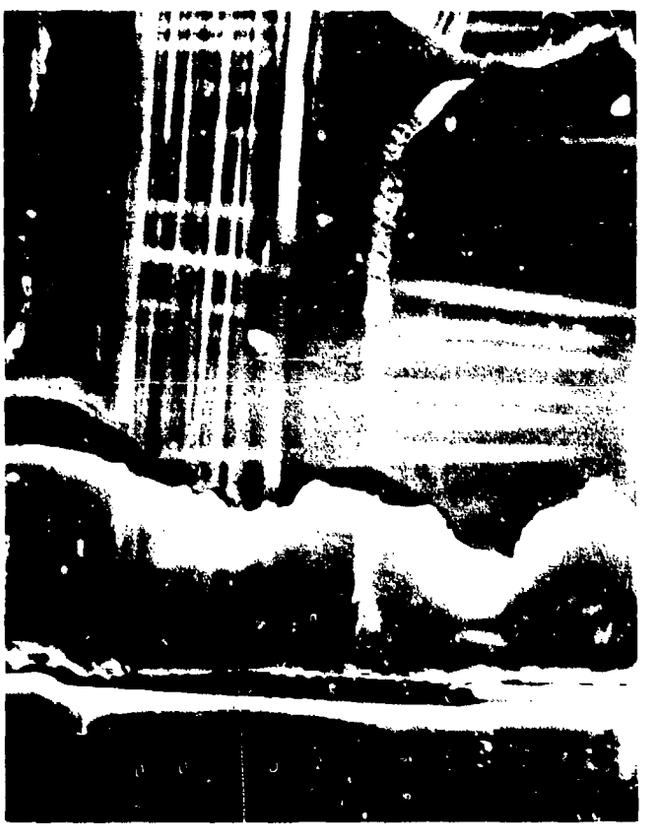

Figure 28. S2 Glass/3501-6, Test Series 6, Specimen 1,1, (200X); side facing bleeder cloth, conditioned for 30 days at 65.5°C, 98% RH. Fibers just below the surface may be seen.

is seen in Figure 29. While not covering as much surface area as in the composites, they are noticed to be present across the surfaces. The roughened area surrounding the crack is due to surface grinding and does

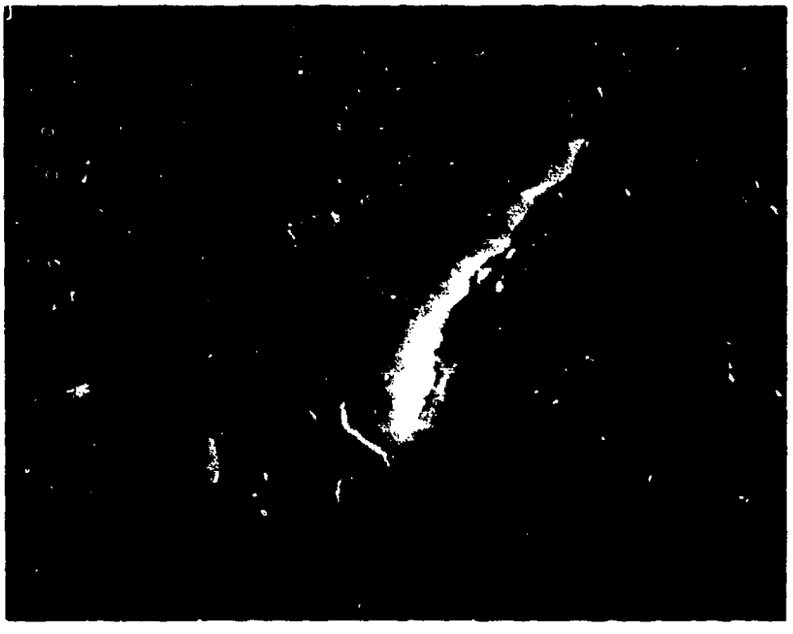

Figure 29. Neat Resin, Test Series 5, Specimen 2,2, (400X); conditioned for 30 days at 65.5°C, 98% RH. Surface ground.

not extend a significant depth into the specimen. Figure 30 is a closeup of Figure 29. The crack is not limited to the local scale as is the grinding-induced roughness. Another example of edge cracking in an

Figure 30. Neat Resin, Test Series 6, Specimen 2,2, (1500X); conditioned for 30 days at 65.5°C, 98% RH. Surface ground. (Closeup of crack in Figure 29.

AS/3501-6 composite is shown in Figure 31. This edge crack is parallel to the fibers and extends for a considerable distance in the vertical direction beyond the field of the photo, showing that these edge cracks are not limited to the smaller scale of the microcracks across the

Figure 31. AS/3501-6, Test Series 6, Specimen 2,1, (200X); conditioned for 30 days at 65.5°C, 98% RH. Fibers run in the vertical direction. This is the side facing the release cloth.

interior. More surface voids on an S2 glass/3501-6 specimen due to the non-permeable steel plate can be seen in Figure 32. The voids at the surface probably do not alter the mechanical properties, but may alter the mode of diffusion. Relatively extensive regions of microcracks are

Figure 32. S2 Glass/3501-6, Test Series 6, Specimen 2,1, (450X): conditioned for 30 days at 65.5°C, 98% RH. Side facing release coated steel plate. Fibers run in the horizontal direction.

seen in some specimens. An example is shown in Figure 33 on an S2 glass/3501-6 specimen. The microcracks are the randomly oriented dark regions on the surface. More microcracks on an S2 glass/3501-6 specimen can be

Figure 33. S2 Glass/3501-6, Test Series 6, Specimen 2,1, (110X); conditioned for 30 days at 65.5°C, 98% RH. Fibers run in the vertical direction. Side which faced the release cloth is shown.

seen in Figure 34. The oval hole at the lower center of the photograph is typical of many of the specimens. After curing, a small web of epoxy resin between the release cloth and the bleeder ply is present. When the composite is peeled away, the epoxy stays on the bleeder ply, exposing

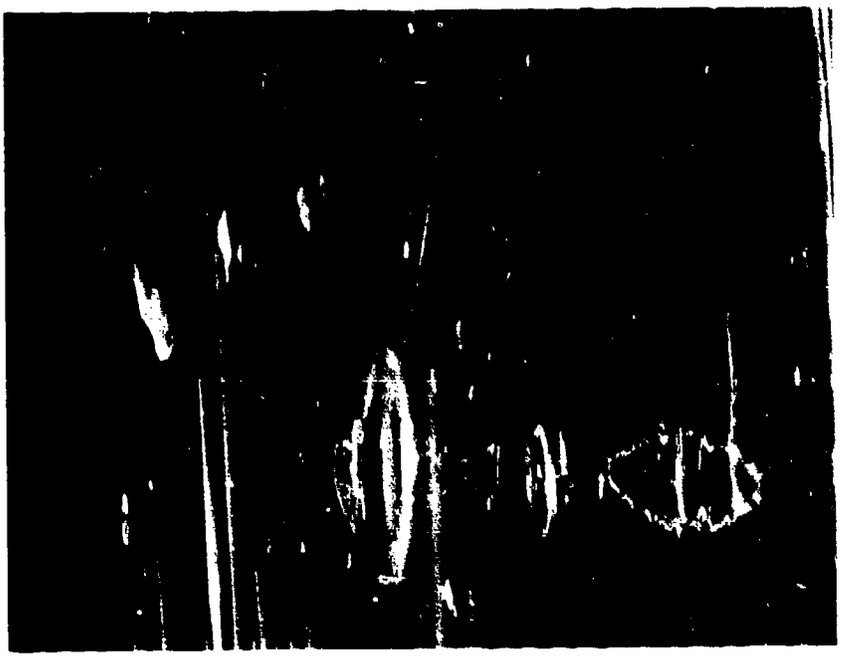

Figure 34. S2 Glass/3501-6, Test Series 6, Specimen 2.1, (110X); conditioned for 30 days at 65.5°C, 98% RH. Fibers run in the vertical direction. Side facing release cloth is shown.

fibers, or remains on the composite, depositing platelike structures. On the epoxy specimens, some small regions of microcracking are found. An example of one of these regions is shown in Figure 35. Again, the relative size differences of the microcracks compared to the surface

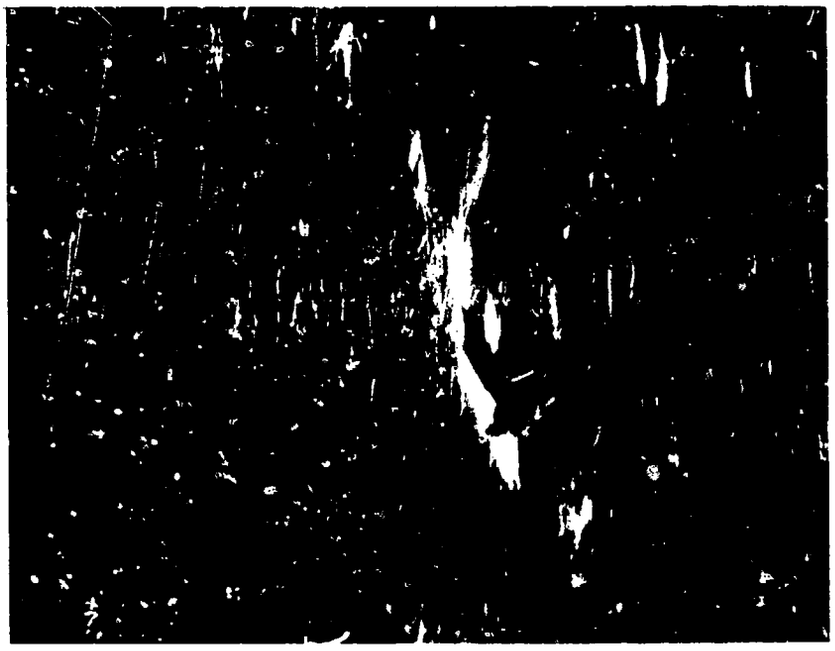

Figure 35. 3501-6 Epoxy Resin, Test Series 5, Specimen 1,1, 400X); conditioned for 30 days at 65.5°C, 98% RH. face ground.

grinding-induced aberrations will be noted. A closeup of Figure 35 is shown as Figure 36. The crack continues down and to the left. The center of the fracture surface is similar to that which is found in a neat epoxy classic brittle fracture [36]. More cracks on the edge of an

Figure 36. 3501-6 Resin, Test Series 5, Specimen 1,1, (1200X); conditioned for 30 days at 65.5°C, 98% RH. Surface ground. (Closeup of Figure 35.)

AS/3501-6 graphite/epoxy specimen are shown in Figure 37. Nearly all sawcut edges in the composites exhibited cracks similar to these. It will be noted that the fibers are separated from the matrix material at the top. The AS/3501-6 specimens also have surface microcracks, as

Figure 37. AS/3501-6, Test Series 5, Specimen 1,1, (150X); conditioned for 30 days at 65.5°C, 98% RH. Side facing the release cloth. Fibers are oriented vertically.

shown in Figure 38. In general, they are not as extensive as in the S2 glass/3501-6 specimens. A typical example can be seen just right of center in the photograph. The microcracks are not as wide as those in the S2 glass/3501-6 composites, but extend a considerable depth into the material. These small cracks were found across the entire surface of the AS/3501-6 specimens.

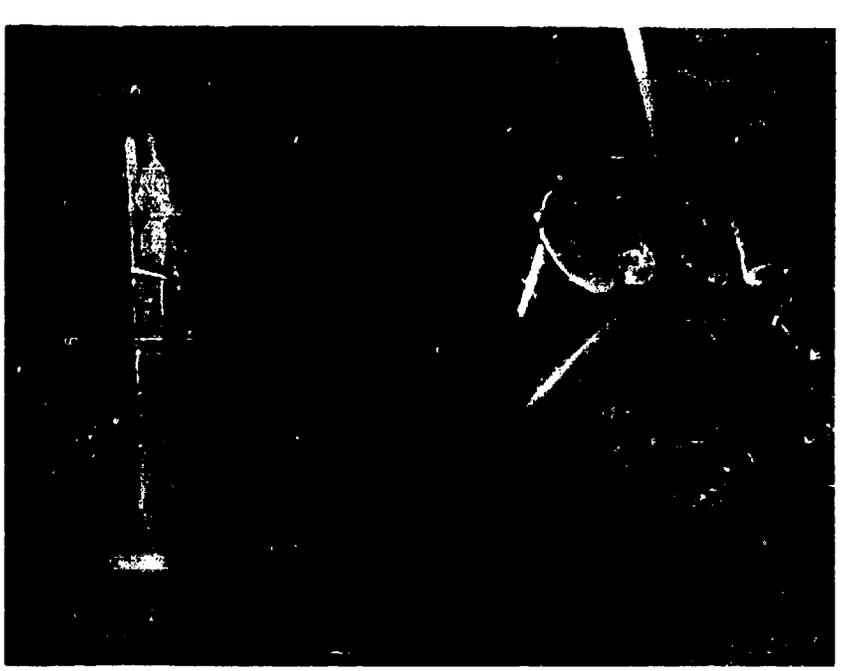

Figure 38. AS/3501-6, Test Series 4, Specimen 1,1, (200X); conditioned for 30 days at 65.5°C, 98% RH. Side facing the release cloth. Fibers run in the vertical direction.

It was desired to know if these specimens exhibited any of these surface anomalies prior to moisture conditioning. Therefore, an SEM study was conducted on unconditioned specimens also.

Figure 39 shows an unconditioned S2 glass/3501-6 specimen. Cracks are seen along the sawcut edges. Since this specimen had seen no conditioning, it appears that these cracks are produced prior to moisture absorption. Small horizontal cracks are seen along the bottom of the

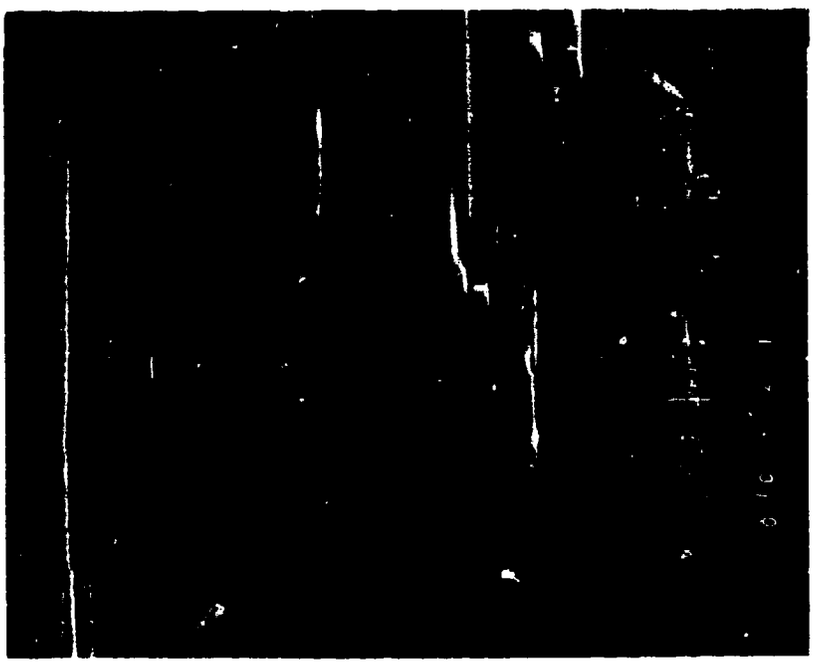

Figure 39. S2 Glass/3501-6, Dry Specimen, (100X); no moisture conditioning. Side facing release coated steel plate. Fibers run in the vertical direction.

photograph. As in the S2 glass/3501-6 specimens, the AS/3501-6 specimens exhibited cracks along sawcut edges before moisture conditioning, as shown in Figure 40. Curing-induced surface imperfections also will be noted, which were also present in the moisture-conditioned specimens. Therefore, these exist before moisture conditioning.

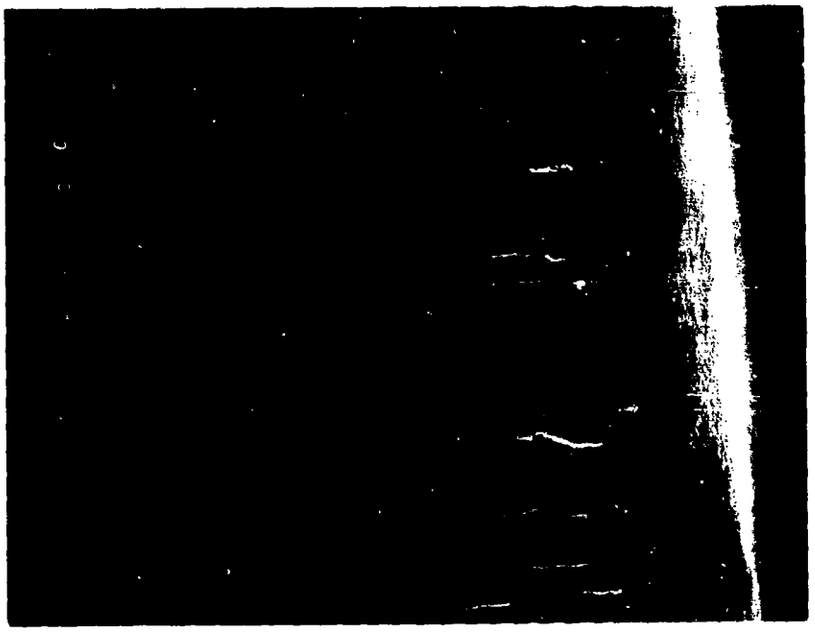

Figure 40. Unconditioned AS/3501-6, (100X); side facing release coated steel plate. Fibers run in the horizontal direction.

Since there is some surface roughness on the ground 3501-6 neat epoxy resin specimens, it was desired to know if these could be totally eliminated. A polished 3501-6 epoxy specimen is shown in Figure 41. This high magnification photograph shows only very superficial surface scratches, residuals from the polishing process. The polishing was accomplished by using a series of polishing wheels down to 0.1μm and with a high-frequency vibrating polishing cloth.

Figure 41. Unconditioned 3501-6 Neat Resin, (1500X); polished.

Microcracks on the surface provide a good explanation for the variation of moisture seen during diffusivity experiments. It is not known at exactly what point during the diffusion process the microcracks form, but the fluctuations are seen shortly after the diffusivity curves level off.

The microcracks absorb and desorb moisture through capillary action. These microcracks have been postulated to change dimensions during moisture-induced dilatation [36]. This would have the effect of forcing the water out and letting it enter back in upon reopening. These small cracks probably do not influence mechanical properties (Young's modulus, ultimate strength, etc.) because they extend only small distances into the thickness of the composite. On sawcut edges, the fiber-matrix debonding may cause local capillary action. While the edges do not represent a large surface area, their influence may still be noticed.

Some of the surface anomalies seen in the moisture-conditioned specimens were also seen in the non-conditioned specimens observed. However, while some cracks were seen, they were observed with far less frequency than in the moisture-conditioned specimens. Polishing the neat resin specimens did eliminate the surface grinding-induced roughness. Since the roughness due to grinding was seen to be very shallow, polishing is not necessary.

Microcracks do exist, and it is felt that these are the primary cause of the nonlinear diffusivity observed.

5.2 Description of Micromechanics Analysis

The Composite Materials Research Group at the University of Wyoming has devoted much time and effort to the development of micromechanics

analyses of composite materials [3,26,27,41]. Micromechanics refers to the analysis of an individual composite lamina on a local scale, in an effort to predict stresses, strains, laminae stiffness properties, and failure under mechanical, moisture, and thermal loadings.

The micromechanics analysis used in this study employs a finite element scheme. A square packing array of fibers is assumed. The analysis uses a generalized plane strain assumption to solve the displacement boundary value problem defined by the repeating square packing array. It evaluates stresses, strains, and material properties after each incremental load is applied. It permits nonlinear moisture and thermal response of the constituent materials. Inelastic behavior is included, using a Prandtl-Reuss flow rule. Complete details of the analysis and related computer programs are presented in References [3, 26,27,41].

In general, constituent material experimental data can be input directly into the analysis. The mechanical response of the matrix material has been characterized at the University of Wyoming [33,42]. Fiber properties are available in the literature [7,8]. These properties are listed in Table 9. Transverse fiber properties are best estimates. The stress-strain response of the matrix is evaluated at each increment using the Richard-Blacklock relation [43].

The micromechanics analysis was first run to simulate the composite curing cycle cooldown to room temperature. This cooldown induces stresses in the composite material due to the mismatch of thermal expansion coefficient of the polymer matrix and fiber. For the dry thermal expansion tests, the composite material was cycled down to -73.3°C (-100°F), then

TABLE 9

CONSTITUENT MATERIAL PROPERTIES FOR AS-GRAPHITE FIBER, S2 GLASS FIBER, AND 3501-6 EPOXY RESIN

Property	Hercules AS-Graphite Fiber [8]	Owens-Corning S2 Glass Fiber [7]	Hercules 3501-6 Epoxy Matrix (Room Temperature, Dry) (from Tensile Test Data [42])	Hercules 3501-6 Epoxy Matrix (Room Temperature, Dry) (from Shear Test Data [33])
Longitudinal Modulus, E_L	GPa 220.6 (Msi 32.0)	86.19 (12.5)	4.27 (0.62)	5.79 (0.84)
Transverse Modulus, E_T	GPa 13.84 (Msi 2.0)	86.19 (12.5)	4.27 (0.62)	5.74 (0.84)
Longitudinal Shear Modulus, G_{LT}	GPa 34.48* (Msi 5.0*)	35.30 (5.12)	1.59 (0.23)	2.14 (0.31)
Transverse Shear Modulus, G_{TT}	GPa 5.52 (Msi 0.80)	35.30 (5.12)	1.59 (0.23)	2.14 (0.31)
Major Poisson's Ratio, ν_{LT}	0.20	0.22	0.34	0.34*
In-Plane Poisson's Ratio, ν_{TT}	0.25	0.22	0.34	0.34*
Longitudinal Tensile Strength, σ_L^u	MPa 3102.45 (ksi 450.0)	4826.5 (700.0)	82.7 (12.0)	169.6 (24.6)

*Estimated

TABLE 9 (continued)

CONSTITUENT MATERIAL PROPERTIES FOR AS-GRAPHITE FIBER, S2 GLASS FIBER, AND 3501-6 EPOXY RESIN

Property	Hercules AS-Graphite Fiber [8]	Owens-Corning S2 Glass Fiber [7]	Hercules 3501-6 Epoxy Matrix (Room Temperature, Dry) (from Tensile Test Data [42])	Hercules 3501-6 Epoxy Matrix (Room Temperature, Dry) (from Shear Test Data [33])
Transverse Tensile Strength, τ_L^u MPa (ksi)	344.75* (50.0*)	4826.5 (700.0)	82.7 (12.0)	169.6 (24.6)
Longitudinal Shear Strength, $\tau_{L\bar{T}}^u$ MPa (ksi)	1551.4 (225.0)	2413.25* (350.0*)	41.4 (6.0)	84.8 (12.3)
Transverse Shear Strength, τ_{TT}^u MPa (ksi)	172.38 (25.0)	2413.25* (350.0*)	41.4 (6.0)	84.8 (12.3)
Longitudinal Coefficient of Thermal Expansion α_L (10^{-6}/°C)	-0.36	5.0	40.91	40.91
Transverse Coefficient of Thermal Expansion α_T (10^{-6}/°C)	18.0*	5.0	40.91	40.91
Coefficient of Moisture Expansion β (10^{-3}/%M)	0	0	3.2	3.2

*Estimated

up to the glass transition temperature of the matrix material (≈175°C). For the moisture correlations, the composite was first cooled to room temperature. Then, it was cycled up to the moisture conditioning temperature of 65.5°C (150°F). Moisture was added in 0.5 percent increments to the matrix. This provided the moisture expansion correlations. The moist material was then cooled down to -73.3°C (-100°F), and back up to the glass transition temperature (≈100°C), to provide the thermal expansion information of the moisture-conditioned material.

Since the thermal expansion of the matrix material is a function of both temperature and moisture (Figures 17 and D17), this had to be taken into account in the micromechanics analysis. That is, a difference in thermal expansion was seen for dry and moisture-conditioned specimens. A linear interpolation was assumed.

Consider that the unconditioned (dry) epoxy matrix thermal strain is of the form:

$$\varepsilon_D = a_0 + a_1 T + a_2 T^2 \qquad (5)$$

where ε_D = strain (with no moisture conditioning)

a_0, a_1, a_2 = curve-fit paramters

T = temperature

Likewise, for the moisture-conditioned (wet) specimens:

$$\varepsilon_W = b_0 + b_1 T + b_2 T^2 \qquad (6)$$

where ε_W = strain (moisture-conditioned)

b_0, b_1, b_2 = curve-fit parameters

T = temperature

The parameters a_0 and b_0 are totally arbitrary since they define the reference point for zero strain. The important quantity used in the

micromechanics analysis is the slope of the curve at any given temperature, which is:

$$\alpha_D = \frac{\partial \varepsilon_D}{\partial T} = a_1 + 2a_2 T \qquad (7)$$

where α_D is the coefficient of thermal expansion for the dry material, and

$$\alpha_W = \frac{\partial \varepsilon_W}{\partial T} = b_1 + 2b_2 T \qquad (8)$$

where α_W is the coefficient of thermal expansion for the wet material. Combining these equations in a linear fashion

$$\alpha_C = \frac{(b_1 - a_1)}{M_m} M + 2\left[\frac{(b_2 - a_2)}{M_m}\right] MT + a_1 + 2a_2 T \qquad (9)$$

where α_C = combined coefficient of thermal expansion

M = moisture content

M_m = maximum moisture content

Note that when $M = 0$, $\alpha_C = \alpha_D$, and when $M = M_m$, $\alpha_C = \alpha_W$, as required.

This equation was used in the micromechanics analysis to provide an estimate of the thermal expansion slope at any given moisture content. It should be stated that the effect of moisture on the coefficient of thermal expansion may not be linear.

5.3 Sensitivity Study

The micromechanics analysis has many uses [3,26,27,39,41], but for the present study it was used in an effort to correlate predicted moisture and thermal expansions with the test results presented in Section 4.2. As will be seen, some of the numerically predicted values show a deviation from experimentally generated results. Thus, a sensitivity study was conducted to determine the relative influence of the various material parameters.

Since, for an isotropic material such as the epoxy matrix used here, E, ν and G are not independent, the shear modulus was varied with a change in Young's modulus or Poisson's ratio according to the relation [44],

$$G = \frac{E}{2(1 + \nu)} \tag{10}$$

where E = Young's modulus

ν = Poisson's ratio

G = shear modulus

to account for the interdependence of these material properties.

5.3.1 Moisture Expansion. The general approach for the sensitivity studies was to take each base constituent material property and divide it by a factor of two and multiply it by a factor of two to examine the influence that each constituent material property had on the predicted composite behavior. Fiber volumes of 60 percent and 70 percent were compared to the base value of 65 percent for the AS/3501-6 composites. For the S2 glass/3501-6 composites, values of 60 percent fiber and 75 percent were compared to the base value of 68 percent.

There is some discrepancy in the measured properties for the matrix material [41]. The matrix is assumed to be isotropic. Unfortunately, data generated from shear tests suggests a different stress-strain response than data generated from tensile tests. The micromechanics analysis was run using both sets of data, with the results presented in Figure 42. While the differences in matrix properties may be significant in predicting other composite material properties, little difference was noticed in the prediction of moisture expansion.

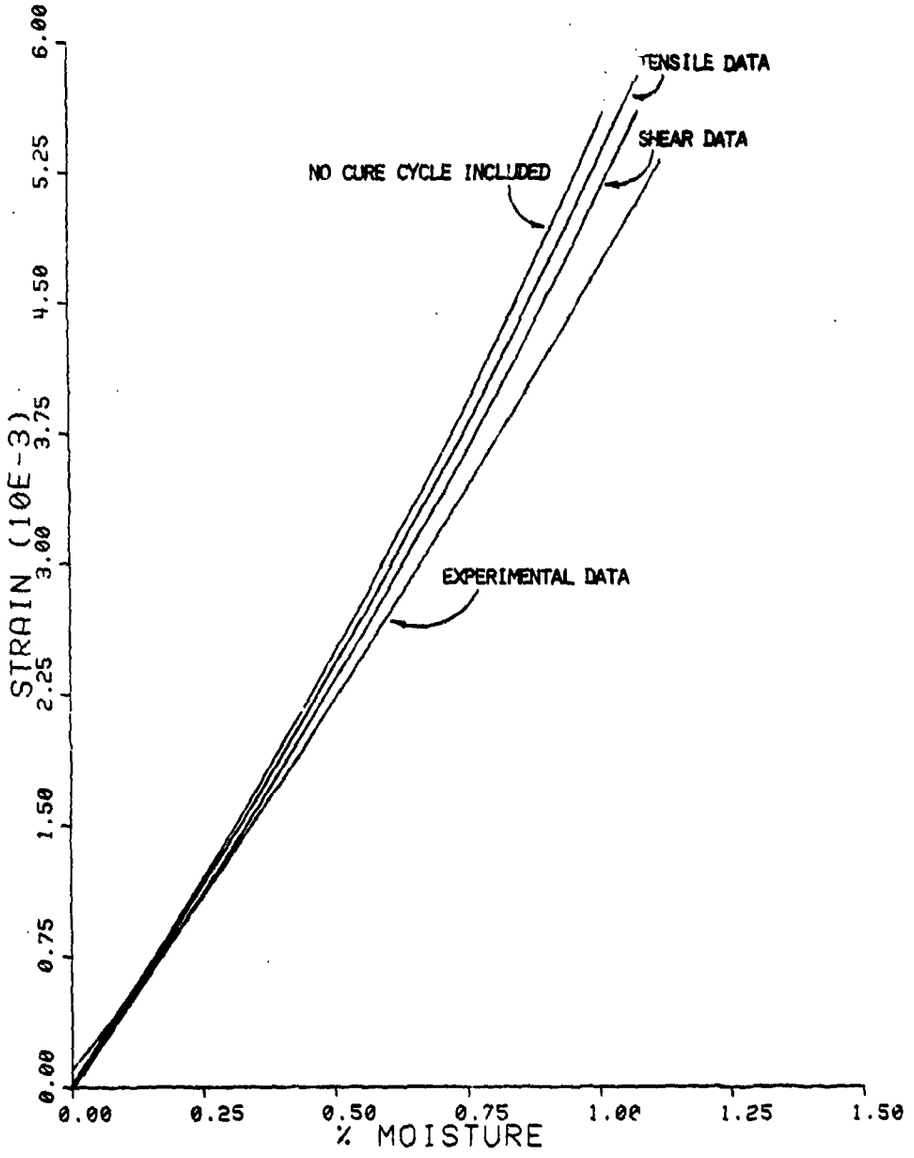

Figure 42. Micromechanics Predictions of Moisture Expansion for AS/3501-6 Graphite/Epoxy in the Transverse Direction

It was also desired to study the effect of curing stresses on the moisture data. Therefore, curves for which curing stresses were neglected are presented along with the tensile and shear data curves. Tensile data were used for this analysis. Interestingly, all three micromechanics-predicted moisture expansion curves vary by only a few percent from each other.

The experimental moisture expansion curves fall only slightly lower than the predicted moisture expansion curves. This small variation is probably due to estimated in-plane fiber constituent properties to be discussed in Section 6.1. Tensile data were also used for the rest of the sensitivity studies. The unchanged micromechanics predictions lie between the curves presented in this section.

Figure 43 shows the effect of the Poisson's ratio of the matrix material on the AS/3501-6 composite moisture expansion. The effect is quite large, showing that this matrix property has a profound influence on moisture expansion. Figure 44 shows the effect of fiber volume on the moisture expansion of the AS/3501-6 composite. For only a 5 percent change in fiber volume, a somewhat larger percentage change in moisture expansion is seen. Since the experimental technique discussed in Appendix C uses density data supplied from other sources than direct measurement [7,8], this could be a source of error.

Figure 45 shows the effect of the transverse Poisson's ratio of tl AS graphite fiber on moisture expansion. While the effect is noticeable, it is small. Figure 46 is a plot of the effect of transverse modulus of the fiber on the composite moisture expansion behavior of the AS/3501-6 system. Again, the change is small, but this fiber constituent property

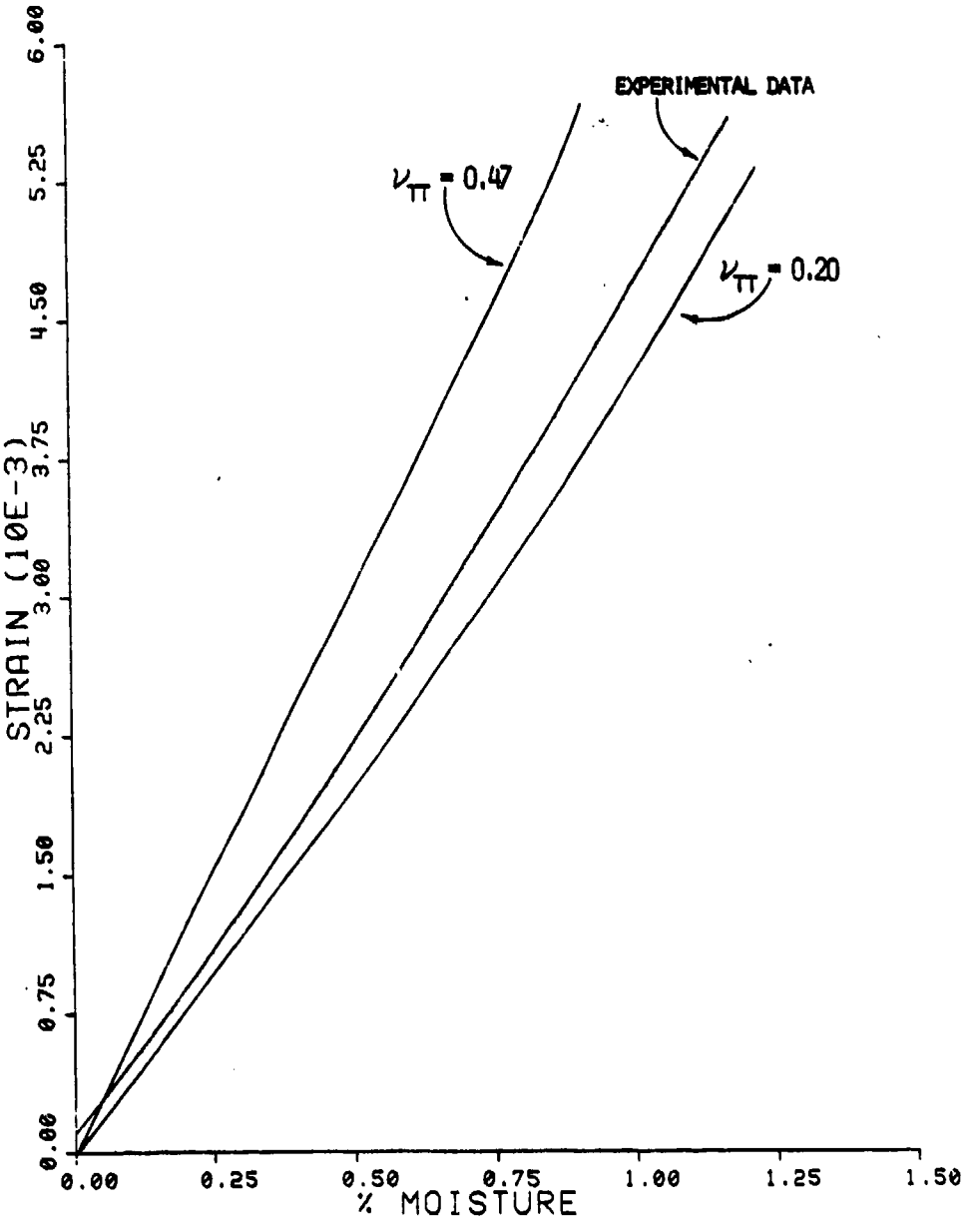

Figure 43. Moisture Expansion Sensitivity to Poisson's Ratio of the Matrix for AS/3501-6 Graphite/Epoxy (Base Value of Matrix ν_{TT} = 0.34)

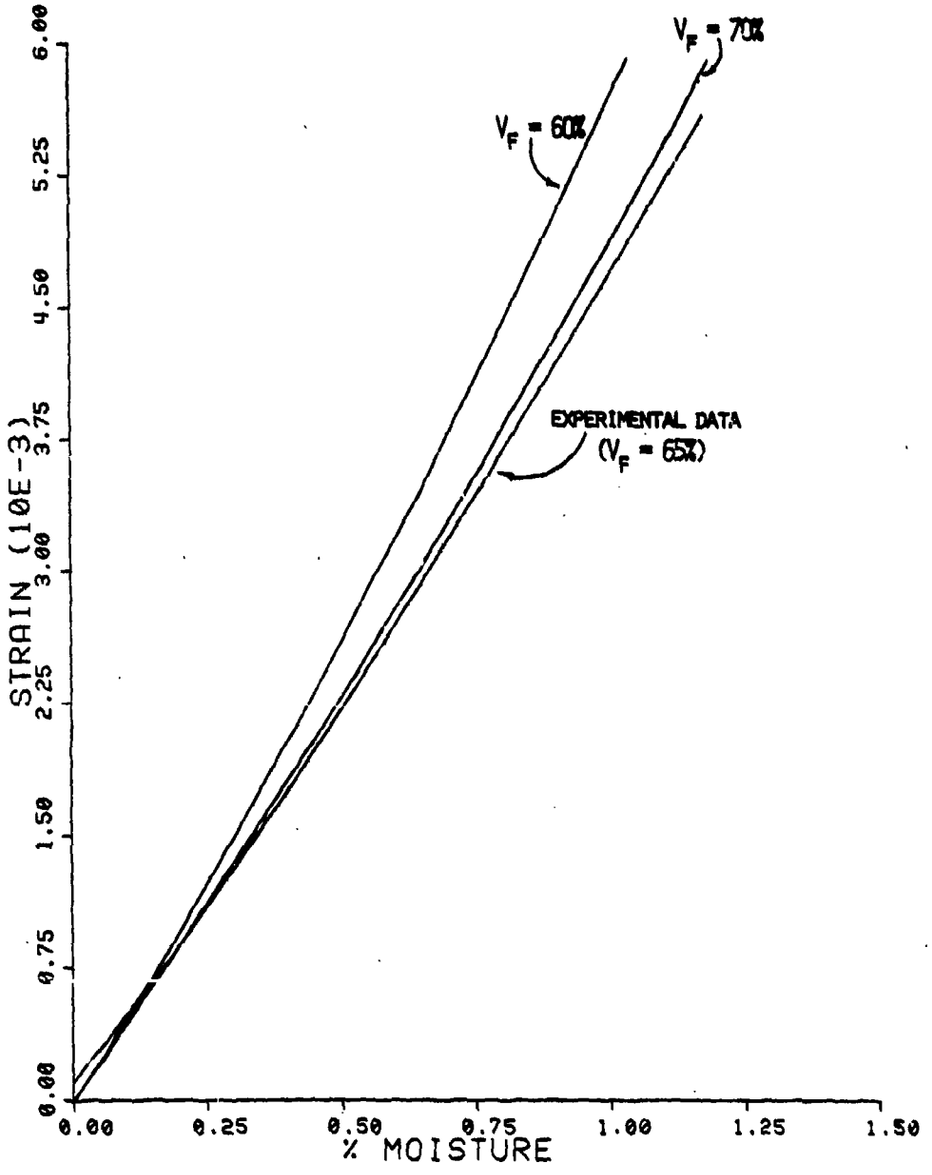

Figure 44. Moisture Expansion Sensitivity to Fiber Volume for AS/3501-6 Graphite/Epoxy

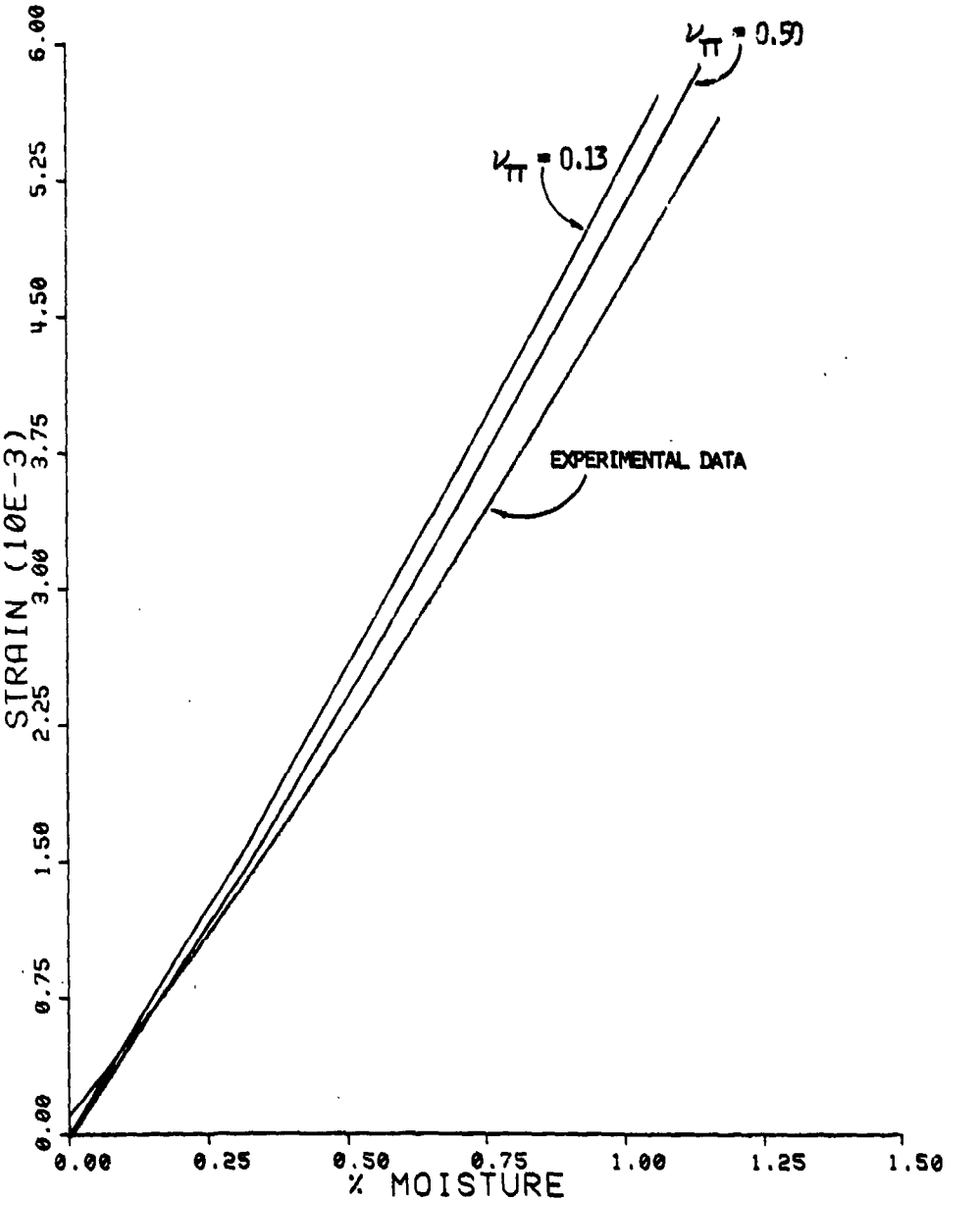

Figure 45. Moisture Expansion Sensitivity to In-Plane Poisson's Ratio of the Fiber for AS/3501-6 Graphite Epoxy (Base Value of Fiber ν_{TT} = 0.25)

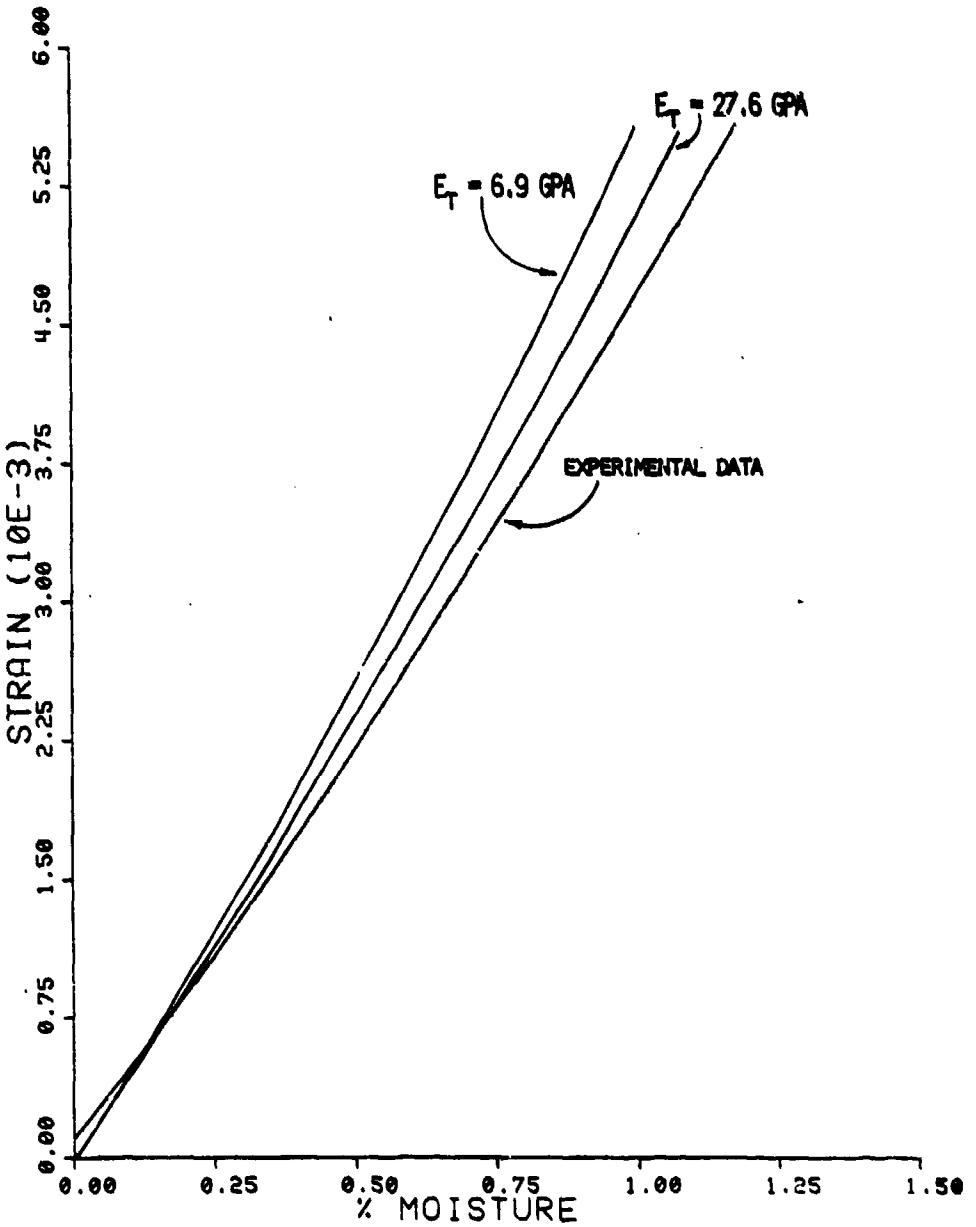

Figure 46. Moisture Expansion Sensitivity to Young's Modulus of the Fiber for Transverse Graphite/Epoxy (Base Value E_T = 13.84 GPa)

has the greatest influence on moisture expansion of any of the fiber properties studied. In general, any decrease in the in-plane modulus of the fiber makes the moisture expansion curves steeper because with any change in stress, a correspondingly higher change in strain is exhibited. In Figure 47, the fiber transverse thermal expansion is seen to have little influence on moisture expansion. This fact should be carefully noted because it becomes important in the thermal expansion studies, to be discussed subsequently. The reason that transverse thermal expansion has any effect at all is due to a difference in residual stresses induced from cooldown after curing. A difference in thermal expansion of the fiber causes a different microstress level at the fiber matrix interface.

Figure 48 shows the micromechanics predictions of moisture expansion for the S2 glass/3501-6 composite. Correlation of experimental data with predicted values is not nearly as close as was shown for the AS/3501-6 composite (Figure 42). However, the difference between no curing cycle using tensile data, tensile data, and shear data of the 3501-6 epoxy matrix is, again, small. The reasons for the predicted values being lower may be due to a degradation of the fiber-matrix interface bond during moisture absorption [45,46,47] (to be discussed in Section 6.1). The micromechanics analysis did not take this into account, since a perfect fiber-matrix bond is assumed.

As was noted for the moisture-induced expansion of the AS/3501-6 composite, the Poisson's ratio of the matrix in the S2 glass/3501-6 composite has a profound influence on moisture expansion, as shown in Figure 49. Unfortunately, the effects are opposite. That is, while a slightly lower value of Poisson's ratio of the 3501-6 epoxy resin seems

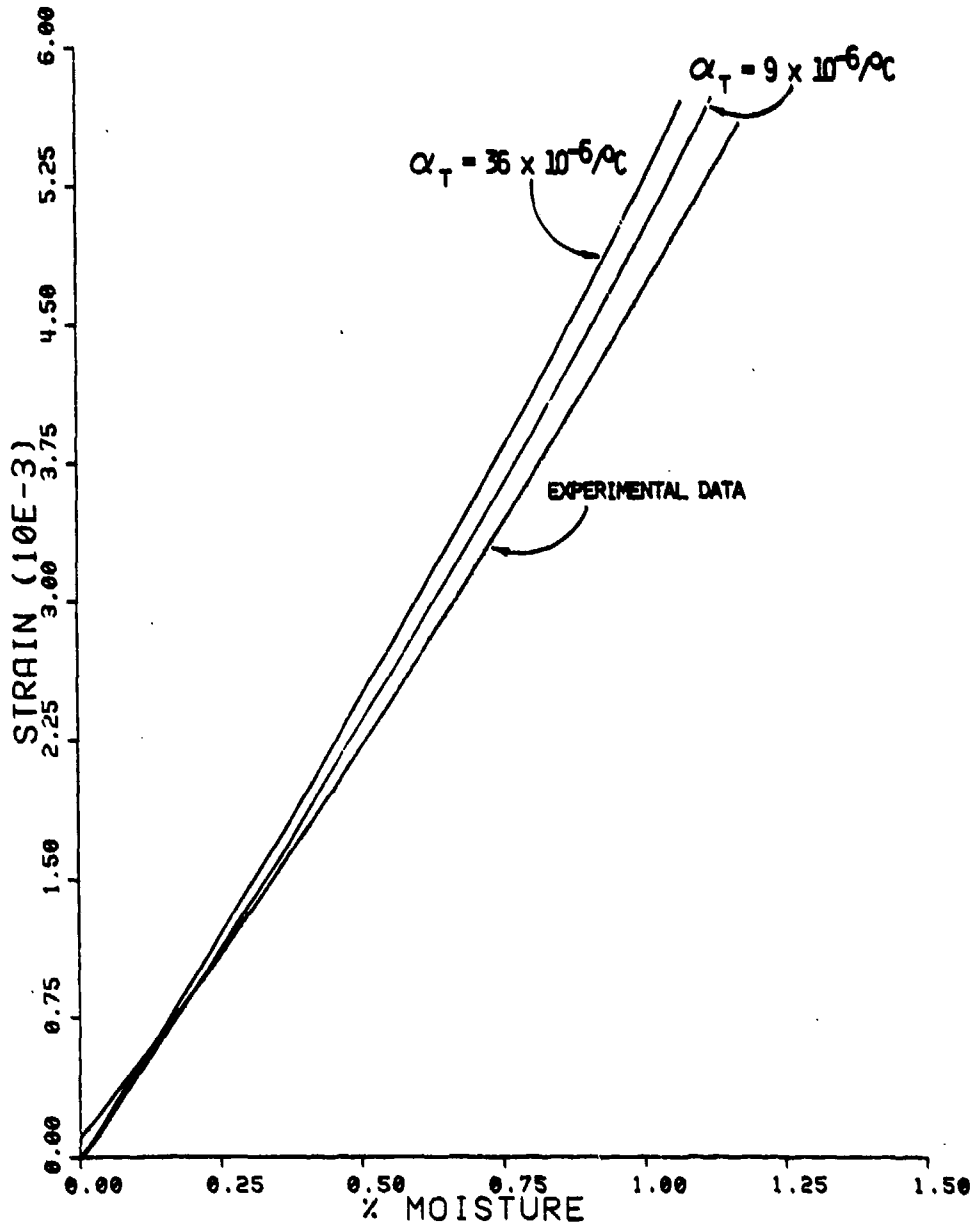

Figure 47. Moisture Expansion Sensitivity to Transverse Thermal Expansion of the Fiber for AS/3501-6 Graphite/Epoxy (Base Value $\alpha_T = 18 \times 10^{-6}/°C$)

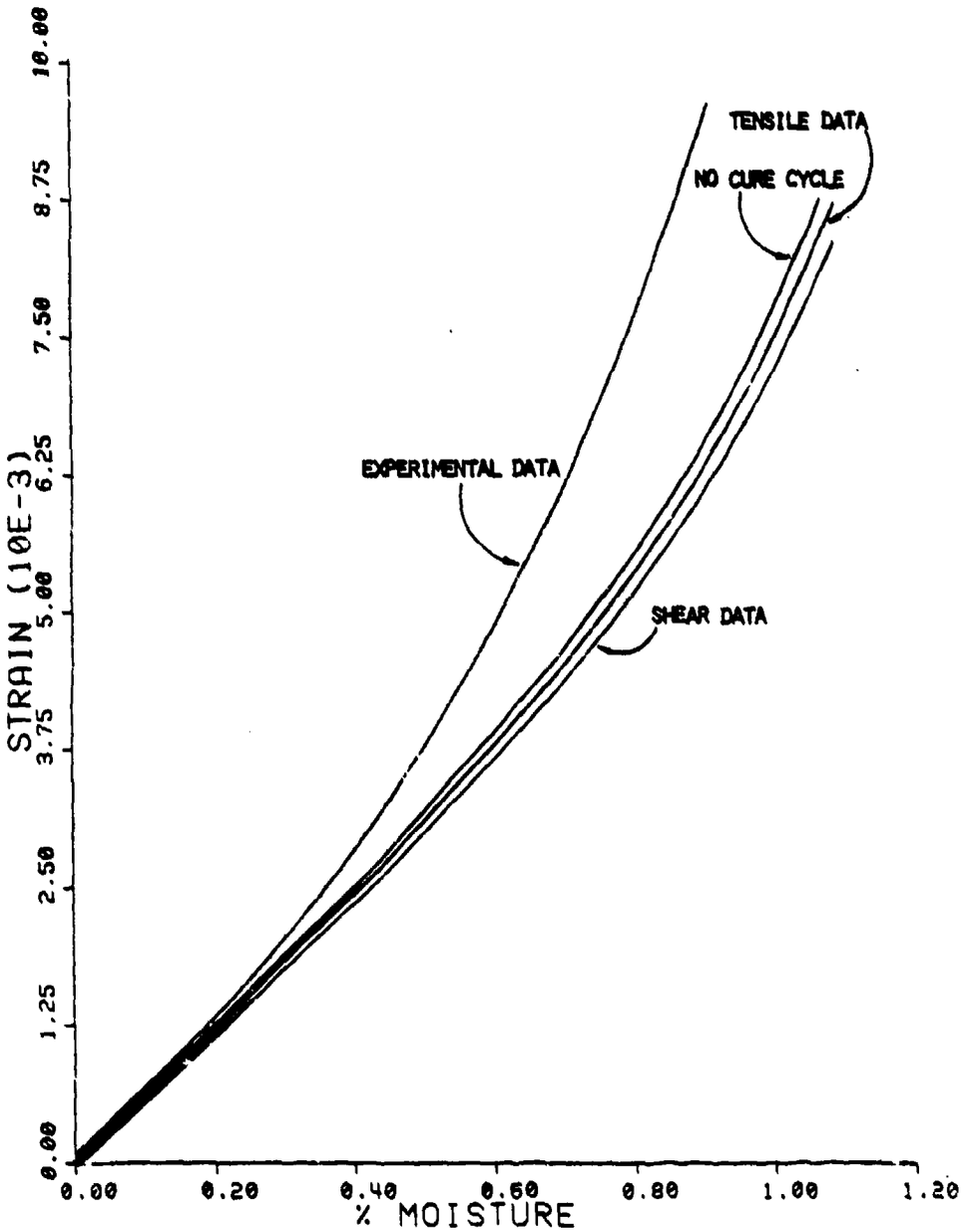

Figure 48. Micromechanics Predictions of Moisture Expansion for S2 Glass/3501-6 Glass/Epoxy in the Transverse Direction

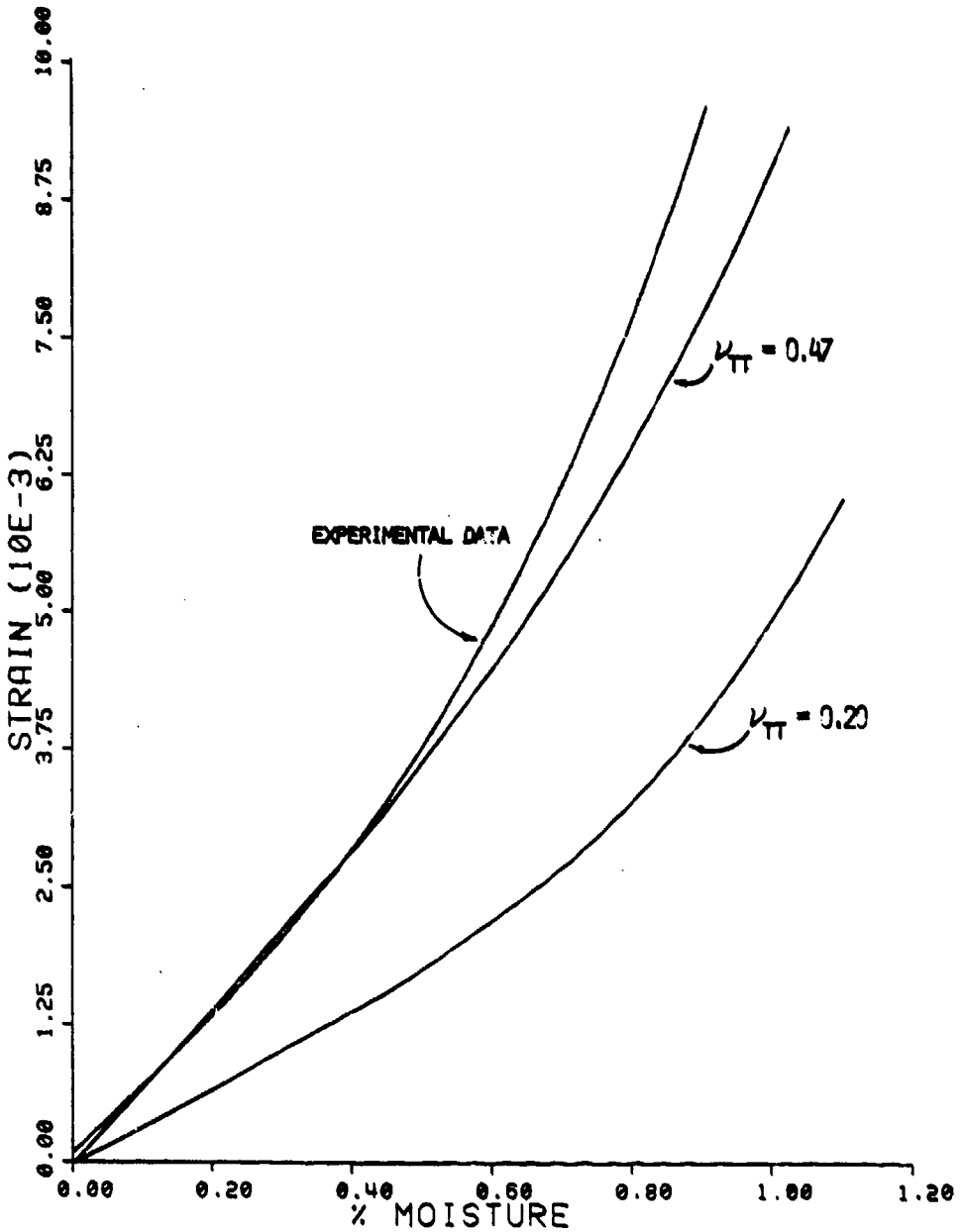

Figure 49. Moisture Expansion Sensitivity to Poisson's Ratio of the Matrix for S2 Glass/3501-6 Glass/Epoxy (Base Value of Matrix ν_{TT} = 0.34)

to improve the correlation for the AS/3501-6 composite, it makes the value of the S2 glass/3501-6 composite off even further. Figure 50 shows the effect of fiber volume on the S2 glass/3501-6 moisture expansion. A large influence is seen. It will be noted that the fiber volume variation is greater in the S2 glass/3501-6 composite than in the AS/3501-6 composite. The larger variation was considered since fiber volume varied more in S2 glass/3501-6 specimens than in AS/3501-6 specimens (Table 6).

Figure 51 shows the effect of Poisson's ratio of the S2 glass fiber on predicted moisture expansion. This Poisson's ratio is independent of direction since the glass fibers are assumed to be isotropic. The Young's modulus of the glass fibers has the most influence on the composite moisture expansion behavior of all constituent material properties, as shown in Figure 52. The transverse thermal expansion of the fiber has little effect, as shown in Figure 53. The effect is, again, due to a difference in residual stresses induced after cooling down from the cure temperature.

As would be expected, the moisture loading plots are very much matrix dominated, corresponding to the negligible moisture absorption of the fibers. That is, a change in matrix properties causes a much more significant change in the results than does a change in the fiber properties. This can readily be seen by comparing the large differences of predicted moisture expansion in Figures 43, 44, 49, and 50, compared to the small changes seen in Figures 45, 46, 47, 51, 52, and 53.

The matrix material appeared to have an essentially linear coefficient of moisture expansion, while the S2 glass/3501-6 and AS/3501-6 were seen to be nonlinear. Tables 10 and 11 present predictions using the micro-

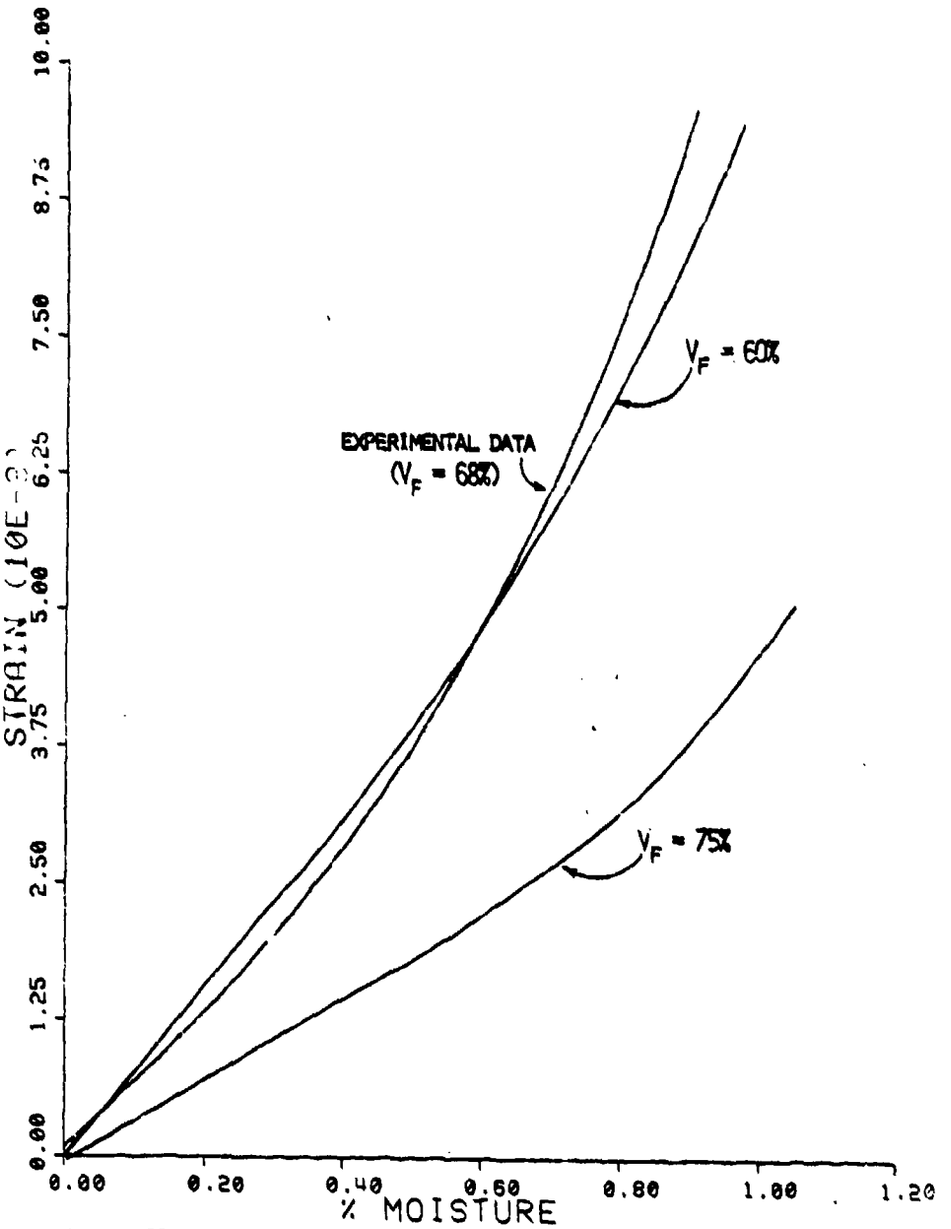

Figure 50. Moisture Expansion Sensitivity to Fiber Volume for S2 Glass/3501-6 Glass/Epoxy

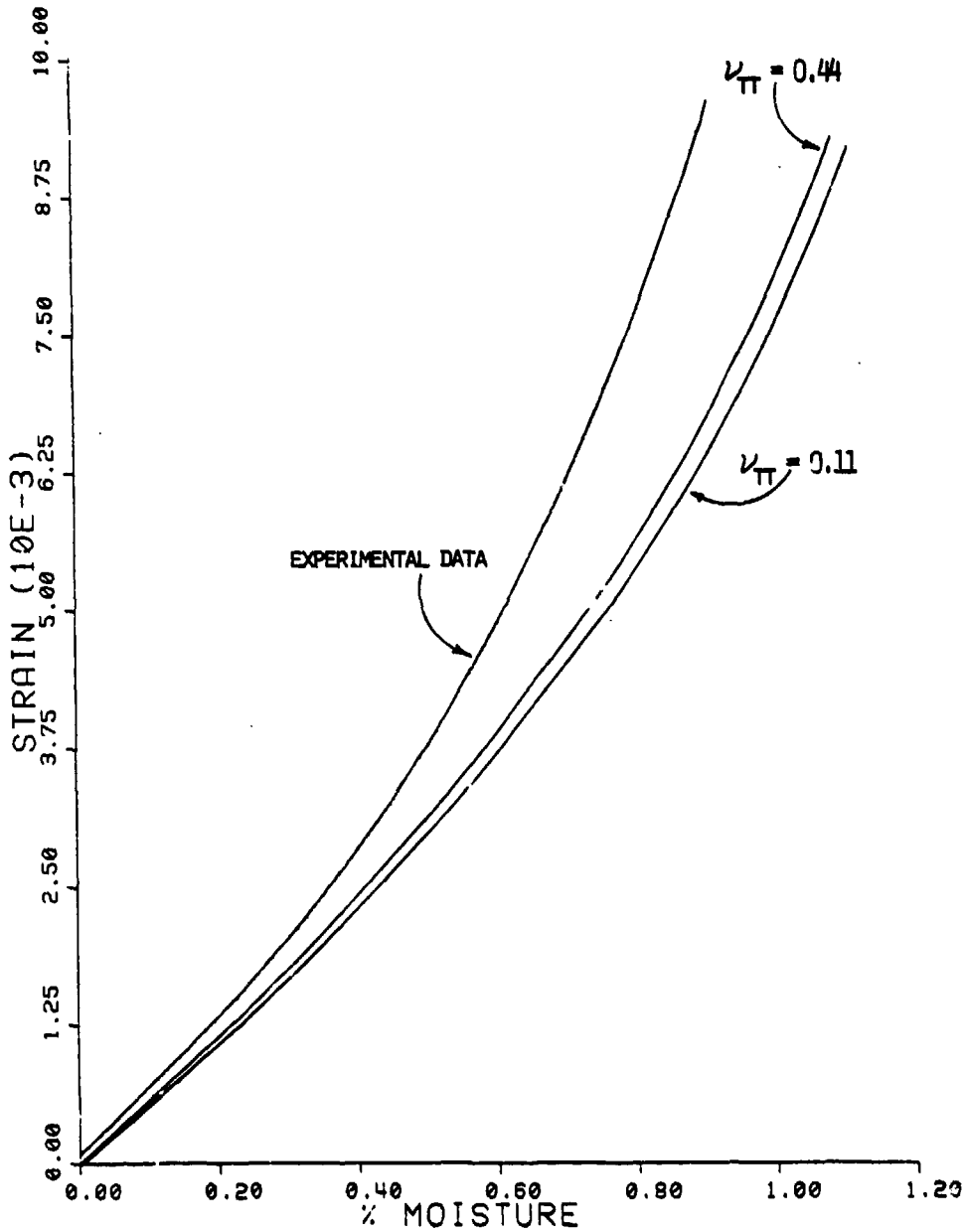

Figure 51. Moisture Expansion Sensitivity to Poisson's Ratio of the Fiber for S2 Glass/3501-6 Glass/Epoxy (Base Value of Fibe ν_{TT} = 0.22)

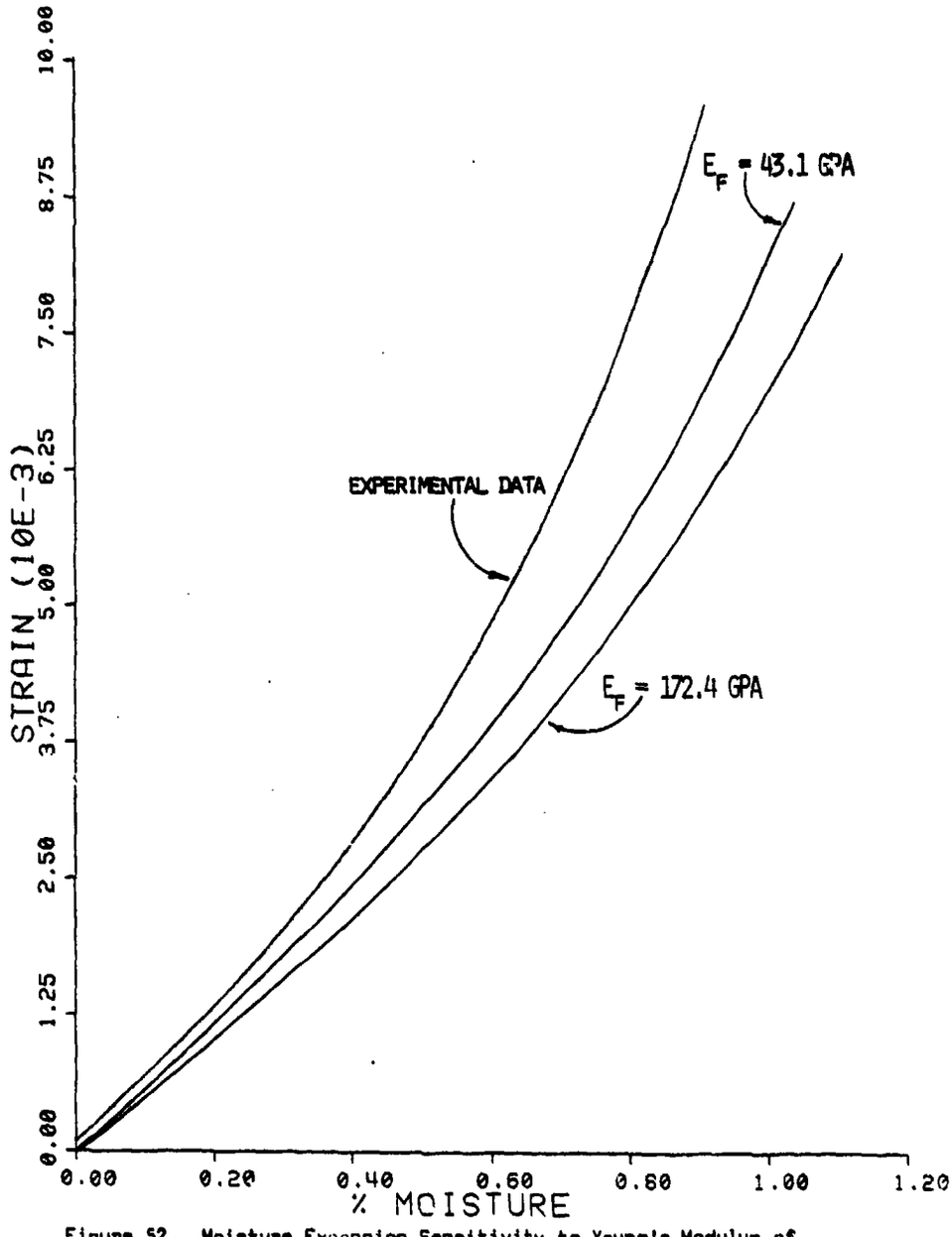

Figure 52. Moisture Expansion Sensitivity to Young's Modulus of the Fiber for S2 Glass/3501-6 Glass/Epoxy (Base Value E_T = 86.19 GPa)

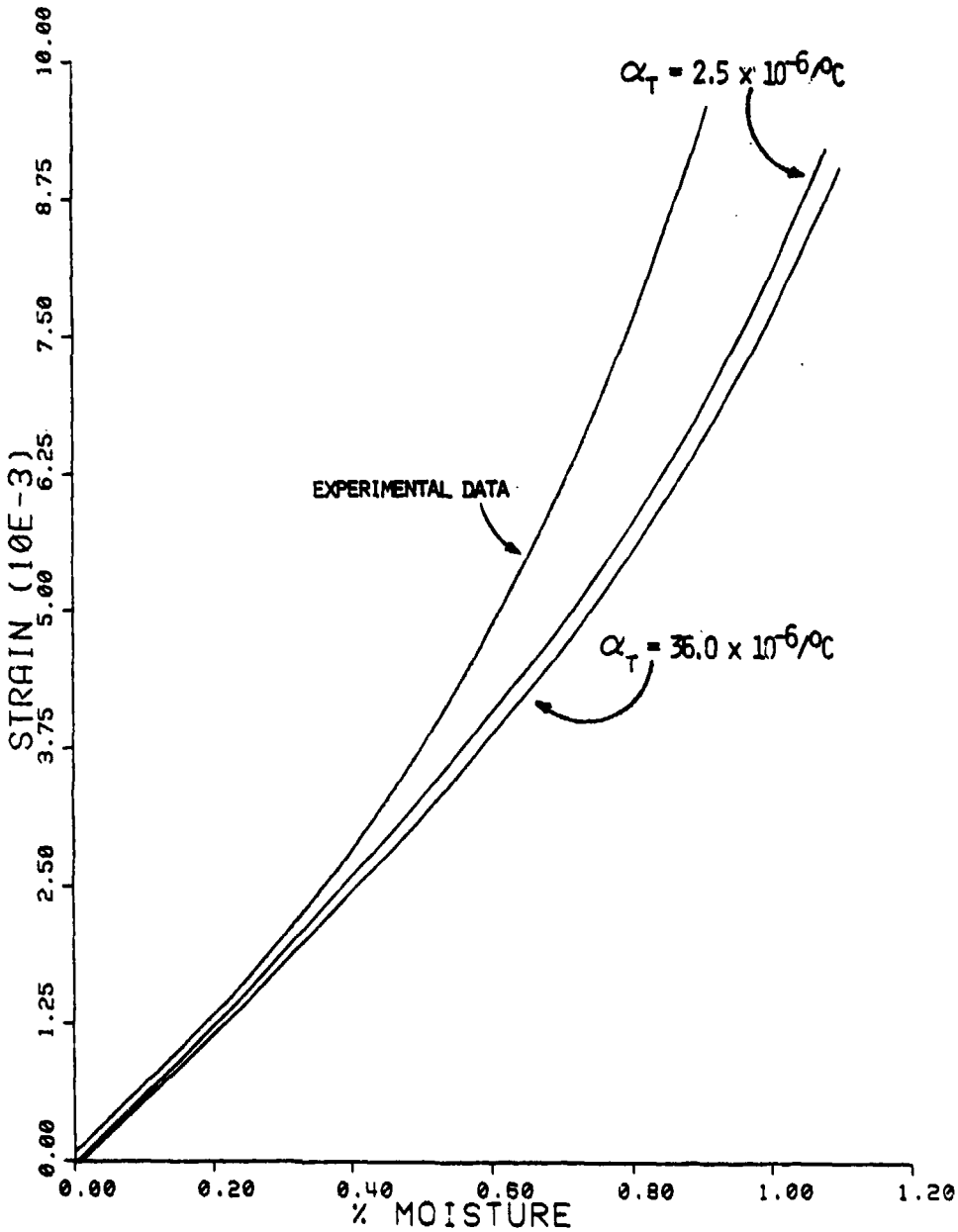

Figure 53. Moisture Expansion Sensitivity to Thermal Expansion of the Fiber for S2 Glass/3501-6 Glass/Epoxy (Base Value α_T = 5.0 x 10^{-6}/°C)

TABLE 10

MICROMECHANICS PREDICTIONS OF MOISTURE-INDUCED TRANSVERSE STRAIN IN THE S2 GLASS/3501-6 COMPOSITE

Temperature = 65.5°C (150°F)

Percent Moisture in Matrix	Percent Moisture in Composite	Incremental Strain (10^{-6})	
0.5	0.107	5.647	
1.0	0.214	5.646	
1.5	0.321	5.644	
2.0	0.429	5.642	
2.5	0.536	5.639	
3.0	0.643	5.635	
3.5	0.750	5.632	Note
4.0	0.857	6.587	
4.5	0.964	6.693	
5.0	1.072	6.923	
5.5	1.179	7.125	
6.0	1.286	7.268	

TABLE 11

MICROMECHANICS PREDICTIONS OF MOISTURE-INDUCED TRANSVERSE STRAIN IN THE AS/3501-6 COMPOSITE

Temperature = 65.5°C (150°F)

Percent Moisture in Matrix	Percent Moisture in Composite	Incremental Strain (10^{-6})	
0.5	0.1401	7.502	
1.0	0.2802	7.497	
1.5	0.4202	7.490	
2.0	0.5605	7.480	
2.5	0.7006	7.467	
3.0	0.8407	7.452	Note
3.5	0.9808	7.541	
4.0	1.1210	7.651	
4.5	1.2611	7.806	
5.0	1.4012	7.954	
5.5	1.5413	8.107	
6.0	1.6814	8.219	

mechanics analysis. The values shown are incremental strain values. Note that there is a slight decrease in incremental strain for each increment of moisture until the level marked by brackets is reached. At this point, the incremental strains take a jump upward, and continue to increase. Crossman, et al., [21] also noted these nonlinearities.

Most effort has been devoted to determining coefficients of moisture expansion of graphite/epoxy composites since these materials are used extensively in spacecraft structures, where dimensional changes are an important consideration. The nonlinearity is much more subtle than for the S2 glass/epoxy composites, as can be seen by comparisons of Tables 10 and 11, due to less mismatch of properties of the fiber and matrix in the transverse direction (see Table 9).

Obviously, in the S2 glass/epoxy, something happens in the increment between 3.5 percent and 4.0 percent moisture by weight in the matrix material.

During the moisture absorption process, the stress state in the matrix becomes very complicated. It is nonhomogeneous, it is triaxial, and it is nonlinear with moisture absorption. The stress state is further complicated with increasing moisture since an increase in moisture changes the matrix constituent properties in a nonlinear fashion also.

The region of closest fiber spacing appears to have the greatest influence on composite strain. Any strain of the matrix in this region has a greater effect due to it being bonded by fibers, which are much stiffer (especially the S2 glass) in this transverse direction. Figure 54 identifies three specific points in this region of closest fiber spacing.

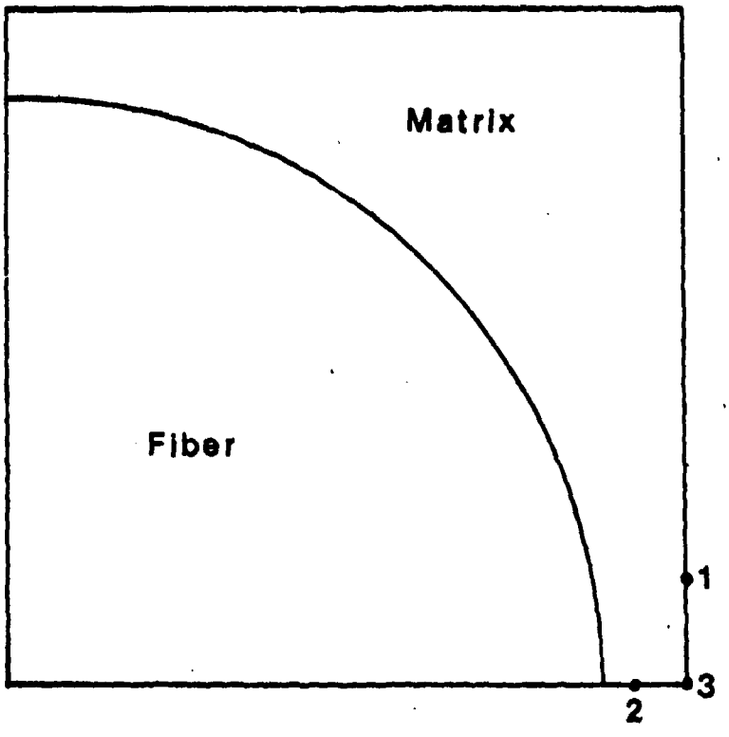

Figure 54. One Quadrant of a Typical Repeating Unit as Modeled by the Micromechanics Analysis, with Three Specific Points in a Region of Closest Fiber Spacing Being Identified

Figure 55 is a plot of the in-plane minimum principal stress in the S2 glass/3501-6 composite during moisture absorption, for Point 1 of Figure 54. Up to 1.5 percent moisture in the matrix material, added moisture tends to decrease the thermally-induced compressive stresses present from cooldown after the curing process. But additional moisture tends to put the matrix material into compression again, which indicates a limitation of expansion transverse to the fiber in this region. At the 3.5 percent moisture content, added moisture changes the slope of the minimum principal stress from negative to positive, indicating an increase in expansion due to moisture loading. In fact, the matrix material quickly goes into tension. That is, after a value of 3.5 percent moisture in the matrix, added moisture has a net positive effect because the added moisture tends to relieve any compressive forces rather than contribute to them.

Figure 56 is a plot of in-plane minimum principal stress present in the matrix material at Point 2 in Figure 54 versus weight percent moisture in the matrix. Again, the general effect is the same, i.e., the large tensile stress increase indicates a proportionally larger increase in composite strain. Figure 57 is the same type of plot for Point 3 of Figure 54. The effect is again the same as shown in the two previous plots. Figures 55 and 57 would be expected to be somewhat similar since both Points 1 and 3 in Figure 54 lie on an axis of symmetry of the repeating quadrant, while Point 2 in Figure 54 does not.

Therefore, it can be seen that an inordinate increase in minimum principal stresses in the region of closest fiber packing causes a correspondingly large increase in composite transverse strain. It should

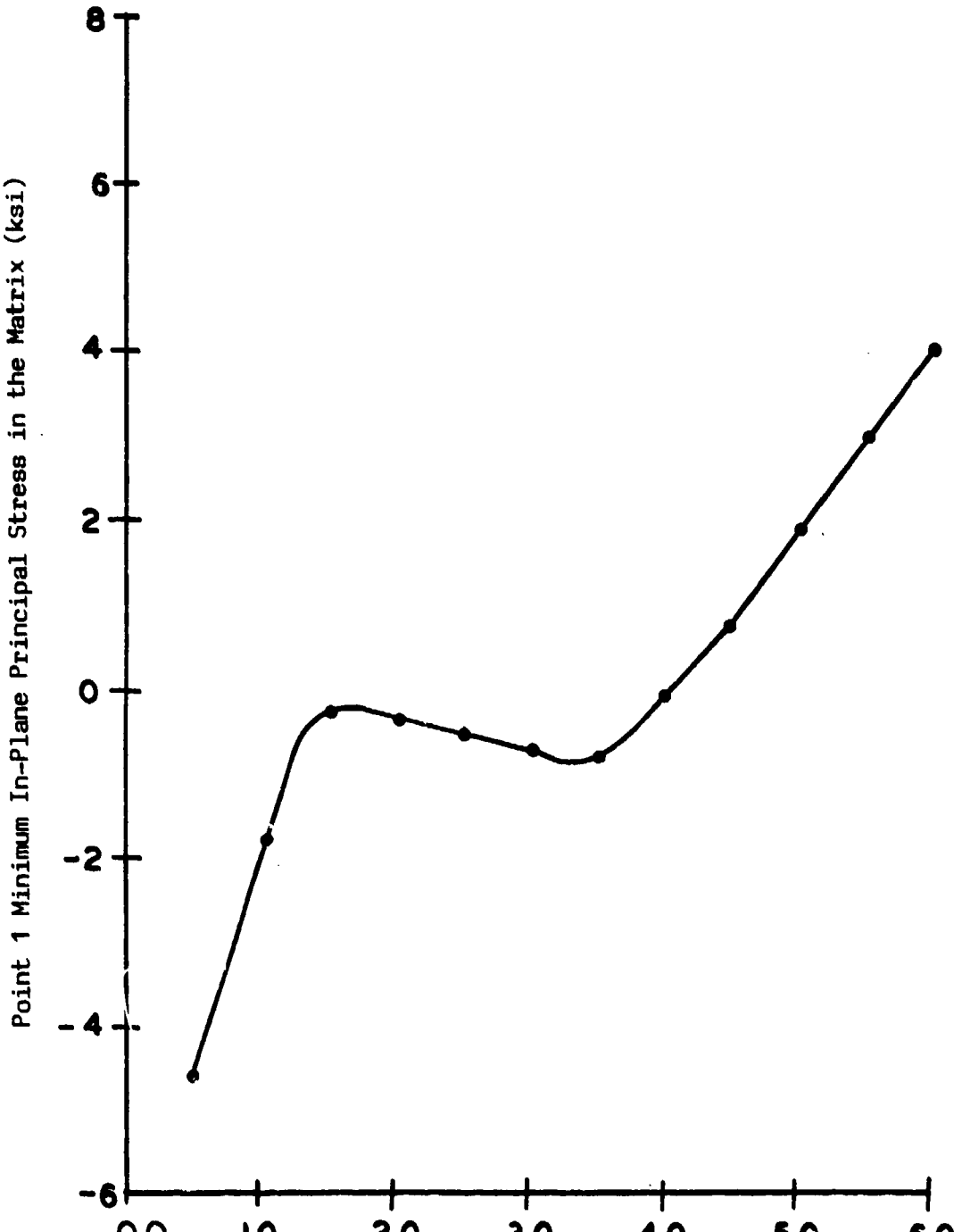

Figure 55. Minimum In-Plane Principal Stress in the Matrix of the S2 Glass/3501-6 Composite at Point 1 as Identified in Figure 54

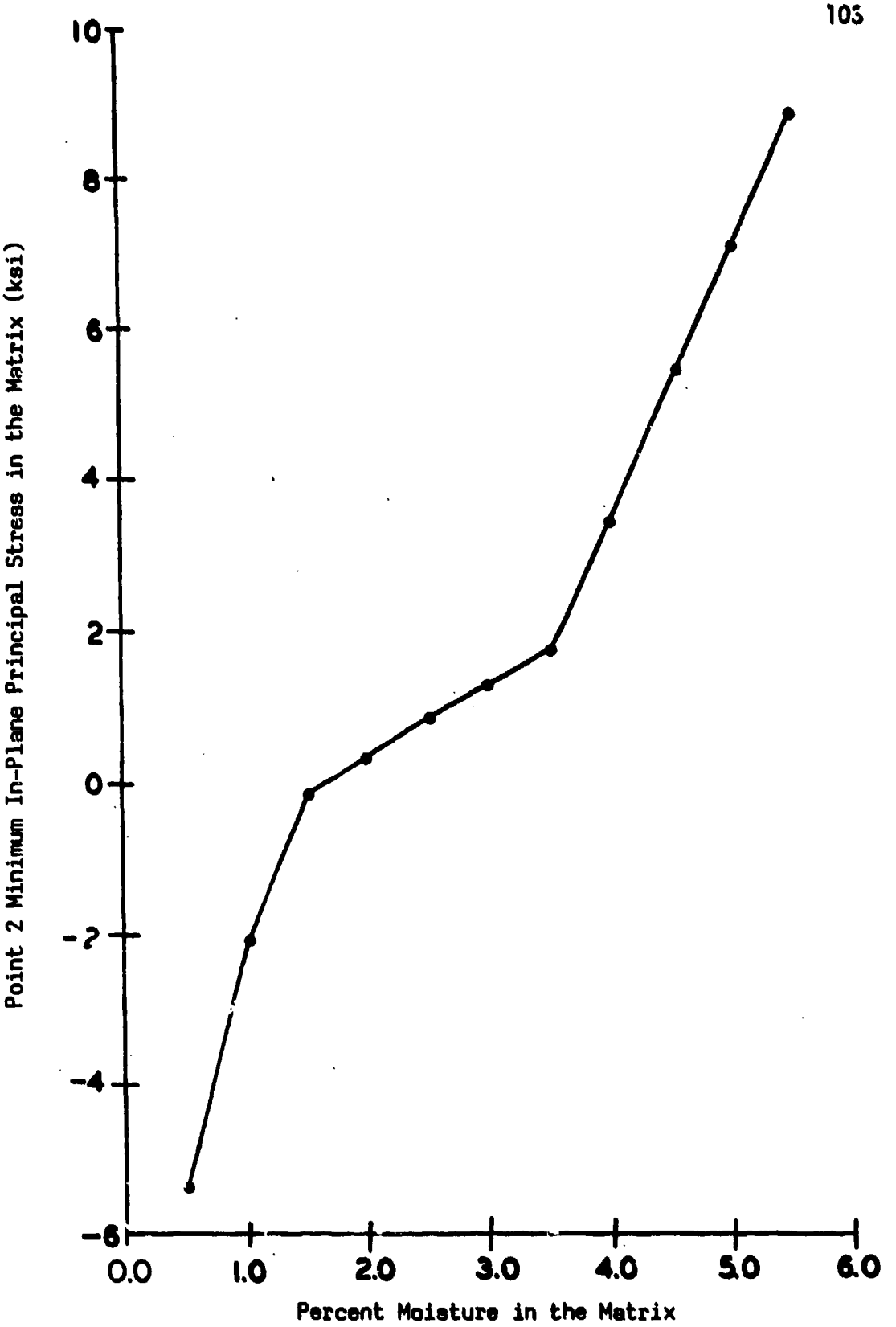

Figure 56. Minimum In-Plane Principal Stress in the Matrix of the S2 Glass/3501-6 Composite at Point 2 as Identified in Figure 54

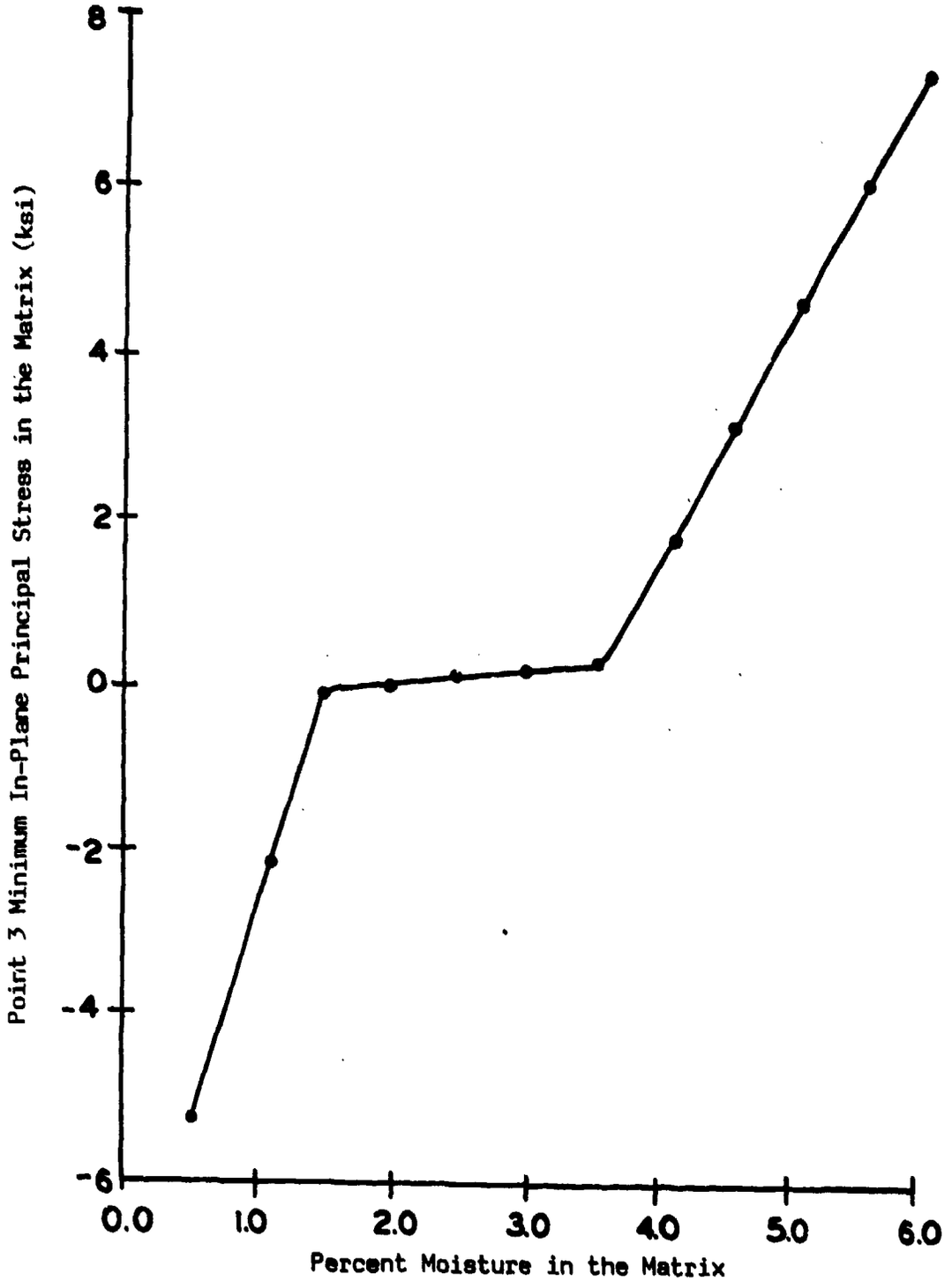

Figure 57. Minimum In-Plane Principal Stress in the Matrix of the S2 Glass/3501-6 Composite at Point 3 as Identified in Figure 54

be noted that this is a local effect. The bulk of the matrix material is in tension after cooldown from the curing temperature. After 1.5 percent moisture absorption of the matrix, the bulk of the matrix material then goes into compression.

The graphite/epoxy composite does not exhibit any of the above phenomena. The matrix material is in a much more uniform and homogeneous stress state. No inordinate changes in stress are seen with increasing moisture, which probably accounts for the far more linear transverse moisture expansion prediction compared to the S2 glass/epoxy predictions (Table 11).

The physical behaviors of S2 glass/epoxy discussed above (see Table 10) do not provide a complete explanation of the nonlinear transverse moisture expansion response observed. Much more analysis needs to be done in this area. It is significant, however, that both theory and experiment show the nonlinear moisture expansion behavior.

5.3.2 Thermal Expansion. The same approach used for the moisture expansion sensitivity studies was taken for the thermal expansion sensitivity studies. Each base constituent material property was first halved, then doubled. The same fiber volumes used for comparison in the moisture expansion sensitivity study were used in the thermal expansion sensitivity study. Comparisons of experimental data with influences of parametric variations of specific fiber and matrix properties generated by the micromechanics analysis for transverse thermal expansion will be presented in this section. Base values lie between the curves shown. In general, the predicted composite response is nonlinear over a wide temperature

range, following the same physical behavior as the 3501-6 epoxy resin. Figure 58 compares experimental data for thermal expansion of unconditioned (dry) AS/3501-6 composites in the transverse direction.

Plots of theoretical predictions using both matrix shear data and tensile data show, once again, little difference. The micromechanics predictions do not agree particularly well with the experimental data, however. Figure 59 shows the influence of the Poisson's ratio of the matrix on the AS/3501-6 transverse thermal expansion in its unconditioned state. The Poisson's ratio of the matrix has a significant influence on the composite behavior, as was also seen for the composite moisture expansion behavior.

Figure 60 shows the effect of fiber volume on thermally-induced transverse strain for the dry AS/3501-6 composite. This effect is also large. The transverse Poisson's ratio of the fiber in an unconditioned AS/3501-6 specimen does not have a significant effect, however, as shown in Figure 61. Likewise, the transverse modulus of the fiber has little influence (see Figure 62).

The coefficient of thermal expansion in the transverse direction of the graphite fiber was shown to have little influence on the moisture-induced strain. This is certainly not the case in the predictions of transverse thermal expansion of the unconditioned AS/3501-6. Figure 63 shows this effect, which is significant. This is as expected since any change in the transverse thermal expansion of the fiber would have an influence on the overall transverse thermal expansion of the composite.

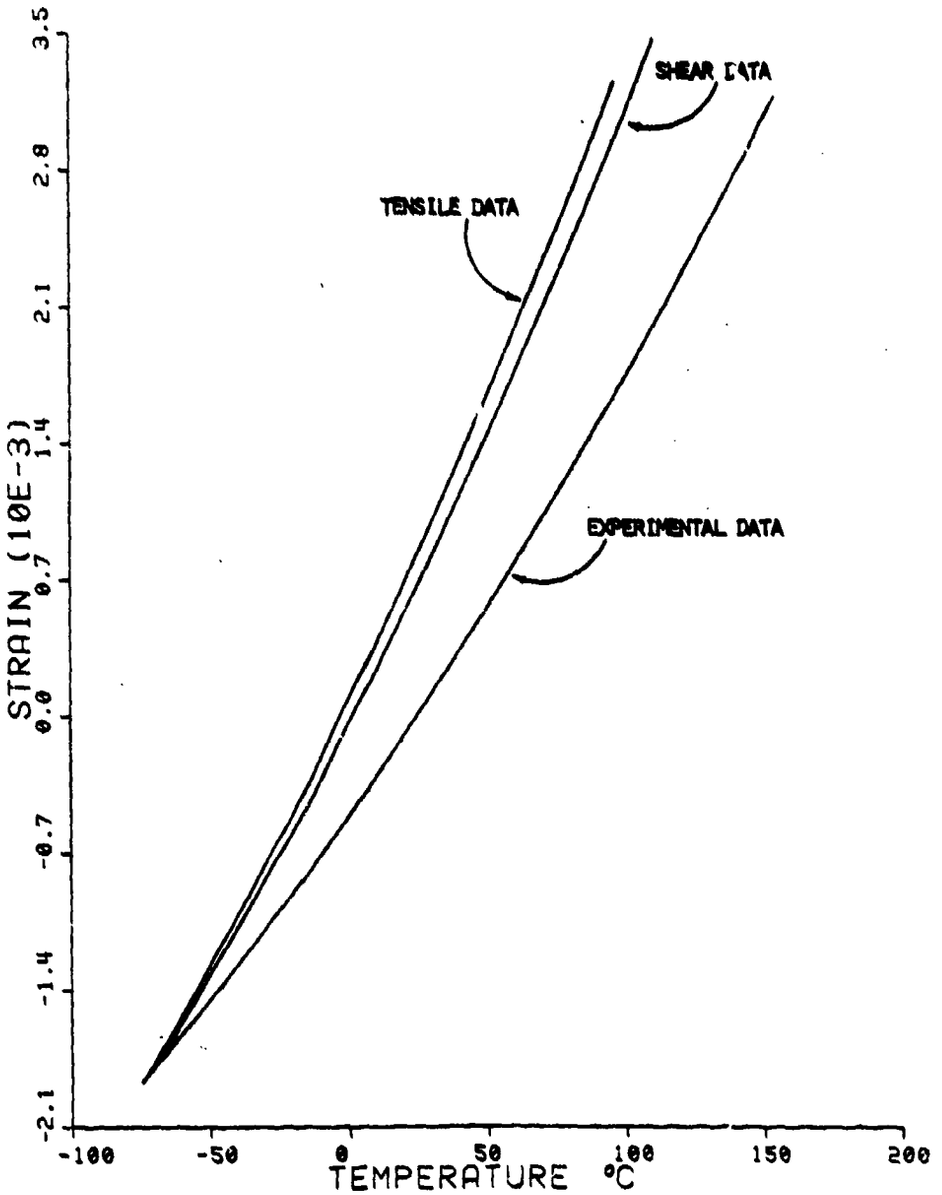

Figure 58. Unconditioned Micromechanics Predictions of Thermal Expansion of the AS/3501-6 Composite in the Transverse Direction

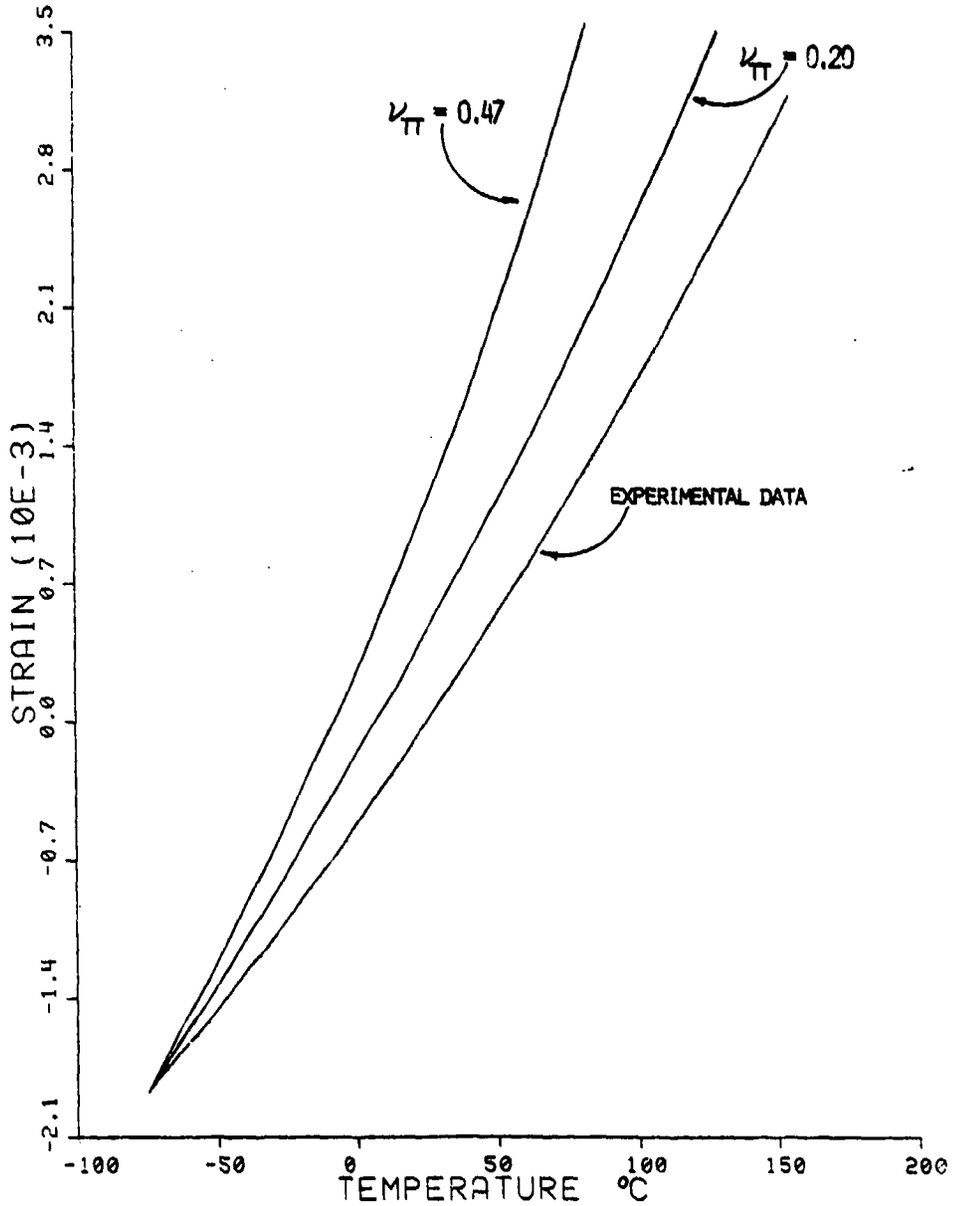

Figure 59. Unconditioned Transverse Thermal Expansion Sensitivity to Poisson's Ratio of the Matrix for AS/3501-6 Graphite/Epoxy (Base Value of Matrix ν_{TT} = 0.34)

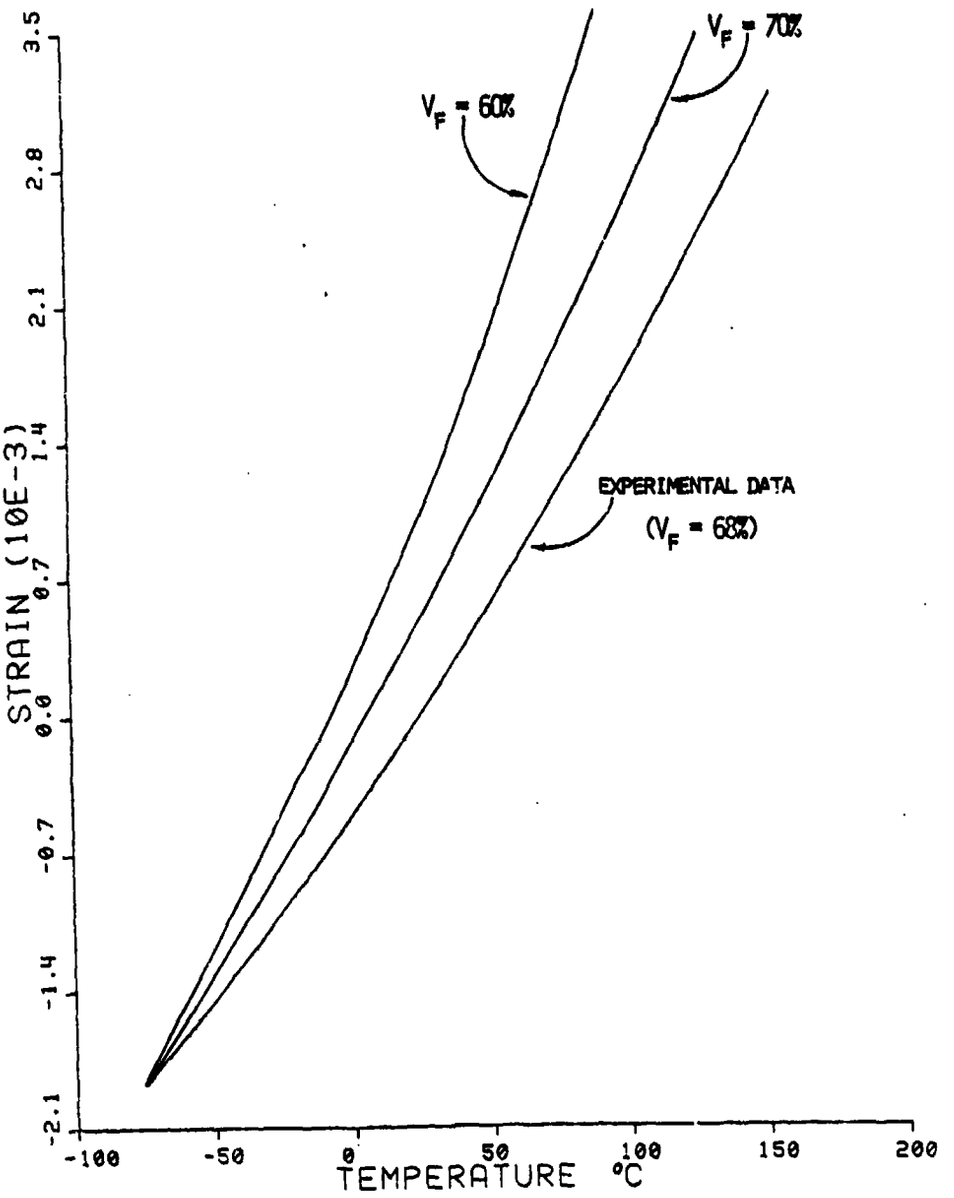

Figure 60. Unconditioned Transverse Thermal Expansion Sensitivity to Fiber Volume for AS/3501-6 Graphite/Epoxy

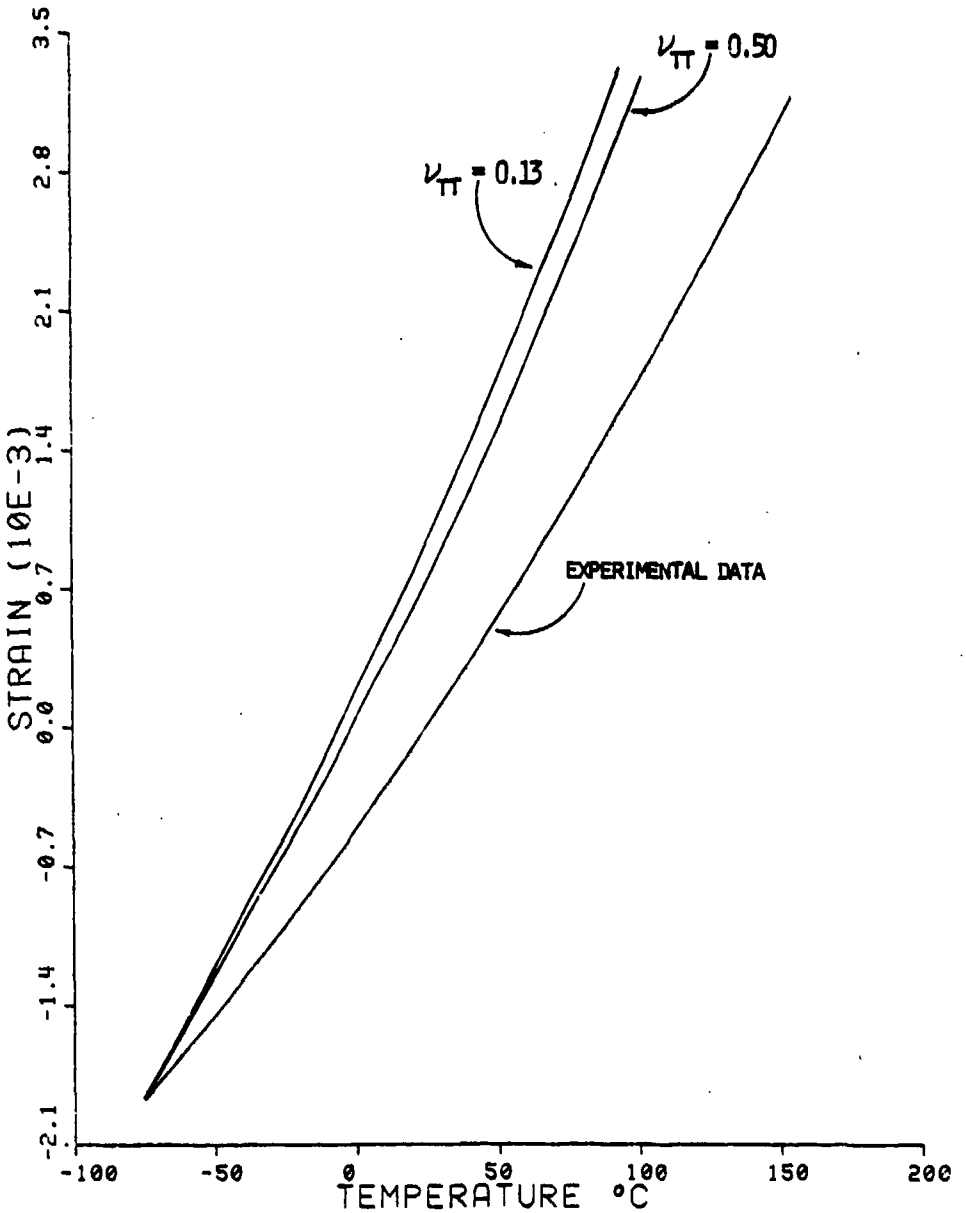

Figure 61. Unconditioned Transverse Thermal Expansion Sensitivity to In-Plane Poisson's Ratio for AS/3501-6 Graphite/Epoxy (Base Value of Fiber ν_{TT} = 0.25)

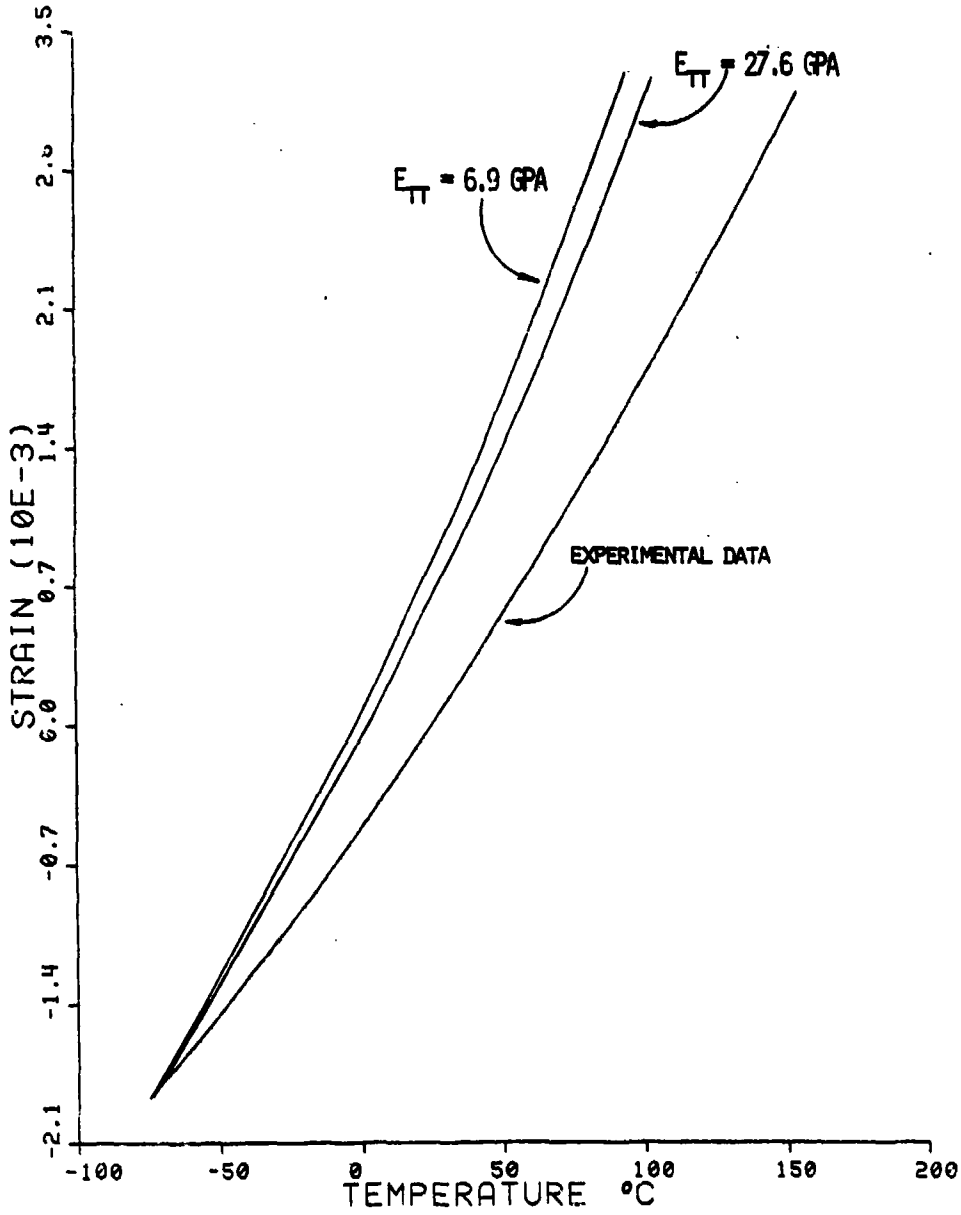

Figure 62. Unconditioned Transverse Thermal Expansion Sensitivity to Transverse Modulus of the Fiber for AS/3501-6 (E_{TT} = 13.8 GPa)

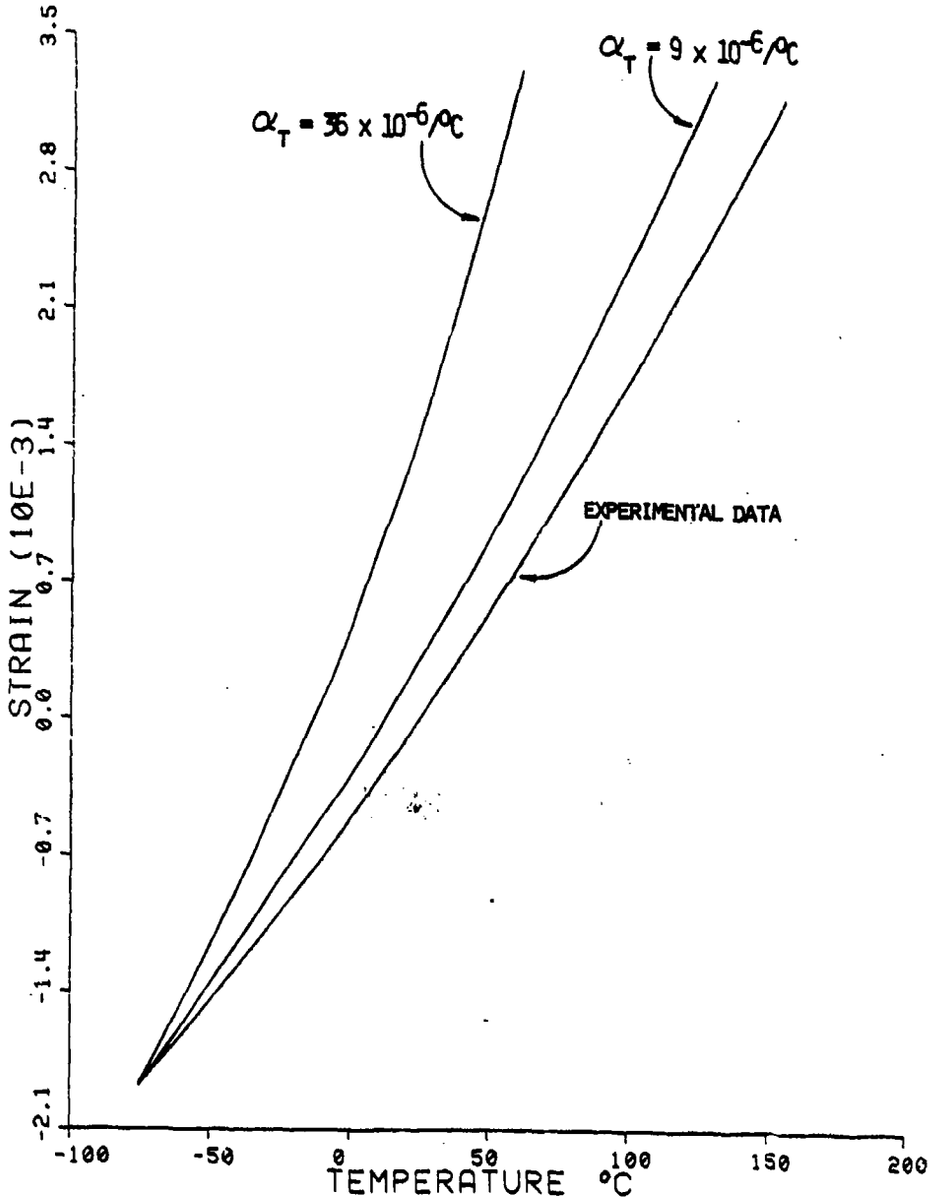

Figure 63. Unconditioned Transverse Thermal Expansion Sensitivity to Transverse Thermal Expansion of the Fiber for AS/3501-6 Graphite/Epoxy (Base Value $\alpha_T = 18 \times 10^{-6}/°C$)

After conditioning, the composites were found to exhibit different characteristics for thermal expansion in the transverse direction. The micromechanics predictions for moisture-conditioned AS/3501-6 graphite/epoxy specimens are shown in Figure 64. Results using both matrix shear data and tensile data are presented. In both cases, the correlation with the experimental data is rather poor. Figure 65 shows the micromechanics predictions of the influence of Poisson's ratio of the matrix on the transverse moisture expansion of the moisture-conditioned AS/3501-6 composite. While the effect is large, it appears to be less than the effect on moisture expansion (Figure 43), and unconditioned transverse thermal expansion (Figure 58).

Fiber volumes, however, do have a significant influence, as shown in Figure 66. The transverse Poisson's ratio and the transverse modulus of the fiber are seen to have relatively little influence on the transverse thermal expansion of the composite, as presented in Figures 67 and 68, respectively. Again, in general, a decrease of in-plane fiber modulus makes the thermal expension higher because with any increase in stress a higher strain is seen. The transverse thermal expansion of a graphite fiber has a significant influence on the moisture-conditioned AS/3501-6 composite transverse thermal strain, as seen in Figure 69. The effect is similar to the dry AS/3501-6 thermal expansion (Figure 63), noted previously.

Parametric sensitivities were also conducted for the S2 glass/3501-6 transverse thermal expansion. Figure 70 presents the micromechanics predictions of unconditioned S2 glass/3501-6 composite transverse thermal strain. Results using both tensile and shear data for the matrix are

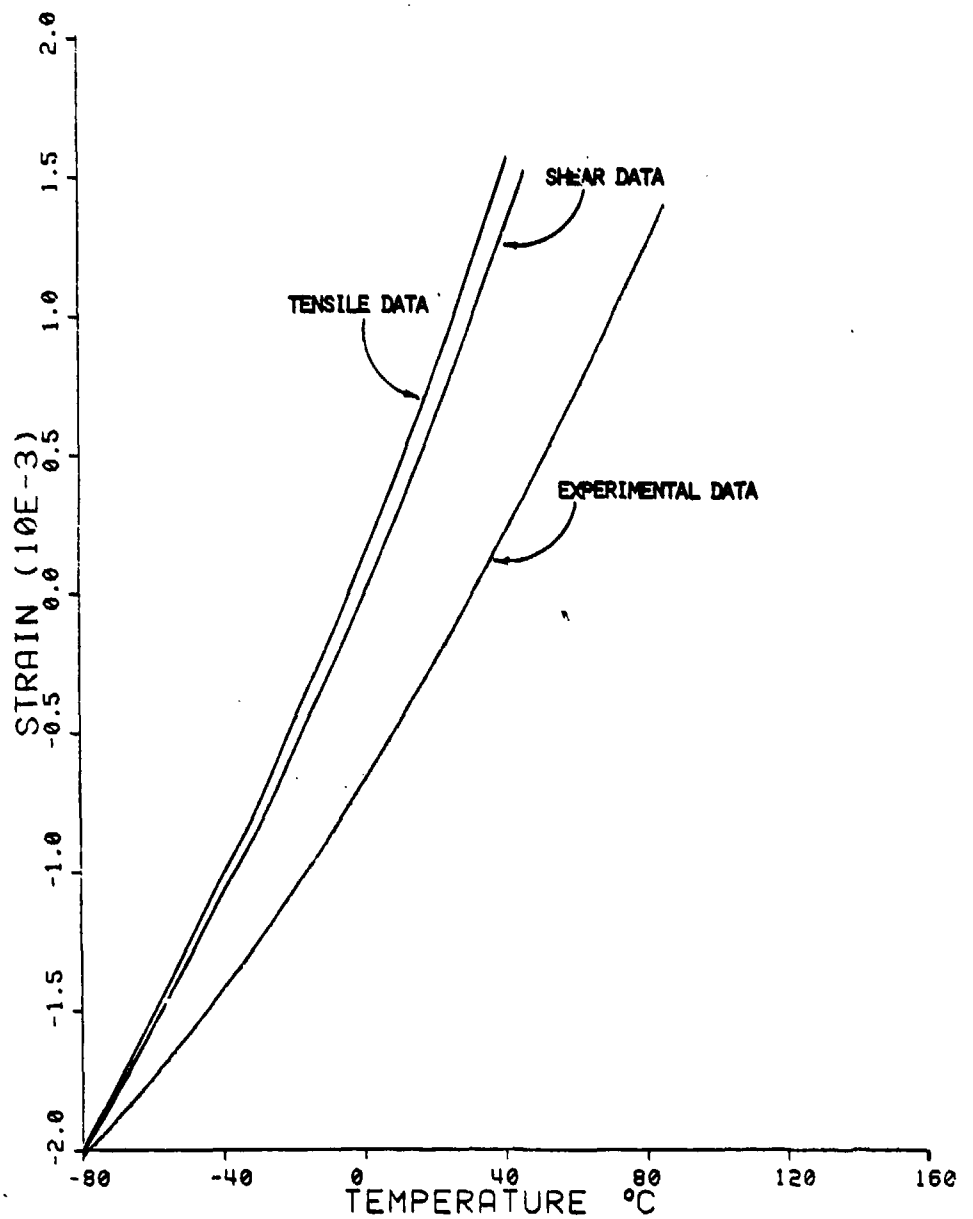

Figure 64. Moisture Conditioned Micromechanics Predictions of Thermal Expansion for AS/3501-6 Graphite/Epoxy in the Composite Transverse Direction

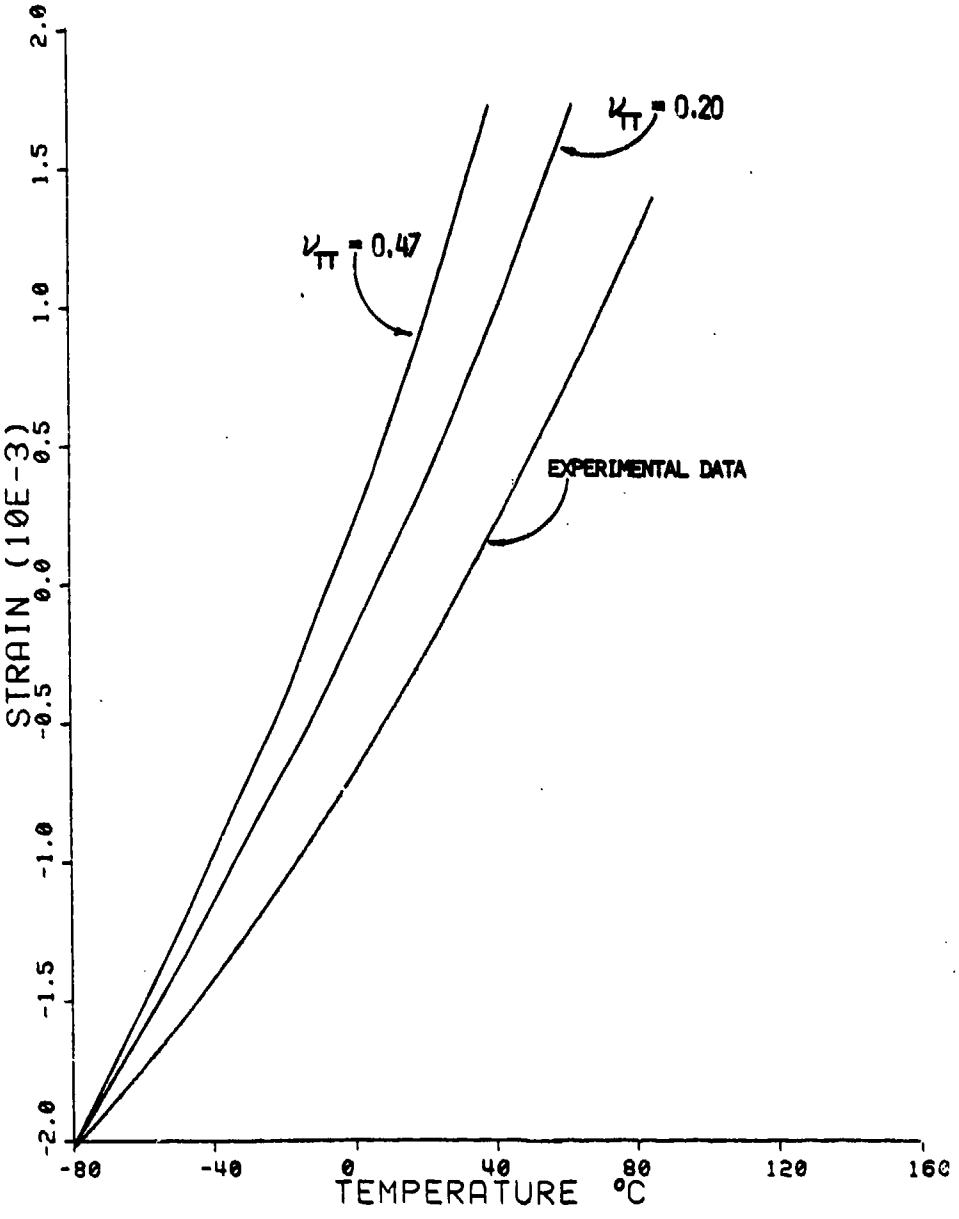

Figure 65. Moisture Conditioned Transverse Thermal Expansion Sensitivity to Poisson's Ratio of the Matrix for AS/3501-6 Graphite Epoxy (Base Value of Matrix ν_{TT} = 0.34)

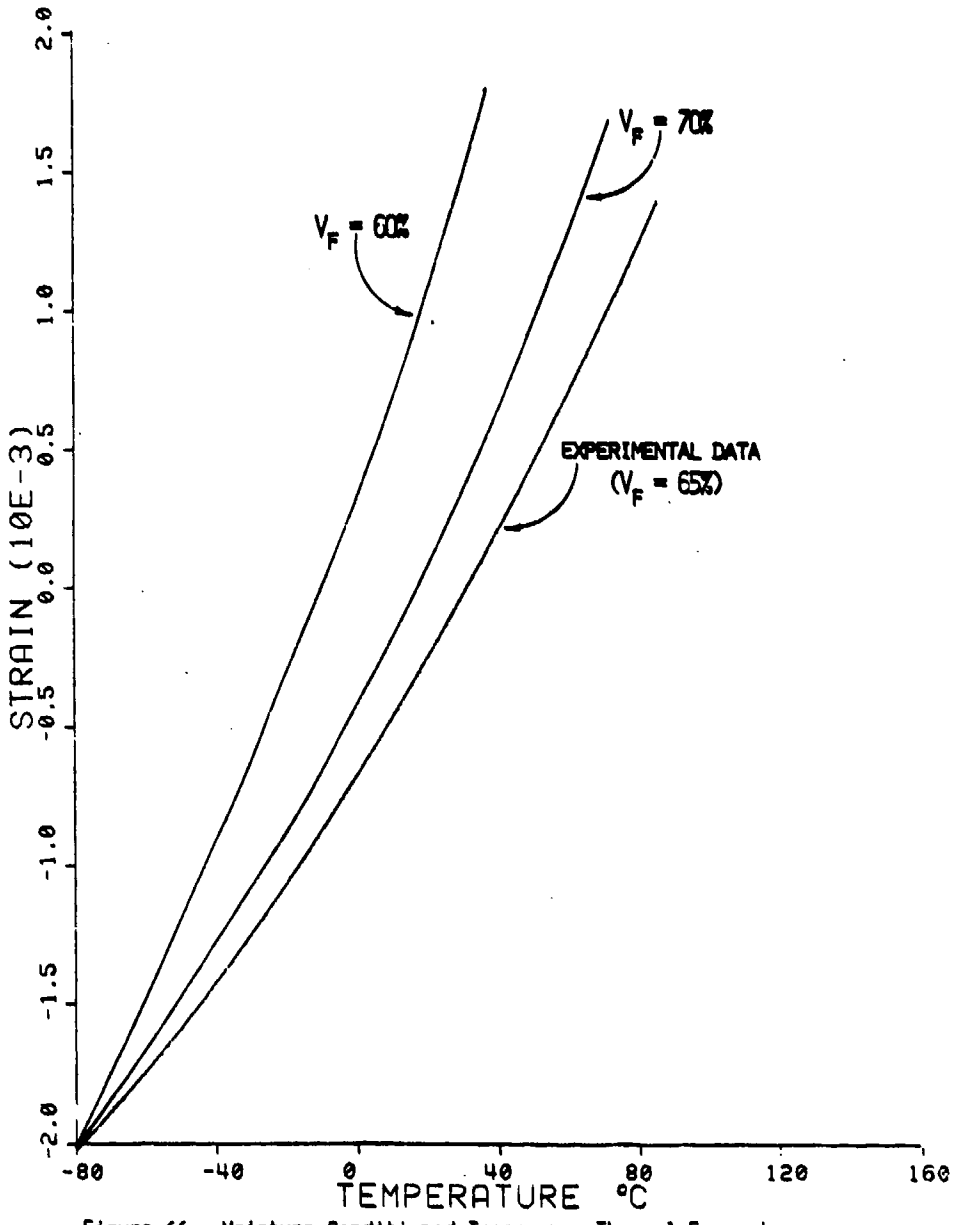

Figure 66. Moisture Conditioned Transverse Thermal Expansion Sensitivity to Fiber Volume for AS/3501-6 Graphite/Epoxy

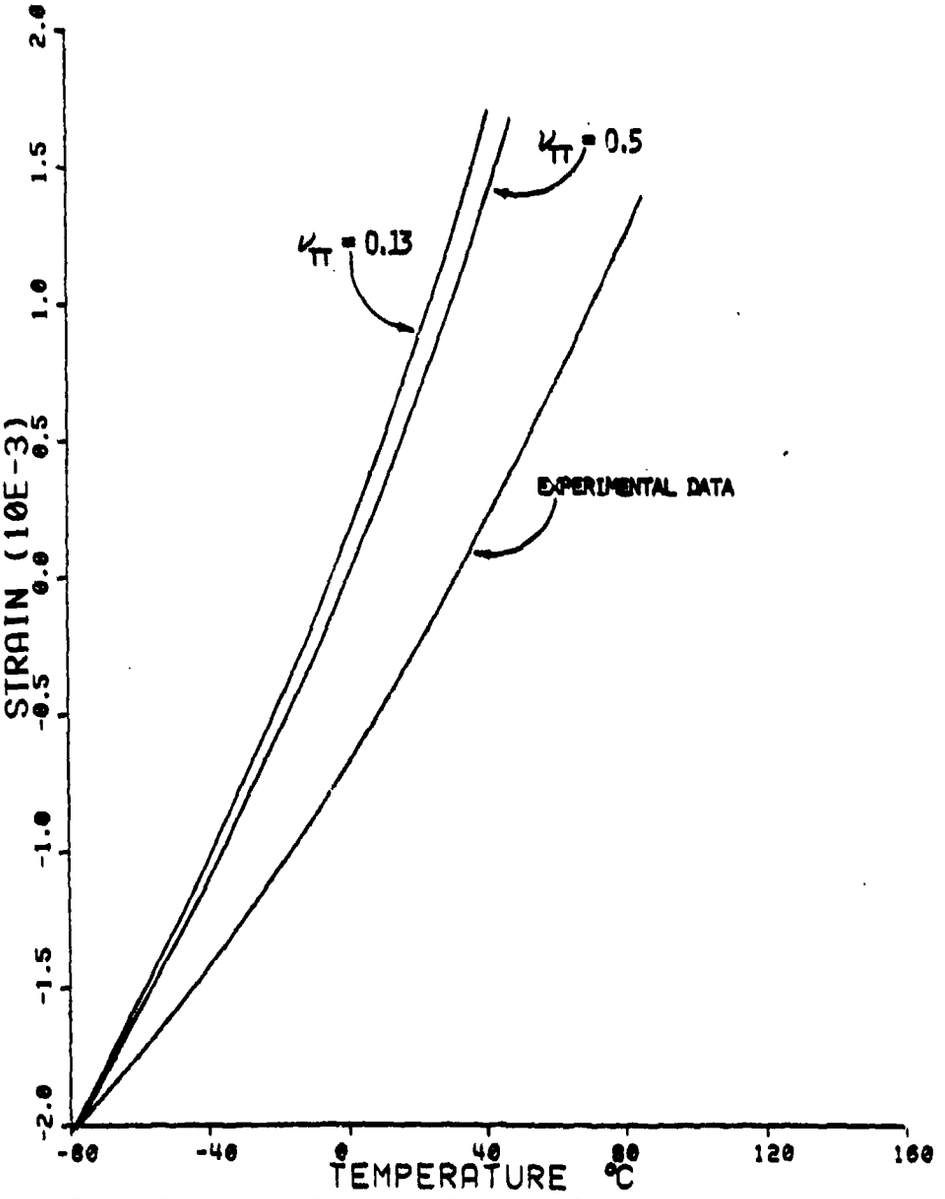

Figure 67. Moisture Conditioned Transverse Thermal Expansion Sensitivity to In-Plane Poisson's Ratio of the Fiber for AS/3501-6 Graphite/Epoxy (Base Value ν_{TT} = 0.25)

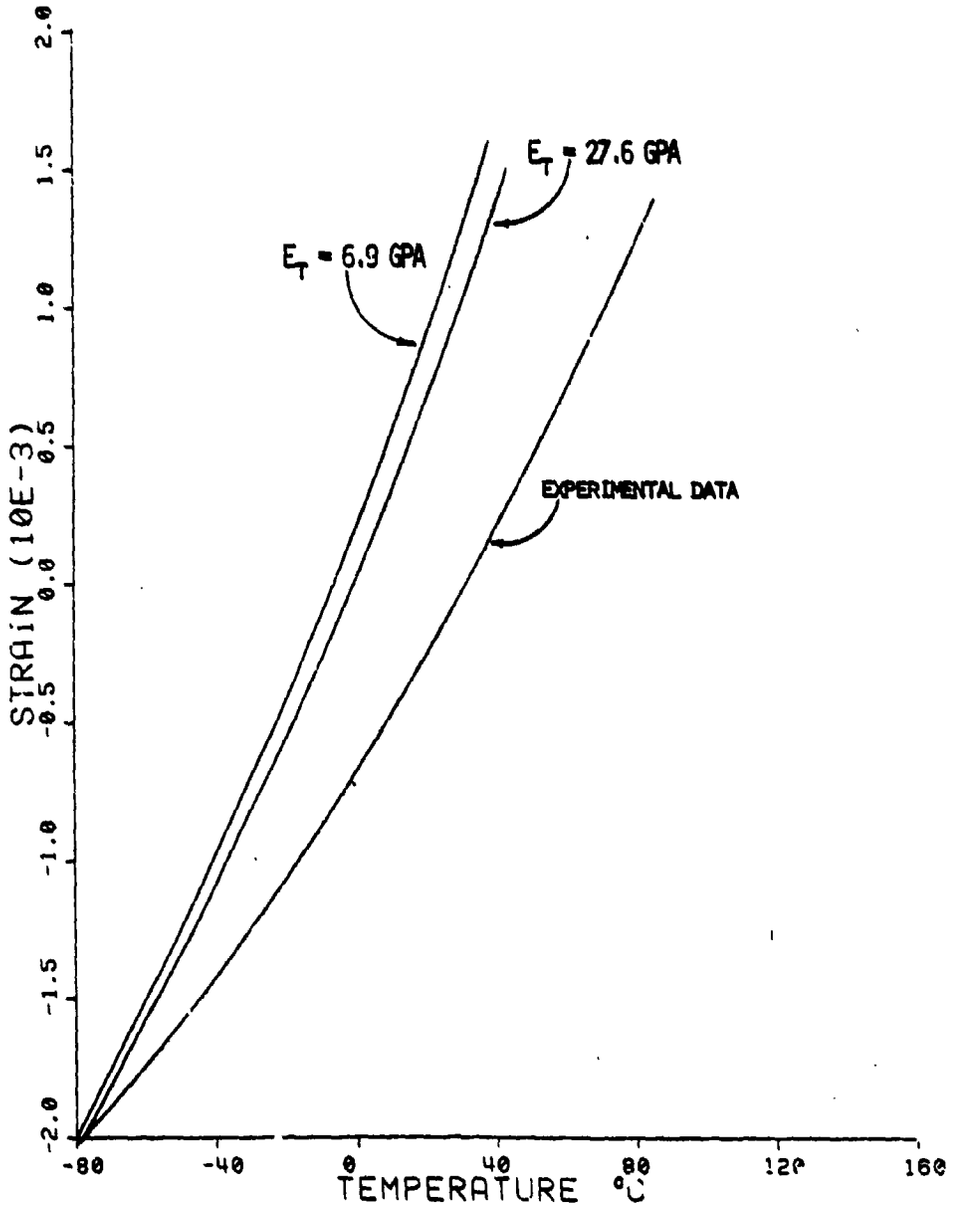

Figure 68. Moisture Conditioned Transverse Thermal Expansion Sensitivity to Transverse Young's Modulus of the Fiber for AS/3501-6 Graphite/Epoxy (Base Value E_T = 13.8 GPa)

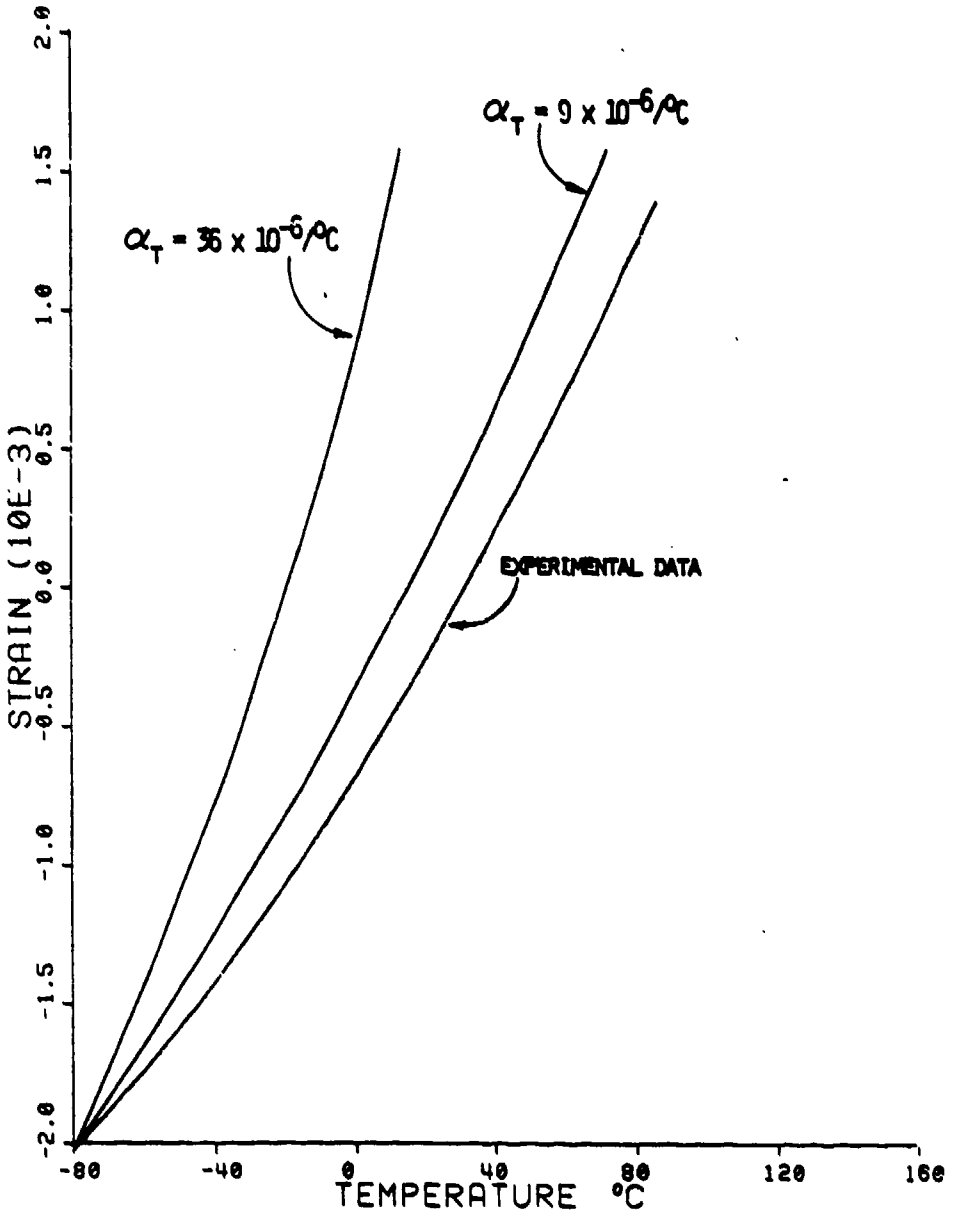

Figure 69. Moisture Conditioned Transverse Thermal Expansion Sensitivity to Transverse Thermal Expansion of the Fiber for AS/3501-6 Graphite/Epoxy (Base Value α_T = 18 x 10^{-6}/°C)

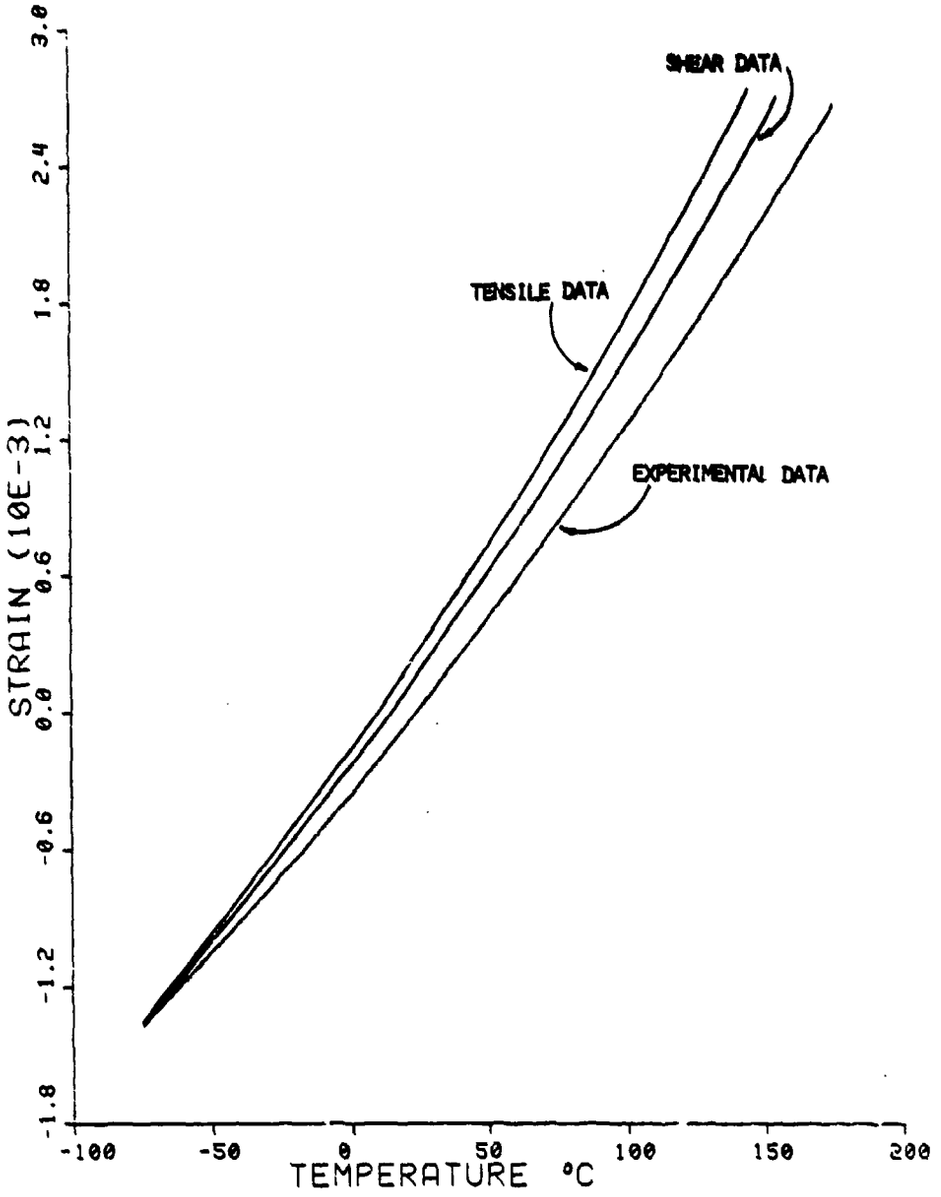

Figure 70. Unconditioned Micromechanics Predictions of Thermal Expansion for S2 Glass/3501-6 Glass/Epoxy in the Transverse Composite Direction

shown. It will be noted that these predicted results correlate much better with the experimental data than the AS/3501-6 transverse thermal expansion corresponded to experimental data (Figure 58). The sensitivity to Poisson's ratio of the matrix of the S2 glass/3501-6 composite is shown in Figure 71. This influence appears to be more pronounced than it was in the unconditioned AS/3501-6 parametric study (Figure 59).

Fiber volume also has a significant influence on the composite behavior, as seen in Figure 72. It will be noted that, again, the range of fiber volume considered for this sensitivity study of the S2 glass/3501-6 composite is greater than the range of fiber volume assumed for the AS/3501-6 composite.

The unconditioned S2 glass/3501-6 is not particularly sensitive to changes of the Poisson's ratio or transverse modulus of the fiber, as seen in Figures 73 and 74, respectively. The transverse thermal expansion of the unconditioned S2 glass/3501-6 is very sensitive to the transverse thermal expansion, however, as shown in Figure 75.

The sensitivity of the S2 glass/3501-6 composites to material constituent properties after moisture conditioning were also conducted. Composite response to tensile and shear data of the matrix is shown in Figure 76. While correlation with the experimental data is not quite as close as was shown for the unconditioned S2 glass/3501-6 (see Figure 70), it is still generally good.

The sensitivity of transverse thermal expansion to the Poisson's ratio of the matrix for conditioned S2 glass/3501-6 composites is shown in Figure 77. A relatively large effect is seen. The sensitivity to fiber volume for transverse thermal expansion of S2 glass/3501-6 composite is found to be large in Figure 78.

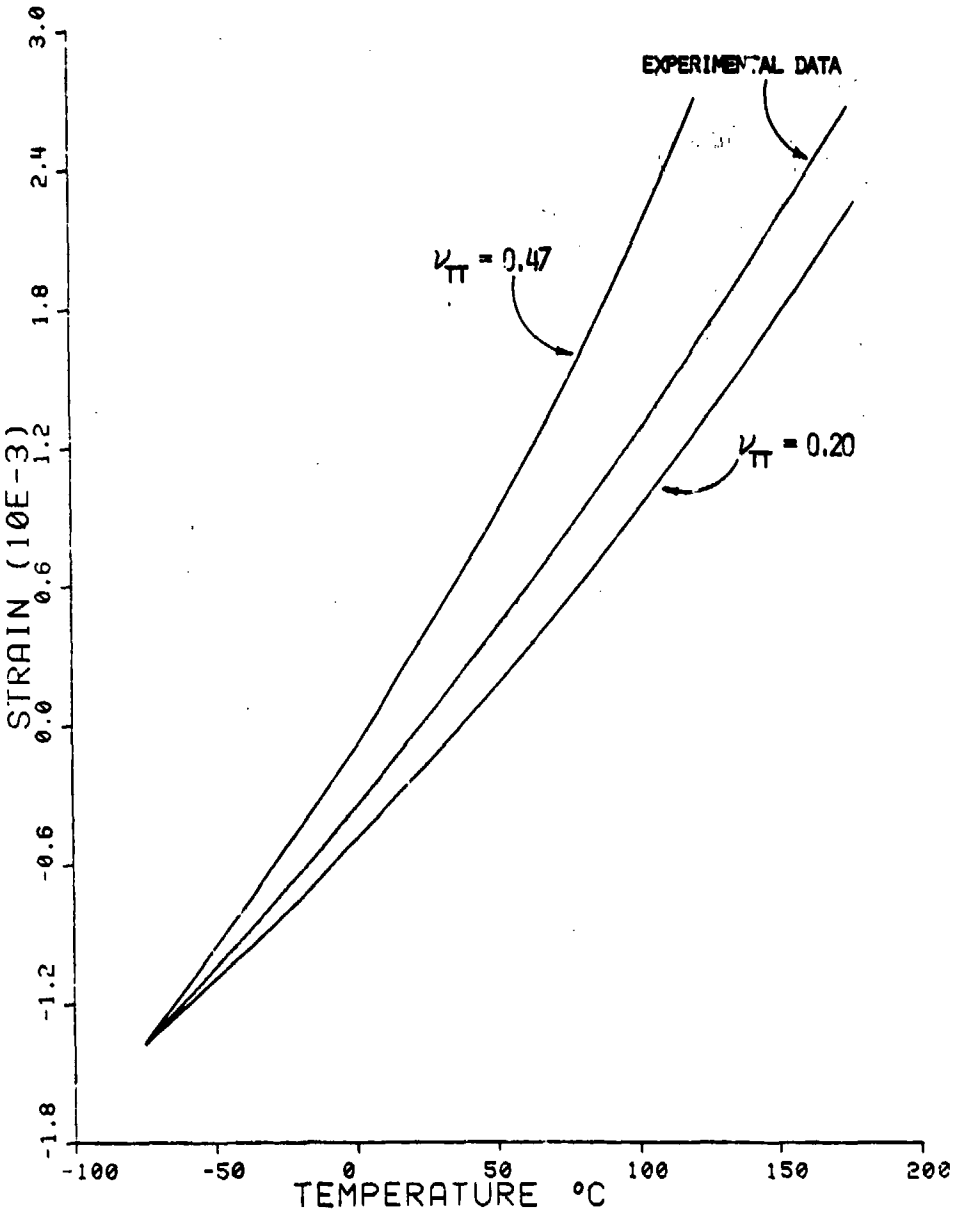

Figure 71. Unconditioned Transverse Thermal Expansion Sensitivity to Poisson's Ratio of the Matrix for S2 Glass/3501-6 Glass/Epoxy (Base Value of Matrix ν_{TT} = 0.34)

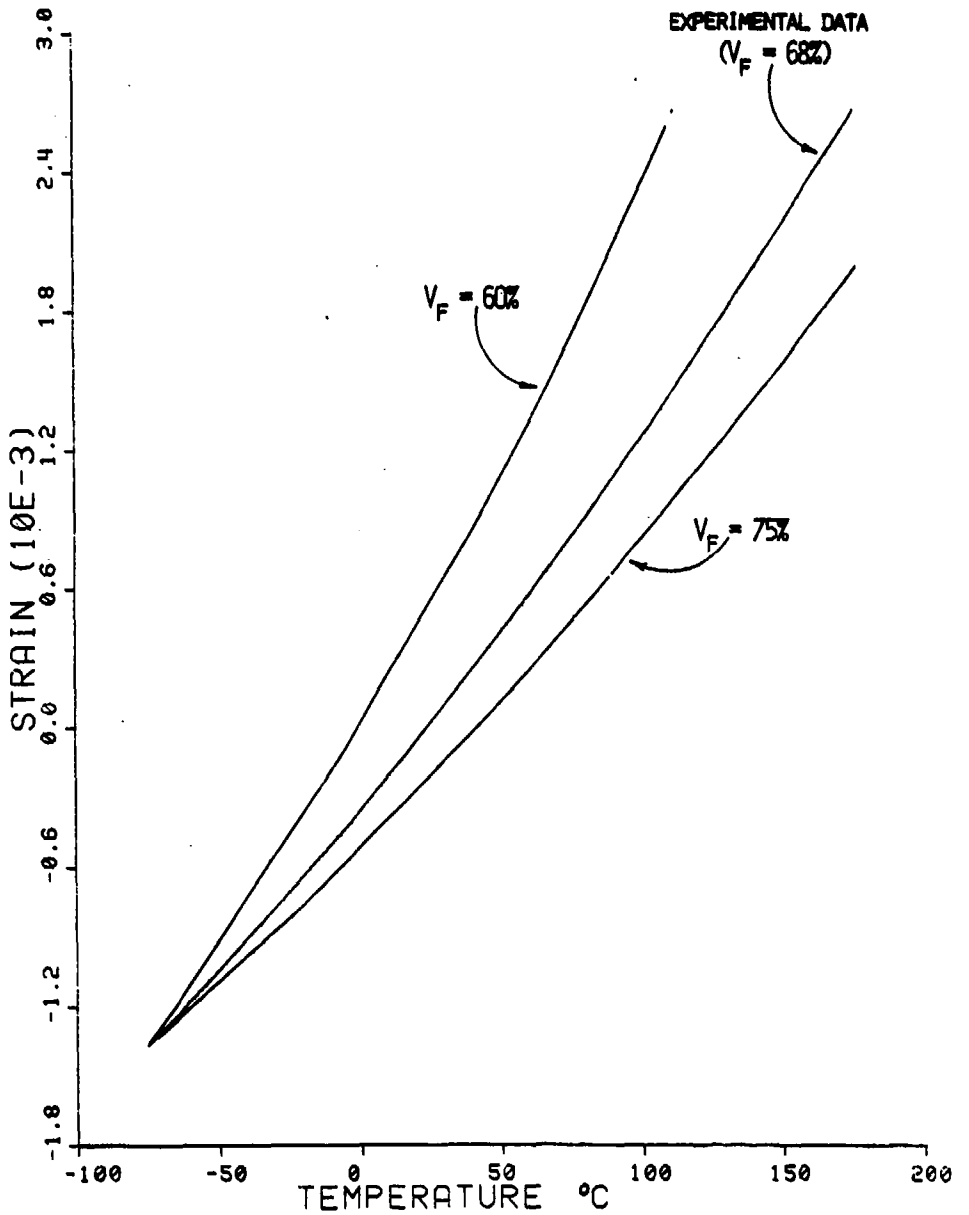

Figure 72. Unconditioned Transverse Thermal Expansion Sensitivity to Fiber Volume for S2 Glass/3501-6 Glass/Epoxy

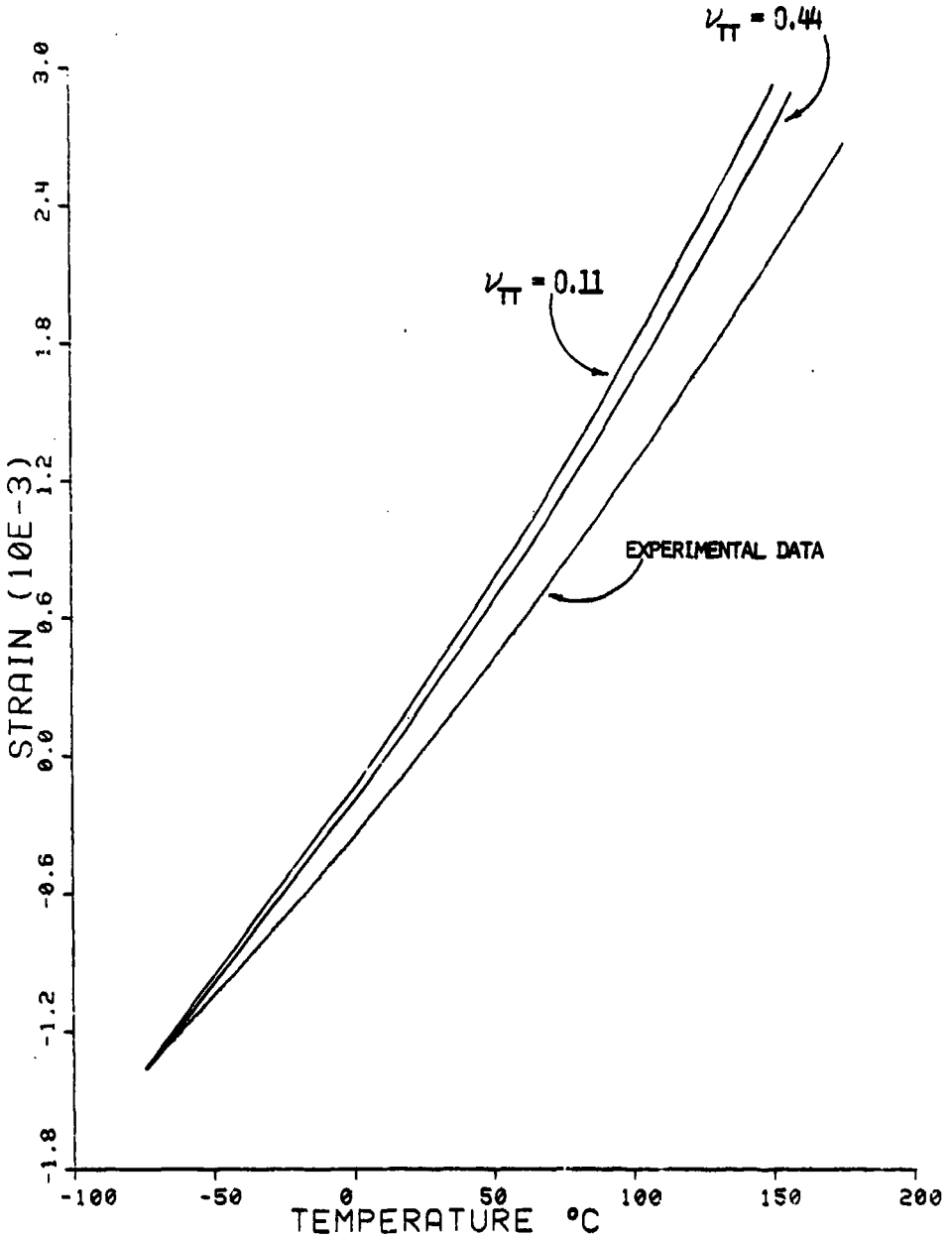

Figure 73. Unconditioned Transverse Thermal Expansion Sensitivity to Poisson's Ratio of the Fiber for S2 Glass/3501-6 Glass/Epoxy (Base Value of the Fiber ν_{TT} = 0.22)

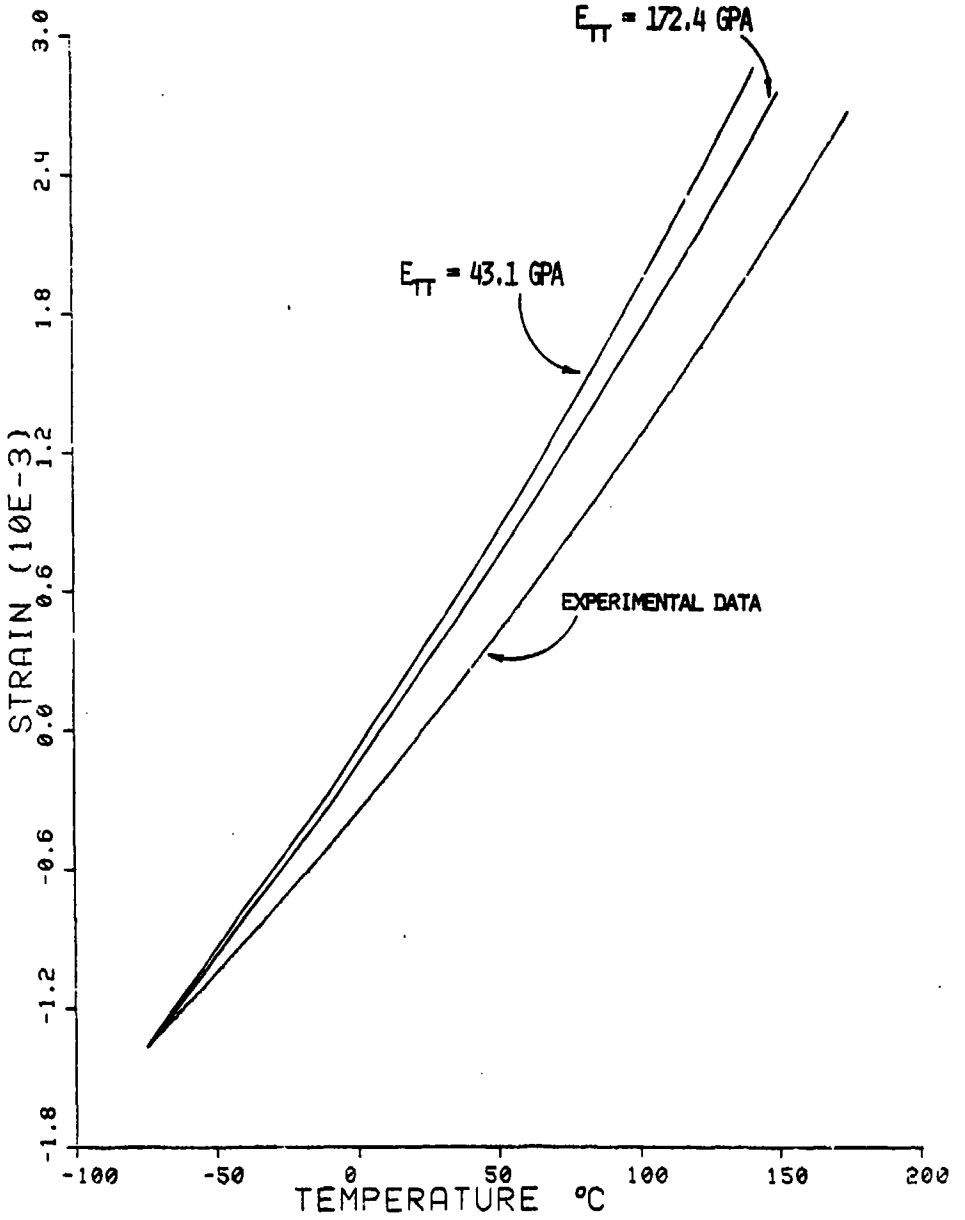

Figure 74. Unconditioned Transverse Thermal Expansion Sensitivity to Young's Modulus of the Fiber for S2 Glass/3501-6 Glass/ Epoxy (Base Value E_{TT} = 86.2 GPa)

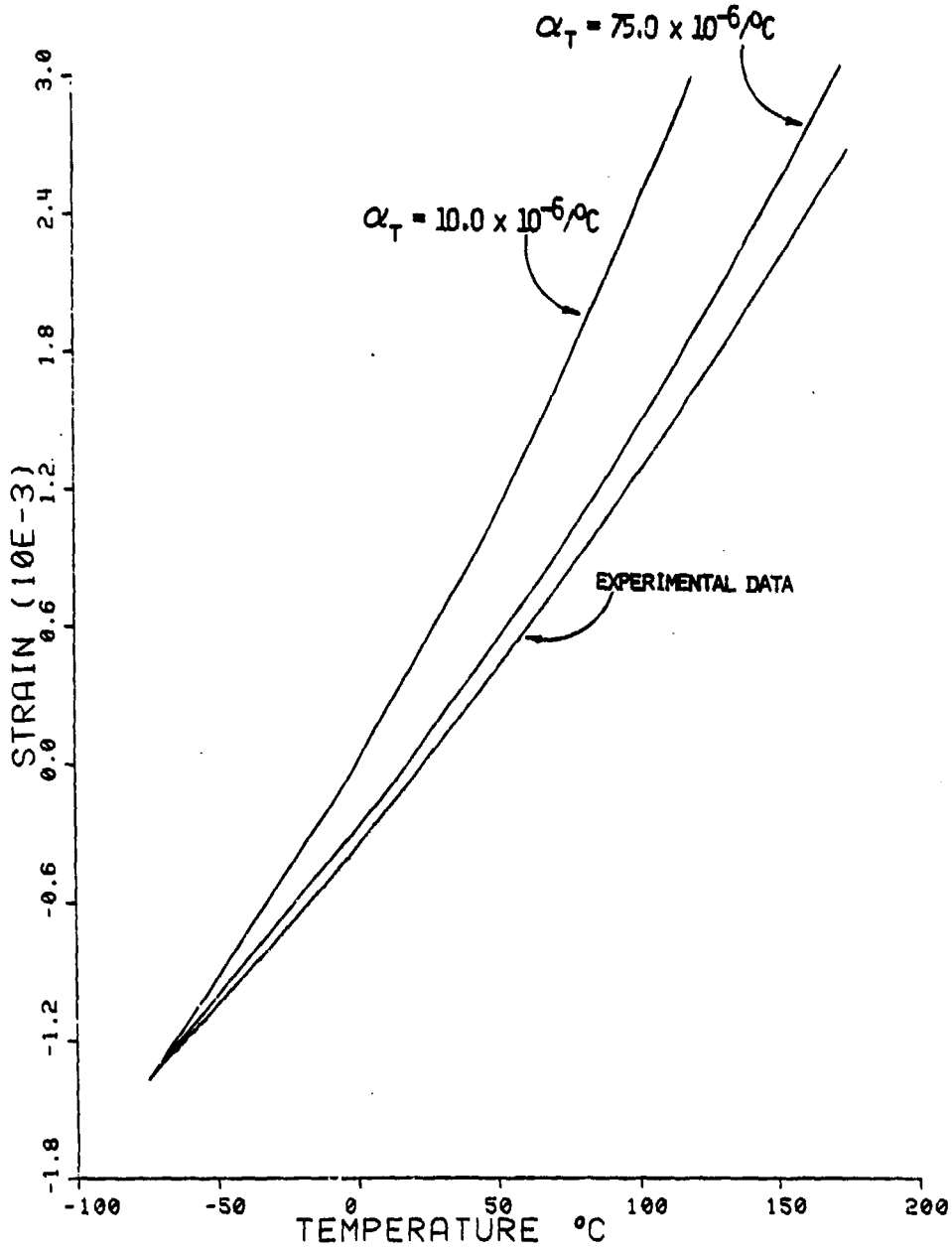

Figure 75. Unconditioned Transverse Thermal Expansion Sensitivity to Thermal Expansion of the Fiber for S2 Glass/3501-6 Glass/Epoxy (Base Value α_T = 5.0 x 10^{-6}/°C)

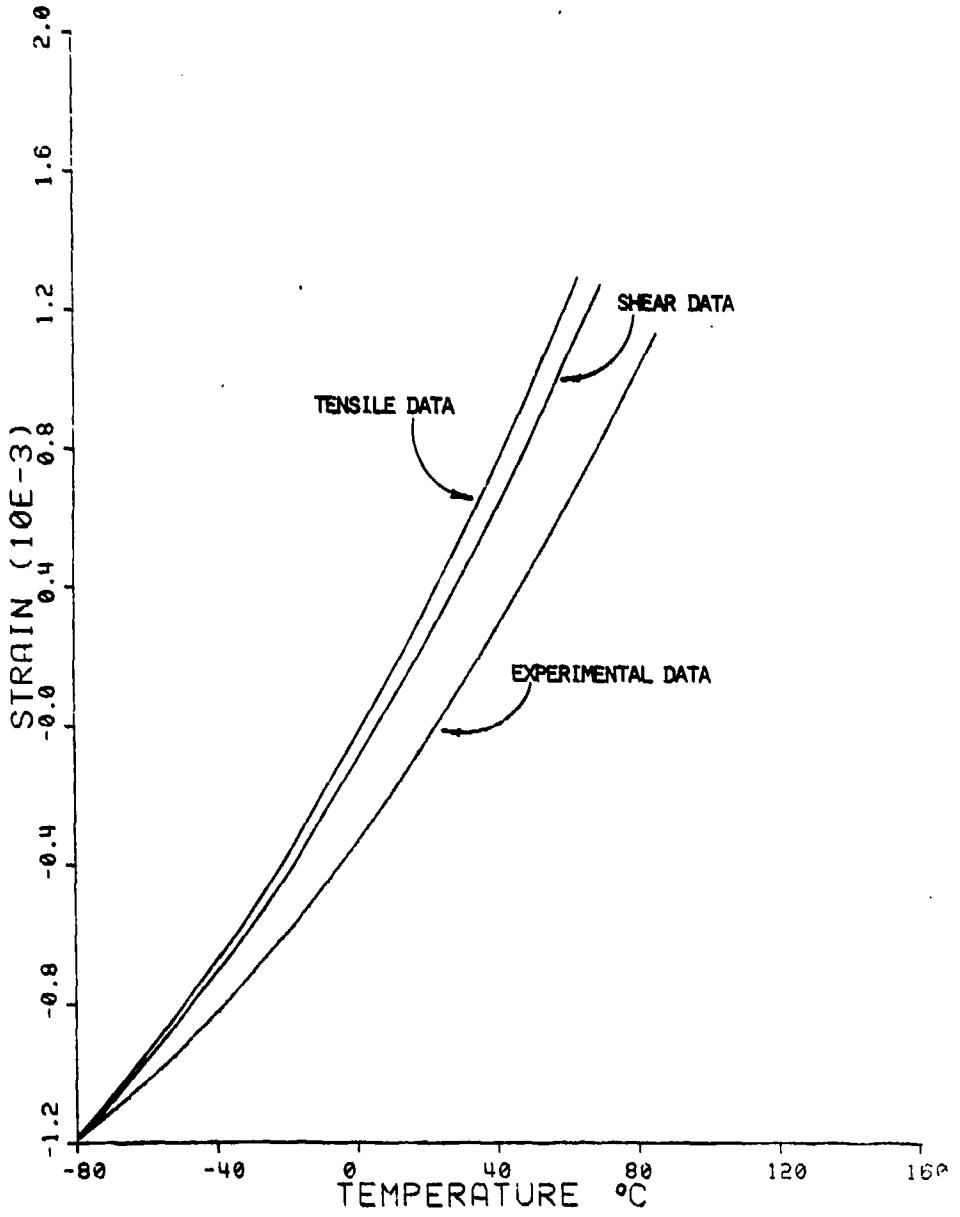

Figure 76. Moisture Conditioned Micromechanics Predictions of Thermal Expansion for S2 Glass/3501-6 Glass/Epoxy in the Composite Transverse Direction

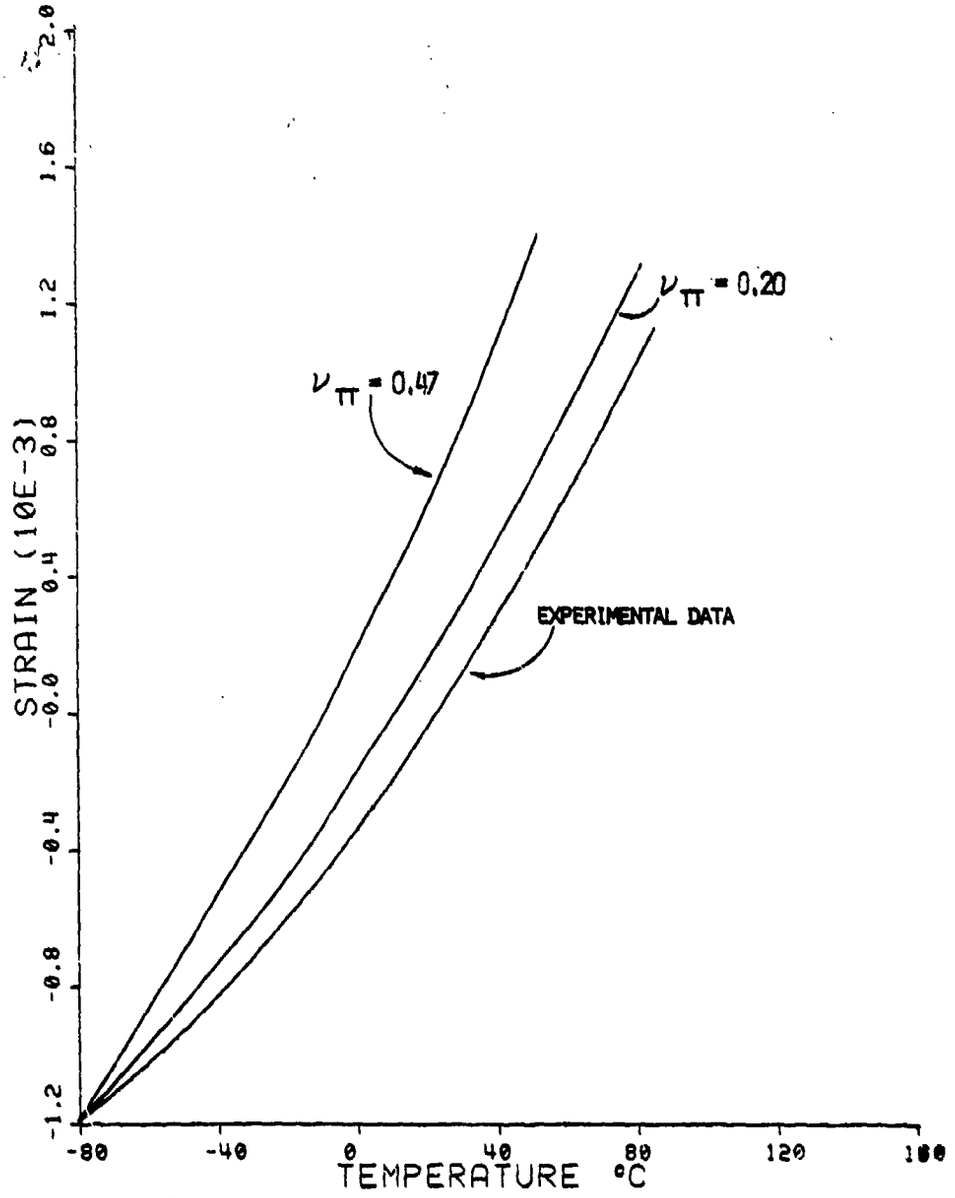

Figure 77. Moisture Conditioned Transverse Thermal Expansion Sensitivity to Poisson's Ratio of the Matrix for S2 Glass/3501-6 Glass/Epoxy (Base Value of Matrix ν_{TT} = 0.34)

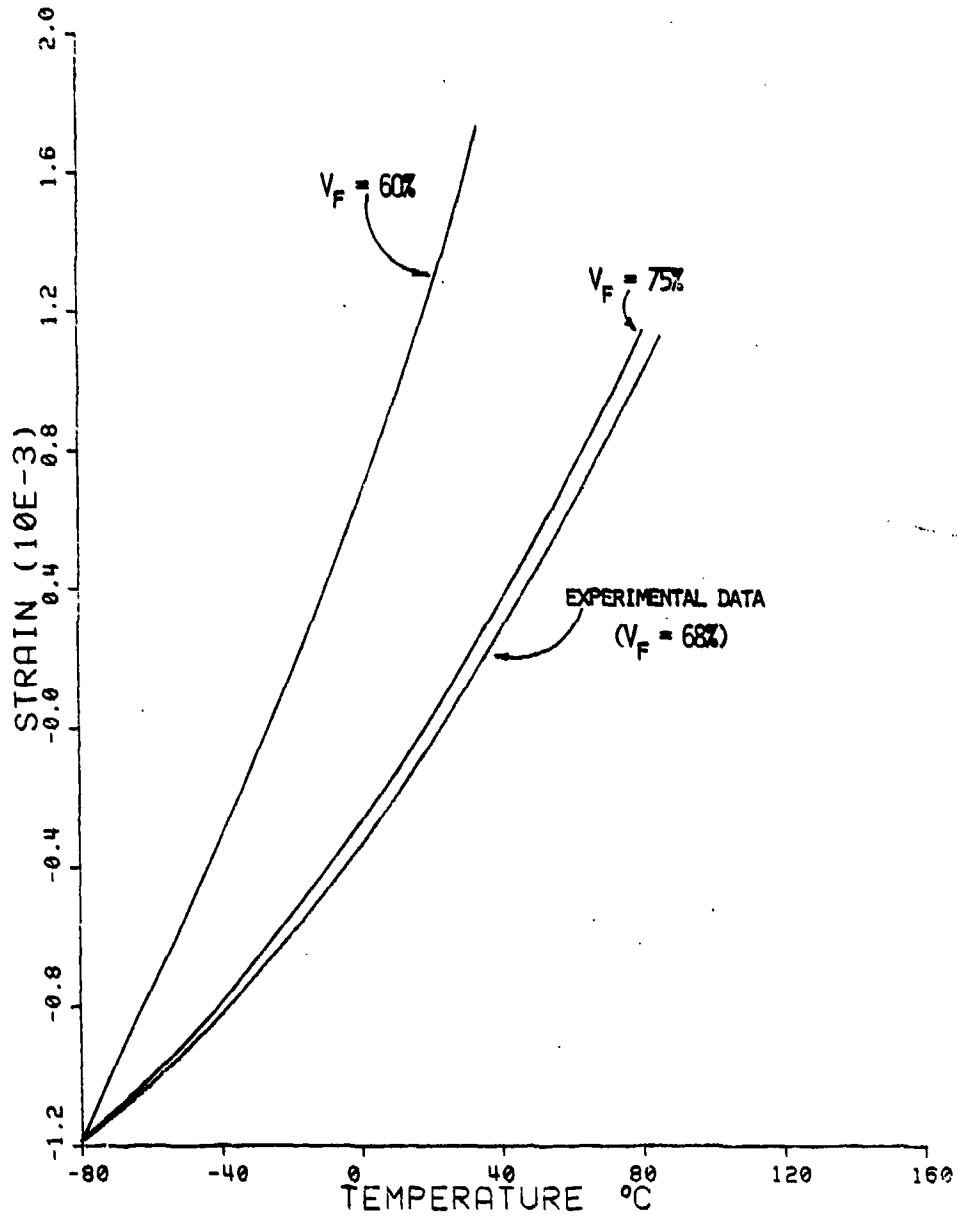

Figure 78. Moisture Conditioned Thermal Expansion Sensitivity to Fiber Volume for S2 Glass/3501-6 Glass/Epoxy

The Poisson's ratio of the fiber has little effect (Figure 79), as does the Young's modulus of the fiber (Figure 80). As seen in all of the composite transverse thermal expansion predictions, the transverse thermal expansion of the fiber is significant (Figure 81).

Since polymers exhibit high coefficients of thermal expansion, and the transverse thermal expansion of the fibers is usually less, the composite would be expected to be, again, matrix dominated. This is the case, with the notable exception of the transverse thermal expansion of the fiber.

It is interesting to note that the micromechanics analysis over-predicts the transverse thermal expansion of both the AS/3501-6 and the S2 glass/3501-6 composites. The transverse coefficient of thermal expansion of an individual graphite fiber is a best estimate since the fibers themselves are anisotropic [8]. A lower value does not change the coefficient of moisture expansion significantly (Figure 47), but it has a substantial influence on the coefficient of thermal expansion (see Figures 60 and 66). As in the moisture expansion case, the Poisson's ratio of the matrix, and the fiber volume, have a large influence on thermal expansion.

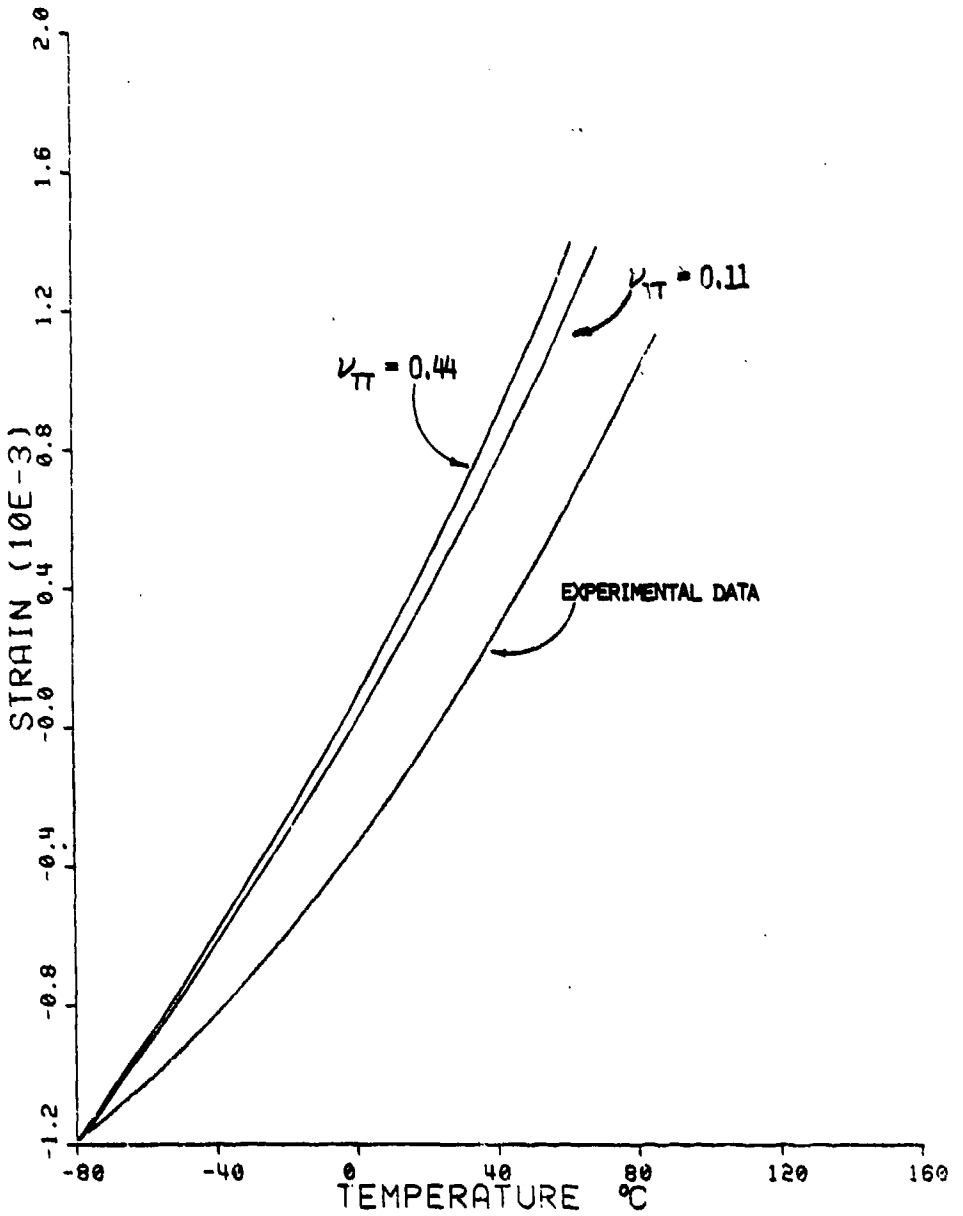

Figure 79. Moisture Conditioned Transverse Thermal Expansion Sensitivity to Poisson's Ratio of the Fiber for S2 Glass/3501-6 Glass/Epoxy (Base Value of Fiber ν_{TT} = 0.22)

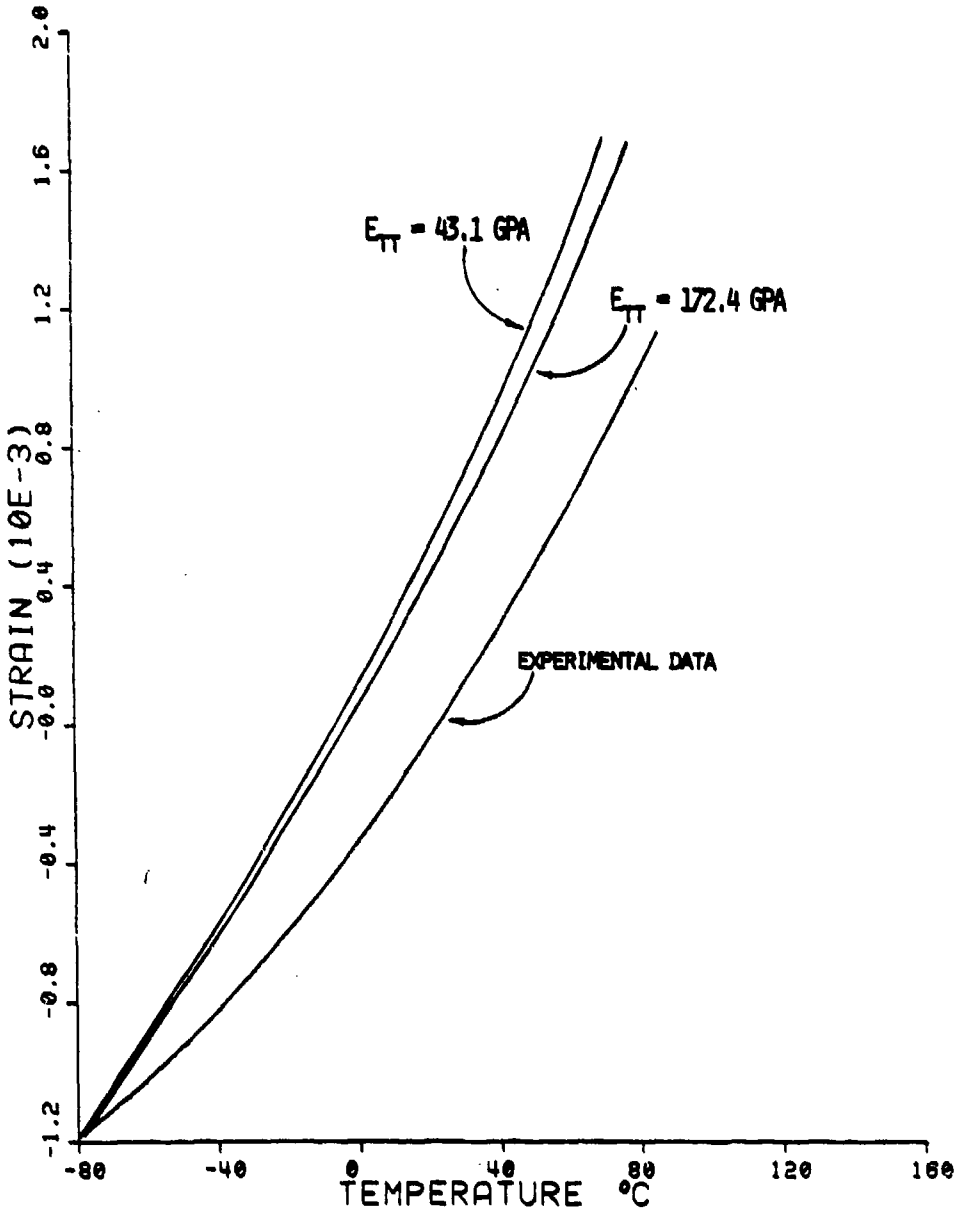

Figure 80. Moisture Conditioned Transverse Thermal Expansion Sensitivity to Young's Modulus of the Fiber for S2 Glass/3501-6 Glass/Epoxy (Base Value E_{TT} = 86.2 GPa)

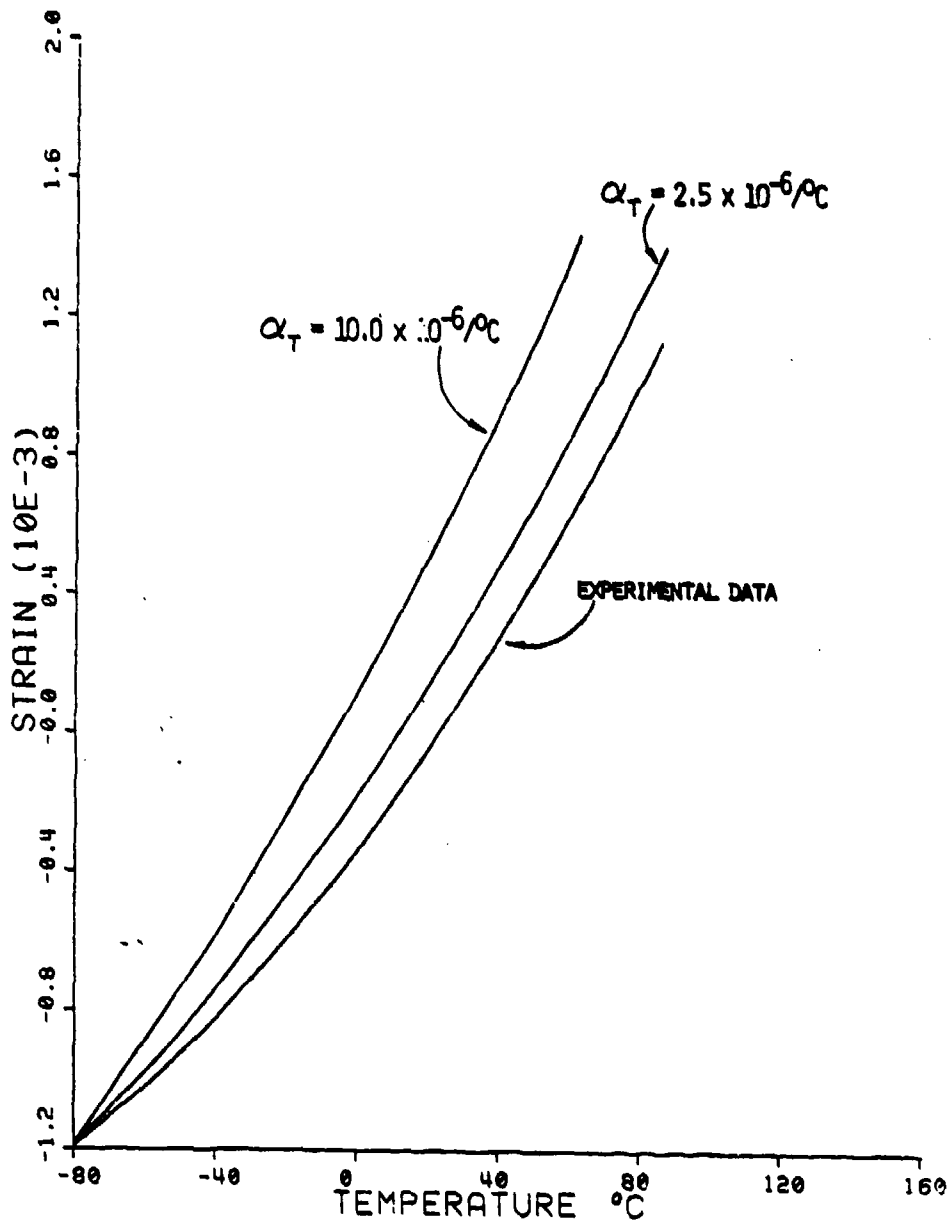

Figure 81. Moisture Conditioned Transverse Thermal Expansion Sensitivity to Transverse Thermal Expansion of the Fiber for S2 Glass/3501-6 Glass/Epoxy (Base Value $\alpha_T = 5.0 \times 10^{-6}/°C$)

SECTION 6

DISCUSSION

6.1 Moisture Expansion Experiments

Using a carefully controlled testing method, reliable moisture expansion data have been determined. The technique developed represents state-of-the-art data acquisition, with a flexibility to accommodate new and more accurate equipment as it becomes available. The data should serve as a base from which designers may account for moisture-induced stresses and strains in composites.

It is appropriate to review some of the major points already discussed. First, although using a matrix material with an essentially linear coefficient of moisture expansion, and fibers with assumed moisture diffusivities of zero, a nonlinear moisture expansion curve was observed, both experimentally and in the micromechanics predictions. This is related to a nonlinear increase of the minimum principal stress in the matrix material in the region at closest fiber packing. The AS/3501-6 graphite/epoxy composite showed far less nonlinearity than did the S2 glass/3501-6 composite. Agreement was quite good, but was probably influenced by fiber material properties such as in-plane Young's modulus or the in-plane coefficient of thermal expansion which are best estimates based on previous knowledge [8]. Therefore, as an approximation, a linear moisture expansion response could probably be assumed for the AS/3501-6, depending on the required accuracy of the application. The slight nonlinearity of the initial portion of the 3501-6 epoxy resin

expansion curves may have been due to moisture filling interstitial voids [21]. This causes the material to have less expansion for a given apparent moisture absorption during this process since less strain is induced in the material. However, this deviation from linearity was observed to be only a few percent of full scale. This deviation can in no way account for the large nonlinearity of the composites, especially the S2 glass/3501-6 laminates. The predicted values would not be influenced much by this since the nonlinearity is small and occurs prior to the moisture level present in the matrix, where the predicted S2 glass/3501-6 composite moisture expansion takes a large incremental increase.

There seems to be a relatively large discrepancy between micromechanics predictions and experimental data for the S2 glass/3501-6 composite. While of the same order of magnitude, the predicted values are lower than the experimentally determined values. It has been postulated that moisture severely degrades mechanical properties at the fiber-matrix interface in glass/epoxy laminates [45,46,47]. Since the micromechanics analysis assumes a perfect fiber-matrix bond, this effect would be totally ignored. A degradation of the fiber-matrix interface would cause a severe decrease in stiffness of the composite, thereby increasing moisture expansion beyond the value predicted, assuming a perfect interface bond. Also, it is generally accepted that glass fibers are isotropic. However, a small degree of anisotropy would also have an influence on the mechanical behavior of the composite [3].

Fiber volumes for the S2 glass/3501-6 composites varied greatly from one specimen to another; a 68 percent average fiber volume was calculated and used in the micromechanics analyses. As shown in the parametric

studies, fiber volume had a significant influence on the moisture expansion. This probably accounts for the high degree of variance seen in the S2 glass/3501-6 composite moisture expansion tests.

The parametric study conducted was incomplete in that the effect of several parameters may operate in a synergistic manner, with only small changes in any one parameter. In addition, it would be very interesting to study in depth the effects that constituent material properties have on the microstress state of the composite, and how these microstresses affect moisture expansion.

While the data obtained represent a good start, further tests at different humidity levels and different temperatures need to be conducted, to provide a greater degree of confidence in the data. This would also provide a family of curves, to determine if these parameters have an effect on moisture expansion. Specifically, strain versus percent equilibrium moisture content tests should be conducted, to verify that the matrix moisture expansion is indeed linear. Also, it would be interesting to numerically generate an S2 glass/3501-6 composite with a much lower modulus at the fiber-matrix interface, to study the effects of the degradation hypothesis.

6.2 Thermal Expansion Experiments

The transverse thermal expansion of the AS/3501-6 and S2 glass/3501-6 composites are both nonlinear over a wide temperature range. This comes as no surprise since the 3501-6 epoxy matrix material exhibits this behavior and the composites behave in a similar manner.

The AS/3501-6 composite specimens did not correlate as well with the theory as did the S2 glass/3501-6 specimens. In both cases, however,

the agreement was acceptable. Since the transverse thermal expansion coefficient of the graphite fiber used in the analysis was an estimate, this could be a source of error. A value of 18 x 10^{-6}/°C for the transverse coefficient of thermal expansion of the graphite fiber was assumed as a base value for the present analysis (see Table 9). Fischbach [48] has stated that a maximum upper limit of 14 x 10^{-6}/°C has been predicted for the thermal expansion for a perfect graphite fiber. Perfect means that all of the graphitic planes are perfectly aligned, and no voids are present in the fiber. In medium modulus fibers such as the Hercules AS graphite fiber used in the present study, the misalignment of the graphitic planes causes a lower transverse coefficient of thermal expansion. Also, microvoids in the fiber tend to accommodate thermal expansion, decreasing the transverse thermal expansion coefficient. Therefore, strong arguments can be made for using the 9 x 10^{-6}/°C transverse coefficient of thermal expansion of the graphite fiber shown in Figures 63 and 69, as being a realistic value. Also, as stated previously, fiber volume has a strong influence, and may be a source of error.

The Poisson's ratio of the matrix was assumed to be a constant for all temperature and moisture conditions. This may not be the case since increased moisture and higher temperatures serve to plasticize the matrix material [21]. This could affect the Poisson's ratio of the matrix material, and the subsequent composite behavior, the composite response having been shown to be highly dependent on Poisson's ratio.

The same problem existed in the thermal expansion parametric study as in the moisture expansion study. That is, it was incomplete in the sense of showing the sensitivity of only one property at a time.

The curve-fitting parameters generated can be used as a design tool. A linear interpolation may be valid over a very small temperature range.

Since composites are gaining acceptance for use in primary structural applications, it is necessary to provide good thermal and moisture expansion data for designers. These data are not only necessary for calculating dimensional changes, but also for predicting moisture- and thermally-induced stresses in composite laminates.

REFERENCES

1. D.F. Adams, "Wind Turbine Blade Materials/Design Technology," Final Report, Faculty Research Participation Program, National Science Foundation Southwest Research Institute, August 1974, pp. 40-62.

2. "KEVLAR, The Fiber That Lets You Re-think Strength and Weight," E.I. DuPont de Nemours & Co. (Inc.), Wilmington, Delaware, 1981, pp. 5-21.

3. A.K. Miller and D.F. Adams, "Inelastic Micromechanical Analysis of Graphite/Epoxy Composites Subject to Hygrothermal Cycling," Advanced Composite Materials - Environmental Effects, ASTM STP 658, American Society for Testing and Materials, Philadelphia, Pennsylvania, 1977, pp. 121-142.

4. R.M. Jones, Mechanics of Composite Materials, Scripta Book Company, Washington D.C., (1975), pp. 147-237.

5. S.J. Davis and D.F. Adams, "Thermal Deformation of Various Composite Material Ski Constructions," Department Report UWME-DR-101-103-1, Department of Mechanical Engineering, University of Wyoming, Laramie, Wyoming, May 1981, pp. 1-9, 85-104, 123-125.

6. L.D. Berman, "Reliability of Composite Zero-Expansion Structures for Use in Orbital Environment," Composite Reliability, ASTM STP 580, American Society for Testing and Materials, Philadelphia, Pennsylvania, 1975, pp. 288-297.

7. "Textile Fibers for Industry," Owens-Corning Fiberglas Corp., Toledo, Ohio (1971), pp. 8-30.

8. "Hercules Magnamite Graphite Fibers," Hercules, Incorporated, Magna, Utah, 1978.

9. D.E. Walrath and D.F. Adams, "Moisture Absorption Analysis of the Thematic Mapper Graphite/Epoxy Composite Structure," Modern Developments in Composite Materials and Structures, The Winter Annual Meeting of The American Society of Mechanical Engineers, New York, New York, December 1979, pp. 289-297.

10. H.S. Carslaw and J.G. Yaeger, Conduction of Heat in Solids, Oxford Press, New York, New York, (1959), pp.

11. G.S. Springer and S.W. Tsai, "Thermal Conductivities of Unidirectional Materials," Journal of Composite Materials, Vol. 1, April 1967, pp. 166-173.

12. J. Crank, The Mathematics of Diffusion, Cambridge University Press, New Rochelle, New York, (1975), pp. 3-27.

13. W. Jost, Diffusion in Solids, Liquids, Gasses, Academic Press, New York, New York, (1965), pp. 3-55.

14. G.S. Springer and C.H. Shen, "Moisture Absorption and Desorption of Composite Materials," Journal of Composite Materials, Vol. 10, January 1976, pp. 2-19.

15. G.S. Springer, "Moisture Content of Composites Under Transient Conditions," Journal of Composite Materials, Vol. 11, January 1977, pp. 107-122.

16. G.S. Springer, "Environmental Effects on Epoxy Matrix Composites," ASTM (Fifth Conference), American Society for Testing and Materials, Philadelphia, Pennsylvania, March 1978, pp. 2-23.

17. A.C. Loos and G.S. Springer, "Moisture Absorption of Graphite-Epoxy Composites Immersed in Liquids and in Humid Air," Journal of Composite Materials, Vol. 13, April 1979, pp. 131-146.

18. E.L. McKague, Jr., J.P. Reynolds and J.E. Halkias, "Moisture Diffusion in Fiber Reinforced Plastics," Transactions of the ASME, Journal of Engineering Materials and Technology, Vol. 98, No. 1 (Series H), January 1976, pp. 92-95.

19. J.M. Augl and A.E. Berger, "The Effect of Moisture on Carbon Fiber Reinforced Composites, III. Prediction of Moisture Sorption in a Real Outdoor Environment," Report No. NSWC/WOL/TR-77-13, White Oak Laboratory, Silver Spring, Maryland, June 1977, pp. 13-18.

20. J.M. Augl, "Moisture Sorption and Diffusion in KEVLAR 49 Aramid Fiber," Report No. NSWCTR 79-51, Naval Surface Weapons Center, White Oak Laboratory, Silver Spring, Maryland, March 1979, pp. 10-34.

21. F.W. Crossman, R.E. Mauri and W.J. Warren, "Moisture-Altered Viscoelastic Response of Graphite/Epoxy Composites," Advanced Composite Materials - Environmental Effects, ASTM STP 658, American Society for Testing and Materials, Philadelphia, Pennsylvania, 1977, pp. 205-220.

22. W.T. Freeman and M.D. Campbell, "Thermal Expansion Characteristics of Graphite Reinforced Composite Materials," Composite Materials: Testing and Design (Second Conference), ASTM STP 497, American Society for Testing and Materials, Philadelphia, Pennsylvania, 1972, pp. 121-142.

23. Unpublished Experimental Data for Hercules AS/3501-6 Graphite/Epoxy System, Composite Materials Research Group, Department of Mechanical Engineering, University of Wyoming, Laramie, Wyoming, 1977.

24. E.G. Wolff and S.A. Eselun, "The Coefficient of Moisture Expansion - Its Measurement and Use," Conference on Advanced Composites - Special Topics Technology Conferences, El Segundo, California, December 1979, pp. 55-68.

25. R.E. Mauri, F.W. Crossman and W.J. Warren, "Assessment of Moisture Altered Dimensional Stability of Structural Composites," Proceedings of the 23rd National SAMPE Symposium, Society for the Advancement of Material and Process Engineering, Azusa, California, April 1978, pp. 1202-1217.

26. D.F. Adams and M.M. Monib, "Moisture Expansion and Thermal Expansion Coefficients of a Polymer-Matrix Composite Material," Proceedings of the Fourth Conference on Fibrous Composites in Structural Design, San Diego, California, November 1978.

27. B.G. Schaffer and D.F. Adams, "Nonlinear Viscoelastic Behavior of a Composite Material Using a Finite Element Micromechanical Analysis," Department Report UWME-DR-001-101-1, Department of Mechanical Engineering, University of Wyoming, Laramie, Wyoming, June 1980.

28. J.E. Ashton, J.C. Halpin and P.H. Petit, Primer on Composite Materials: Analysis, Technomic Publishing Co., Westport, Connecticut, (1969), pp. 88-89.

29. T. Ishikawa, "Thermal Expansion Coefficients of Unidirectional Composites," Journal of Composite Materials, Vol. 12, April 1978, pp. 153-168.

30. J.W. Dally and W.F. Riley, Experimental Stress Analysis, McGraw-Hill Book Company, New York, New York, (1965), pp. 165-220.

31. C.D. Shirrell, "Diffusion of Water Vapor in Graphite/Epoxy Composites," Advanced Composite Materials - Environmental Effects, ASTM STP 658, American Society for Testing and Materials, Philadelphia, Pennsylvania, 1977, pp. 21-42.

32. "Maintaining Constant Relative Humidity by Means of Aqueous Solutions," ASTM Designation E 104-51 (Reapproved 1971), 1975 Annual Book of ASTM Standards, American Society of Testing and Materials, Philadelphia, Pennsylvania, 1975, pp. 852-855.

33. Unpublished Experimental Data for Hercules 3501-6 Epoxy Resin, Composite Materials Research Group, Mechanical Engineering Department, University of Wyoming, Laramie, Wyoming, 1978.

34. R. DeIasi and J.B. Whiteside, "Effect of Moisture on Epoxy Resins and Composites," Advanced Composite Materials - Environmental Effects, ASTM STP 658, American Society for Testing and Materials, Philadelphia, Pennsylvania, 1977, pp. 2-20.

35. J.M. Whitney and C.E. Browning, "Some Anomalies Associated with Moisture Diffusion in Epoxy Matrix Composites Materials," Advanced Composite Materials - Environmental Effects, ASTM STP 658, American Society for Testing and Materials, Philadelphia, Pennsylvania, 1977, pp. 43-60.

36. C.E. Browning, "The Mechanisms of Elevated Temperature Property Losses in High Performance Structural Epoxy Resin Matrix Materials After Exposures to High Humidity Environments," Report No. AFML-TR-76-153, Air Force Materials Laboratory, Wright-Patterson Air Force Base, Ohio, March 1977.

37. J.M. Augl and A.E. Berger, "Moisture Effect on Carbon Fiber Epoxy Composites," Proceedings of the 8th National SAMPE Conference, Society for the Advancement of Material and Process Engineering, Azusa, California, October 1976, pp. 383-427.

38. Y.A. Tajima, "The Diffusion of Moisture in Graphite Fiber Reinforced Epoxy Laminates," SAMPE Quarterly, Society for the Advancement of Material and Process Engineering, Azusa, California, July 1980, pp. 1-9.

39. G.C. Grimes and D.F. Adams, "Investigation of Compression Fatigue Properties of Advanced Composites," Northrop Technical Report NOR 79-17, Northrop Corporation, Hawthorne, California, October 1979, pp. 82-88.

40. C.E. Browning, C.E. Husman and W.M. Whitney, "Moisture Effects in Epoxy Matrix Composites," Report No. AFML-TR-77-17, Air Force Materials Laboratory, Wright-Patterson Air Force Base, Ohio, May 1977, pp. 16-22.

41. D.A. Crane and D.F. Adams, "Finite Element Micromechanical Analysis of a Unidirectional Composite Including Longitudinal Shear Loading," Department Report UWME-DR-001-101-1, Department of Mechanical Engineering, University of Wyoming, Laramie, Wyoming, February 1981.

42. D.E. Walrath and D.F. Adams, "Fatigue Behavior of Hercules 3501-6 Epoxy Resin," Report No. NADC-78139-60, Naval Air Development Center, Warminster, Pennsylvania, January 1980.

43. R.M. Richard and J.M. Blacklock, "Finite Element Analysis of Inelastic Structures," AIAA Journal, Vol. 7, No. 3, March 1969, pp. 432-438.

44. A.P. Boresi and P.P. Lynn, Elasticity in Engineering Mechanics, Prentice-Hall, Inc., Englewood Cliffs, New Jersey, (1974), p. 174.

45. D.H. Kaeble, P.J. Dynes and L.W. Crane, "Interfacial Mechanisms of Moisture Degradation in Graphite Epoxy Composites," Journal of Adhesion, Vol. 7, April 1974, pp. 25-54.

46. D.J. Vaughan and E.L. McPherson, "The Effects of Adverse Environmental Conditions on the Resin-Glass Interface of Epoxy Composites," Proceedings of the 27th Annual Conference, Reinforced Plastics/Composites Institute, The Society of the Plastics Industry, Inc., New York, New York, 1972 , Section 21-C, pp. 1-7.

47. W.J. Eakens, "Effect of Water on Glass Fiber Resin Bonds," Interfaces in Composites, ASTM STP 452, American Society for Testing and Materials, Philadelphia, Pennsylvania, 1969, pp. 137-148.

48. D.B. Fischbach, Personal Correspondence, Professor of Ceramic Engineering, University of Washington, Seattle, Washington, August 1981.

49. P.G. Hodge, Jr., Continuum Mechanics, An Introductory Text for Engineers, McGraw-Hill Book Company, New York, New York, (1970), pp. 35-36, 55-56.

APPENDIX A

EQUATIONS OF THERMAL AND MOISTURE DIFFUSION

APPENDIX A

EQUATIONS OF THERMAL AND MOISTURE DIFFUSION

The purpose of this Appendix is to present the general equations for thermal diffusion, and then apply them to the case of moisture diffusion since the solutions of both are similar. The equations have been formulated previously in classic works on diffusion. All equations will be presented in standard tensorial form [49].

A1. Thermal Diffusion in an Anisotropic Solid

Thermal diffusion appears to follow the Fourier equation of heat transver [10], i.e.,

$$\rho c \frac{\partial T}{\partial t} = \frac{\partial}{\partial x_i}\left[K_{ij} \frac{\partial T}{\partial x_j}\right] = (K_{ij}\, T_{,j})_{,i} \qquad (A.1a)$$

where ρ = material density

c = specific heat

T = temperature

t = time

x = material coordinates

K_{ij} = thermal conductivity tensor

If K_{ij} is not a function of temperature and position, the above simplifies to

$$\rho c \frac{\partial T}{\partial t} = K_{ij} \frac{\partial^2 T}{\partial x_i \partial x_j} \qquad (A.1b)$$

The heat flux vector represents the rate of heat transfer per unit area per unit time and may be written as Fourier's Second Law [10]

$$-q_i = K_{ij} \frac{\partial T}{\partial x_j} \tag{A.2}$$

For the most general material form (triclinic, i.e., no material planes of symmetry), the thermal conductivity tensor has the form [10]

$$\begin{pmatrix} K_{11} & K_{12} & K_{13} \\ K_{21} & K_{22} & K_{23} \\ K_{31} & K_{32} & K_{33} \end{pmatrix} \tag{A.3a}$$

For the monoclinic system (one plane of symmetry), the tensor simplifies to

$$\begin{pmatrix} K_{11} & K_{12} & 0 \\ K_{21} & K_{22} & 0 \\ 0 & 0 & K_{33} \end{pmatrix} \tag{A.3b}$$

An orthorhombic material has two perpendicular diad axes (symmetry about 180° rotation) or a diad axis with a plane of symmetry through it, the conductivities are

$$\begin{pmatrix} K_{11} & 0 & 0 \\ 0 & K_{22} & 0 \\ 0 & 0 & K_{33} \end{pmatrix} \tag{A.3c}$$

Single crystals are usually orthorhombic materials.

The materials of the present study are orthotropic, with conductivities K_{11}, K_{22}, K_{33} in three mutually perpendicular directions. The conductivities are

$$\begin{pmatrix} K_{11} & 0 & 0 \\ 0 & K_{22} & 0 \\ 0 & 0 & K_{33} \end{pmatrix} \tag{A.3d}$$

with the above statement of orthogonality kept in mind. The conductivity K_{11} is along the fiber axis of a unidirectional lamina, while conductivities K_{22} and K_{33} are transverse to the fiber in the x_2 and x_3 directions, respectively. If, in addition to the above, the material is transversely isotropic (material properties independent of direction transverse to the fiber), the conductivity matrix becomes

$$\begin{bmatrix} K_{11} & 0 & 0 \\ 0 & K_{22} & 0 \\ 0 & 0 & K_{22} \end{bmatrix} \tag{A.3e}$$

The components of the heat flux vector for this condition are

$$\begin{aligned} q_1 &= -K_{11} \frac{\partial T}{\partial x_1} \\ q_2 &= -K_{22} \frac{\partial T}{\partial x_2} \\ q_3 &= -K_{22} \frac{\partial T}{\partial x_3} \end{aligned} \tag{A.4}$$

Consider the case of a unidirectional fiber reinforced composite material, with the following assumptions [11];

a) The composite is macroscopically homogeneous.

b) The matrix and fiber are homogeneous and isotropic locally.

c) Thermal contact resistance between fiber and matrix is negligible.

d) The problem is two dimensional, i.e., temperature distribution is independent of x_3 (see Figure A1).

e) The fibers are circular in cross section and the packing array is rectangular.

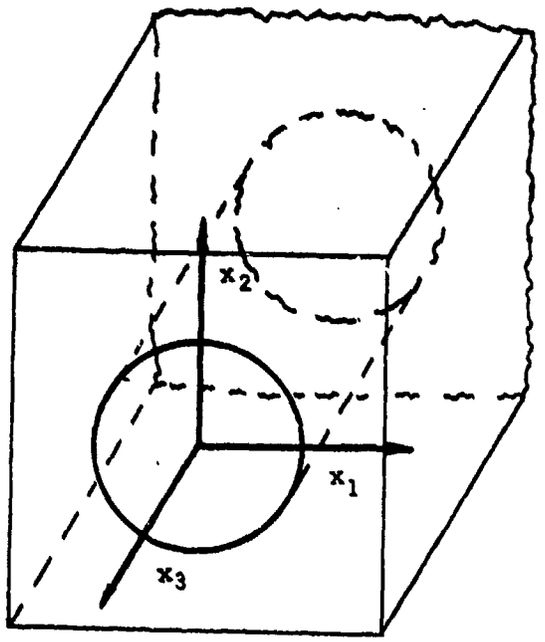

Figure A1. Rectangular Array for Fiber Imbedded in Matrix

The problem considered is that of a thin orthotropic plate, with fiber orientation shown in Figure A2.

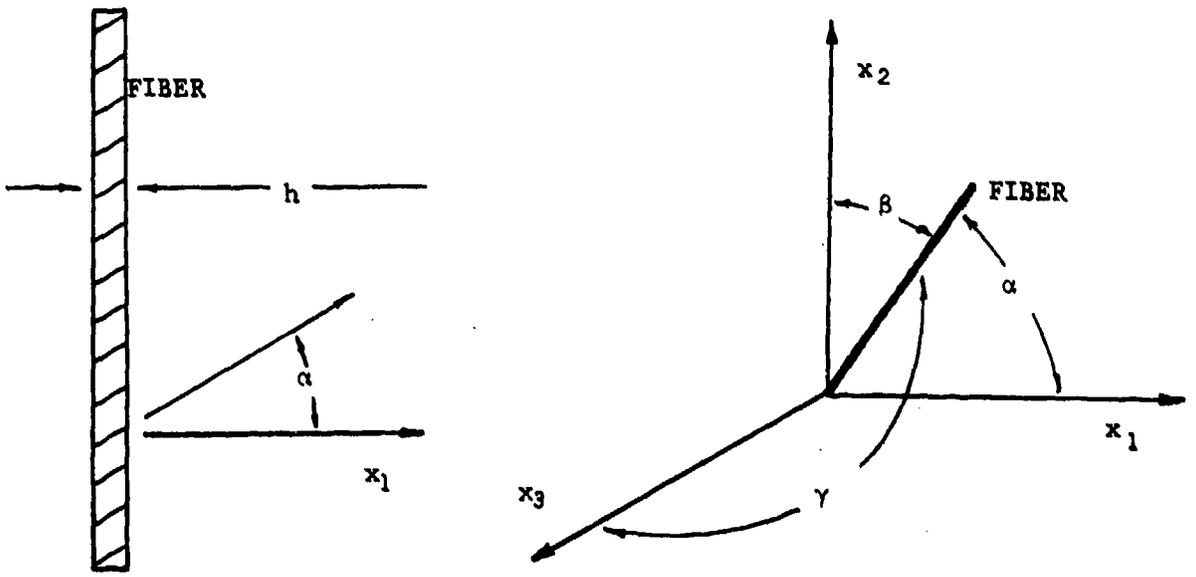

a) Plate Geometry b) Fiber Orientation in Plate

Figure A2. General Fiber Orientation

From the initial assumption that the temperature is independent of the x_3 direction, Eq. (A.5) is obtained

$$K_{\alpha\beta} = a_{\lambda\alpha}\, a_{\gamma\beta}\, K'_{\lambda\gamma} \tag{A.5}$$

where $a_{\lambda\alpha}$, $a_{\gamma\beta}$ are direction cosines of a given rotation, $K_{\alpha\beta}$ are the conductivities according to the specimen geometry, and $K'_{\lambda\gamma}$ are the conductivities along the three mutually perpendicular axes of a unidirectional lamina. For a transversely isotropic lamina, K_{11}' is along the fiber axis and K_{22}' is transverse to the fiber axis. From these assumptions

$$K_{11} = a_{11}a_{11}K_{11}' + a_{21}a_{21}K_{22}' + a_{11}a_{12}K_{12}' + a_{21}a_{11}K_{21}' \tag{A.6a}$$

$$K_{12}' = K_{21}' = 0 \text{ from (A.3c)}$$

so,
$$K_{11} = K_{11}'\cos^2\alpha + K_{22}'\sin^2\alpha$$

similarly,

$$K_{22} = K_{11}'\cos^2\beta + K_{22}'\sin^2\beta \tag{A.6b}$$

$$K_{33} = K_{11}'\cos^2\gamma + K_{22}'\sin^2\gamma \tag{A.6c}$$

Springer and Tsai approximated K_{11}' and K_{22}' [11] by the following set of equations, subject to the previous assumptions (a-e).

$$K_{11}' = (1 - V_f)K_r + V_f K_f \tag{A.7}$$

$$K_{22}' = \left[1 - 2\sqrt{\frac{V_f}{\pi}}\right]K_r + \frac{K_r}{B_k}\left[\pi - 4\tan^{-1}\frac{\sqrt{1 - B_k^2\frac{V_f}{\pi}}}{1 + \sqrt{B_k^2\frac{V_f}{\pi}}}\right] \tag{A.8}$$

where V_f = fraction volume of fiber

K_r = thermal conductivity of resin

K_f = thermal conductivity of fiber

$$B_k = 2\left(\frac{K_r}{K_f} - 1\right)$$

For a rotation about the x_1 axis

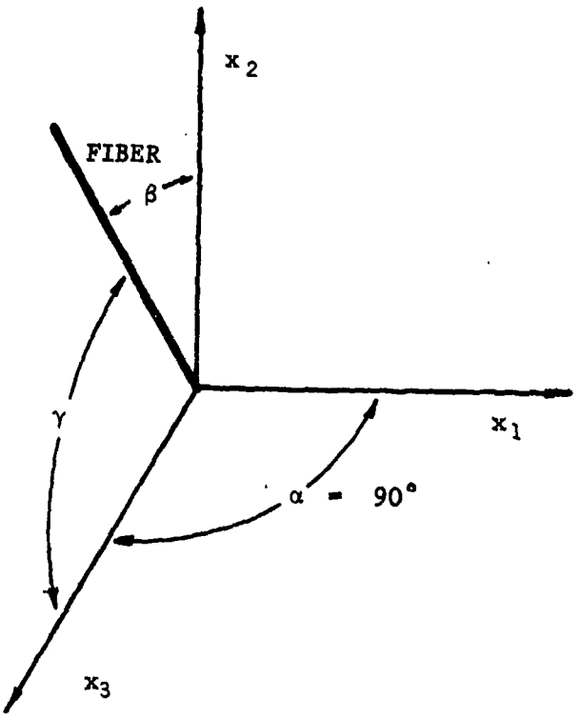

Figure A3. Planar Fiber Orientation

$$K_{11} = K_{11}'\cos^2\alpha + K_{22}'\sin^2\alpha = K_{22}' \qquad \text{(A.9a)}$$

$$K_{22} = K_{11}'\cos^2\beta + K_{22}'\sin^2\beta \qquad \text{(A.9b)}$$

and, since $\gamma = 90^\circ - \beta$

$$K_{33} = K_{11}'\cos^2(90^\circ - \beta) + K_{22}'\sin^2(90^\circ - \beta)$$
$$= K_{11}'\sin^2\beta + K_{22}'\cos^2\beta \qquad \text{(A.9c)}$$

It should be noted (demonstrated in Section A2), that the above equations must be solved for each individual lamina in a laminate if the laminate contains any off axis plies.

A2. Diffusion of Moisture into a Thin Anisotropic Plate

Since temperature reaches equilibrium quickly with time for a thin plate, transient conditions play a smaller role for thermal considerations than they do for moisture diffusion. In fact, the ratio of moisture diffusivity to thermal diffusivity is of the order of 10^{-6} for a typical fiber reinforced plastic [14].

Several models have been proposed for the diffusion of moisture in composites. Fick's Second Law for anisotropic media appears to correspond well to experimental data. This is

$$\frac{\partial c}{\partial t} = \frac{\partial}{\partial x_i}\left[D_{ij}\frac{\partial c}{\partial x_j}\right] \qquad \text{(A.10)}$$

where c = concentration of moisture

D_{ij} = diffusivity tensor

It has been observed that [14] D_{ij} varies little with moisture content (hence x_i), so that the above may be rewritten

$$\frac{\partial c}{\partial t} = D_{ij}\frac{\partial^2 c}{\partial x_i \partial x_j} \qquad \text{(A.11)}$$

If one goes through similar arguments developed in the previous section for conductivities normal and transverse to the fiber direction

under the same assumption of transverse isotropy, a similar scheme of diffusivities is obtained.

$$D_{ij} = \begin{bmatrix} D_{11} & 0 & 0 \\ 0 & D_{22} & 0 \\ 0 & 0 & D_{22} \end{bmatrix} \qquad (A.12)$$

Equation (A.11) has initial and boundary conditions [13] as follows:

$$c = c_0 \qquad 0 < x < h \qquad t \leq 0$$

$$c = c_{ambient} \qquad x = 0;\ x = h \qquad t > 0$$

For a specimen configuration as in Figure 4, subject to assumptions stated in Section A1, a solution to Eq. (A.11) is obtained for the x_1 direction. The solution is [13]

$$\frac{c-c_0}{c_m-c_0} = 1 - \frac{4}{\pi} \sum_{j=1}^{\infty} \frac{1}{(2j+1)} \sin \frac{(2j+1)\pi x_1}{h} \left[\exp \frac{-(2j+1)^2\pi^2 \left(\frac{D_{11}t}{h^2} \right)}{(2j+1)^2} \right] \qquad (A.13)$$

where c_m = maximum concentration (mass/unit volume)

The total weight of moisture in the plate due to diffusion in the x_1 direction is obtained by integrating the above over the entire thickness h and multiplying by the gravitational constant g [14].

The result of this integration is

$$\frac{M-M_0}{M_m-M_0} = 1 - \frac{8}{\pi^2} \sum_{j=1}^{\infty} \frac{\exp \left[-(2j+1)^2\pi^2 \frac{D_{11}t}{h^2} \right]}{(2j+1)^2} \equiv G \qquad (A.14)$$

where G may be considered the ratio of moisture at a given time to the maximum possible moisture, and M_m = maximum moisture content possible.

The approximate time to reach $M = .99M_m$, or the time for the amount of moisture to reach 99 percent of maximum is

$$t = \frac{.67h^2}{D_{11}} \tag{A.15}$$

G may be approximated by the numerically generated solution [14]

$$G \approx 1 - \exp\left[-.73 \left(\frac{D_{11}t}{h^2}\right)^{.75} \right] \tag{A.16}$$

As a function of position and time

$$\frac{c - c_0}{c_m - c_0} = 1 - \text{erf}\left(\frac{x_1}{2\sqrt{D_{11}t}} \right) \tag{A.17}$$

where erf = error function

for the x_1 direction [13]. Eq. (A.13) may be used to find concentration profiles through the thickness of a laminate. If the laminate is infinitely long and wide, Eqs. (A.10)-(A.13) represent all of the relations needed to describe the moisture diffusion process. If, however, the plate has edges, this boundary effect must be taken into account.

Consider the specimen configuration below, shown in Figure A4.

A moisture flux vector can be defined [12] which represents the amount of moisture entering or leaving any surface per unit area per unit time, i.e.,

$$-J_i = D_{ij} \frac{\partial c}{\partial x_j} \tag{A.18}$$

Eq. (A.18) is completely analogous to Eq. (A.2) stated previously.

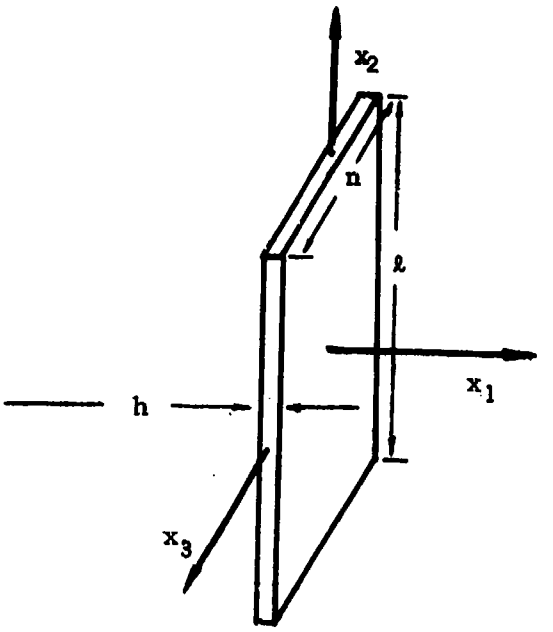

Figure A4. Specimen Configuration

On a given side of the composite, assuming no coupling between sides*, the moisture that enters or leaves a side over a given period of time is

$$M_i = \int_0^t - A\, J_i\, dt$$
$$= \int_0^t - A\, D_{ij} \left.\frac{\partial c}{\partial x_j}\right|_{x=0} dt \qquad (A.19)$$

where A = area of the side

For the case of an orthotropic, transversely isotropic material, the diffusion matrix is Eq. (A.12), and the following equations analogous to Eqs. (A.6a), (A.6b), and (A.6c) hold.

$$D_{11} = D_{11}'\cos^2\alpha + D_{22}'\sin^2\alpha \qquad (A.20a)$$

*This assumption appears to be valid if nh, ℓh << ℓn

$$D_{22} = D_{11}'\cos^2\beta + D_{22}'\sin^2\beta \qquad \text{(A.20b)}$$

$$D_{33} = D_{11}'\cos^2\gamma + D_{22}'\sin^2\gamma \qquad \text{(A.20c)}$$

Integrating (A.19), following Reference [13]:

$$M_1 = 2Ag\,(c_m - c_0)\sqrt{\frac{D_{11}t}{\pi}} \qquad \text{(A.21a)}$$

$$M_2 = 2Ag\,(c_m - c_0)\sqrt{\frac{D_{22}t}{\pi}} \qquad \text{(A.21b)}$$

$$M_3 = 2Ag\,(c_m - c_0)\sqrt{\frac{D_{33}t}{\pi}} \qquad \text{(A.21c)}$$

Thus, the total weight of moisture entering the specimen shown in Figure A4. is;

$$M_{total} = 4g(c_m - c_0)\left[n\ell\sqrt{D_{11}} + nh\sqrt{D_{22}} + h\ell\sqrt{D_{33}}\right]\sqrt{\frac{t}{\pi}} \qquad \text{(A.22)}$$

The weight of a dry specimen is [14]:

$$Wd = \rho ghn\ell$$

where ρ = mass density

g = gravitational constant

h = thickness

n = width

ℓ = length

if $c_0 = 0$

$$\%M = \frac{w-w_d}{w_d} \times 100 = \frac{m}{w_d} \times 100 = \frac{4c_m}{\rho h}\left[\sqrt{D_{11}} + \frac{h}{\ell}\sqrt{D_{22}} + \frac{h}{n}\sqrt{D_{33}}\right]\sqrt{\frac{t}{\pi}} \qquad \text{(A.23)}$$

where %M = percent moisture content by weight

m = weight of moisture absorbed

w = weight of specimen after exposure to a moist environment.

The above equation is helpful for experimental results.

Note that $M_m = c_m/\rho$ so that

$$M = \frac{4M_m}{h}\left(\sqrt{D_{11}} + \frac{h}{\ell}\sqrt{D_{22}} + \frac{h}{n}\sqrt{D_{33}}\right)\sqrt{\frac{t}{\pi}} \tag{A.24}$$

The above may be rewritten [14]

$$M = \frac{4M_m}{h}\sqrt{\frac{t}{\pi}}\sqrt{D} \tag{A.25}$$

where

$$D = D_{11}\left[1 + \frac{h}{\ell}\sqrt{\frac{D_{22}}{D_{11}}} + \frac{h}{n}\sqrt{\frac{D_{33}}{D_{11}}}\right]^2 \tag{A.26}$$

analogous to Equations (A.7) and (A.8) are [14]

$$D_{11}' = (1 - V_f)D_r + V_f D_f \tag{A.27}$$

$$D_{22}' = 1 - 2\sqrt{\frac{V_f}{\pi}}D_r + \frac{D_r}{B_D}\left[\pi - \frac{4}{\sqrt{1 - B_D{}^2\frac{V_f}{\pi}}}\tan^{-1}\left[\frac{\sqrt{1 - B_D{}^2\frac{V_f}{\pi}}}{1 + \sqrt{B_D{}^2\frac{V_f}{\pi}}}\right]\right] \tag{A.28}$$

where D_r = diffusivity of the resin

D_f = diffusivity of the fiber

$$B_D = 2\left(\frac{D_r}{D_f} - 1\right) \tag{A.29}$$

For the fiber orientation of Figure A3) $\alpha = 90^\circ$, $\gamma = 90^\circ - \beta$.

Thus,
$$D_{11} = D_{11}'\cos^2(90) + D_{22}'\sin^2(90) \tag{A.30a}$$
$$= D_{22}'$$
$$D_{22} = D_{11}'\cos^2\beta + D_{22}'\sin^2\beta \tag{A.30b}$$
$$D_{33} = D_{11}'\sin^2\beta + D_{22}'\cos^2\beta \tag{A.30c}$$

If, in addition, $D_f = 0$, a good assumption for most fiber reinforcing materials, Eq. (A.26) becomes (A.31)

$$D = D_r\left(1 - 2\sqrt{\frac{V_f}{\pi}}\right)\left[1 + \frac{h}{\ell}\sqrt{\frac{(1-V_f)\cos^2\beta}{1-2\sqrt{\frac{V_f}{\pi}}} + \sin^2\beta} + \frac{h}{n}\sqrt{\frac{(1-V_f)\sin^2\beta}{1-2\sqrt{\frac{V_f}{\pi}}} + \cos^2\beta}\right]^2$$

The above represents the approximate diffusion coefficient for each indificual lamina. For a laminate, D must be summed over the entire thickness [14]. Let h_i = thickness of the i^{th} ply and β_i = angle with respect to the x_1 axis for the i^{th} ply, and n = total number of plies. Then, (A.32)

$$D_{total} = D_r\left(1 - 2\sqrt{\frac{V_f}{\pi}}\right)\left[1 + \frac{h}{\ell}\sqrt{\frac{(1-V_f)\sum_{i=1}^{n} h_i\cos^2\beta_i}{1-2\sqrt{\frac{V_f}{\pi}}\sum_{i=1}^{n} h_i} + \frac{\sum_{i=1}^{n} h_i\sin^2\beta_i}{\sum_{i=1}^{n} h_i}}\right.$$

$$\left. + \frac{h}{n}\sqrt{\frac{(1-V_f)\sum_{i=1}^{n} h_i\sin^2\beta_i}{1-2\sqrt{\frac{V_f}{\pi}}\sum_{i=1}^{n} h_i} + \frac{\sum_{i=1}^{n} h_i\cos^2\beta_i}{\sum_{i=1}^{n} h_i}}\right]^2$$

This is a brief summary of the governing equations for thermal and moisture diffusion. In closing, a review of the simplifying assumptions is appropriate. First, the material is assumed to be either orthotropic or transversely isotropic. These assumptions led to the K_{ij} and D_{ij} matrices, where all of these conductivities and diffusivities are mutually perpendicular. The assumptions stated in Section A1 led to the subsequent development of Eqs. (A.6) and (A.20).

The K_r and D_r were assumed to be constant throughout the thickness. If hn, hℓ are of order ℓn, the edge correction factor and subsequent resulting Equation (A.34) is not valid; for a three-dimensional diffusion problem is encountered. In the present summary, D_f was assumed to be zero. This assumption is not valid for all fibers, e.g., aramid or other organic fiber reinforcing materials. If $D_f \neq 0$, Eq. (A.32) becomes slightly more complicated. This summary represents the state-of-the-art to date. An obvious next step would be to extend the theory to the most general three-dimensional case.

APPENDIX B

FIBER VOLUMES AND RESIN WEIGHT FRACTION MEASUREMENTS

APPENDIX B

FIBER VOLUMES AND RESIN WEIGHT FRACTION MEASUREMENTS

Fiber volume measurements are necessary to correlate experimentally determined data to numerical data (Section 5). The theoretical data was very sensitive to changes in fiber volume, so accurate measurements are mandatory.

Fiber volumes were calculated by taking three samples from each material and weighing them. The specimens were then placed in nitric acid, heated by a water bath at 50°C (122°F), until all epoxy resin was dissolved. The specimens were cleaned with acetone and weighed again. The resin weight fractions were calculated from

$$1 - \frac{W_f}{W_c} = F_r \tag{B.1}$$

where W_f = weight of fiber

W_c = weight of composite

F_r = weight fraction of epoxy resin

Fiber volumes were calculated according to

$$V_f = \frac{1}{1 + \frac{\rho_f}{\rho_r}\left[\frac{W_t}{W_f} - 1\right]} \tag{B.2}$$

where V_f = volume fraction of the fiber

ρ_f = density of the fiber

ρ_r = density of the resin

W_t = total weight of the sample

W_f = weight of the fiber

Eq. (B.3) may be used to estimate the moisture content of the resin in a composite.

$$M_c = M_r F_r \tag{B.3}$$

where M_c = moisture content of the composite

M_r = moisture content of the epoxy resin

F_r = weight fraction of the epoxy resin

Table 6 showed the results of volume fraction calculations. The S2 glass/3501-6 specimens were manufactured here under relatively uncontrolled conditions. Therefore, there is much scatter in the data as compared to the commercially available AS/3501-6 prepreg system.

APPENDIX C

COMPUTER CODES

```
 PAGE 0001  FTN.  11:49 AM  WED., 26  AUG., 1981

0001  FTN4,L
0002        PROGRAM MPLOT
0003  C ***************************************************
0004  C
0005  C  THIS PROGRAM READS FILES CREATED BY THE OPERATOR
0006  C  AND PLOTS DIFFUSIVITY AND MOISTURE DILATATION
0007  C               INFORMATION
0008  C
0009  C ***************************************************
0010  C
0011        COMMON IDCB(144),ICOM(170)
0012        REAL TIME(100),MOIS(100),DISP(100),LNOT,SQTR(100),WGHT(100),
0013       1 STRN(100),WNOT
0014        INTEGER SPNAME(3),IREC(36),IDX(11),IDY(24),IX(11),IY(10)
0015  C ***************************************************************
0016  C THIS SECTION DEFINES LABELS FOR PLOTTING
0017  C ***************************************************************
0018  C
0019        DATA  IDX/2HSQ,2HRT,2H (,2HHR,2HS),2H  ,2H  ,2H  ,2H  ,2H  ,
0020       1 2H  /
0021        DATA  IDY/2H% ,2HMO,2HIS,2HTU,2HRE,2H  ,2H  ,2H  ,
0022       1 2H  ,2H  ,2H  ,2H  ,2H  ,2H  ,2H  ,2H  ,2H  ,2H  ,2H  ,
0023       2 2H  ,2H  ,2H  ,2H  ,2H  /
0024        DATA  IX/2H% ,2HMO,2HIS,2HTU,2HRE,2H  ,2H  ,2H  /
0025        DATA  IY/2HST,2HRA,2HIN,2H (,2H10,2HE-,2H3),2H  ,2H  ,2H  /
0026     10 WRITE(1,1000)
0027  C ***************************************************************
0028  C THIS SECTION READS DATA FILES
0029  C ***************************************************************
0030        READ(1,2000)SPNAME
0031        IF(SPNAME(1).EQ.2HST)STOP
0032        CALL OPEN(IDCB,IERR,SPNAME)
0033        IF(IERR.GE.0)GOTO 20
0034        WRITE(1,1010)SPNAME
0035        GOTO 10
0036     20 CALL READF(IDCB,IERR,IREC,36)
0037        CALL CODE
0038        READ(IREC,*)NPTS,LNOT,WNOT
0039        WRITE(11,1030)NPTS,LNOT,WNOT
0040        WRITE(11,1040)
0041        DO 30 I=1,NPTS
0042        CALL READF(IDCB,IERR,IREC,36)
0043        CALL CODE
0044        READ(IREC,*)TIME(I),DISP(I),WGHT(I)
0045  C ***************************************************************
0046  C THIS SECTION PRINTS, AT THE OPERATOR'S OPTION, TIMES, DISPLACEMENTS
0047  C AND WEIGHTS
0048  C ***************************************************************
0049  C       WRITE(11,1020)TIME(I),DISP(I),WGHT(I)
0050     30 CONTINUE
0051        CALL CLOSE(IDCB,IERR)
0052  C ***************************************************************
0053  C THIS SECTION CALCULATES STRAINS,SQUARE ROOT OF TIME, AND
0054  C                 %MOISTURE
0055  C ***************************************************************
```

Figure C1. MPLOT FORTRAN Code

```
0056          DO 50 I=1,NPTS
0057       50 STRN(I)=(DISP(I)/LNOT)*1000.
0058          DO 60 I=1,NPTS
0059       60 SQTR(I)=TIME(I)**.5
0060          DO 70 I=1,NPTS
0061       70 MOIS(I)=((WGHT(I)-WNOT)/WNOT)*100.
0062          WRITE(11,1060)
0063    C ***************************************************
0064    C THIS SECTION PRINTS THE SQUARE ROOT OF TIME,
0065    C STRAIN, AND %MOISTURE IF DESIRED
0066    C ***************************************************
0067    C     DO 80 I=1,NPTS
0068    C  80 WRITE(11,1070)SQTR(I),STRN(I),MOIS(I)
0069    C ***************************************************
0070    C THIS SECTION IS THE PLOTTING ROUTINE
0071    C ***************************************************
0072          PMOIS=3.2
0073          PTIME=30
0074          DX=PTIME/6
0075          DY=PMOIS/8
0076          CALL MODE(0,1.,1.,1.)
0077          CALL MODE(3,9999.,-1.5,9999.)
0078          CALL MODE(8,0.,DX,0.)
0079          CALL MODE(9,0.,DY,0.)
0080          CALL DRAW(SQTR,MOIS,NPTS,441)
0081          CALL AXES(22.0,IDX,48.1,IDY)
0082          CALL DRAW(0.,0.,1,9000)
0083    C
0084    C *****************************************
0085    C
0086    C LFIT MAY BE UNCOMMENTED TO PROVIDE A LINEAR
0087    C INTERPOLATION OF THE DATA POINTS
0088    C
0089    C *****************************************
0090    C
0091    C     CALL LFIT(MOIS,STRN,NPTS,SLOPE,YINT,RSQ)
0092    C     WRITE (11,1050)SLOPE,YINT,RSQ
0093          PMOIS=1.8
0094          PSTRN=12.
0095          DY=PSTRN/8
0096          DX=PMOIS/6
0097          CALL MODE(8,0.,DX,0.)
0098          CALL MODE(9,0.,DY,0.)
0099    C     PMOIS1=-YINT/SLOPE
0100    C     CALL DRAW(PMOIS1,0.,1,440)
0101    C     PSTRN2=PMOIS*SLOPE+YINT
0102    C     CALL DRAW(PMOIS,PSTRN2,1,449)
0103          CALL AXES(22.1,IX,20.2,IY)
0104          DO 40 I=1,NPTS
0105       40 CALL NOTE(MOIS(I),STRN(I),42,-1)
0106          CALL DRAW(0.,0.,1,9000)
0107          CALL DRAW(0,0,0,9999)
0108          STOP
0109     1000 FORMAT(" ENTER SPECIMEN NAME  ST TO STOP _")
0110     1010 FORMAT(" FILE DOES NOT EXIST!")
0111     1020 FORMAT(3E12.3)
0112     1030 FORMAT("NPTS = ",I5,2X,"LNOT= ",F10.5,2X,"WNOT= ",F10.5)
0113     1040 FORMAT(5X,"TIME",4X,4X,"DISP",5X,3X,"MOIS",5X)
0114     1050 FORMAT(/,"SLOPE= ",1PE10.3,/,"Y INTERCEPT= ",E10.3,/,
0115         1 "RSQ= ",E10.3)
0116     1060 FORMAT(5X,"SQRT",4X,4X,"STRN",5X,4X,"% MOIS",5X)
0117     1070 FORMAT(3F10.4)
0118     2000 FORMAT(3A2)
0119          END
```

Figure C1. MPLOT FORTRAN Code (continued)

```
 PAGE 0001  FTN.   9:58 AM  THU., 27  AUG., 1981
0001   FTN4,L
0002         PROGRAM NPLOT
0003   C
0004   C *********************************************************
0005   C
0006   C THIS PROGRAM READS FILES GENERATED BY THE PROGRAM
0007   C DLTLG AND PLOTS DIFFUSIVITY AND MOISTURE DILATATION
0008   C                 INFORMATION
0009   C
0010   C *********************************************************
0011   C
0012   C
0013   C *********************************************************
0014   C THIS SECTION DEFINES COMMONS AND READS THE FILES
0015   C *********************************************************
0016   C
0017         COMMON IDCB(144),ICOM(170)
0018         COMMON / MEM / DISP(1000),SQTR(1000),
0019        1               WGHT(1000),MOIS(1000),STRN(1000)
0020         REAL MOIS,DISP,LNOT,SQTR,
0021        1 WGHT,STRN,WNOT
0022         INTEGER SPNAME(3),IREC(36),IDX(11),IDY(24),IX(11),IY(10)
0023         COMMON / RECRD / STNUM,SPNUM,DAYS,HRS,MINS,TEMP,DISPL,
0024        1                 HUMID,WEIGHT,BALST
0025         INTEGER STNUM,SPNUM,DAYS,HRS,MINS
0026         REAL TEMP,DISPL,HUMID,WEIGHT
0027         LOGICAL BALST(3)
0028         DOUBLE PRECISION STME,TIME
0029         INTEGER WRTBUF(16),IANS(3)
0030         REAL WT,PWT
0031         EQUIVALENCE(WRTBUF,STNUM)
0032   C
0033   C *********************************************************************
0034   C
0035   C THIS SECTION DEFINES LABELS FOR GRAPHS
0036   C
0037   C *********************************************************************
0038         DATA  IDX/2HSQ,2HRT,2H (,2HHR,2HS),2H  ,2H  ,2H  ,3H  ,
0039        1 2H  ,2H  /
0040         DATA  IDY/2H% ,2HMO,2HIS,2HTU,2HRE,2H  ,2H  ,2H  ,2H  ,
0041        1 2H  ,2H  ,2H  ,2H  ,2H  ,2H  ,2H  ,2H  ,2H  ,2H  ,2H  ,
0042        2 2H  ,2H  ,2H  ,2H  /
0043         DATA  IX/2H% ,2HMO,2HIS,2HTU,2HRE,2H  ,2H  ,2H  /
0044         DATA  IY/2HST,2HRA,2HIN,2H (,2H10,2HE-,2H3),2H  ,2H  ,2H  /
0045      10 WRITE(1,1000)
0046         READ(1,2000) (SPNAME(I),I=1,3)
0047         WRITE(1,2000) SPNAME
0048         IF(SPNAME(1).EQ.2HST)STOP
0049         WRITE(1,3000)
0050         READ(1,3500) LNOT
0051         WRITE(1,4000)
0052         READ(1,4500) WNOT
0053         IF(SPNAME(1).EQ.2HST)STOP
0054         CALL OPEN(IDCB,IERR,SPNAME)
0055         IF(IERR.GE.0)GOTO 20
```

Figure C2. NPLOT FORTRAN Code

```
 PAGE 0002  NPLOT  9:58 AM  THU., 27  AUG., 1981

0056          WRITE(1,1010)SPNAME
0057          GOTO 10
0058       20 ICNT = 1
0059          WT=0.0
0060          PWT=0.0
0061          WRITE(1,9000) SPNAME
0062       25 CALL READF(IDCB,IERR,WRTBUF,16,LEN)
0063          IF(LEN.EQ.-1) GO TO 40
0064          IF(ICNT.EQ.1) STME=DBLE(FLOAT(DAYS))*1440.+DBLE(FLOAT(HRS))*60.
0065         1 +DBLE(FLOAT(MINS))
0066    C
0067    C ***************************************************************
0068    C
0069    C THIS SECTION HAS BEEN COMMENTED OUT BUT MAY BE UNCOMMENTED
0070    C TO GIVE RAW DATA READ FROM THE DLTLG FILES.  ALSO, IF THE BALANCE
0071    C HAS BEEN RETARED, IT ADDS THE NEW WEIGHT TO THE PREVIOUS WEIGHT.
0072    C
0073    C***************************************************************
0074    C       WRITE(11,9009)STNUM,SPNUM,DAYS,HRS,MINS,
0075    C      1 TEMP,DISPL,HUMID,WEIGHT,BALST
0076          DISP(ICNT)=DISPL
0077          IF(BALST(3).EQ..TRUE.)PWT=0.0
0078          WT=WT+WEIGHT-PWT
0079          PWT=WEIGHT
0080          WGHT(ICNT)=WT
0081    C
0082    C ***************************************************************
0083    C
0084    C THIS SECTION CALCULATES HOURS FROM THE REAL TIME CLOCK,
0085    C THEN CALCULATES THE SQUARE ROOT OF TIME.
0086    C
0087    C ***************************************************************
0088    C
0089          TIME = DBLE(FLOAT(DAYS))*1440.+DBLE(FLOAT(HRS))*60. +
0090         1 DBLE(FLOAT(MINS)) - STME
0091          SQTR(ICNT) = SNGL(DSQRT(TIME)/DSQRT(DBLE(60.)))
0092          ICNT=ICNT+1
0093          GOTO 25
0094       40 NPTS = ICNT - 1
0095          WRITE(1,9001) NPTS
0096          IF(NPTS .EQ. 0) GO TO 100
0097          CALL CLOSE(IDCB,IERR)
0098    C ***************************************************************
0099    C
0100    C THIS SECTION CALCULATES STRAIN AND %MOISTURE
0101    C
0102    C ***************************************************************
0103          DO 50 I=1,NPTS
0104       50 STRN(I)=(DISP(I)/LNOT)*1000.
0105          WRITE(1,9005)
0106          DO 70 I=1,NPTS
0107       70 MOIS(I)=(WGHT(I)/WNOT)*100.
0108          WRITE(1,9007)
0109          WRITE(11,1060)
0110    C
```

Figure C2. NPLOT FORTRAN Code (continued)

```
 PAGE 0003  NPLOT  9:58 AM  THU., 27  AUG., 198:

0111   C ************************************************************
0112   C
0113   C THIS SECTION MAY BE UNCOMMENTED TO GIVE A PRINTOUT OF
0114   C SQUARE ROOT OF TIME, STRAIN, AND %MOISTURE
0115   C
0116   C ************************************************************
0117         DO 80 I=1,NPTS
0118      80 WRITE(11,1070)SQTR(I),STRN(I),MOIS(I)
0119         WRITE(1,9008)
0120   C
0121   C ************************************************************
0122   C
0123   C THIS FINAL SECTION IS THE PLOTTING ROUTINE
0124   C
0125   C ************************************************************
0126         PMOIS=12.
0127         PTIME=30
0128         DX=PTIME/6
0129         DY=PMOIS/8
0130         WRITE(1,9010)
0131         READ(1,2000) IANS
0132         IF(IANS(1) .EQ. 2HNO) GO TO 99
0133         WRITE(1,9002)
0134         CALL MODE(0,1.,1.,1.)
0135         CALL MODE(3,9999.,-1.5,9999.)
0136         CALL MODE(8,0.,DX,0.)
0137         CALL MODE(9,0.,DY,0.)
0138         CALL DRAW(SQTR,MOIS,NPTS,441)
0139         CALL AXES(22.0,IDX,48.1,IDY)
0140         CALL DRAW(0.,0.,1,9000)
0141   C
0142   C ********************************************
0143   C
0144   C LFIT MAY BE UNCOMMENTED TO PROVIDE A LINEAR
0145   C INTERPOLATION OF THE DATA POINTS
0146   C
0147   C ********************************************
0148   C
0149   C     CALL LFIT(MOIS,STRN,NPTS,SLOPE,YINT,RSQ)
0150   C     WRITE (11,1059)SLOPE,YINT,RSQ
0151         PMOIS=6.0
0152         PSTRN=16.0
0153         DY=PSTRN/8
0154         DX=PMOIS/6
0155         CALL MODE(8,0.,DX,0.)
0156         CALL MODE(9,0.,DY,0.)
0157   C     PMOIS1=-YINT/SLOPE
0158   C     CALL DRAW(PMOIS1,0.,1,440)
0159   C     PSTRN2=PMOIS*SLOPE+YINT
0160   C     CALL DRAW(PMOIS,PSTRN2,1,449)
0161         CALL AXES(22.1,IX,20.2,IY)
0162   C     DO 90 I=1,NPTS
0163   C  90 CALL NOTE(MOIS(I),STRN(I),42,-1)
0164         CALL DRAW(MOIS,STRN,NPTS,441)
0165         CALL DRAW(0.,0.,1,9000)
```

Figure C2. NPLOT FORTRAN Code (continued)

```
 PAGE 0004  NPLOT  9:58 AM  THU., 27  AUG., 1981

0166          CALL DRAW(0,0,0,9999)
0167       99 STOP
0168      100 WRITE(1,5000) SPNAME
0169          STOP
0170     1000 FORMAT(" ENTER SPECIMEN NAME  ST TO STOP _")
0171     1010 FORMAT(" FILE ",3A2," DOES NOT EXIST!")
0172     1020 FORMAT(3E12.3)
0173     1040 FORMAT(5X,"TIME",4X,4X,"DISP",5X,3X,"MOIS",5X)
0174     1050 FORMAT(/,"SLOPE= ",1PE10.3,/,"Y INTERCEPT= ",E10.3,/,
0175         1 "RSQ= ",E10.3)
0176     1060 FORMAT(5X,"SQRT",4X,4X,"STRN",5X,4X,"% MOIS",5X)
0177     1070 FORMAT(3F10.4)
0178     2000 FORMAT(3A2)
0179     3000 FORMAT("ORIGINAL LENGTH IS")
0180     3500 FORMAT(F8.4)
0181     4000 FORMAT("ORIGINAL WEIGHT IS")
0182     4500 FORMAT(F8.4)
0183     5000 FORMAT(1X,3A2," IS AN EMPTY FILE.")
0184     9000 FORMAT(1X,"READING FILE ",3A2)
0185     9001 FORMAT(1X,"NUMBER OF READINGS IN FILE = ",I10)
0186     9002 FORMAT(1X,"PLOTING THE FILE NOW.")
0187     9005 FORMAT(1X,"CALCULATING STRN")
0188     9006 FORMAT(1X,"CALCULATING SQTR")
0189     9007 FORMAT(1X,"CALCULATING MOIS")
0190     9008 FORMAT(1X,"PRINTING CALCULATIONS")
0191     9009 FORMAT(5I10,4F10.5,3L1)
0192     9010 FORMAT(1X,"OK TO PLOT THIS DATA? _")
0193          END
0194          BLOCK DATA RD
0195          COMMON / RECRD / STNUM,SPNUM,DAYS,HRS,MINS,TEMP,DISPL,
0196         1                 HUMID,WEIGHT,BALST(3)
0197          INTEGER STNUM,SPNUM,DAYS,HRS,MINS
0198          REAL TEMP,DISPL,HUMID,WEIGHT
0199          LOGICAL BALST
0200          COMMON / MEM / DISP(1000),SQTR(1000),
0201         1               WGHT(1000),MOIS(1000),STRN(1000)
0202          REAL MOIS,DISP,SQTR,WGHT,STRN
0203          END

  FTN4 COMPILER: HP92060-16092 REV. 2026 (800423)

  **  NO WARNINGS **  NO ERRORS **

 BLOCK COMMON RECRD  SIZE =  00016

 BLOCK COMMON MEM    SIZE =  10000
```

Figure C2. NPLOT FORTRAN Code (continued)

```
 READY.
LIST

 81/08/24. 14.42.24.
PROGRAM   DILGLAS

2 REM THIS PROGRAM CALCULATES COEFFICIENTS OF MOISTURE
3 REM DILATATION FOR S-GLAS/3501-6 ACCORDING TO THE EQUATION
4 REM A0 + A1(%M) + A2(%M)**2 + A3(%M)**3 = STRAIN
5 OPTION BASE 1
10 DIM A(127),X(127,4),T(4,127),B(127,127),I(127,127),Y(127)
15 DIM C(4)
20 N=127
30 FOR I=1 TO N
40 READ X,Y
50 Y(I)=Y
60 X(I,1)=1
70 X(I,2)=X
80 X(I,3)=X*X
85 X(I,4)=X**3
90 NEXT I
100 MAT T= TRN(X)
110 MAT B =T*X
120 MAT I= INV (B)
130 MAT A= T*Y
140 MAT C= I*A
150 FOR I= 1 TO N
160 PRINT X(I,2),Y(I)
170 NEXT I
180 PRINT C(1),C(2),C(3),C(4)
200 DATA .0001,0,.0441,.0003,.0860,.0005,.1306,.0009
210 DATA .2184,.0013,.2654,.0016,.3114,.0018,.3695,.0024
220 DATA .4345,.0034,.4985,.0035,.5414,.0039,.5891,.0044
230 DATA .6542,.0045
240 DATA .0011,0,.0523,.0003,.0942,.0006,.1427,.0007
250 DATA .2408,.0011,.3,.0016,.3595,.0018,.4397,.0025
260 DATA .5421,.0033,.5770,.0034,.6247,.0038,.6596,.0040
270 DATA .7492,.0042
280 DATA .0002,0,.0360,.0003,.0777,.0005,.1184,.0011
290 DATA .1964,.0018,.2312,.0022,.2637,.0027,.2996,.0028
300 DATA .3656,.0033,.4201,.0037,.4572,.0039,.5187,.0040
310 DATA .5396,.0045,.5582,.0046
320 DATA .0001,0,.0917,.0005,.1587,.0014,.2551,.0019
330 DATA .3726,.0028,.4713,.0034,.5462,.0037,.67,.0058
340 DATA .6794,.006,.6987,.0065,.7092,.0065,.7299,.0073
350 DATA .7410,.0071,.7452,.0074,.7417,.0073,.7487,.0073
```

Figure C3. DILGLAS BASIC Code

```
360 DATA .7499,.0074,.7628,.0075,.7646,.0073,.7711,.0072
370 DATA .7734,.0075,.7746,.0075,.7711,.0075,.7746,.0077
380 DATA .7734,.0076,.7793,.0077,.7781,.0077
390 DATA .0004,0,.0797,.0005,.1254,.0015,.2297,.0019
400 DATA .3645,.0028,.4618,.0032,.5389,.0037,.6587,.0055
410 DATA .6611,.0059,.6855,.0062,.6855,.0068,.6951,.0075
420 DATA .7019,.0070,.6986,.007,.6927,.0073,.7068,.0072
430 DATA .7068,.0074,.7220,.0071,.7267,.0071,.7267,.0068
440 DATA .7232,.0072,.7279,.0069,.7302,.0073,.7279,.0075
450 DATA .7267,.0077,.7220,.0077,.7279,.0077
460 DATA .001,0,.1037,.0006,.1933,.0013,.2817,.0019
470 DATA .3819,.0024,.4821,.0031,.5505,.0036,.5976,.0041
480 DATA .6471,.0046,.6813,.0051,.6978,.0055,.7131,.0060
490 DATA .7343,.0062,.7450,.0064,.7744,.0065,.7650,.0067
500 DATA .7803,.0067,.7933,.0070,.7886,.0071,.7921,.0071
510 DATA .7945,.0072,.8039,.0073,.8027,.0074,.8157,.0074
520 DATA .8239,.0079,.8227,.0079,.8122,.0078,.8180,.0079
530 DATA .8227,.0080,.8216,.0079,.8381,.0078,.8298,.0077
540 DATA .0551,.00024,.3501,.00096,.6444,.00261,.7198,.00378
550 DATA .7927,.00416,.8564,.00464,.8656,.00501,.8530,.00556
560 DATA .8472,.00525,.8289,.00567,.8449,.00584,.8461,.00584
570 DATA .8415,.00594,.8484,.00594,.8679,.00594,.8702,.00601
580 DATA .9000,.00622,.9046,.00646,.8817,.00628
590 DATA .0545,.00024,.1505,.0005818,.2300,.00120,.4765,.00346
600 DATA .5815,.0040,.6164,.0040,.6828,.00434,.7053,.00479
610 DATA .7528,.00510,.7528,.00507,.7776,.00520,.7836,.00537
620 DATA .7859,.00530,.7954,.00572,.7765,.00554,.8203,.00599
630 DATA .8263,.00582,.8263,.00565,.8156,.00599,.7966,.00565
640 DATA .7966,.00582,.8061,.00592
999 END

 READY.
```

Figure C3. DILGLAS BASIC Code (continued)

```
 READY.
LIST

 81/08/25. 10.35.47.
PROGRAM   CARBON

2 REM THIS PROGRAM CALCULATES COEFFICIENTS OF DRY AS/3501-6 THERMAL
3 REM DILATATION ACCORDING TO THE EQUATION
4 REM A0 + A1(TEMP) + A2(TEMP)**2 = STRAIN
5 OPTION BASE 1
10 DIM A(33),X(33,3),T(3,33),B(33,33),I(33,33),Y(33)
15 DIM C(3)
16 DIM D(33,2)
20 N=33
30 FOR I=1 TO N
40 READ X,Y
50 Y(I)=Y
60 X(I,1)=1
70 X(I,2)=X
80 X(I,3)=X*X
90 NEXT I
100 MAT T= TRN(X)
110 MAT B =T*X
120 MAT I= INV (B)
130 MAT A= T*Y
140 MAT C= I*A
150 FOR I= 1 TO N
160 PRINT X(I,2),Y(I)
170 NEXT I
180 PRINT C(1),C(2),C(3)
200 DATA -73.3,-.00167,-73.3,-.00218,-73.3,-.00162
210 DATA -45.6,-.0012,-45.6,-.00145,-45.6,-.0012
220 DATA -7.78,-.000713,-7.78,-.000953,-7.78,-.000740
230 DATA 10,-.000260,10,-.000272,10,-.000231
240 DATA 22.7,0,22.7,0,22.7,0
250 DATA 37.8,.000312,37.8,.000408,37.8,.000324
260 DATA 65.6,.000847,65.6,.000998,65.6,.000925
270 DATA 93.3,.00152,93.3,.00159,93.3,.00153
280 DATA 121.1,.00218,121.1,.00231,121.1,.00222
290 DATA 148.8,.00308,148.8,.00286,148.8,.00305
300 DATA 176.67,.00401,176.67,.00354,176.67,.00407
999 END

 READY.
```

Figure C4. CARBON BASIC Code

```
 READY.
LIST

 81/08/25. 10.34.49.
PROGRAM   MCAR

2 REM THIS PROGRAM CALCULATES COEFFICIENTS OF MOISTURE CONDITIONED
3 REM AS/3501-6 THERMAL DILATATION SPECIMENS ACCORDING TO THE EQUATION
4 A0 + A1(TEMP) + A2(TEMP)**2 = STRAIN
5 OPTION BASE 1
10 DIM A(24),X(24,3),T(3,24),B(24,24),I(24,24),Y(24)
15 DIM C(3)
16 DIM D(24,2)
20 N=24
30 FOR I=1 TO N
40 READ X,Y
50 Y(I)=Y
60 X(I,1)=1
70 X(I,2)=X
80 X(I,3)=X*X
90 NEXT I
100 MAT T= TRN(X)
110 MAT B =T*X
120 MAT I= INV (B)
130 MAT A= T*Y
140 MAT C= I*A
150 FOR I= 1 TO N
160 PRINT X(I,2),Y(I)
170 NEXT I
180 PRINT C(1),C(2),C(3)
200 DATA -73.3,-.00193,-73.3,-.00175,-73.3,-.00183
210 DATA -4.56,-.0014000,-4.56,-.00134,-4.56,-.00128
220 DATA -7.78,-.000883,-7.78,-.00071,-7.78,-.00084
230 DATA 10,-.000321,10,-.000280,10,-.000279
240 DATA 22.7,0,22.7,0,22.7,0
250 DATA 37.8,.000321,37.8,.000280,37.8,.000360
260 DATA 65.6,.000950,65.6,.000840,65.6,.001040
270 DATA 93.3,.00156,93.3,.00142,93.3,.00151
999 END

 READY.
```

Figure C5. MCAR BASIC Code

```
 PAGE 0001  FTN.   9:08 AM  TUE., 25  AUG., 1981

0001  FTN4,L
0002  C ***************************************
0003  C                                        *
0004  C THIS PROGRAM PLOTS STRAIN VS. %MOIS    *
0005  C FOR MOISTURE EXPANSION SPECIMENS       *
0006  C IT REQUIRES COEFFICIENTS ACCORDING     *
0007  C TO THE EQUATION                        *
0008  C A0 + A1(%M) + A2(%M)**2 +A3(%M)**3 =   *
0009  C STRAIN                                 *
0010  C                                        *
0011  C ***************************************
0012  C
0013        PROGRAM NLDIL
0014        COMMON IDCB(144),ICOM(170)
0015        REAL MOIS(48),STRN(48),ANOT,AONE,ATWO,ATHR
0016        INTEGER IDX(11),IDY(10)
0017        DATA IDX/2H% ,2HMO,2HIS,2HTU,2HRE,2H  ,2H  ,2H  ,2H  ,2H  ,2H  /
0018        DATA IDY/2HST,2HRA,2HIN,2H (,2H10,2HE-,2H3),2H  ,2H  ,2H  /
0019        MOIS(1)=0.0001
0020        WRITE(1,1000)
0021        READ(1,*)ANOT,AONE,ATWO,ATHR
0022        DO 10 I=2,49
0023        STRN(I-1)=(ANOT+AONE*MOIS(I-1)+ATWO*(MOIS(I-1)**2)+
0024       1 ATHR*(MOIS(I-1)**3))*1000.
0025        IF(I.EQ.49)GO TO 10
0026        MOIS(I)=MOIS(I-1)+.025
0027     10 CONTINUE
0028        PMOIS=1.2
0029        WRITE(1,3000)
0030        READ(1,*)PSTRN
0031        WRITE(1,5050)PSTRN
0032        DX=PMOIS/6
0033        DY=PSTRN/8
0034        CALL MODE(0,1.,1.,1.)
0035        CALL MODE(3,9999.,-1.5,9999.)
0036        CALL MODE(8,0.,DX,0.)
0037        CALL MODE(9,0.0,DY,0.0)
0038        CALL DRAW(MOIS,STRN,48,441)
0039        CALL AXES(20.2,IDX,20.2,IDY)
0040        CALL DRAW(0.,0.,1,9000)
0041        CALL DRAW(0,0,0,9999)
0042   1000 FORMAT("ENTER A0,A1,A2,A3")
0043   3000 FORMAT("ENTER THE STRAIN SPAN")
0044   3050 FORMAT(E10.6)
0045   5050 FORMAT(E10.6)
0046        END

 FTN4 COMPILER: HP92060-16092 REV. 2026 (800423)
```

Figure C6. NLDIL FORTRAN Code

```
PAGE 0001  FTN.   9:10 AM  TUE., 25  AUG., 1981

0001  FTN4,L
0002  C ************************************
0003  C                                    *
0004  C THIS PROGRAM PLOTS STRAIN VS. TEMP  *
0005  C FOR MOISTURE CONDITIONED SPECIMENS  *
0006  C THE PROGRAM REQUIRES COEFFICIENTS   *
0007  C ACCORDING TO THE EQUATION           *
0008  C A0 + A1(TEMP) + A2(TEMP)**2 = STRAIN *
0009  C                                    *
0010  C ************************************
0011        PROGRAM MGLAS
0012        COMMON IDCB(144),ICOM(170)
0013        REAL TEMP(34),STRN(34),ANOT,AONE,ATWO,STY
0014        INTEGER IDX(11),IDY(10)
0015        DATA IDX/2HTE,2HMP,2HER,2HAT,2HUR,2HE ,2H C,2H  ,2H  ,
0016       1 2H  ,2H  /
0017        DATA IDY/2HST,2HRA,2HIN,2H (,2H10,2HE-,2H3),2H  ,2H  ,2H  /
0018        TEMP(1)=-80.
0019        WRITE(1,1000)
0020        READ(1,*)ANOT,AONE,ATWO
0021        DO 10 I=2,35
0022        STRN(I-1)=(ANOT+AONE*TEMP(I-1)+ATWO*(TEMP(I-1)**2))
0023       1 *1000.
0024        IF(I.EQ.35)GO TO 10
0025        TEMP(I)=TEMP(I-1)+5.
0026       10 CONTINUE
0027        PTEMP=240.
0028        WRITE(1,3000)
0029        READ(1,*)PSTRN
0030        WRITE(1,3050)PSTRN
0031        DX=PTEMP/6
0032        DY=PSTRN/8
0033        WRITE(1,5000)
0034        READ(1,*)STY
0035        WRITE(1,5050)STY
0036        CALL MODE(0,1.,1.,1.)
0037        CALL MODE(3,9999.,-1.5,9999.)
0038        CALL MODE(8,-80.0,DX,0.)
0039        CALL MODE(9,STY,DY,0.0)
0040        CALL DRAW(TEMP,STRN,34,441)
0041        CALL AXES(22.0,IDX,20.1,IDY)
0042        CALL DRAW(0.,0.,1,9000)
0043        CALL DRAW(0,0,0,9999)
0044   1000 FORMAT("ENTER A0,A1,A2")
0045   3000 FORMAT("ENTER THE STRAIN SPAN")
0046   3050 FORMAT(E10.6)
0047   5000 FORMAT("ENTER THE INITIAL Y VALUE")
0048   5050 FORMAT(E10.6)
0049        END

FTN4 COMPILER: HP92060-16092 REV. 2026 (800423)
```

Figure C7. MGLAS FORTRAN Code

```
 PAGE 0001  FTN.   9:09 AM  TUE., 25  AUG., 1981

0001  FTN4,L
0002  C ***************************************
0003  C                                        *
0004  C THIS PROGRAM PLOTS STRAIN VS. TEMP     *
0005  C FOR UNCONDITIONED SPECIMENS            *
0006  C THE PROGRAM REQUIRES COEFFICIENTS      *
0007  C ACCORDING TO THE EQUATION              *
0008  C A0 + A1(TEMP) +A2(TEMP)**2 = STRAIN    *
0009  C                                        *
0010  C ***************************************
0011        PROGRAM CLASS
0012        COMMON IDCB(144),ICOM(170)
0013        REAL TEMP(51),STRN(51),ANOT,AONE,ATWO,STY
0014        INTEGER IDX(11),IDY(10)
0015        DATA IDX/2HTE,2HMP,2HER,2HAT,2HUR,2HE ,2H C,2H   ,
0016       1 2H   ,2H   ,2H   /
0017        DATA IDY/2HST,2HRA,2HIN,2H (,2H10,2HE-,2H3)/
0018        TEMP(1)=-75.
0019        WRITE(1,1000)
0020        READ(1,*)ANOT,AONE,ATWO
0021        DO 10 I=2,52
0022        STRN(I-1)=(ANOT+AONE*TEMP(I-1)+ATWO*(TEMP(I-1)**2))
0023       1 *1000.
0024        IF(I.EQ.52)GO TO 10
0025        TEMP(I)=TEMP(I-1)+5.
0026     10 CONTINUE
0027        PTEMP=300.
0028        WRITE(1,3000)
0029        READ(1,*)PSTRN
0030        WRITE(1,3050)PSTRN
0031        DX=PTEMP/6
0032        DY=PSTRN/8
0033        WRITE(1,5000)
0034        READ(1,*)STY
0035        WRITE(1,5050)STY
0036        CALL MODE(0,1.,1.,1.)
0037        CALL MODE(3,9999.,-1.5,9999.)
0038        CALL MODE(8,-100.0,DX,0.)
0039        CALL MODE(9,STY,DY,0.0)
0040        CALL DRAW(TEMP,STRN,51,441)
0041        CALL AXES(22.0,IDX,20.1,IDY)
0042        CALL DRAW(0.,0.,1,9000)
0043        CALL DRAW(0,0,0,9999)
0044   1000 FORMAT("ENTER A0,A1,A2")
0045   3000 FORMAT("ENTER THE STRAIN SPAN")
0046   3050 FORMAT(E10.6)
0047   5000 FORMAT("ENTER THE INITIAL Y VALUE")
0048   5050 FORMAT(E10.6)
0049        END

 FTN4 COMPILER: HP92060-16092 REV. 2026 (800423)
```

Figure C8. GLASS FORTRAN Code

APPENDIX D

EXPERIMENTAL DATA

APPENDIX D-1

MOISTURE EXPANSION TESTS

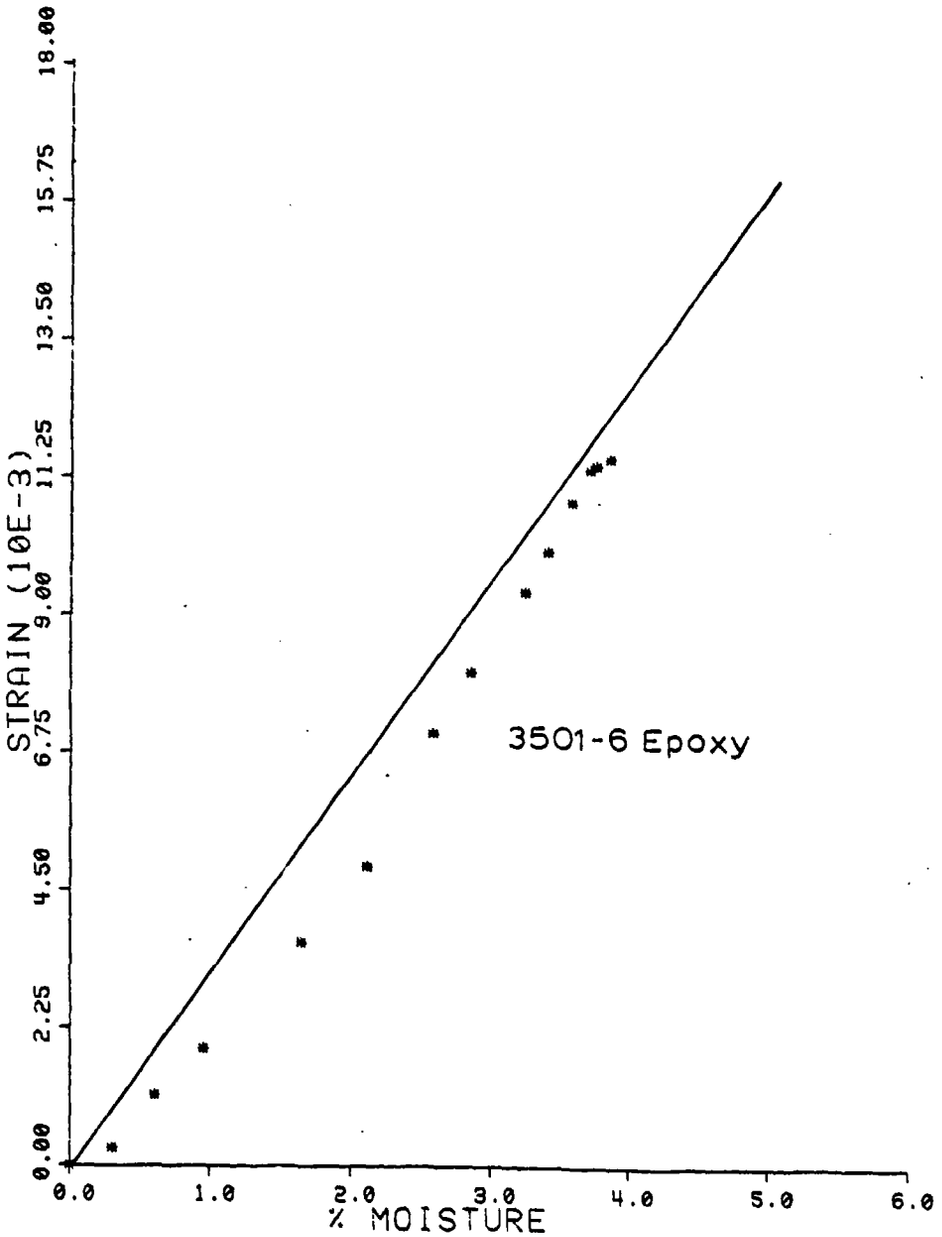

Figure D1. Results of Test 3, Station 1, 10 days @ 98% RH, 65.5°C (150°F)

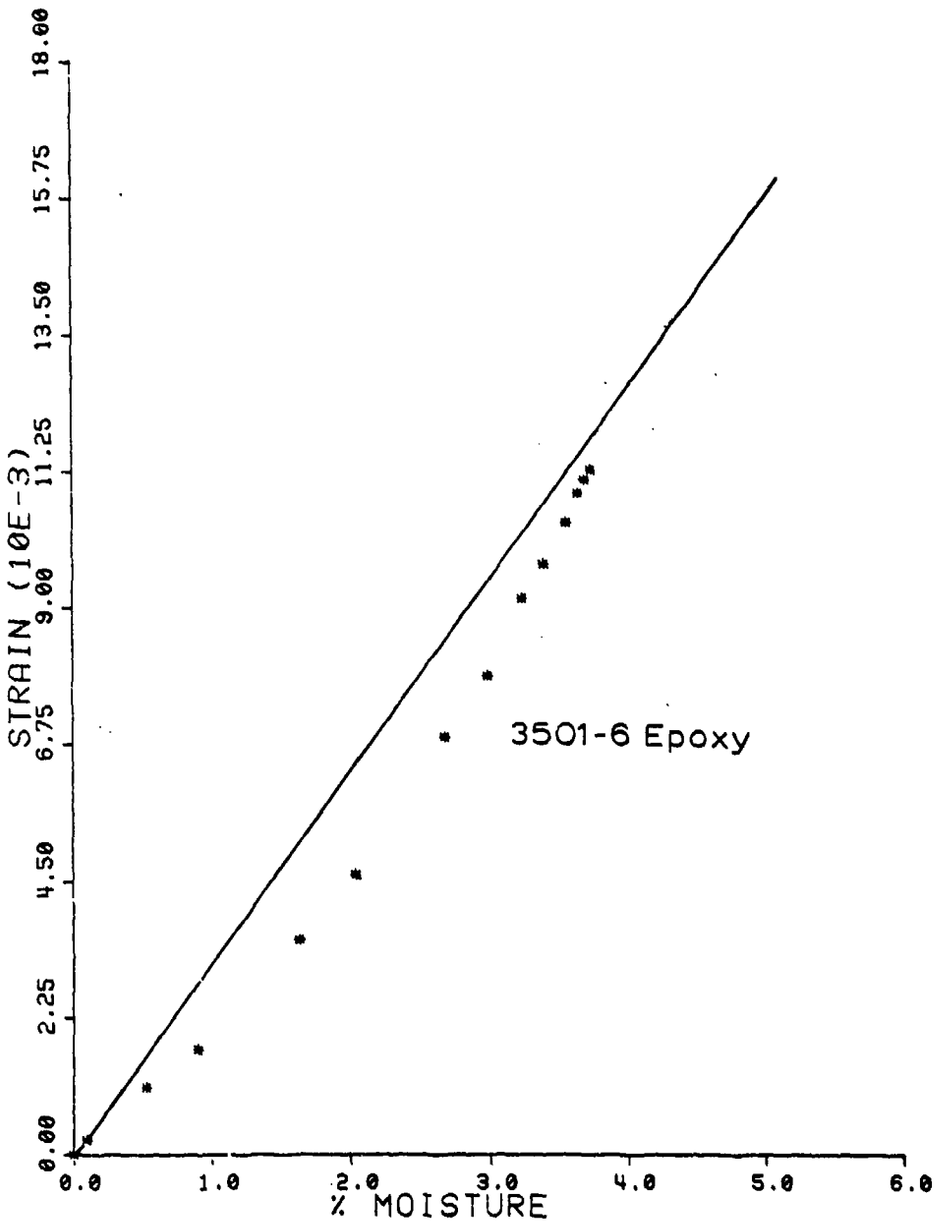

Figure D2. Results of Test 3, Station 2, 10 days @ 98% RH, 65.5°C (150°F)

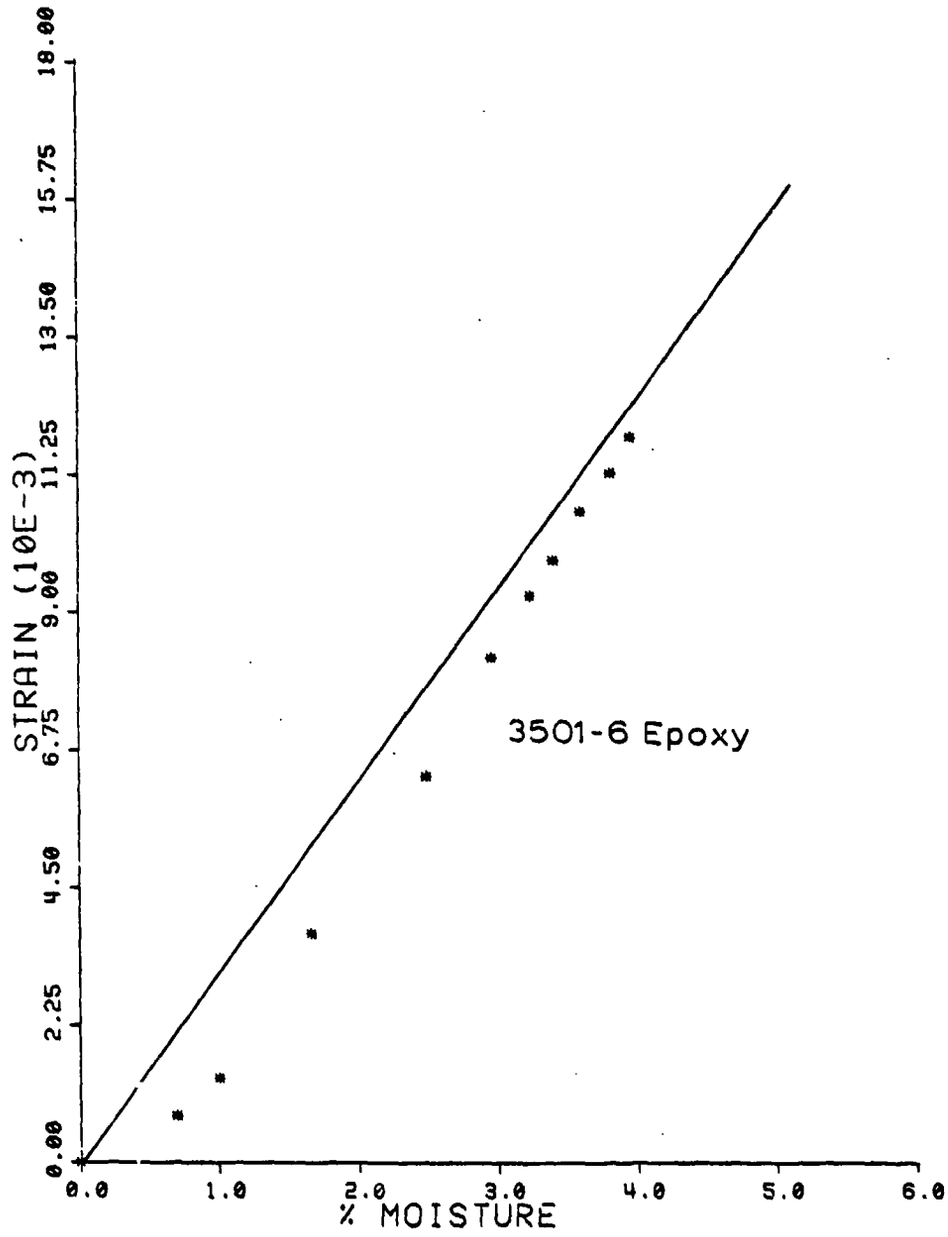

Figure D3. Results of Test 3, Station 3, 10 days @ 98% RH, 65.5°C (150°F)

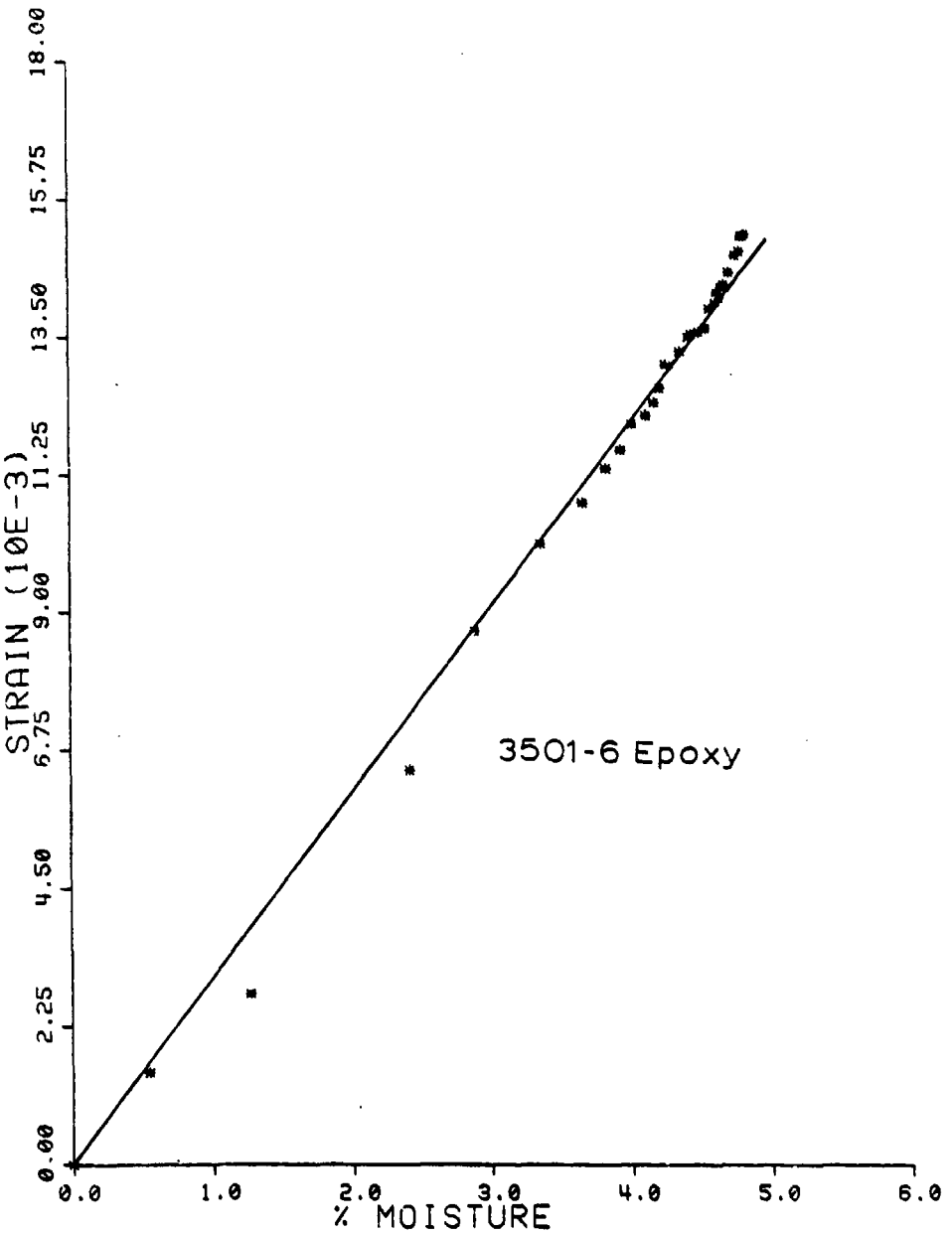

Figure D4. Results of Test 5, Station 1, 30 days @ 98% RH, 65.5°C (150°F)

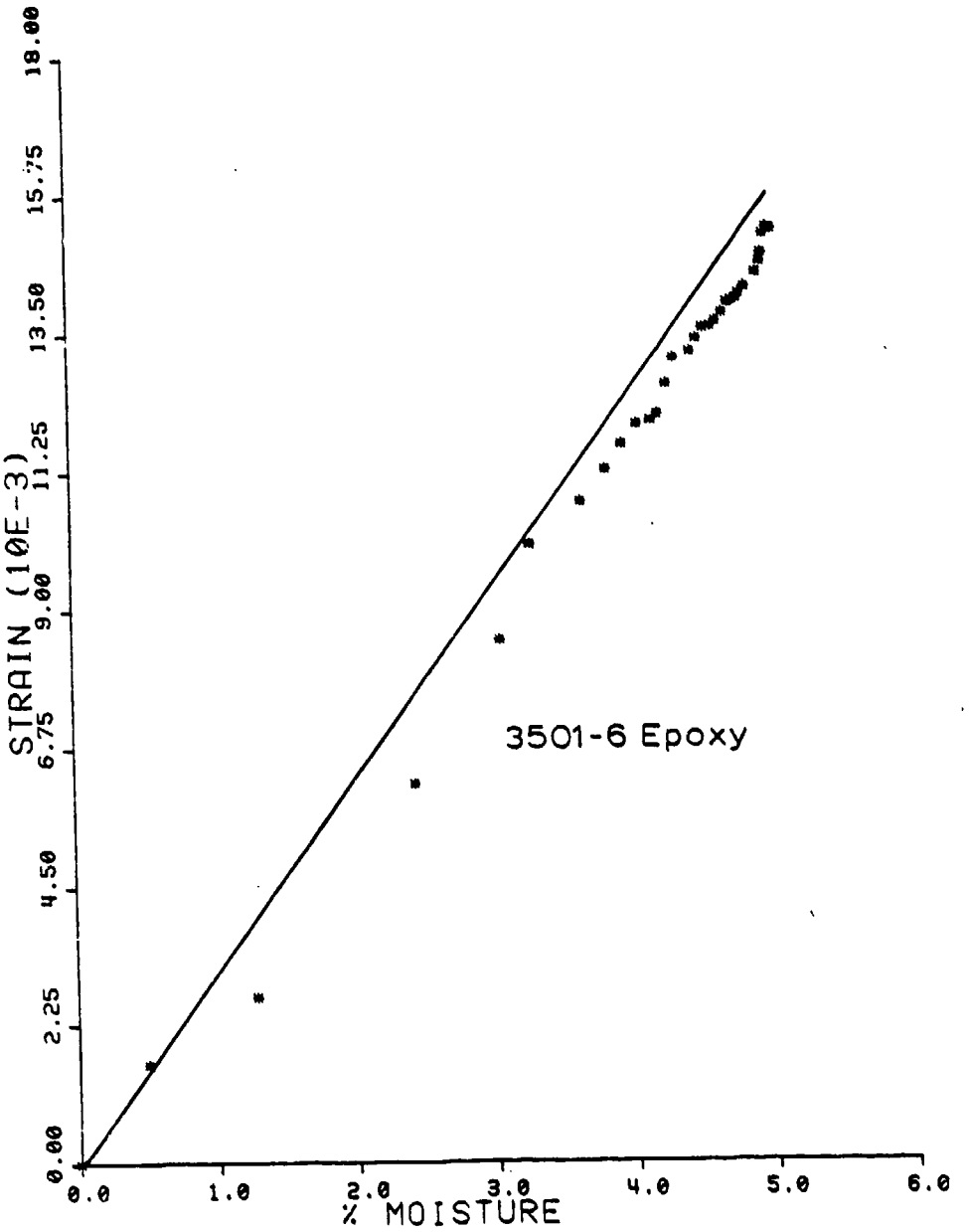

Figure D5. Results of Test 5, Station 3, 30 days @ 98% RH, 65.5°C (150°F)

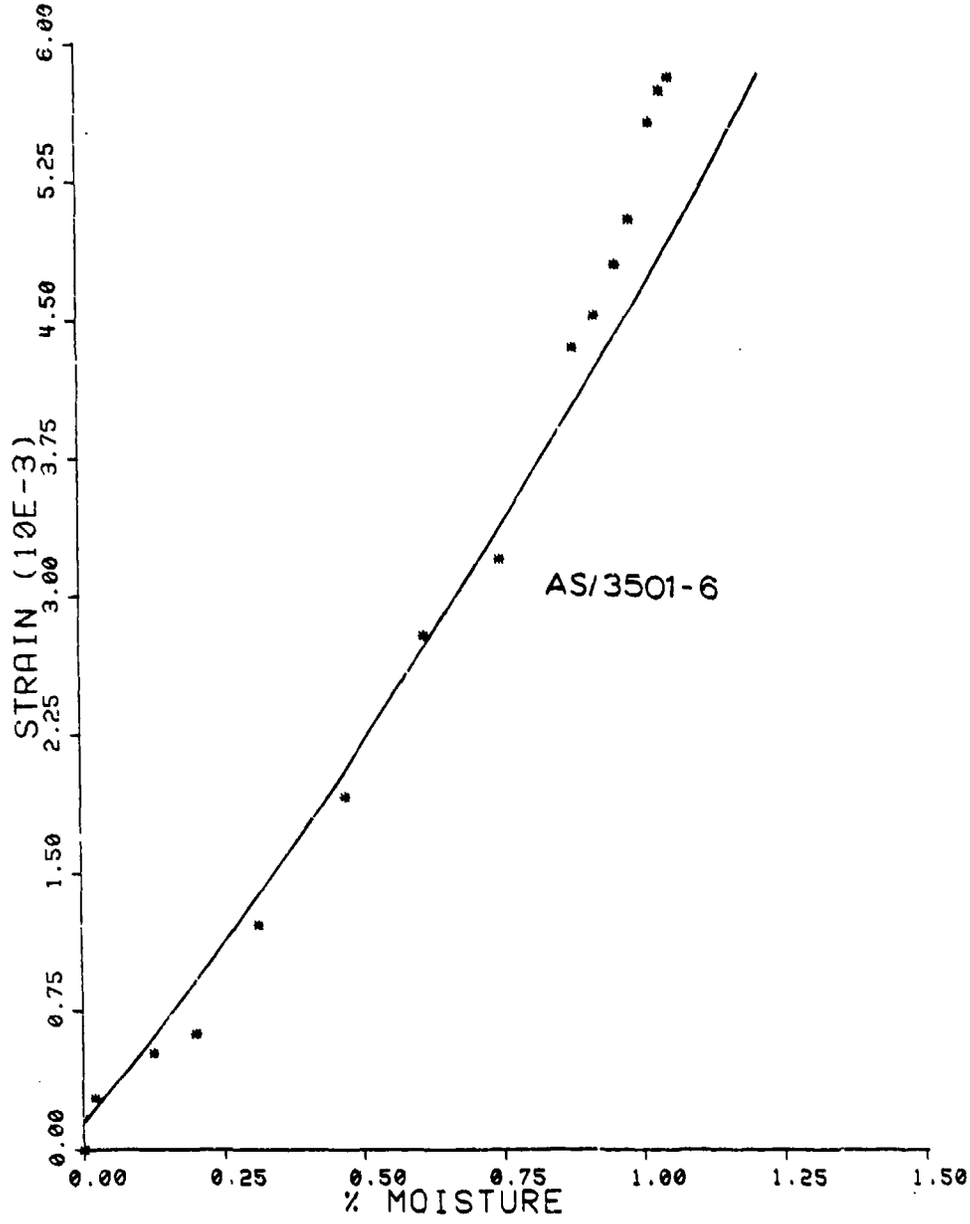

Figure D6. Results of Test 1, Station 1, 10 days @ 98% RH, 65.5°C (150°F)

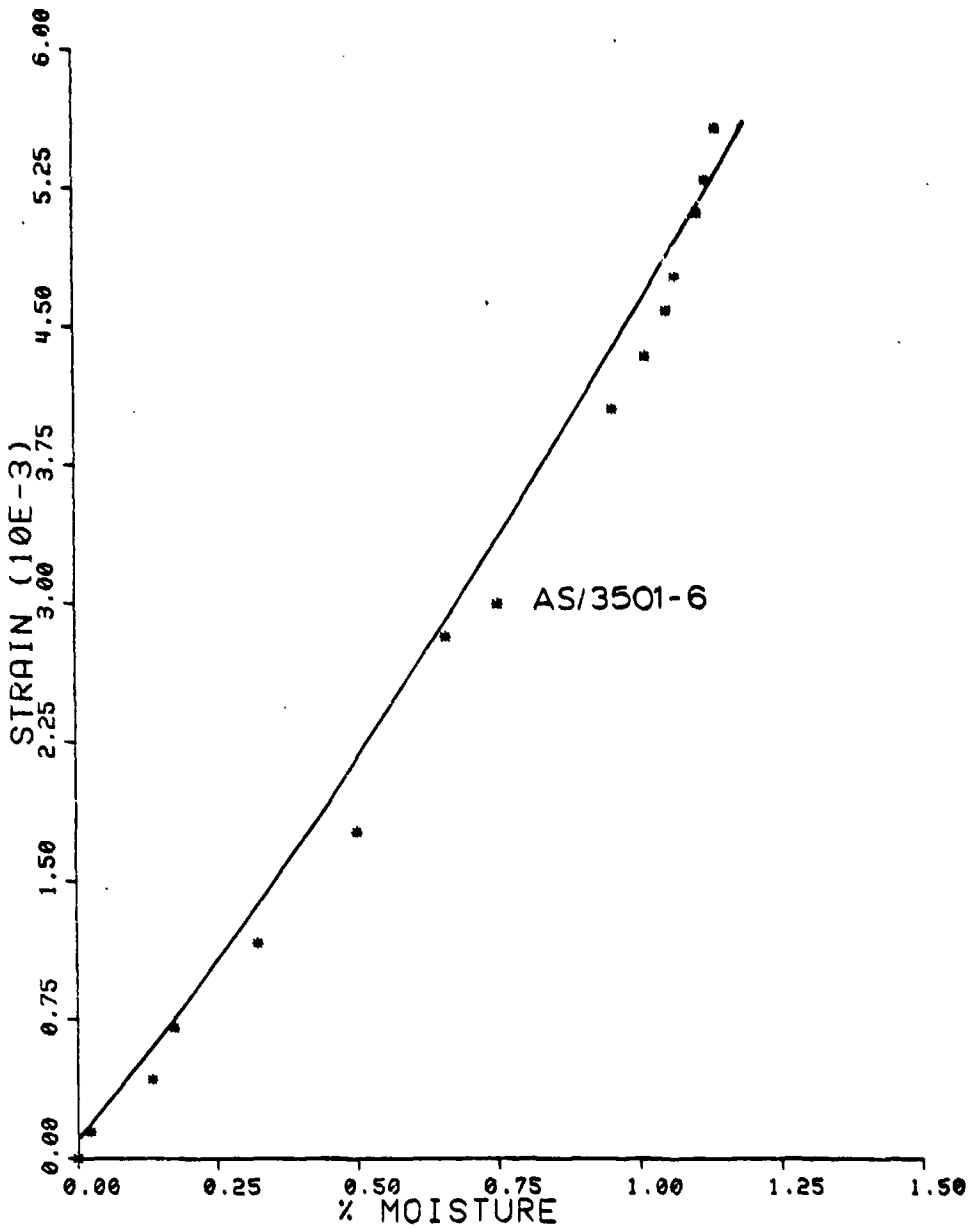

Figure D7. Results of Test 1, Station 2, 10 days @ 98% RH, 65.5°C (150°F)

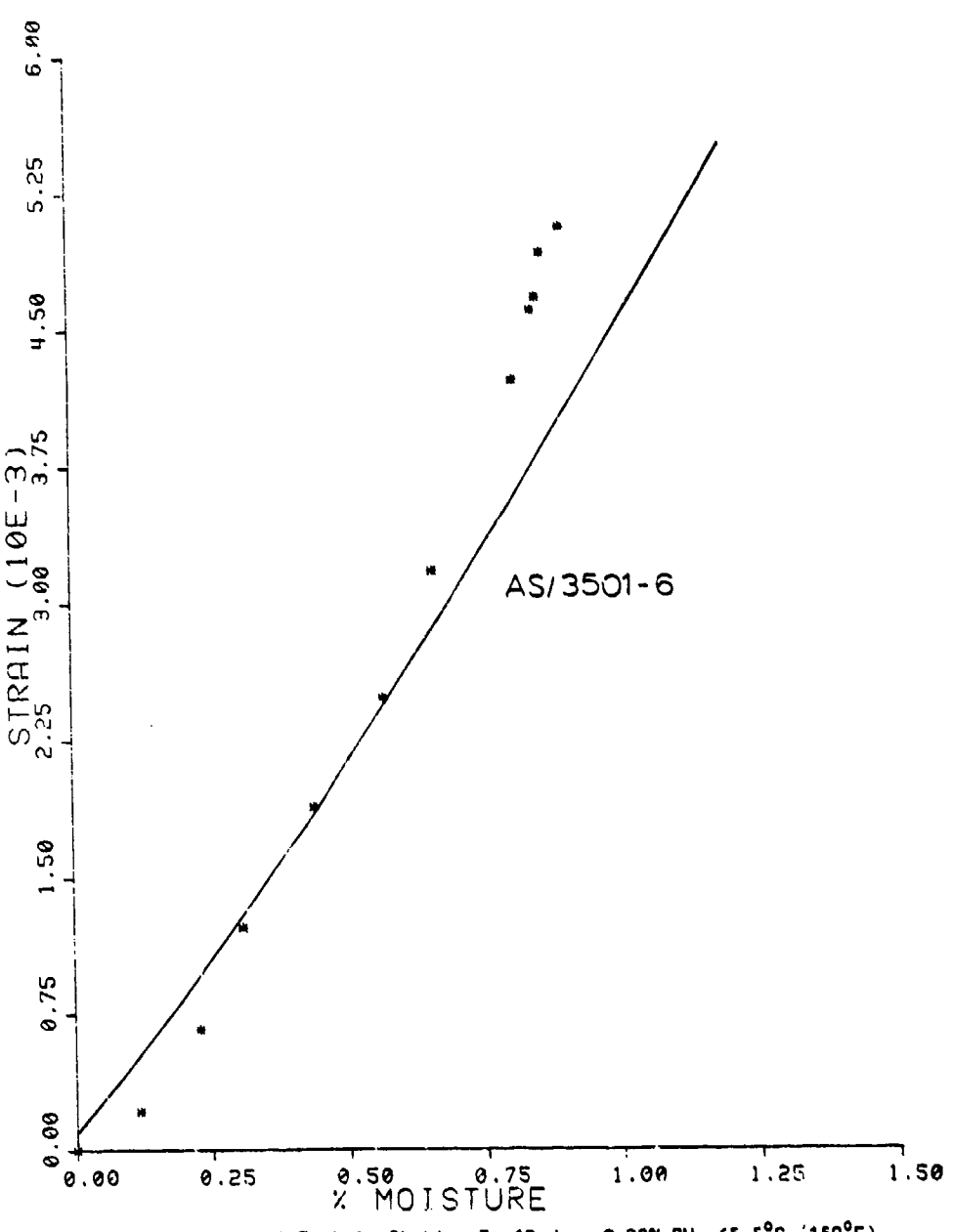

Figure D8. Results of Test 1, Station 3, 10 days @ 98% RH, 65.5°C (150°F)

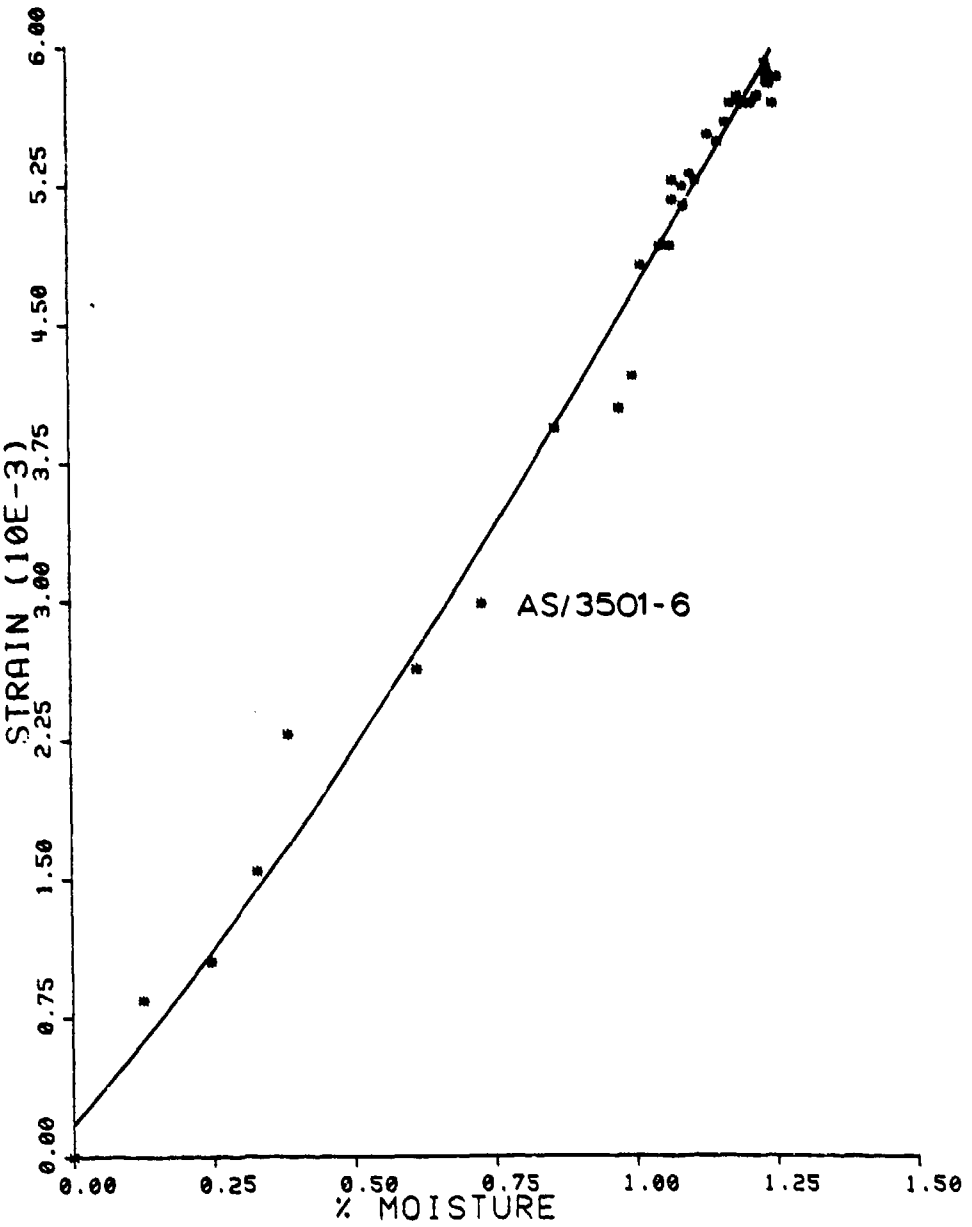

Figure D9. Results of Test 4, Station 1, 30 days @ 98% RH, 65.5°C (150°F)

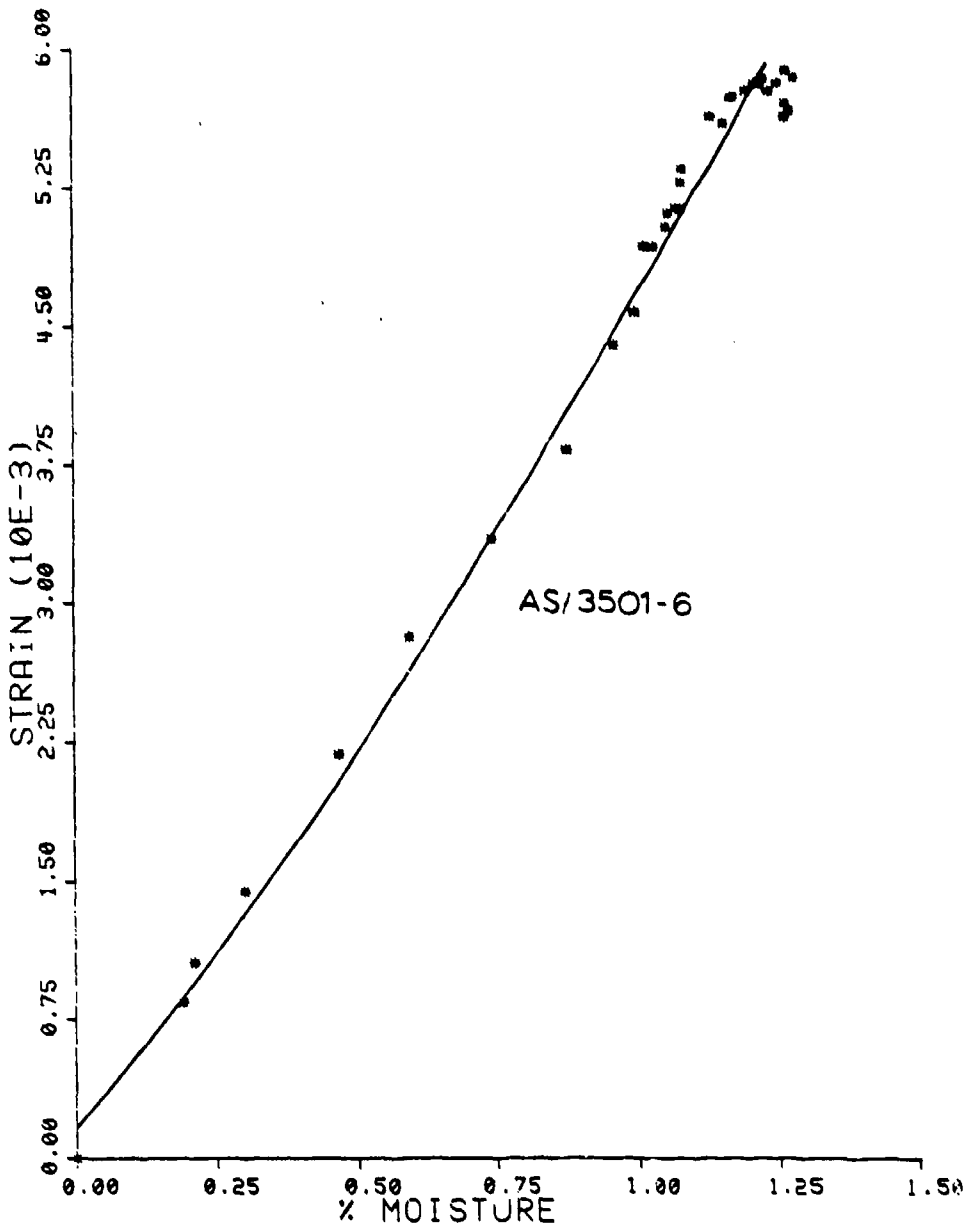

Figure D10. Results of Test 4, Station 2, 30 days @ 98% RH, 65.5°C (150°F)

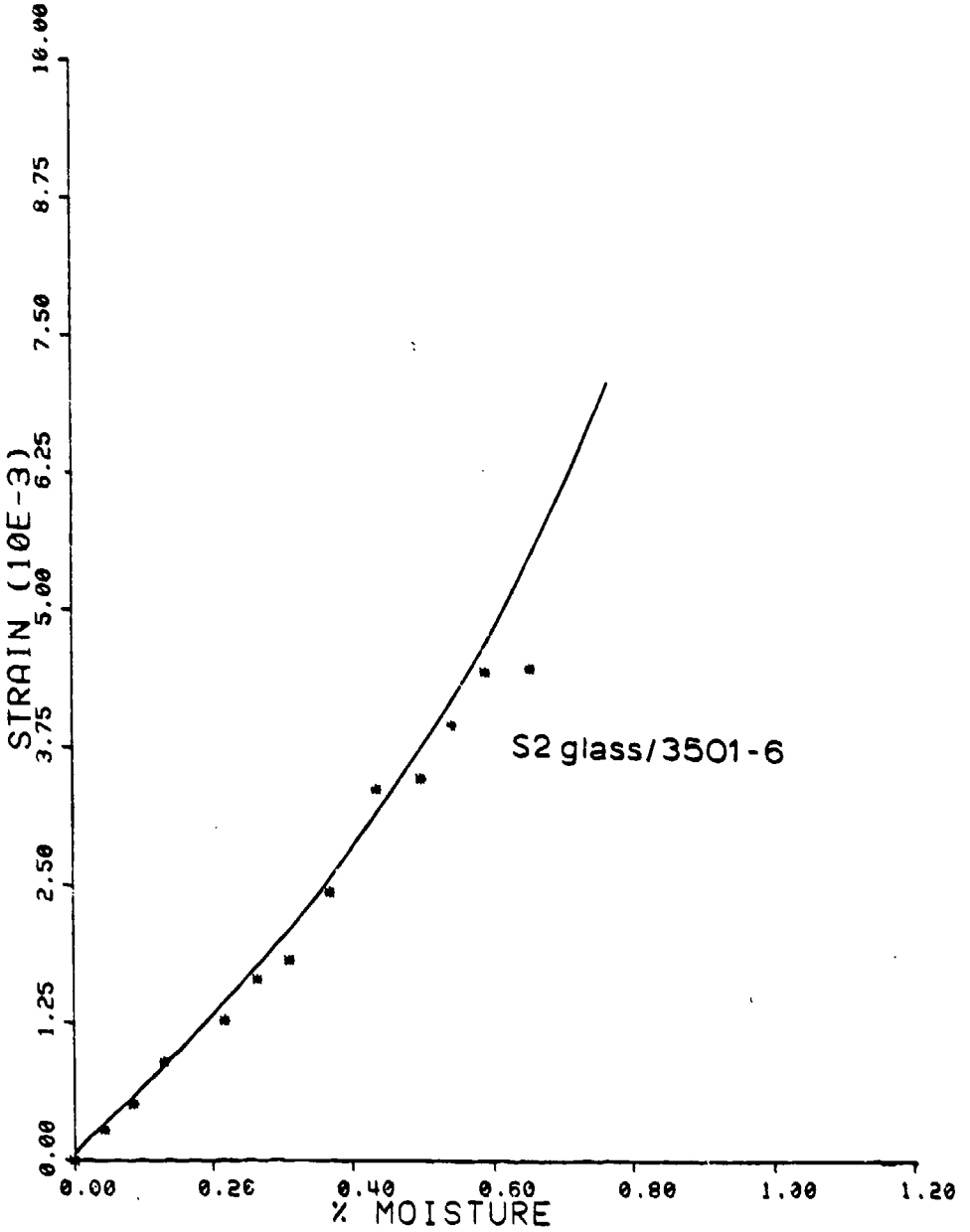

Figure D11. Results of Test 2, Station 1, 10 days @ 98% RH, 65.5°C (150°F)

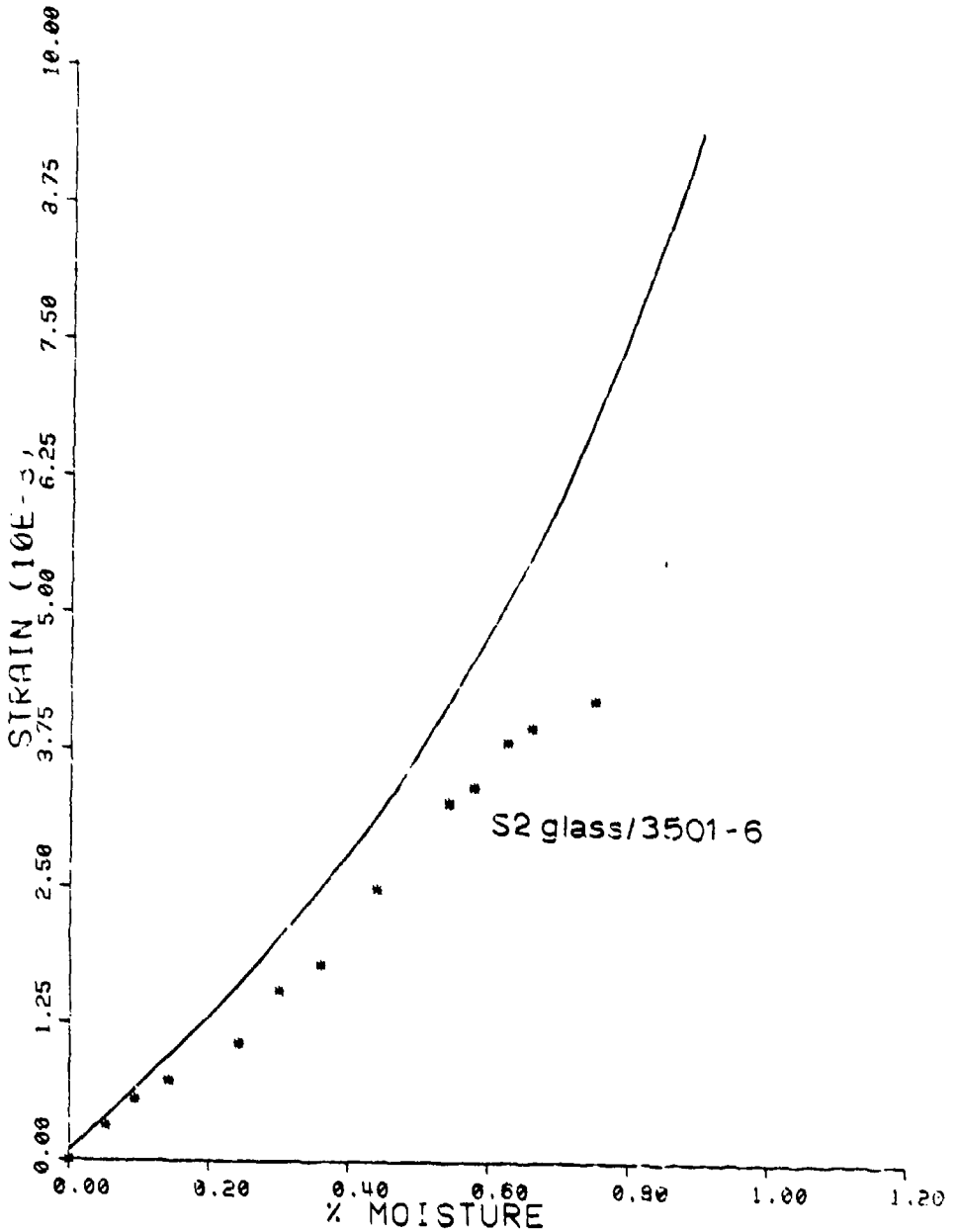

Figure D12. Results of Test 2, Station 2, 10 days @ 98% RH, 65.5°C (150°F)

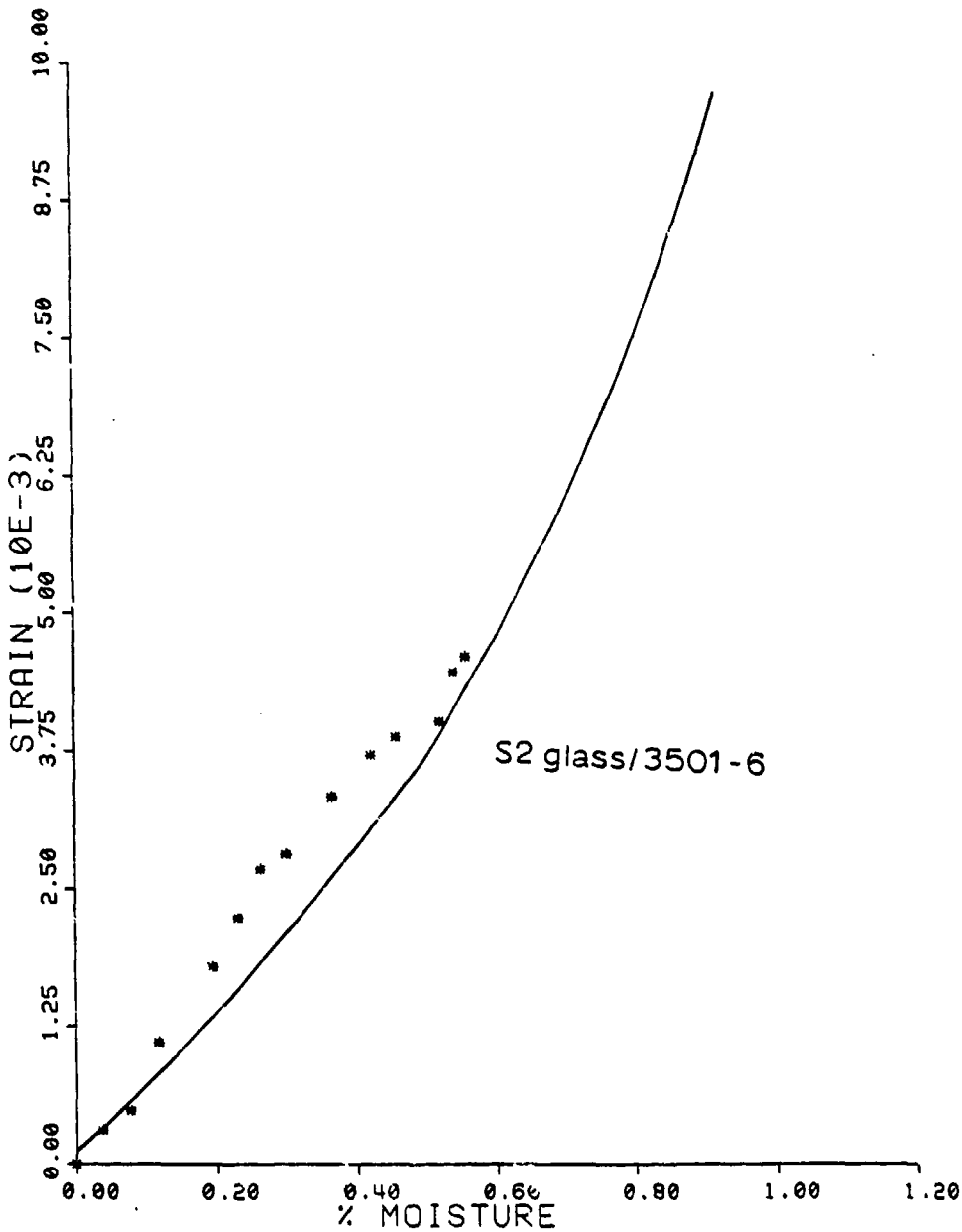

Figure D13. Results of Test 2, Station 3, 10 days @ 98% RH, 65.5°C (150°F)

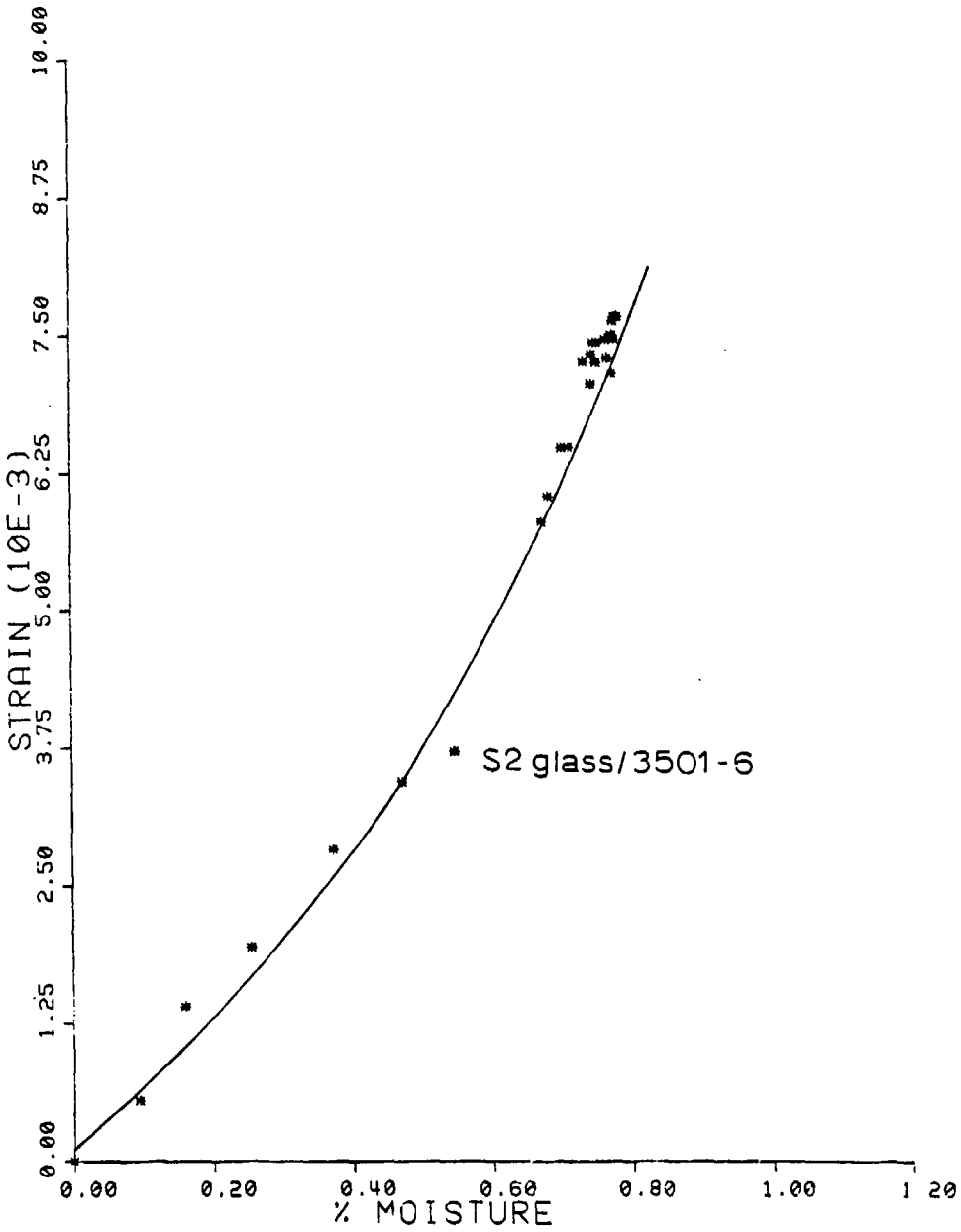

Figure D14. Results of Test 6, Station 1, 30 days @ 98% RH, 65.5°C (150°F)

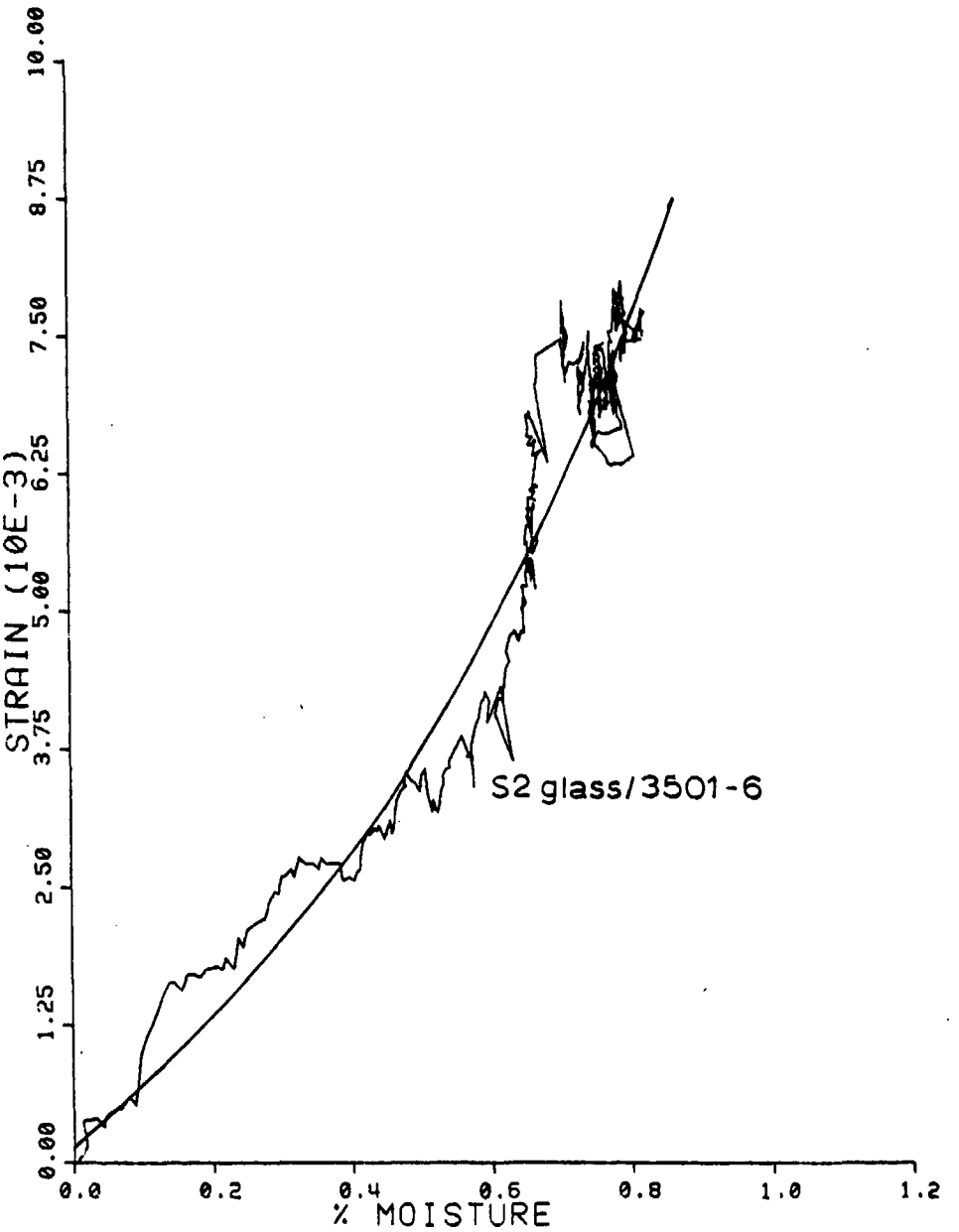

Figure D15. Results of Test 6, Station 2, 30 days @ 98% RH, 65.5°C (150°F)

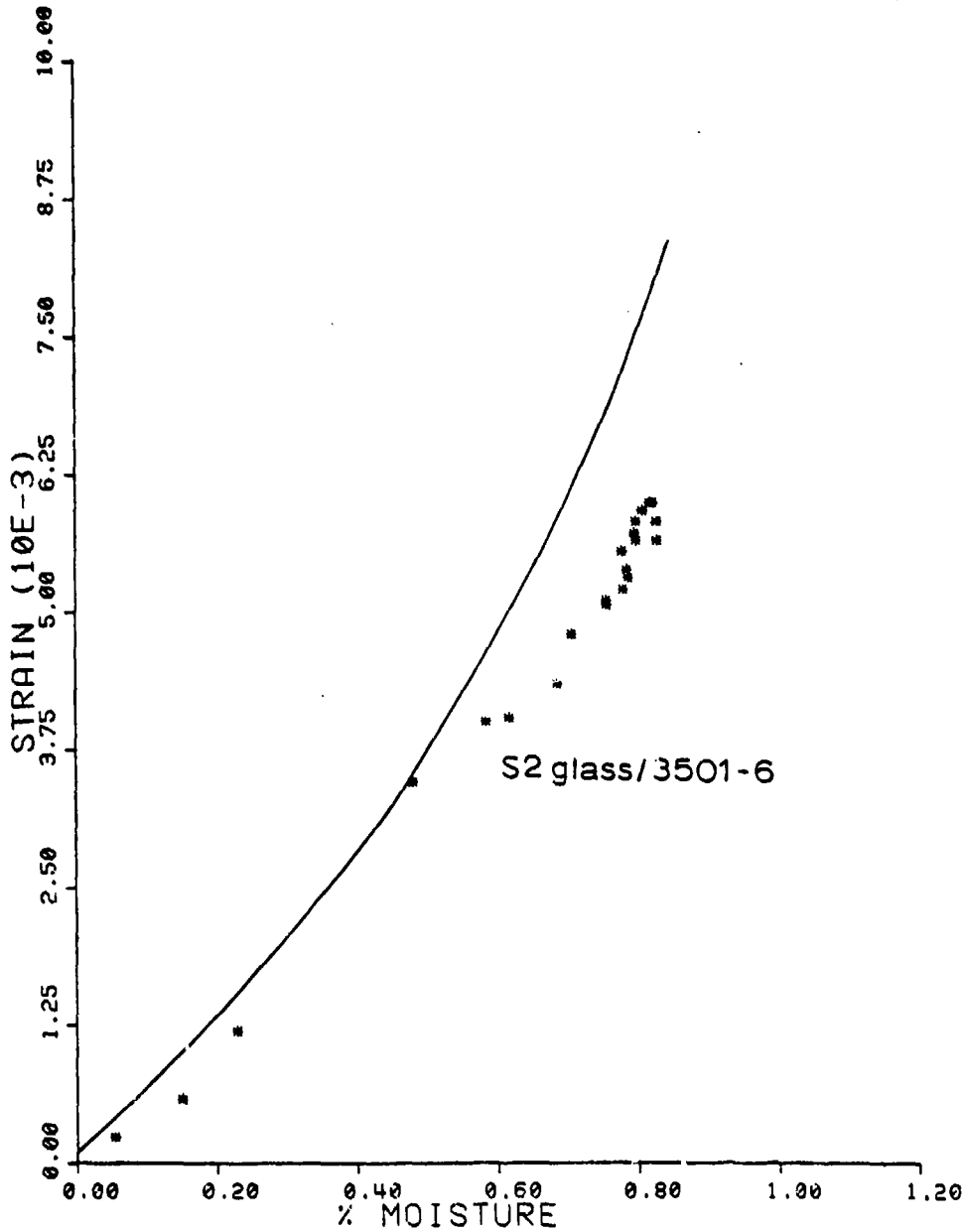

Figure D16. Results of Test 7, Station 2, 20 days @ 98% RH, 70.0°C (167°F)

APPENDIX D-2

THERMAL EXPANSION TESTS

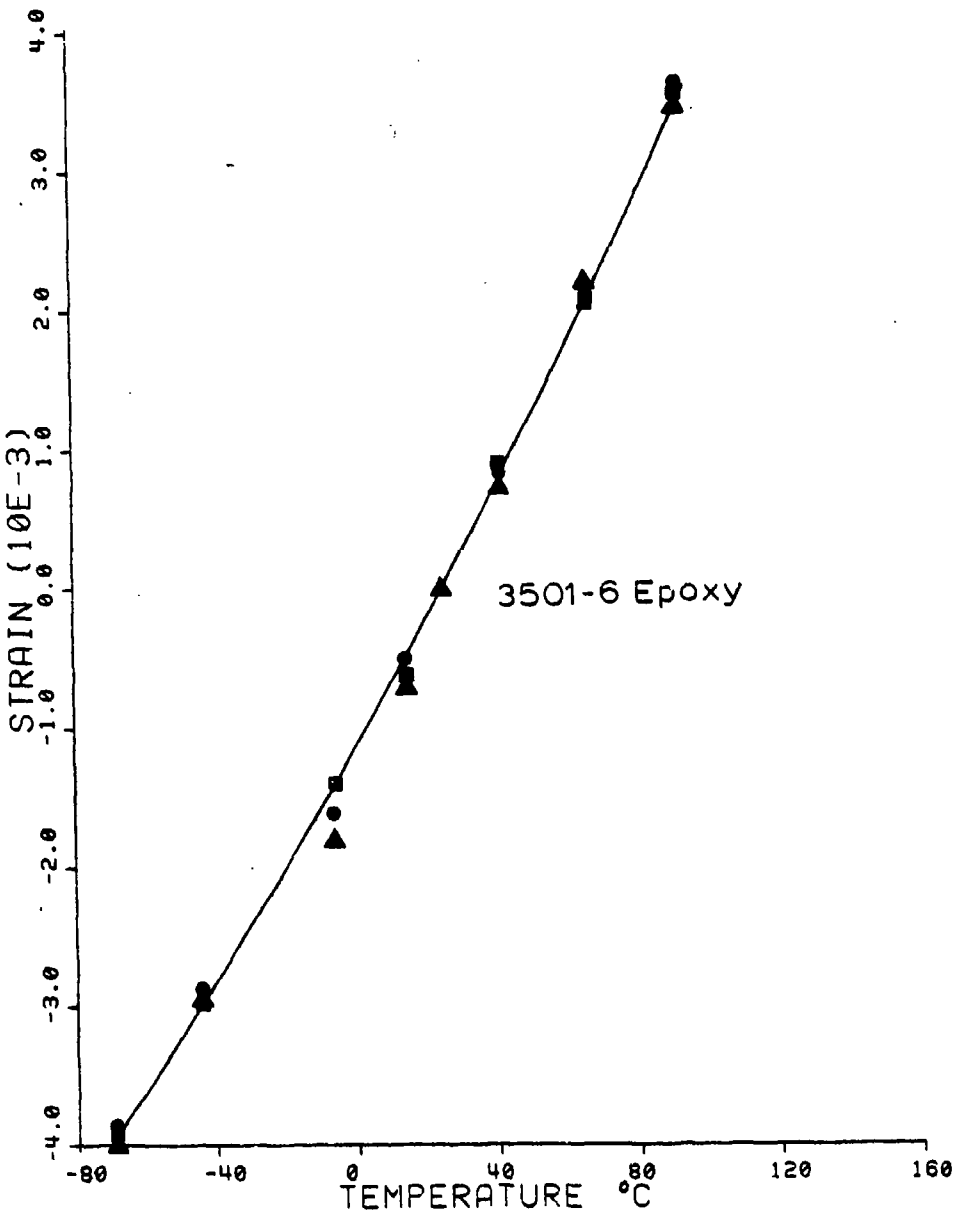

Figure D17. Thermal Expansion Data for Conditioned 3501-6 Resin; Average Percent Moisture = 6.02

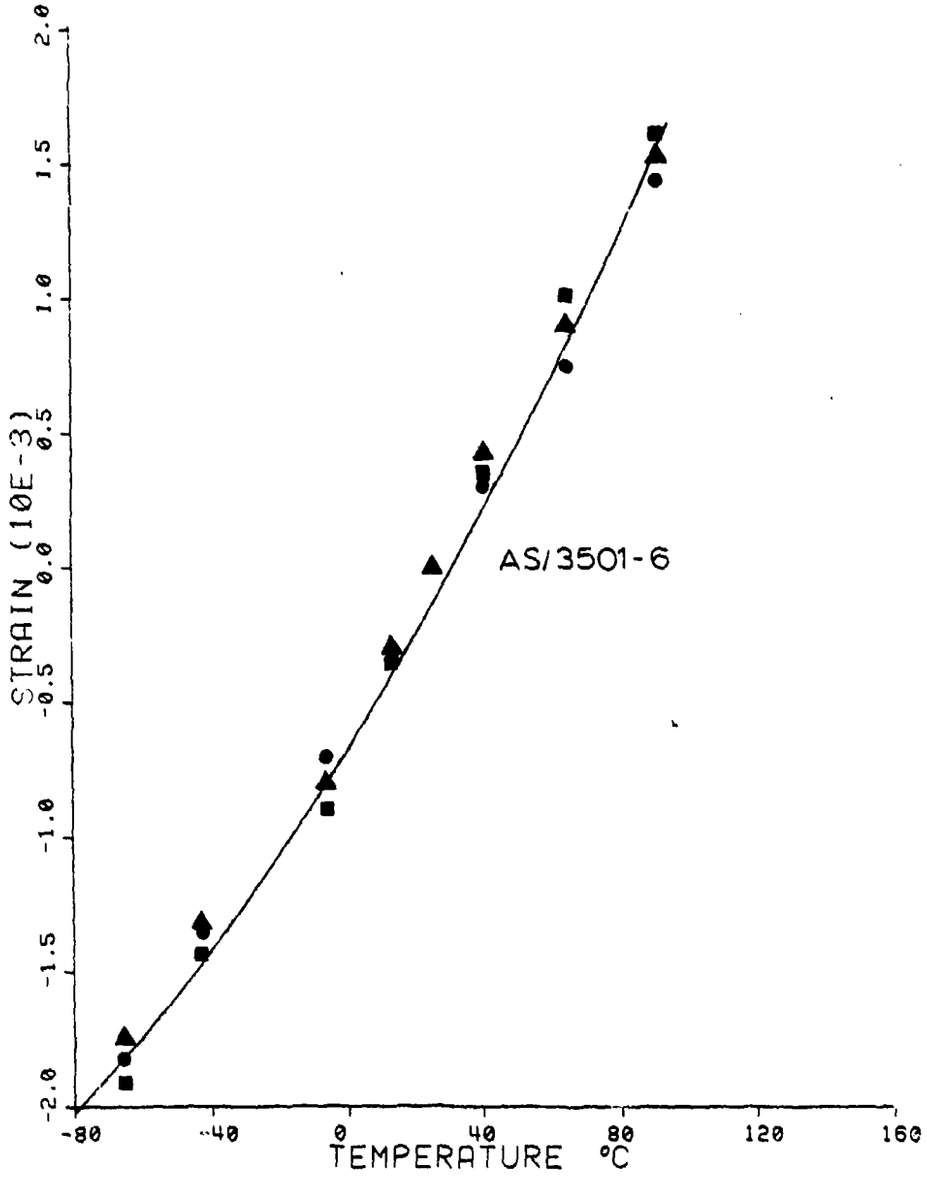

Figure D18. Thermal Expansion Data for Conditioned AS/3501-6; Average Percent Moisture = 1.69

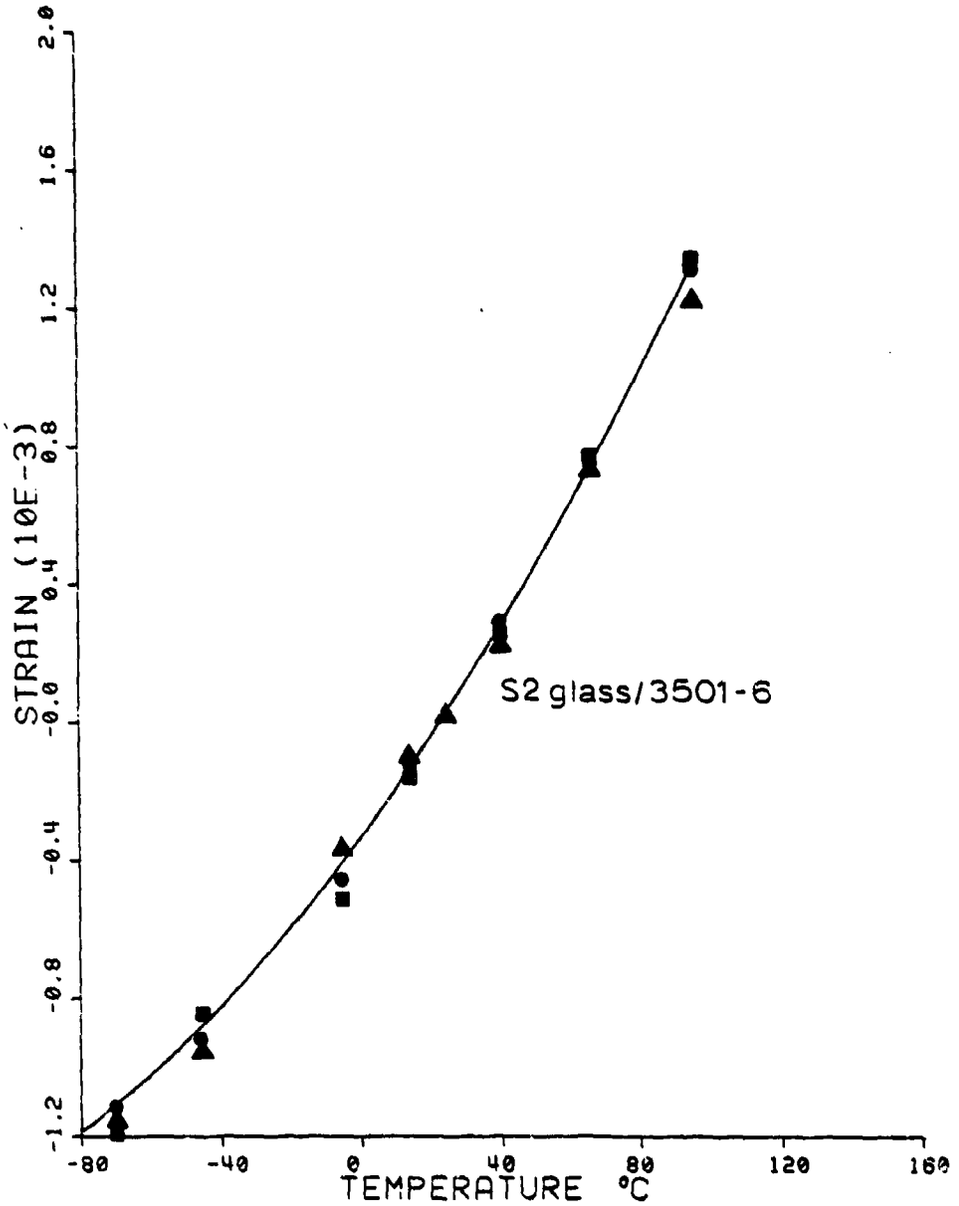

Figure D19. Thermal Expansion Data for Conditioned S2 Glass/3501-6; Average Percent Moisture = 1.13